

ANDRÉ CRUZ DE OLIVEIRA

Identificação e caracterização de mecanismos celulares e moleculares envolvidos na regulação da massa muscular esquelética durante o hipertireoidismo experimental

Tese apresentada ao Programa de Pós-graduação em Biologia de Sistemas do Instituto de Ciências Biomédicas da Universidade de São Paulo, para obtenção do Título de Doutor em Ciências.

São Paulo
2021

ANDRÉ CRUZ DE OLIVEIRA

Identificação e caracterização de mecanismos celulares e moleculares envolvidos na regulação da massa muscular esquelética durante o hipertireoidismo experimental

Tese apresentada ao Programa de Pós-graduação em Biologia de Sistemas do Instituto de Ciências Biomédicas da Universidade de São Paulo, para obtenção do Título de Doutor em Ciências.

Área de concentração: Biologia Morfofuncional

Orientador: Prof. Dr. Anselmo Sigari Moriscot

Versão corrigida

São Paulo
2021

CATALOGAÇÃO NA PUBLICAÇÃO (CIP)
Serviço de Biblioteca e informação Biomédica
do Instituto de Ciências Biomédicas da Universidade de São Paulo

Ficha Catalográfica elaborada pelo(a) autor(a)

de Oliveira, André Cruz
Identificação e caracterização de mecanismos
celulares e moleculares envolvidos na regulação da
massa muscular esquelética durante o
hipertireoidismo experimental / André Cruz de
Oliveira; orientador Anselmo Sigari Moriscot. --
São Paulo, 2021.
164 p.

Tese (Doutorado) -- Universidade de São Paulo,
Instituto de Ciências Biomédicas.

1. Músculo Esquelético. 2. Hipertireoidismo. 3.
Rptor. 4. MDM2. 5. Miostatina. I. Moriscot, Anselmo
Sigari, orientador. II. Título.



Janus

Universidade de São Paulo

ATA DE DEFESA

Aluno: 42138 - 9756434 - 1 / Página 1 de 1

Ata de defesa de Tese do(a) Senhor(a) André Cruz de Oliveira no Programa: Biologia de Sistemas, do(a) Instituto de Ciências Biomédicas da Universidade de São Paulo.

Aos 03 dias do mês de novembro de 2021, no(a) via remota realizou-se a Defesa da Tese do(a) Senhor(a) André Cruz de Oliveira, apresentada para a obtenção do título de Doutor intitulada:

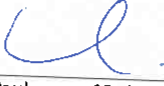
"Identificação e caracterização de mecanismos celulares e moleculares envolvidos na regulação da massa muscular esquelética durante o hipertireoidismo experimental"

Após declarada aberta a sessão, o(a) Sr(a) Presidente passa a palavra ao candidato para exposição e a seguir aos examinadores para as devidas arguições que se desenvolvem nos termos regimentais. Em seguida, a Comissão Julgadora proclama o resultado:

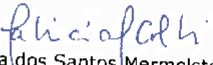
Nome dos Participantes da Banca	Função	Sigla da CPG	Resultado
Anselmo Sigari Moriscot	Presidente	ICB - USP	Não Votante
Francemilson Goulart da Silva	Titular	ICB - USP	<u>APROVADO</u>
Claudia dos Santos Mermelstein	Titular	UFRJ - Externo	<u>APROVADO</u>
Lucia Elvira Alvares	Suplente	UNICAMP - Externo	<u>APROVADO</u>

Resultado Final: APROVADO

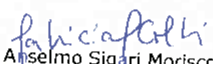
Parecer da Comissão Julgadora *

Eu, Lucianna Vicente da Silva , lavrei a presente ata, que assino juntamente com os(as) Senhores(as). São Paulo, aos 03 dias do mês de novembro de 2021.

pl 
Francemilson Goulart da Silva

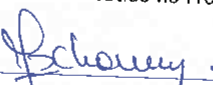
p | 
Claudia dos Santos Mermelstein

pl 
Lucia Elvira Alvares

p | 
Anselmo Sigari Moriscot
Presidente da Comissão Julgadora

* Obs: Se o candidato for reprovado por algum dos membros, o preenchimento do parecer é obrigatório.

A defesa foi homologada pela Comissão de Pós-Graduação em 09/11/2021 e, portanto, o(a) aluno(a) André Cruz de Oliveira jus ao título de Doutor em Ciências obtido no Programa Biologia de Sistemas - Área de concentração: Biologia Morfofuncional.


Presidente da Comissão de Pós-Graduação

Profa. Dra. Maria Luiza Moraes Baneto de Unaves
Presidente da Comissão de Pós-Graduação
ICB/USP



Cidade Universitária "Armando de Salles Oliveira", Butantã, São Paulo, SP - Av. Professor Lineu Prestes, 2415 - ICB III - 05508-000
Comissão de Ética no Uso de Animais - Telefone (11) 3091-7733 - e-mail: cep@icb.usp.br

Of.Circ.CEUA.03.2020

São Paulo, 31 de janeiro de 2020.

Prezado(a) Professor(a),

Lembramos que a validade do protocolo nº **4/2016**, referente ao projeto intitulado **"Impacto do hipertireoidismo induzido sobre a interação entre a via da miostatina e Akt/mTOR no músculo esquelético de ratos"**, para o uso de animais em experimentação sob sua responsabilidade, aprovado por esta comissão em 15/03/2016, encerrar-se-á em **15/03/2020**.

Desta forma, se o projeto não foi concluído, deverá ser encaminhada **até a data do vencimento uma solicitação fundamentada de extensão da vigência da referida licença, conforme modelo constante na página da internet: ww2.icb.usp.br/ich/ceua**.

Ressaltamos ainda, a necessidade de enviar a esta CEUA o **relatório parcial/final**, conforme modelo constante na página da internet citada acima, tanto se o projeto estiver encerrado quanto se houver a necessidade de fazer a renovação do certificado.

Contando com a sua atenção e providências, despeço-me.

Cordialmente,

Luciane Valéria Sita

Prof.a Dra. **Luciane Valéria Sita**
Coordenadora da CEUA - ICB/USP

Sr.(a)
Prof.(a) Dr.(a) **Anselmo Sigari Moriscot**
Departamento de Anatomia - ICB USP



Cidade Universitária "Amendo de Salles Oliveira", Butantã, São Paulo, SP - Av. Professor Lineu Prestes, 2415 - ICB III - 05508-000
Comissão de Ética no Uso de Animais - Telefone (11) 3091-7733 - e-mail: cep@icb.usp.br

Of. CEUA.16.2020

São Paulo, 16 de março de 2020.

Prezado(a) Professor(a),

Informo que o projeto intitulado: **"Impacto do hipertireoidismo induzido sobre a interação entre a via da miostatina e Akt/mTOR no músculo esquelético de ratos"**, registrado sob o protocolo nº **4/2016** e aprovado em 15/03/2016, que envolve a produção, manutenção e/ou utilização de animais pertencentes ao filo Chordata, subfilo Vertebrata (exceto o homem), para fins de pesquisa científica, foi **prorrogado por 17 meses, até 15/08/2021**.

Autorizamos a prorrogação de vigência de licença, com a declaração de que não houve alteração da metodologia e das técnicas descritas na licença inicial para o uso de animais, ou inclusão de animais, para continuidade ao referido projeto.

Reitero que havendo alteração de metodologia e inserção de novos alunos ao projeto de pesquisa vinculado à referida licença a CEUA-ICB deverá ser informada.

Cordialmente,

Luciane Valéria Sita

Profa. Dra. **Luciane Valéria Sita**
Coordenadora CEUA-ICB/USP

Prof.(a) Dr.(a) **Anselmo Sigari Moriscot**
Departamento de **Anatomia**
Instituto de Ciências Biomédicas - USP

Dedico este trabalho a todos os seres que direta e indiretamente me possibilitaram o privilégio de dedicar a vida à busca do conhecimento.

AGRADECIMENTOS

Agradeço a:

Maria Regina, por priorizar minha educação até nas horas mais difíceis.

Paula Alves, companheira de vida, por todo seu amor, paciência e colaboração. Seus ensinamentos foram alicerces essenciais para cada conquista. Sua força e alegria são um porto seguro na tempestade de minhas ideias.

Nilton Cruz, sua presença desde os primórdios da minha caminhada foi crucial para meu desenvolvimento emocional e intelectual. Sem cada um dos seus conselhos eu não chegaria até aqui, fazendo o mundo girar.

Heloi Cruz, por toda a ajuda em um dos momentos mais difíceis. Nosso reencontro foi o elixir para a mudança.

Talitha Érica, por me ensinar que a felicidade vem de dentro.

Moisés Henry, por colocar arte nos meus dias.

Rodrigo Bastos, por me mostrar, pela força do exemplo, que é possível superar os desafios.

Erivaldo Valério, que me fez observar o poder da disciplina.

Marcelo Meratti, por identificar e cultivar em mim o gosto pela ciência. Sempre me senti um verdadeiro biólogo quando juntos pelas matas aprendia de ti a cada relance com plantas e animais.

Anselmo Moriscot, pela oportunidade de trocar o facão por uma pipeta. Sou grato por sua paciência, confiança e pelos sábios conselhos compartilhados. Sua orientação ao longo desses anos foi indispensável para minha formação profissional e pessoal. Muito obrigado por sempre me instigar a evoluir.

William Silva, por me ensinar tanta coisa nos laboratórios científicos e da vida. Sua garra, humildade e incansável amizade me fizeram ter coragem de encarar os desafios, juntos alcançamos lugares que não imaginávamos. Sou grato por sua presença nos momentos bons e ruins.

Lucas Ariel, por sua energia contagiante que sempre me fez ver novas portas.

Jéssica Duarte, por sua sinceridade, amizade e cuidado com o desenvolvimento das pessoas.

Marcos Esteca, por todo o suporte no laboratório e por me inspirar a ter uma esperança incansável.

Luciano Leonel e Denício de Sousa, pela amizade, momentos de descontração e toda ajuda quanto ao estudo e ensino da anatomia humana. Vocês me ensinaram que é possível ter esforço com leveza e trabalho com alegria.

Afonso Melazzo, por sua amizade e todo auxílio no laboratório. Obrigado por renovar meu olhar sobre a ciência e influenciar a busca de um equilíbrio sustentável.

Andrei Rozanski, por seu auxílio essencial na base dos projetos e seu apoio diligente.

Aos colegas de laboratório João Silvestre, Mirella Bento, Flávia Graça, Andrea Ferrian, Gabriela Lima, Rita Rodrigues e Fernando Ribeiro, por todo suporte e conversas.

Siegfried Labeit, Volker Adams e as equipes das Universidades de Heidelberg e Dresden, pela paciência e colaboração produtiva.

Sou grato à Fundação de Amparo à Pesquisa do Estado de São Paulo (FAPESP) pelo financiamento #2017/09398-8 e # 2019/06819-8. Além disso, agradeço a Coordenação de Aperfeiçoamento de Pessoal de Nível Superior (CAPES) pela bolsa emergencial de demanda social, crucial para minha manutenção no programa de pós-graduação.

“Her damos de nossos antepassados um profundo desejo por um conhecimento unificado e abrangente. (...) Por outro lado, tornou-se quase impossível para uma só mente dominar por completo mais que uma pequena porção especializada do conhecimento”.

(Erwin Schrödinger, 2007)

RESUMO

Oliveira AC. Identificação e caracterização de mecanismos celulares e moleculares envolvidos na regulação da massa muscular esquelética durante o hipertireoidismo experimental. São Paulo. Tese [Doutorado em Ciências] – Instituto de Ciências Biomédicas, Universidade de São Paulo, São Paulo; 2021.

Os hormônios tireoidianos são fundamentais no controle dos processos celulares, sobretudo através da regulação da transcrição gênica desencadeada pela triiodotironina (T3). Entretanto, níveis supra fisiológicos deste hormônio, hipertireoidismo, alteram o fenótipo dos tecidos-alvo estabelecendo patologias. No músculo esquelético o hipertireoidismo correlaciona-se com atrofia como a resultante de processos que podem englobar estímulo proteolítico e inibição da síntese proteica. Com o intuito de compreender de forma ampla a ação do T3 no músculo esquelético buscou-se identificar novos alvos da regulação hormonal por meio da análise da expressão global dos genes envolvidos nas vias de síntese e degradação proteica. Acerca do eixo catabólico, identificou-se a regulação positiva da proteína E3 ligase MDM2 exclusivamente nas fibras musculares rápidas. Nestas fibras o MDM2 encontra-se no citoplasma e núcleo, neste último, colocalizado com o fator de transcrição PAX7. Em resposta ao T3 há o aumento de translocação nuclear de MDM2 entretanto a co-marcação com PAX7 é diminuída. De forma semelhante, a elevação dos níveis de T3 inibem a translocação de FOXO3, um fator de transcrição passível de desativação por MDM2. Além disso, a inibição farmacológica de MDM2 em cultura de miotubos potencializou os efeitos do T3 ao gerar estruturas menores e com expressão elevada de atrogenes. Assim, nossos resultados indicam que o MDM2 pode estar envolvido em uma resposta pro-trófica ao T3 no músculo esquelético. Por outro lado, a análise dos componentes da via de síntese mTOR indicou queda rápida e expressiva de Rptor, uma subunidade fundamental para o pleno funcionamento de mTORC1. Surpreendentemente, não há elementos responsivos ao T3 na região promotora de Rptor, de forma que se explorou a hipótese da inibição indireta de Rptor por intermédio da via da miostatina. De fato, verificou-se elevados níveis de miostatina em resposta ao T3, contudo houve menor marcação nuclear de SMAD3. Além disso, os elevados níveis de T3 intensificaram a síntese proteica *de novo* apesar da

diminuta fosforilação de mTOR e P70S6K. Por fim, o silenciamento da miostatina ou a expressão ectópica de Rptor protegeram o músculo esquelético da atrofia induzida por T3. Dessa forma, concluímos que a inibição Rptor é essencial para o estabelecimento da atrofia induzida por T3, que por sua vez se estabelece a despeito dos elevados níveis de síntese proteica.

Palavras-chave: Músculo esquelético. Hipertireoidismo. Rptor. MDM2. Miostatina.

ABSTRACT

Identification and characterization of cellular and molecular mechanisms responsible for the regulation of skeletal muscle mass during experimental hyperthyroidism. São Paulo. Thesis [Doctorate in Sciences] - Institute of Biomedical Sciences, University of São Paulo, São Paulo; 2021.

Thyroid hormones are essential players on cellular signaling, primarily through the regulation of gene transcription by triiodothyronine (T3). However, supraphysiological levels of T3, also called hyperthyroidism, leads to pathological changes in target tissues. In skeletal muscle, hyperthyroidism is related to atrophy throughout mechanisms that may include proteolytic stimulation and inhibition of protein synthesis. To get new insights about T3 action upon skeletal muscle, we sought to identify new regulation targets by analyzing the global expression of genes involved on both protein synthesis and degradation pathways. Regarding the catabolic axis, we identified upregulation of the MDM2 E3 ligase exclusively in fast twitch fibers. Additionally, MDM2 is found in the cytoplasm and nucleus, in the latter colocalized with the transcription factor PAX7. In response to T3, there is augmented MDM2 nuclear translocation and reduced PAX7 colocalization. Similarly, T3 inhibits FOXO3 nuclear translocation suggesting a MDM2-dependent inactivation mechanism. Furthermore, pharmacological MDM2 inhibition in cell culture intensified T3 effects, resulting smaller myotubes with high atrogenes expression. Thus, our results indicate that MDM2 may integrate a protrophic response to T3 in skeletal muscle. On the other hand, the analysis of mTOR components showed a swift and strong downregulation of Rptor, a fundamental subunit of mTORC1 complex. Surprisingly, we did not find T3-responsive elements in the promoter region of Rptor, so we explored the hypothesis of indirect inhibition of Rptor by T3 through the myostatin pathway. In fact, we verified myostatin positive response to T3. However, we identified inhibited SMAD3 nuclear translocation. Furthermore, T3 level levels enhanced de novo protein synthesis despite the low phosphorylation of mTOR and P70S6K. Finally, myostatin silencing or Rptor ectopic expression protected skeletal muscle from T3-induced atrophy. Thus, we

conclude that Rptor inhibition is essential for the establishment of T3-induced atrophy, which in turn takes place regardless of the levels of protein synthesis levels.

Keywords: Skeletal muscle. Hyperthyroidism. Rptor. MDM2. Myostatin.

PREFÁCIO

Esta tese segue a estrutura e regras para depósito de coletânea de artigos segundo Resolução CoPGr 7617, de 21/02/2019. Desta forma, o tópico Introdução, precede os artigos que são apresentados na íntegra no tópico Resultados e por fim relacionados no tópico Discussão.

LISTA DE ABREVIATURAS

ATP – adenosina trifosfato
CO₂ – dióxido de carbono
Dio1 – desiodase do tipo 1
Dio2 – desiodase do tipo 2
Dio3 – desiodase do tipo 3
DIT – diiodotirosina
HPT – hipotálamo-pituitária-tireoide
HT – hormônio tireoidiano
LUCA – último ancestral unicelular comum
MIT – moniodotirosina
NIS – cotransportador de sódio e iodo ATP-ase
O₂ – oxigênio
RHT α – receptor de hormônio Tireoidiano Alfa
RHT β – receptor de hormônio Tireoidiano Beta
RHT – receptor de hormônio Tireoidiano
TBG – globulina ligante de tiroxina
TBPA – transtirretina
THR – hormônio liberador de tireotrofina
THRE – elemento responsivo ao hormônio tireoidiano
TPO – peroxidase tireoidiana
TRIAC – 3,5,3'-ácido triiodotiroacético
TSH - hormônio estimulante da tireoide
T3 – triiodotironina
T4 – tetraiodotironina

LISTA DE FIGURAS

Figure 1 Microarray based global gene expression analysis of proteolytic pathways responsive to T3 in the soleus muscle.....	48
Figure 2: T3 increases MDM2 expression in vivo and in vitro.....	50
Figure 3: mRNA expression levels of MDM2 in soleus muscle in different models of atrophy.....	51
Figure 4: Tissue localization of MDM2 by immunofluorescence and skeletal muscle fiber identity by ATPase assay.....	52
Figure 5: MDM2 is expressed in satellite cells.....	54
Figure 6: Influence T3 and Nutlin3 (MDM2 inhibitor) on diameter of myotubes.....	56
Figure 7: FOXO3 is deactivated by T3 in skeletal muscle.....	57
Supplemental Figure 1: Detection of myogenic factors in primary myoblast culture.....	58
Artigo 2 Figure 1: T3 supraphysiological injections for seven days resulted in decreased fibre's cross-sectional area and slow-to-fast type switch in the soleus muscle of rats.....	89
Artigo 2 Figure 2: T3 supraphysiological injections for fourteen days resulted in decreased fibre's cross-sectional area and slow-to-fast type switch in the soleus muscle of rats.....	90
Artigo 2 Figure 3: Rptor gene expression and protein levels were downregulated during experimental hyperthyroidism on the soleus muscle of rats.....	92
Artigo 2 Figure 4: Myostatin gene expression and protein levels were upregulated during experimental hyperthyroidism.....	94
Artigo 2 Figure 5: SMAD3 nuclei colocalisation inquiry by confocal immunofluorescence analysis.....	95
Artigo 2 Figure 6: Protein levels of mTORC1 components during experimental hyperthyroidism.....	97
Artigo 2 Figure 7: Thyroid hormone treatment induces morphological and molecular alterations in mature myotubes.....	99
Artigo 2 Figure 8: Myostatin knockdown blocked T3 effects upon myotube size and Rptor gene expression.....	101

Artigo 2 Figure 9: Myostatin knockdown and RPTOR overexpression protect skeletal muscle from seven-day T3-induced atrophy.....	103
Artigo 2 Figure 10: Myostatin knockdown and RPTOR overexpression protect skeletal muscle from fourteen-day T3-induced atrophy.....	104
Artigo 2 Supplemental Figure 1: Soleus muscle electroporation efficiency.....	105

SUMÁRIO

1	INTRODUÇÃO.....	21
1.1.	OS HORMÔNIOS TIREOIDIANOS E O PROCESSO EVOLUTIVO.....	21
1.2.	A GLÂNDULA TIREOIDE.....	26
1.2.1.	Características anatômicas	26
1.2.2.	Características Histológicas	28
1.3.	HORMÔNIOS TIREOIDIANOS	29
1.3.1.	Biossíntese dos hormônios tireoidianos T3 e T4	29
1.3.2.	Controle da secreção hormonal	32
1.3.3.	Controle da sinalização hormonal nos tecidos-alvo	33
1.3.4.	Mecanismos de Ação dos Hormônios Tireoidianos	34
1.3.5.	Desbalanço dos níveis hormonais.....	35
1.4.	MÚSCULO ESQUELÉTICO.....	36
1.4.1.	Processo Evolutivo	36
1.4.2.	Plasticidade Muscular Esquelética	37
1.4.3.	Vias intracelulares de Controle de Massa	39
2	OBJETIVOS	42
2.1.	OBJETIVOS ESPECÍFICOS.....	42
3	RESULTADOS	43
3.1.	ARTIGO PUBLICADO: “THYROID HORMONE UPREGULATES MDM2 IN RAT TYPE I FIBER: IMPLICATIONS FOR SKELETAL MUSCLE MASS REGULATION”	43
3.1.1.	Introduction	44
3.1.2.	Results	46
<u>3.1.2.1.</u>	<u>Effect of T3 on body, heart, and skeletal muscle weights and on serum T4 levels</u>	<u>46</u>
<u>3.1.2.2.</u>	<u>Gene Expression Level of E3-ligases by Microarray and RT-PCR.....</u>	<u>47</u>
<u>3.1.2.3.</u>	<u>MDM2 expression levels in vivo and in vitro</u>	<u>48</u>
<u>3.1.2.4.</u>	<u>MDM2 gene expression in different atrophy models.....</u>	<u>50</u>
<u>3.1.2.5.</u>	<u>MDM2 is up regulated by T3 in type I fibers.....</u>	<u>50</u>
<u>3.1.2.6.</u>	<u>Cellular localization of MDM2 in skeletal muscle</u>	<u>52</u>
<u>3.1.2.7.</u>	<u>MDM2 is a player in controlling myotube trophicity.....</u>	<u>54</u>
3.1.3.	Discussion.....	57
3.1.4.	Materials and Methods	63
<u>3.1.4.1.</u>	<u>Experimental Procedures</u>	<u>63</u>
<u>3.1.4.2.</u>	<u>Tissue Samples</u>	<u>64</u>
<u>3.1.4.3.</u>	<u>Serum parameters</u>	<u>64</u>
<u>3.1.4.4.</u>	<u>Microarray analysis.....</u>	<u>64</u>

3.1.4.5.	<i>Gene expression by RT- PCR</i>	65
3.1.4.6.	<i>Western blot (WB)</i>	66
3.1.4.7.	<i>Immunofluorescence (IF)</i>	67
3.1.4.8.	<i>Enzyme histochemical staining</i>	68
3.1.4.9.	<i>Cell Culture of myoblasts</i>	69
3.1.4.10.	<i>Myotube Measurements</i>	70
3.1.4.11.	<i>Statistical Analysis</i>	70
3.1.5.	<i>The completion of the Copyright Transfer and Affirmation of Originality</i>	71
3.1.6.	<i>Author contributions</i>	71
3.1.7.	<i>Acknowledgements</i>	71
3.1.8.	<i>References</i>	71
3.2.	<i>ARTIGO SUBMETIDO: “RPTOR INHIBITION IS ESSENTIAL FOR T3-INDUCED SKELETAL MUSCLE ATROPHY INDEPENDENTLY OF mTORC-1”</i>	75
3.2.1.	<i>Introduction</i>	76
3.2.2.	<i>Materials and Methods</i>	79
3.2.2.1.	<i>Experimental hyperthyroidism in a rat model</i>	79
3.2.2.2.	<i>Biological samples</i>	79
3.2.2.3.	<i>Thyroxin (T4) serum levels</i>	80
3.2.2.4.	<i>Skeletal muscle transfection in vivo</i>	80
3.2.2.5.	<i>Plasmid Constructions</i>	81
3.2.2.6.	<i>Global gene expression</i>	81
3.2.2.7.	<i>Gene expression by Real-Time PCR</i>	81
3.2.2.8.	<i>Protein level by Western Blotting</i>	82
3.2.2.9.	<i>Histological analysis and immunofluorescence</i>	84
3.2.2.10.	<i>Cell Culture of Myoblasts and RNAi transfection</i>	85
3.2.2.11.	<i>Statistical analysis</i>	85
3.2.3.	<i>Results</i>	85
3.2.3.1.	<i>Effects of supraphysiological T3 dose upon biometric features</i>	85
3.2.3.2.	<i>Global gene expression analysis of mTOR components</i>	89
3.2.3.3.	<i>T3 inhibits Raptor and promotes Myostatin expression</i>	91
3.2.3.4.	<i>T3 supraphysiological injections increase de novo protein synthesis despite reduced mTOR phosphorylation</i>	94
3.2.3.5.	<i>T3 triggers in vivo similar alterations in myotubes from C2C12 lineage</i>	96
3.2.3.6.	<i>Myostatin knockdown protects myotubes from T3 effects in vitro</i>	98
3.2.3.7.	<i>Myostatin knockdown and Rptor overexpression protects skeletal muscle from T3-induced atrophy</i> 100	
3.2.4.	<i>Discussion</i>	104
3.2.5.	<i>Acknowledgements</i>	107

3.2.6.	<i>Funding</i>	107
3.2.7.	<i>Availability of data and materials</i>	108
3.2.8.	<i>Author's contributions</i>	108
3.2.9.	<i>Ethics approval and consent to participate</i>	108
3.2.10.	<i>Patient consent for publication</i>	108
3.2.11.	<i>Competing interests</i>	109
3.2.12.	<i>References</i>	109
4	APRESENTAÇÃO DOS ARTIGOS (DISCUSSÃO)	116
5	REFERÊNCIAS	119
6	ANEXOS	125
6.1.	AUTORIZAÇÃO USO ARTIGO “<i>THYROID HORMONE UPREGULATES MDM2 IN RAT TYPE I FIBRE: IMPLICATIONS FOR SKELETAL MUSCLE MASS REGULATION</i>”	125
6.2.	AUTORIZAÇÃO PARA USO DO ARTIGO “<i>SKELETAL MUSCLE ANTI-ATROPHIC EFFECTS OF LEUCINE INVOLVE MYOSTATIN INHIBITION</i>”	131
6.3.	ARTIGOS PUBLICADOS EM COLABORAÇÃO	133
6.3.1.	<i>“miR-29c improves skeletal muscle mass and function throughout myocyte proliferation and differentiation and by repressing atrophy-related genes”</i>	133
6.3.2.	<i>“The E3 ligase MuRF2 plays a key role in the functional capacity of skeletal muscle fibroblasts”</i> 134	
6.3.3.	<i>“Small-Molecule Chemical Knockdown of MuRF1 in Melanoma Bearing Mice Attenuates Tumor Cachexia Associated Myopathy”</i>	135
6.3.4.	<i>“Leucine Supplementation Decreases HDAC4 Expression and Nuclear Localization in Skeletal Muscle Fiber of Rats Submitted to Hindlimb Immobilization”</i>	136
6.3.5.	<i>“Regulation of Glucose Metabolism by MuRF1 and Treatment of Myopathy in Diabetic Mice with Small Molecules Targeting MuRF1”</i>	137
6.4.	ARTIGOS COMPLETOS PUBLICADOS – PRIMEIRA AUTORIA	138

1 INTRODUÇÃO

1.1. Os hormônios tireoidianos e o processo evolutivo

Os hormônios tireoidianos (HTs) são moléculas constituídas pela associação do aminoácido tirosina e o elemento químico iodo. Nos mamíferos, classe que inclui os humanos e roedores, os hormônios tireoidianos são um heterogêneo de tetraiodotironina (T4) e triiodotironina (T3), estruturas formadas pela ligação de quatro ou três iodos, respectivamente. O arranjo dessas moléculas é amplamente conservado no subfilo dos vertebrados, denotando um caráter ancestral. De fato, é possível que moléculas precursoras dos hormônios tireoidianos tenham se organizado nos primórdios do planeta e contribuído para o desenvolvimento de funções biológicas desde o último ancestral unicelular comum, o LUCA¹[2].

O LUCA é uma aproximação teórica da primeira forma de vida celular ativa à 3.95 bilhões de anos, do qual derivou-se as bactérias, arqueias e eucariotos². Esse organismo primordial, possuía metabolismo anaeróbico autótrofo³ utilizando uma molécula precursora da acetilcoenzima A para fixar o abundante dióxido de carbono (CO₂) atmosférico e produzir energia (moléculas de adenosina trifosfato ou ATP). Na ausência de enzimas, essas reações ocorriam espontaneamente a partir dos elementos disponíveis na atmosfera e nos oceanos, dessa forma LUCA prosperou em correntes termais nas quais as altas temperaturas garantiam a efetividade das reações [3].

¹ Do inglês, Last Unicellular Common Ancestor.

² A posição desses táxons é fonte de grande discussão. Árvores filogenéticas colocam LUCA como precursor direto dos três táxons enquanto outras focam apenas na ancestralidade direta de bactérias e arqueias, tendo os eucariotos derivado das arqueias posteriormente na escala evolutiva. A capacidade desses organismos unicelulares transferirem genes lateralmente acrescenta mais uma camada de complexidade ao intuito de descobrir quais genes necessariamente vieram do ancestral comum [3].

³ Há argumentos na literatura defendendo o estilo de vida autótrofo e heterotrófico. Entretanto Weiss e colaboradores apresentam argumentos convincentes sobre o possível autotrofismo (3).

Além da obtenção de energia, o LUCA se ajustava ao ambiente. Ao ser extremamente adaptado à anaerobiose, o LUCA era sensível ao contato com oxigênio (O_2), dessa forma, este organismo gerou um gradiente de iodo reativo na sua região pericelular, protegendo seu conteúdo interno da oxidação. Posteriormente, a excessiva permeabilidade da membrana celular rudimentar permitiu a admissão do iodo reativo, por sua vez, esse novo componente intracelular permitiu a catalisação não enzimática da síntese de tirosina [2]. A tirosina é um aminoácido importante para o funcionamento da fotossíntese, mecanismo que utiliza a luz solar para fixar carbono e gerar energia [4,5], e sua disponibilidade pode ter sido central para a derivação deste processo biológico [2].

A fotossíntese derivou-se no Reino das bactérias mais especificamente nas cianobactérias, há 3.4 bilhões de anos⁴. Ao longo do tempo, a atividade desses organismos propiciou alterações profundas nas características do planeta. O oxigênio, subproduto da fotossíntese, acumulou-se na atmosfera acarretando diminuição nos níveis de metano e CO_2 , além de formar a camada de ozônio. Por fim, esses fatores propiciaram o resfriamento do planeta [6] e o carregamento de iodo para a atmosfera, gerando uma ciclagem global através das chuvas [2]. Nesse sentido, é importante observar que os primeiros registros de fotossíntese vegetal foram observados a 1.2 bilhões de anos [6], ou seja, após a estabilização da produção de tirosinas e o aumento da disponibilidade de iodo em ambiente terrestre.

⁴ Hipotetiza-se que o desenvolvimento da fotossíntese foi estabelecido inicialmente no Reino das bactérias e que a incorporação simbiótica de bactérias fotossintetizantes por células eucarióticas a derivação dos cloroplastos (6).

Dessa forma, expandiu-se a disponibilidade de iodotirosinas, precursoras dos hormônios tireoidianos, devido a reatividade espontânea entre iodo e tirosinas. Essas moléculas eram extremamente reativas e facilmente difundidas através da membrana celular rudimentar, tornando-se componentes ativos da sinalização celular e valiosas bioquimicamente. Essa sinalização foi essencial para a organização dos primeiros organismos multicelulares ancestrais, seu estabelecimento e conservação ainda é observado em animais e plantas [2].

A absorção de derivados do iodo é essencial para o crescimento e desenvolvimento das plantas. A presença de iodo orgânico, na forma dos precursores hormonais monoiodotirosina (MIT), diiodotirosina (DIT) e do próprio hormônio tireoidiano T3, foi constatada tanto em algas quanto em plantas superiores (na alface, por exemplo). Entretanto, são desconhecidos os processos de síntese e metabolismo desses compostos [7–10]. Além disso, é possível observar a conservação da sinalização dos hormônios tireoidianos através da resposta cruzada entre os animais e vegetais. Nesse sentido, demonstrou-se que o extrato de algumas plantas é capaz de estimular o receptor de hormônio tireoidiano beta (RHT β) em humanos [11], e o aporte exógeno (através da alimentação) de MIT e DIT é suficiente para desencadear processo de metamorfose em larvas de animais [12,13].

Nos animais, a responsividade as iodotironinas é observada em diversos grupos⁵. Nos filos⁶ *porífera* (esponjas-do-mar) e *cnidária* (águas-viva e corais), por exemplo, são bem descritas a síntese e armazenamento de iodotironinas, principalmente, MIT, DIT e

⁵ É importante ressaltar que os parágrafos abaixo descrevem o processo evolutivo de uma maneira linear, com o intuito de facilitar o entendimento do leitor. Entretanto, o processo de formação e especialização da sinalização dos hormônios tireoidianos podem ter ocorrido de maneira independente em diferentes grupos.

⁶ Filo é um nível de classificação taxonômica, encontrado abaixo de Reino e acima de Classe.

T4. Nestes animais, T4 induz o processo de diferenciação e reprodução assexuada para o desenvolvimento de formas livres em águas-viva, além disso provoca aumento na deposição de cálcio e crescimento de corais [14,15]. Esses efeitos, contudo, são provavelmente regulados por mecanismos não-gênicos do T4, pois não foram identificadas a presença de receptores de hormônio tireoidiano (RHT) ou homólogos no genoma desses animais [15]. Por sua vez, síntese e responsividade aos HTs e a presença de ortólogos de RHT é extremamente difundida nos diversos filos invertebrados de *Bilateria*⁷, nematódeos (vermes), moluscos (ostra, vieira), insetos (drosófila, barata), crustáceos (lagosta), equinodermos (ouriço-do-mar, bolacha-da-praia, estrela-do-mar) [2,14,15].

Entretanto, é no ramo dos cordados que identificamos a especialização de um órgão para a produção de HTs e a presença de RHTs conservados com grande impacto sobre o genoma. Nos cefalocordados (anfioxo), tanto as larvas quanto organismos adultos produzem HTs em um tecido chamado endóstilo, este tecido metaboliza T3 e T4 em 3,5,3'-ácido triiodotiroacético (TRIAC) que, ao interagir com os RHTs, induz a metamorfose dos animais [2,14,15]. Por outro lado, no grupo basal dos vertebrados chamado ciclostomados (lampreias), o endóstilo está presente na fase larval, sua atividade aumenta o aporte de HTs aos tecidos, induzindo a metamorfose da fase adulta e o desenvolvimento da glândula tireoide. Este novo órgão é mantido como componente de todos os organismos grupo dos vertebrados (peixes, aves, répteis, anfíbios, mamíferos) [2,15].

⁷ Agrupamento dos animais com simetria bilateral, em oposição a *Radiata* que apresentam simetria radial.

As primeiras hipóteses sobre o desenvolvimento da sinalização dos HTs propuseram que, as iodotironinas presentes nos animais basais e invertebrados eram oriundas inteiramente do aporte alimentar, fator crítico para o estabelecimento dos processos de metamorfose [14,16]. Entretanto, investigações atuais demonstram que esses organismos são capazes de produzir HTs [15], o que indica que o aporte alimentar era o fator limitante para atingir os níveis elevados de HT necessários para iniciar os processos de desenvolvimento. O surgimento da glândula tireoide nos vertebrados permitiu maior estabilidade na sinalização, reduzindo a dependência das iodotironinas provenientes da alimentação e das flutuações ambientais. Conjectura-se que a sinalização dos HTs permitiu amplo controle da regulação osmótica e adaptabilidade nos peixes, processo que desencadeou, primeiramente, a colonização dos corpos de água doce a partir dos oceanos e, posteriormente, o desenvolvimento do pulmão e regulação térmica, possibilitando à colonização do ambiente terrestre [2,13].

Por fim, no contexto do desenvolvimento humano, estudos sugerem que duas espécies do gênero *Homo* (*H. neandertalis* e *H. florencis*) sofriam os efeitos deletérios das flutuações patológicas dos HTs. Como consequência de seu modo de vida caçador-coletor, esses ancestrais humanos obtinham dieta pobre em iodo, o que prejudicava a síntese de HTs e causava severo hipotireoidismo. Esse quadro causava cretinismo, baixo desenvolvimento cerebral, rebaixamento mental, comprometimento do sistema imunológico e reprodutivo, e perda de função do músculo esquelético. Neste contexto, a espécie *Homo sapiens* apresentava maior capacidade de síntese de HTs, compatível com a dieta de baixo teor de iodo, característica que concedeu vantagem evolutiva e flexibilidade adaptativa à espécie [13]. Além disso, a formação em folículos da glândula

tireoide permite o armazenamento de iodo⁸ e tiroglobulinas, de forma que a sinalização hormonal não é comprometida por variações sazonais na ingestão de iodo [17].

Mesmo que muitas dessas hipóteses se enquadrem em um contexto amplo, com diversas explicações e outros mecanismos celulares e moleculares em curso, é pertinente ressaltar que a vida não seria como conhecemos hoje sem a participação das iodotironinas [2].

1.2. A glândula tireoide

1.2.1. Características anatômicas

A tireoide é a maior glândula estritamente endócrina do corpo humano [18], origina-se na quarta semana de gestação como uma projeção do tecido epitelial do assoalho da faringe na base da língua. Durante o desenvolvimento do trato digestório,⁹ este órgão se desloca à cavidade visceral do pescoço ao longo do desenvolvimento [19,20]. Após o nascimento, a glândula tireoide está localizada na base do pescoço, ao nível das vértebras cervical V e torácica I, em posição posterior aos músculos esteno-hióideo, esterno-tireóideo e omo-hióideo ocupando o espaço imediatamente anterior e lateral da traqueia. A glândula é composta por uma massa globular, em formato de H,

⁸ A glândula tireoide humana pode armazenar de 3 a 20 mg de iodo.

⁹ Após o nascimento o ponto de origem é marcado pelo forame cego da língua (19).

subdivida em dois lobos à direita e à esquerda¹⁰, conectados por um istmo na altura da segunda e terceira cartilagem da traqueia [18,19].

A extensa vascularização necessária para o estabelecimento das funções endócrinas da glândula tireoide é atendida principalmente por dois vasos, a artéria tireóidea superior e a artéria tireóidea inferior. A artéria tireóidea superior origina-se bilateralmente do primeiro ramo da artéria carótida externa, irrigando sobretudo a porção superior da glândula, já a artéria tireóidea inferior origina-se da artéria subclávia, irrigando principalmente a porção inferior da glândula tireoide. Entretanto, esses ramos inferiores e superiores bilaterais fazem extensas anastomoses no interior do tecido glandular, assegurando fluxo abundante e proporcionando potencial circulação colateral [18,19].

A drenagem do tecido ocorre por intermédio de três veias, a veia tireóidea superior que drena principalmente a área irrigada pela artéria tireóidea superior e as veias tireóideas média e inferior, que drenam o restante da tireoide. Por fim, as veias tireóideas superior e média desembocam na veia jugular interna e as tireóideas inferiores desembocam nas veias braquiocefálicas [19].

A inervação da glândula tireoide é derivada do sistema nervoso autônomo simpático. Ramificações dos gânglios cervicais superiores, médio e inferiores chegam ao tecido através dos plexos cardíaco e periarteriais tireóideos. Esses ramos são compostos por fibras vasomotoras, que controlam a constrição dos vasos sanguíneos presentes na

¹⁰ Aproximadamente metade da população possui uma variação anatômica com a presença do lobo piramidal. Nesta variação o tecido glandular se entende superiormente a partir do istmo (que pode ser incompleto ou ausente), podendo se inserir até o osso hioide (18).

glândula tireoide, o controle da secreção da glândula é feito hormonalmente pela hipófise, não possuindo componente secretomotor [18].

Por fim, ressalta-se que os aspectos anatômicos relativos à origem, localização e vascularização da glândula tireoide são semelhantes entre humanos e roedores (ratos e camundongos), entretanto, são notáveis as diferenças proporcionais entre as espécies. Em humanos a glândula tireoide tem cerca de 15-25 gramas¹¹ (g) de massa, com dimensões aproximadas de $5-6 \times 2-2.5 \times 2$ centímetros (cm); já nos roedores a massa varia entre 13-24 mg e 1,3-2,6 mg e dimensões de $7 \times 3 \times 3$ mm e $2 \times 1 \times 0,5$ mm, para ratos e camundongos, respectivamente [21].

1.2.2. Características Histológicas

O parênquima da glândula tireoide é formado por dois tipos de células, as células foliculares (também chamadas de “células principais”) e as células parafoliculares (também chamadas de “células C”) [20–22], sendo as últimas contribuintes com apenas 0.1% do conteúdo celular. Tanto a estrutura quanto origem histológica do tecido da glândula tireoide são semelhantes entre humanos e roedores (ratos e camundongos)[21].

As células foliculares são as produtoras dos hormônios tireoidianos, seu formato está relacionado ao nível de atividade, apresentando-se geralmente em formato cúbico, mas assumindo característica em escamas ou em colunas com a menor ou maior atividade, respectivamente [20–22]. Além disso, apresentam especializações que caracterizam as atividades de secreção e absorção, como por exemplo, a presença de

¹¹ A média de peso da glândula na população Humana decresceu discretamente até a atualidade, provavelmente devido a maior disponibilidade de iodo na alimentação (17).

microvilosidades em sua porção apical e a alta concentração de retículo endoplasmático rugoso em sua região basal [20].

A partir da 14^a semana de gestação, as células foliculares se organizam em uma estrutura circular na qual a face celular apical delimita um lúmen central, preenchido por uma solução gelatinosa chamada coloide e com o exterior abalizado pela face celular basal apoiada sobre a lâmina basal [20]. Essa estrutura circular chama-se folículo e compreende a menor unidade funcional da glândula tireoide. Neste tecido glandular, centenas de milhares de folículos são circundados por tecido conjuntivo, capilares sanguíneos e anastomoses que formam a matriz extra celular [20,22].

Por outro lado, as células parafoliculares, que produzem o hormônio calcitonina, localizam-se abaixo das células foliculares, apoiadas à lâmina basal, de forma que não possuem acesso ao lúmen[20,21]. Geralmente, as células parafoliculares apresentam maior presença do complexo de Golgi e menor densidade de retículo endoplasmático rugoso em comparação com as células foliculares. As células parafoliculares são incorporadas ao tecido da glândula tireoide durante a sétima semana de gestação a partir do último corpo branquial [20,21].

1.3. Hormônios Tireoidianos

1.3.1. Biossíntese dos hormônios tireoidianos T3 e T4

O iodo, juntamente com as tiroglobulinas, são os componentes básicos para a síntese dos hormônios tireoidianos nas células foliculares. Portanto, o consumo satisfatório de iodo é crucial para o funcionamento da glândula tireoide [20,23], uma vez

que o iodo consumido na alimentação é reduzido para iodeto, absorvido pela mucosa do estômago e do intestino delgado e disponibilizado na corrente sanguínea [17,24].

Oriundo da circulação, o iodeto é internalizado na região látero-basal das células foliculares por intermédio de proteínas cotransportadoras de sódio e iodo ATP-ase dependentes (*Na⁺/I⁻ symporters – NIS*), que ativamente bombeiam os íons para o citoplasma das células estabelecendo um transporte ativo secundário que gera uma concentração de aproximadamente quarenta vezes maior de iodeto no meio intracelular quando comparado com o sangue ou líquido extracelular (processo chamado de “*iodine trapping*”). Em seguida, os íons de iodo se difundem para a região apical das células, onde são transportados para o lúmen por intermédio de proteínas transportadoras de iodo e cloro (pendrinas). Ao iniciar sua difusão no coloide, ainda na região das microvilosidades apicais o iodeto é oxidado a iodo, sua forma mais ativa, na presença de peróxido de hidrogênio em uma reação catalisada pela atividade das peroxidases tireoidianas (“*thyroid peroxidase – TPO*”) [20,23–25].

Já as tiroglobulinas são homodímeros de glicoproteínas com aproximadamente 130 resíduos de tirosina. Essas proteínas são produzidas no retículo endoplasmático rugoso das células foliculares, posteriormente glicosiladas e empacotadas no complexo de Golgi e finalmente secretadas para o lúmen como componente do coloide [20,24,25]. Com a presença dos componentes individuais, a biossíntese dos hormônios tireoidianos segue os passos abaixo:

1. Iodação da tiroglobulina ou organificação do iodo: Na região das microvilosidades, os átomos de iodo são adicionados em unidade ou duplas aos resíduos de tirosina nas tiroglobulinas, formando MITs and DITs, respectivamente.

Dentre os 130 resíduos de tirosina presentes, apenas 25-30 deles são iodinados, essas reações são catalisadas pelas TPOs [20,23–25].

2. Formação dos hormônios tireoidianos: Os hormônios tireoidianos são formados pelo acoplamento oxidativo de pares de MITs e DITs dentro das tiroglobulinas. O acoplamento de duas DITs forma uma molécula de T4, já a ligação de uma MIT e uma DIT origina uma molécula de T3. Geralmente, cada tiroglobulina contém de 3-4 moléculas de T4, enquanto apenas 1/5 das tiroglobulinas apresentam uma molécula de T3 [20,23–25].
3. Reabsorção do coloide e secreção hormonal: As células foliculares absorvem a tiroglobulina por endocitose mediada por receptores, as vesículas internalizadas são transportadas para endossomos iniciais, que se maturam em lisossomos, fundindo-se e originando os corpos de reabsorção de coloide. Nessas estruturas, as tiroglobulinas são degradadas em aminoácidos e carboidratos pela ação de proteases catepsina-D e D-like Thiol proteinases, liberando seu conteúdo de T3, T4, DIT e MIT. As iodotirosinas DIT e MIT são rapidamente deiodinadas (com o auxílio de isoenzimas deiodinaseses Dhal1 e Dhal1b) e o iodeto reciclado [20,24,25].
4. Liberação de T3 e T4 – Por fim as células foliculares secretam os hormônios para a circulação em uma proporção de 20:1 de T4 para T3. Ao serem secretados, a maior parte dos hormônios é imediatamente ligada a proteínas plasmáticas globulina ligante de tiroxina (TBG) e transtirretina (também chamada de thyroxine-binding prealbumin - TBPA), sendo a ligação do T4 mais forte à TGB e a ligação do T3 à transtirretina e uma parte menor se liga à albumina, deixando apenas 1%

¹² dos hormônios livres para exercer suas funções biológicas. O controle do *feedback* hormonal e liberação do hormônio estimulante da tireoide (TSH) ocorre por intermédio dos hormônios tireoidianos livres, sendo que variações hormonais totais podem não necessariamente se correlacionar à proporção de hormônios ativos, como por exemplo na gravidez, onde a liberação de T4 aumenta, mas o T4 livre permanece normal [20,23]. Após a liberação na corrente sanguínea, a meia vida dos hormônios tireoidianos nos humanos é de aproximadamente 5-9 dias para o T4 e 1 dia para o T3, enquanto para ratos varia de 12-24 horas e 6 horas, respectivamente. Esse fenômeno pode estar relacionado ao fato de que os hormônios dos roedores encontram-se principalmente em sua forma livre, o que facilita seu processo de metabolismo e excreção [17,21].

1.3.2. Controle da secreção hormonal

Tanto a biossíntese quanto a liberação dos hormônios tireoidianos são controladas pelos hormônios TSH e liberador de tireotrofina¹³ (THR), secretados respectivamente pela pituitária anterior e hipotálamo, em um mecanismo regulatório envolvendo o eixo hipotálamo-pituitária-tireoide (HPT) [17,23,26]. Baixos níveis de T3 ou T4 estimulam a produção de THR no hipotálamo, que por sua vez, flui pela veia porta hipofiseal para a pituitária anterior estimulando os tireotrofos a produzirem TSH. O TSH então estimula praticamente todos os aspectos da atividade das células foliculares (sequestro de iodo, síntese hormonal, secreção e crescimento das células foliculares).

¹² Alguns autores citam diferentes proporções, como por exemplo: 0,04% de T4 e 0,4% de T3 (23).

¹³ Também chamado de tiro liberina.

Níveis altos de hormônios tireoidianos, principalmente T3¹⁴, inibem a liberação de THR e TSH em um *feedback* negativo [23,26]. Além disso, o controle da secreção pode ser realizado pelos elementos de autorregulação do iodo, como por exemplo excesso de iodo e lítio [23] e da sinalização da dopamina [17]. Esses mecanismos funcionam de maneira similar nos roedores [21,25].

Além disto, destaca-se que estímulos físicos e características ambientais influenciam os níveis internos dos hormônios tireoidianos. Por exemplo, no hemisfério Norte observa-se um aumento de aproximadamente 15% nos níveis de TSH e 5% nos níveis de T3 durante o inverno com redução similar durante o verão. Nesse sentido, regiões com frio extremo (-20°C/-24°C) induzem redução de aproximadamente 7% nos níveis de T3 e T4, mesmo com um aumento de 30% nos níveis de TSH. Com relação aos estímulos físicos, nota-se que o jejum e o envelhecimento induzem redução de TSH e T3, enquanto privação de sono afeta principalmente nos níveis de TSH [17].

1.3.3. Controle da sinalização hormonal nos tecidos-alvo

Visto o discutido nos aspectos evolutivos das iodotirosinas, não é surpresa verificar que os hormônios tireoidianos potencialmente regulam todas as células de um organismo. Seus efeitos passam pelo desenvolvimento e maturação de órgãos até manutenção tecidual e resposta a estímulos ambientais. Assim, torna-se claro que os níveis hormonais circulantes não permitem regulações teciduais e temporais específicas para cada tipo celular concomitantemente, de forma que a presença e proporção de T3 e T4 na corrente sanguínea é relativamente constante e, o ajuste específico da

¹⁴ Outros autores apontam que essa inibição ocorre principalmente em resposta ao T4 circulante (17).

intensidade da regulação hormonal ocorre de maneira mais ampla nos tecidos-alvo pelo controle de transportadores intracelulares dos hormônios (MCT8, MCT10, OATP1 e LAT) e pela atividade das desidases [27–29].

As desidases fazem parte do grupo das seleno proteínas com capacidade catalítica sobre os anéis aromáticos dos hormônios tireoidianos, resultando na diminuição do número de iodos na cadeia [28,29]. As desidases do tipo 1¹⁵ e 2 (Dio1 e Dio2, respectivamente), sendo que esta última apresenta maior afinidade ao T4, podem remover o anel exterior de T4, resultando em moléculas de T3, o que incrementa a sinalização hormonal devido ao maior papel biológico de T3. Já as desidases do tipo 3 (Dio 3), podem desidar T3 em T2 reduzindo a sinalização hormonal [29].

1.3.4. Mecanismos de Ação dos Hormônios Tireoidianos

Após sua admissão nas células, os hormônios tireoidianos exercem sua ação de duas formas principais envolvendo ou não o controle da expressão gênica, conhecidas respectivamente como ações genômicas e não genômicas. Em ambos os casos, os efeitos dos hormônios tireoidianos são mediados pelos receptores dos hormônios tireoidianos (RHT). Os RHTs fazem parte da família de receptores nucleares e suas isoformas alfa e beta são as principais mediadoras das ações genômicas do T3, enquanto formas truncadas de RHT α medeiam ações não genômicas [27,30,31].

Com relação à regulação da transcrição gênica pelos HTs, na ausência ou em níveis baixos do ligante, os RHTs estão associados a sequências específicas no DNA,

¹⁵ Quando a desidase do tipo 1 cliva o anel interior de T4 o resultado é T3 reverso, sem ação biológica descrita. As desidases do tipo 1 são pouco conhecidas, em humanos elas estão relacionadas à produção de níveis altos de T3 no soro durante o hipertireoidismo (29).

os elementos responsivos aos hormônios tireoidianos (THRE). Essa ligação pode ocorrer como monômeros, homodímeros ou heterodímeros que recrutam proteínas corepressoras que podem inibir ou ativar a transcrição basal de genes. Na presença de T3, os RHTs alteram sua conformação, acarretando na liberação dos corepressores e no assentamento de coativadores, que induzirão a transcrição dos genes positivamente regulados e a inibição dos genes negativamente regulados [30,32–34]. Além disso, é importante ressaltar que diferentes autores demonstram que parte dos genes responsivos aos HTs são associados aos RHTs apenas após sua ligação com o T3, indicando migração nuclear. Outro fator curioso é a atividade paradoxal dos corepressores e coativadores, que geram inibição ou ativação transcricional dependente de HTs de formas distintas nos diferentes tecidos e tipos celulares [27].

Enquanto os processos que envolvem a transcrição gênica podem levar várias horas até culminarem na modulação do conteúdo proteico, observa-se que os THs regulam vias celulares minutos após sua administração [35,36]. Esses processos não genômicos são mediados por integrinas e formas truncadas de TR α na membrana plasmática, que induzem a fosforilação de vias e ativação de quinases na presença de THs [35,37,38].

1.3.5. Desbalanço dos níveis hormonais

O extenso desenvolvimento ao longo do processo evolutivo e a ampla atividade dos hormônios tireoidianos no controle dos mecanismos celulares são refletidos na influência dos níveis hormonais ao longo da vida dos organismos. Durante o desenvolvimento, os HTs controlam o metabolismo e diferenciação de vários tecidos [39–

41]. Neste período, os HTs induzem o desenvolvimento dos somitos e dermomiótomo nas linhagens musculares, controlam a proliferação e migração de neurônios, e são essenciais para a maturação dos pulmões, do fígado e dos músculos esqueléticos [34,40–43]. Desta forma, distúrbios na sinalização do T3 podem causar graves patologias, tais como cretinismo, surdez, deficiências cognitivas, ossificação prematura e insuficiência cardíaca [39,41,44,45].

Após o nascimento, a sinalização do T3 é necessária para a homeostase do indivíduo e, alterações nos níveis fisiológicos do hormônio desencadeiam modificações marcantes nos tecidos alvo [46]. No tecido cardíaco, o hipertireoidismo inicialmente altera a velocidade e força da contração de maneira benéfica, mas culmina em hipertrofia do miocárdio, desarranjo sarcomérico e insuficiência cardíaca [46]. Já no músculo esquelético, o hipertireoidismo estabelece diminuição da força e resistência muscular, assim como degeneração das fibras musculares com redução na área de secção transversal e proteólise severa [43,47–49].

1.4. Músculo Esquelético

1.4.1. Processo Evolutivo

De forma semelhante aos hormônios tireoidianos, os primórdios do tecido muscular esquelético se estabelecem nos ramos basais do desenvolvimento evolutivo, com a marcante presença do movimento nos seres vivos. Em um nível microscópico é possível identificar movimentos intracelulares (alinhamento de organelas e movimentação cromossômica) [50–52] e celulares (produzidos por cílios ou flagelos como nas plânulas e protozoários, respectivamente). Posteriormente, em organismos

complexos, observa-se a movimentação das plantas, essenciais na busca de nutrientes e na dispersão de sementes que marcaram a vanguarda na colonização do ambiente terrestre.

No ramo dos animais, no grupo dos bilaterados, originou-se um aparato contrátil especializado na geração de movimentos rápidos e amplos. Esta apomorfia contribuiu para a sofisticação da interação dos organismos com o ecossistema, diversificando suas estratégias de caça e fuga de predadores [51–53]. Finalmente, nos vertebrados, as grandes células contráteis, chamadas de fibras, formam o tecido muscular esquelético que é especializado na geração de tensão por contração coordenada.

Nos humanos, o tecido muscular esquelético corresponde a aproximadamente 40% da massa corporal [54] e assume papéis centrais na homeostase do organismo. Nesse sentido o músculo esquelético está associado a regulação do metabolismo da glicose, participa da produção de calor e do retorno venoso, e é componente crucial no processo de ventilação e reserva nutricional [55–57]. Além disso, o músculo esquelético aprimorou-se em um tecido extremamente plástico, capaz de alterar suas características fenotípicas em resposta a alterações ambientais, garantindo vantagem na obtenção de alimentos e fuga de predadores. De tal forma que estas especializações foram um fator crucial no desenvolvimento da cognição e comportamentos sociais em humanos [52,53,58].

1.4.2. Plasticidade Muscular Esquelética

Como citado anteriormente, o músculo esquelético responde às demandas ambientais acomodando seu fenótipo ao novo equilíbrio fisiológico exigido por alterações

no estresse mecânico, aporte nutricional e sinalização hormonal [57]. Em resposta ao aumento da demanda mecânica e indução anabólica por ação hormonal, por exemplo, há o característico quadro de hipertrofia, com aumento da síntese de proteínas e maior área das fibras musculares que culmina no incremento de massa e força [59–61]. Por outro lado, diminuição da demanda muscular, restrição nutricional e ação anormal dos hormônios tireoidianos desencadeia elevada degradação de proteínas, perda de sarcômeros em série e organelas, culminando em menor área na secção transversal das fibras e perda de força muscular [62,63].

Apesar dos processos de atrofia e hipertrofia serem fenômenos bem estabelecidos, a forma que os mecanismos intracelulares se modulam e interagem ainda necessitam de esclarecimentos. Nesse sentido, o processo envolvendo o equilíbrio entre síntese e degradação proteica possui papel central nos processos de regulação da massa muscular. De maneira clássica, na hipertrofia, a síntese de proteínas prevalece em relação aos processos de degradação [64]. Por outro lado, nos quadros de atrofia, foi bem estabelecido que o aumento da degradação se sobressai à síntese basal de proteínas [65]. Contudo, a regulação do *turnover* de proteínas nos diferentes modelos de atrofia e hipertrofia demonstrou-se mais complexa, uma vez que as vias de síntese e degradação são moduladas de forma diferente. Por exemplo, a via de indução de síntese proteica encontra-se ativada em condições sarcopenicas. Além disso, o regulador negativo da massa muscular, miostatina, está relacionada à indução de condições atroficas ou hipertróficas de forma condicionada a quais vias *downstream* estão ativadas [66–68].

Os mecanismos moleculares que participam do *turnover* de proteínas foram extensivamente investigados e, são agora apreciados como vias de sinalização distintas

que regulam a massa muscular. Por exemplo, a sinalização anabólica para a síntese de proteínas é associada as via do IGF1-PI3K-AKT-mTOR [69], óxido nítrico [70], SRF [71], e β 2-adrenoceptores [72]. Por outro lado, a inibição da síntese proteica pode ser relacionada à via da miostatina [73] e a degradação proteica inclui os processos de autofagia, calpaínas [74] e do sistema ubiquitina proteassoma.

1.4.3. Vias intracelulares de Controle de Massa

A proteína mTOR é o componente central da atividade do complexo regulatório da síntese de proteínas, foi inicialmente identificada por grupos distintos que buscavam os mecanismos mediadores da atividade antiploriferativa da rapamicina [75,76]. Posteriormente, estabeleceu-se que a mTOR é conservada entre os seres vivos, controlando diferentes mecanismos celulares como crescimento, diferenciação, autofagia, sobrevivência e metabolismo em resposta a diferentes tipos de estímulo, entre os mais conhecidos como a resposta ao IGF-1 e a disponibilidade de aminoácidos através da via RAG [76].

Para exercer a resposta adequada, a mTOR, que é uma proteína quinase, funciona como a porção catalítica do complexo mTORC1, formado com as proteínas regulatórias RPTOR, PRAS40, DEPTOR e MLST8 [76,77]. O complexo então, controla a síntese proteica ao ativar por fosforilação P70S6K que, por sua vez, exerce controle da atividade ribossomal ao fosforilar o S6, componente da porção ribossomal 40S. Além disso, mTORC1 fosforila 4EBP1, enfraquecendo sua ligação com o fator transcricional EIF4 e assim, aumentando a tradução [76–78].

Por outro lado, a regulação negativa da atividade de mTORC1 está relacionada a via da miostatina [68,79–81]. A sinalização canônica dessa via inicia-se com sua ligação ao receptor de membrana ActRIIB, que desencadeia a fosforilação de SMADs, que migram para o núcleo e induzem ou inibem a transcrição gênica. Nesse sentido, são bem identificados os efeitos inibitórios da via canônica da miostatina sobre a atividade dos microRNAs 486 e 29, o que aumenta a atividade de PTEN e reduz atividade de Akt que, por sua vez, diminui a sinalização para via de síntese mTOR ao mesmo tempo que induz a degradação proteica ao aumentar transcrição dos genes atroficos Atrogin-1 e MuRF-1, via FoxO ou independentemente via NFκB [79,81–83].

Atrogin-1 e MuRF-1 são ubiquitina ligases, componentes do sistema proteolítico ubiquitina proteassoma. Esse sistema é o principal responsável pela degradação proteica no músculo esquelético e está implicado em diferentes processos atroficos [84–88]. Nesse sistema, as proteínas são marcadas para degradação através do processo de ubiquitinação. Primeiramente, a ubiquitina é ativada pela atividade das proteínas ativadoras de ubiquitina (E1), e então direcionada pelas proteínas carreadoras de ubiquitina (E2), para então ser conjugada às proteínas alvo pelas proteínas ubiquitina-ligases (E3) e degradadas no complexo 26S do proteassoma [89].

2 Objetivos

O objetivo deste trabalho foi identificar novos alvos de regulação do hormônio tireoidiano T3 e explorar sua função no controle da massa muscular esquelética.

2.1. *Objetivos específicos*

Os objetivos específicos estão divididos nas duas publicações relacionadas no corpo deste trabalho.

1. “Thyroid hormone upregulates MDM2 in rat type I fiber: Implications for skeletal muscle mass regulation”:
 - Investigar o padrão global de expressão de componentes das vias proteolíticas regulados por T3 visando selecionar um novo alvo de interesse;
 - Caracterizar a responsividade do alvo de interesse ao hormônio tireoidiano T3 *in vivo* e *ex vivo*;
 - Explorar a relação do alvo selecionado e o trofismo muscular.
2. “Rptor inhibition is essential for T3-induced skeletal muscle atrophy independently of mTORC1”:
 - Investigar o padrão global de expressão de componentes da via Akt/mTOR regulados por T3 visando selecionar um novo alvo de interesse;
 - Caracterizar a responsividade do alvo de interesse ao hormônio tireoidiano T3 *in vivo* e *ex vivo*;
 - Explorar a relação do alvo selecionado e o trofismo muscular.

3 RESULTADOS

3.1. Artigo publicado: “Thyroid hormone upregulates MDM2 in rat type I fiber: Implications for skeletal muscle mass regulation”

Received: 25 April 2017 | Revised: 24 October 2017 | Accepted: 22 November 2017

DOI: 10.1111/apha.13003

ORIGINAL ARTICLE

ACTA PHYSIOLOGICA

Thyroid hormone upregulates MDM2 in rat type I fibre: Implications for skeletal muscle mass regulation

G. V. Ramos | A. Cruz  | W. J. Silva | A. Rozanski | I. L. Baptista | J. G. Silvestre | A. S. Moriscot

Department of Anatomy, Institute of Biomedical Sciences, University of Sao Paulo, Sao Paulo, Brazil

Correspondence

A. S. Moriscot, Department of Anatomy, Institute of Biomedical Sciences, University of São Paulo, São Paulo, Brazil.
Email: moriscot@usp.br

Funding information

This work was supported by the Sao Paulo Research Foundation (FAPESP) fellowships #2010/50321-0, #2012/22488-2, #2012/13315-7, #2012/13071-0, #2012/22488-4, #2017/09398-8, and by the Research Grant 2015/04090-0. This work was also supported by the Brazilian National Research Foundation CNPq grant #201123/2010-1.

Abstract

Aim: Based upon a microarray assay, we have identified that triiodothyronine (T3) upregulates MDM2 gene expression in the rat skeletal muscle. As MDM2 protein is an E3 ligase, we hypothesized that this enzyme could play a role in T3 effects on skeletal muscle mass control.

Methods: To test our hypothesis, male rats (2 months old) were randomly assigned into the following groups: intact controls, treated with 20 physiological doses of T3 for 0.5, 1 and 7 days, or with 5, 20 and 50 physiological doses of T3 for 7 days. For in vitro experiments, myotubes and C2C12 cells were treated with T3 for 3 days.

Results: After validation of the microarray finding throughout RT-PCR and confirmation that T3 induces increases in MDM2 protein expression in a dose-dependent manner, we observed that MDM2 was upregulated by T3 exclusively in fibre type I. Moreover, detailed histological evaluation showed that MDM2 over-expression distributes punctiformly along the cross section of the fibre and also inside nuclei. MDM2 colocalizes with PAX7 in control muscle and T3 downregulates this myogenic factor. Pharmacological inhibition of MDM2 in cultured myotubes caused a severe decrease in their diameter (~35%, $P < .001$ vs Control), enhancing the effect of T3 (from ~12% to ~35%, $P < .001$) alone upon myotube diameter and mRNA levels of atrogenes. Finally, we observed that FOXO3 (MDM2 target) is kept outside the nucleus under T3 stimulation.

Conclusion: Our results indicate that MDM2 might be involved in the trophic effects of T3 in skeletal muscle.

KEYWORDS

atrophy, E3 Ligase, MDM2, skeletal muscle, T3

1 | INTRODUCTION

T3 is a key hormone broadly involved in many biological processes, including development, differentiation and metabolism. It is well known that hypothyroidism can lead to

developmental malformations including delayed growth, abnormal neurogenesis, deafness and cardiac defects.¹ The importance of T3 is also well recognized by its conserved expression from amphioxus to humans.²

At the molecular level, T3 is well known to act as an activator of the receptors TR α and TR β . These receptors are expressed in different tissues in the postnatal phase and

Ramos and Cruz equally contributed to this study.

Acta Physiologica. 2018;222:e13003.
<https://doi.org/10.1111/apha.13003>

wileyonlinelibrary.com/journal/apha

© 2017 Scandinavian Physiological Society. | 1 of 15
Published by John Wiley & Sons Ltd

3.1.1. Introduction

T3 is a key hormone broadly involved in many biological processes, including development, differentiation, and metabolism. It is well known that hypothyroidism can lead to developmental malformations including delayed growth, neurogenesis, deafness, and cardiac defects.¹ The importance of T3 is also well recognized by its conserved expression in primitive organisms such as amphioxus to humans.²

At the molecular level, T3 is well known to act as an activator of the receptors TR α and TR β . These receptors are expressed in different tissues in the postnatal phase and are associated with specific DNA sequences denominated THREs (Thyroid Hormone Responsive Element), located in target genes. These receptors can form homodimers or heterodimers with partners such as RAR, RXR and VDR. When the complex T3-TR is formed, transcriptional modulation of the target gene occurs, a mechanism that mediates most of the biological effects of the hormone and is known as genomic action. More recently, non-genomic effects mediated by T3 in the plasma membrane, cytoplasm and mitochondria have been well described.³ Furthermore, T3 signaling is modulated by plasma membrane selective transport, interactions of TR with co-repressors and co-activators, cross-talk with other intracellular pathways and by the configuration of the THREs. Finally, levels of T3 also can be regulated by deiodinases.^{1,4}

An interesting aspect of T3 action is its dual effect in many systems: for example, elevated levels of this hormone can increase lipogenesis and lipolysis in both white and brown fat tissue.⁵ In bone tissue T3 can simultaneously increase osteoblastic and osteoclastic activity.⁶ In skeletal muscle supra-physiological levels of T3 can increase expression of fast twitch myosin heavy chain proteins and simultaneously increase

mitochondrial content and myoglobin expression, leading to skeletal muscle fibers that have increased fast twitch power and also increased aerobic capacity.⁷ Regarding skeletal muscle mass control, T3 is well described to increase protein breakdown.^{8,9} On the other hand, it has been suggested that T3 can also activate protein synthesis pathways.¹⁰ The net output of these two opposing forces results in a sarcopenic status. The precise molecular players in these two effects (catabolic vs anabolic) of T3 are not well understood and their identification and characterization can unravel new targets for therapeutic strategies emphasizing spared mass.

Previous observations have shown that high levels of T3 stimulates the ubiquitin proteasome-dependent protein breakdown in skeletal muscle^{11,12}, which is considered to be the main pathway of proteolysis of myofibrillar proteins in skeletal muscle.¹³ In this system, E3 ligases ubiquitinate target proteins that will be directed and degraded at the 26S proteasome. F-box protein 32 (MAFbx/Atrogin-1) and tripartite motif containing 63 (muscle RING Finger 1/MuRF1) are two E3 ligases abundantly expressed in skeletal muscles and have been directly implicated in muscle wasting in several catabolic conditions, therefore they were named as atrogenes.¹⁴⁻¹⁶ On the other hand, it is unlikely that these two E3 ligases can account for all the massive ubiquitination that occurs under atrophic conditions, therefore it is possible that additional E3 ligases play a role in skeletal muscle mass control. Accordingly, new E3 ligases need to be identified and explored to deepen the understanding on the effects of T3 upon skeletal muscle.

In the present study, we have used a microarray approach aiming to identify novel E3 ligases responsive to thyroid hormone. Out of the E3 ligases identified, MDM2 caught our attention because of reproducibility and levels of responsiveness to T3. MDM2 is an oncogene overexpressed in several types of human sarcomas. Oliner and colleagues¹⁷

have shown amplification of MDM2 in approximately 30% of osteosarcomas and soft tissue tumors. Previous observations have evidenced that MDM2 speeds the tumor cells growth throughout interactions with several cell cycle regulatory proteins, including P53 a key cell cycle restrainer. Under physiological conditions, MDM2 plays a crucial role for cell survival by keeping P53 appropriated repressed into the cell. This regulatory mechanism is important because increased P53 levels can cause cell cycle arrest and apoptosis.^{18,19}

In this study we have identified and characterized MDM2 gene responsiveness to T3 in skeletal muscle, determining expression levels and tissue/cellular localization. Furthermore, we have shown *in-vitro* that MDM2 is essential for myotube diameter maintenance. These data emphasizes that in addition to activating proteolytic pathways, T3 might also involve in contention of proteolysis by increasing MDM2 expression.

3.1.2. Results

3.1.2.1. Effect of T3 on body, heart, and skeletal muscle weights and on serum T4 levels

Our first step was to confirm the recognized effects of supra physiological doses of T3 upon body, heart and skeletal muscle weight and serum T4 levels. We observed no significant differences in body weight among all groups. On the other hand, heart weight and heart weight/naso-tail length ratio were significantly increased after 7 days of treatment with T3 (~11.5% and ~11.8% higher than control respectively, $p < 0.05$, Table 1). Accordingly, soleus muscle weight and weight/naso-tail length ratio significantly decreased (~11.4% and ~13.5% lower than control respectively, $p < 0.05$, Table 1) at 7 days of treatment with T3. As expected, treatment with T3 decreased T4 plasma levels (~90.8% lower than Control, $p < 0.05$, Table 1).

Table 1 – General Data of Serum Hormone Levels, Body Weight (BW), Naso-Tail (NT), Heart Weight (HW), Muscle Weight (MW) and HW/NT, MW/NT ratios of animals treated with 20 physiological doses of T3.

Groups	BW (g) (n=8)	NT (cm) (n=8)	T4 (nmol/L) (n=8)	HW (mg) (n=8)	Soleus MW (mg) (n=8)	HW/NT(mg/cm) (n=8)	MW/NT(mg/cm) (n=8)
Control	246.33 ± 24.11	21.09 ± 0.46	44.23 ± 13.59	851.00 ± 48.18	89.00 ± 8.12	40.34 ± 1.68	4.22 ± 0.33
T3-0.5 days	218.35 ± 7.79	20.68 ± 0.79	33.24 ± 10.25	803.13 ± 39.72	80.31 ± 6.31	38.89 ± 2.24	3.88 ± 0.22
T3 -1 day	217.89 ± 19.08	20.21 ± 0.57*	27.89 ± 9.34*	775.50 ± 35.58	81.69 ± 6.98	38.40 ± 2.11	4.01 ± 0.32
T3 -7 days	228.08 ± 14.25	21.06 ± 0.50	4.05 ± 0.54*	949.38 ± 84.42*	78.81 ± 6.15*	45.12 ± 4.49*	3.65 ± 0.45*

Values expressed as mean ± SD.
* p < 0.05 vs. Control

3.1.2.2. Gene Expression Level of E3-ligases by Microarray and RT-PCR

By using the microarray approach, it was possible to simultaneously analyze 425 genes corresponding to proteolytic pathways (GO: Protein catabolism process, ubiquitination and proteolysis). Out of those genes, 54% (233 genes) were regulated by T3 (Figure 1a) and interestingly, out of those, 185 genes belonged to the ubiquitin-proteasome pathway category (Figure 1a). The majority of the T3 responsive genes in the ubiquitin-proteasome category corresponded to E3 ligases (166 genes) (Figure 1a). The responsiveness of E3 ligases that presented elevated expression at all experimental time points is shown in figure 1B. Among T3 responsive E3 ligases, MDM2 caught our attention because of the similarity of response comparing to MuRF1 and also because of high gross basal expression (~1500, data not shown), in contrast to the other top responsive genes (FBXO45:~7, ASB3:~130, BIRC3:~180, KLHL2:~140, data not shown). Therefore we decided to focus the investigation on MDM2. The up regulation of MDM2 to T3 was validated by RT-PCR (Figure 1c). Similarly to the microarray assay, MDM2 showed up-regulation after 12 hours onset of T3 treatment and lasted up to 7 days. For comparison purposes, the responsiveness of two classical E3 ligases were measured: MAFbx/Atrogin-1 and MuRF1 in skeletal muscle. As expected those E3 were up-regulated by T3 (Figure 1c).

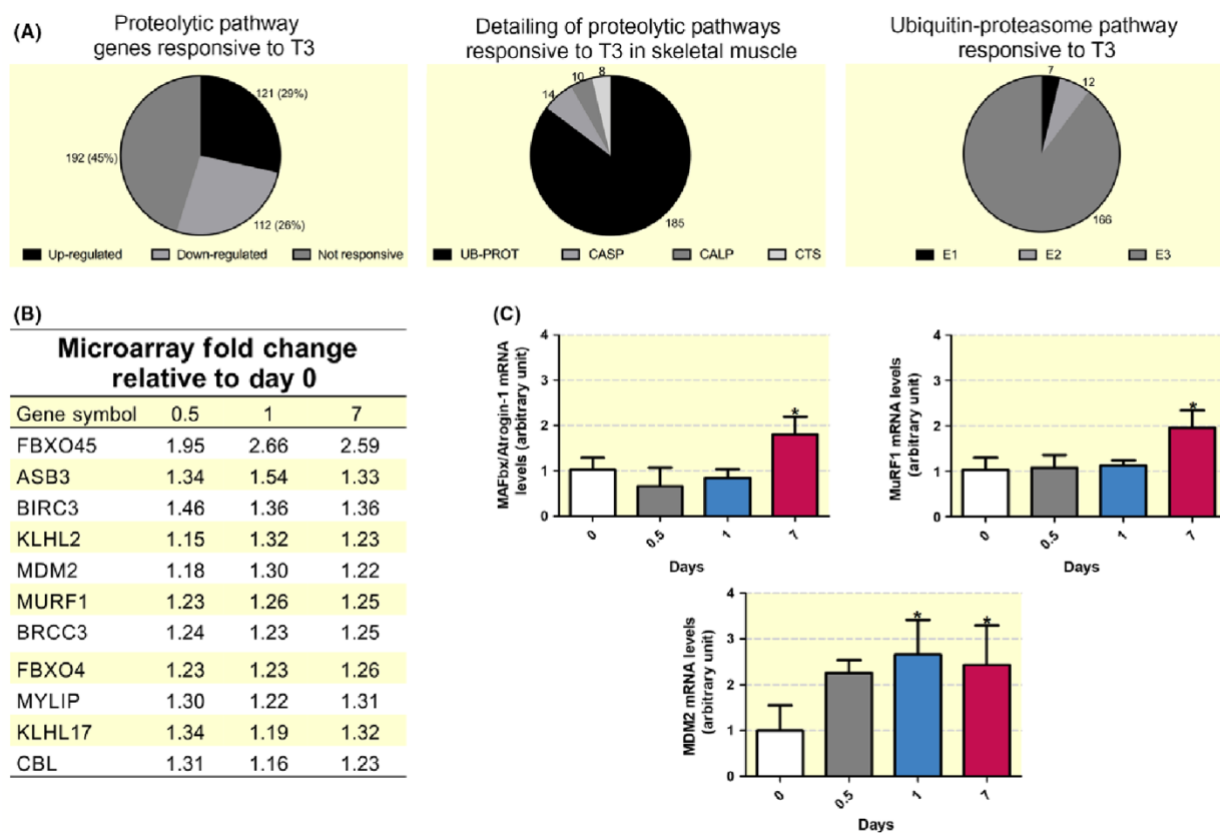


Figure 1: Microarray based global gene expression analysis of proteolytic pathways responsive to T3 in the soleus muscle. (a) Proteolysis overall gene expression responsiveness to T3; categories considered were ubiquitin-proteasome, calpains, caspases and cathepsins. (b) Fold change in mRNA levels of responsive E3 ligases after 0.5, 1 and 7 days of treatment with T3 (fold Change of > 1.15 relative to the control group was considered responsive) (c) mRNA levels of Mafbx/Atrogin-1, MuRF1 and MDM2 after treatment with T3 for 0.5, 1 and 7 days determined by RT-PCR. Values were expressed as means \pm SD. * p <0.05 vs control group.

3.1.2.3. MDM2 expression levels in vivo and in vitro

In agreement with mRNA levels, we found that T3 increased MDM2 protein levels at 7 days of treatment (Figure 2a, p <0.05). Next we evaluated the effect of increasing doses of T3 upon MDM2 gene and protein expression. MDM2 mRNA expression was increased by 20 physiological doses of T3 (2.4 fold, p <0.05) and non-responsive at 5 and 50 physiological doses of T3 (Figure 2b). These results were also noticed at the protein level, except at 50 physiological doses where we observed lower levels of MDM2 protein

when compared to control (Figure 2c; $p < 0.05$). In a primary myoblast culture differentiated to myotubes we observed that MDM2 is also up-regulated by T3 (~1.8 fold, Figure 2d, $p < 0.05$). Similar response can be observed at a C2C12 culture differentiated to myotubes treated with T3 for 48 hours (~1.4 fold, Figure 2d, $p < 0.05$).

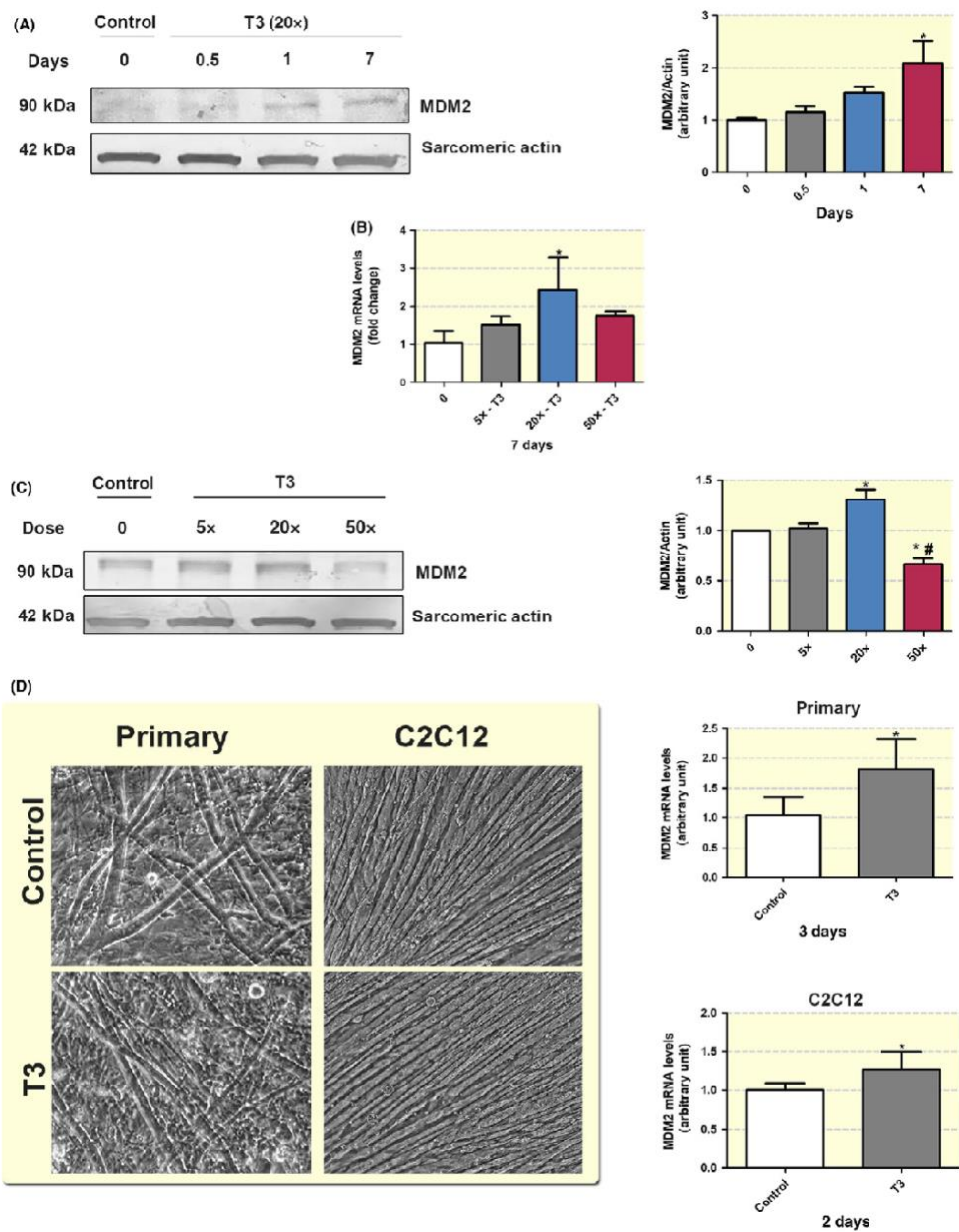


Figure 2: T3 increases MDM2 expression in vivo and in vitro. (a) MDM2 protein expression in soleus muscle of T3 (20 physiological doses) treated animals for 0.5, 1 and 7 days. (b) MDM2 mRNA expression level in soleus muscle after treatment with different doses T3 (5, 20 and 50 physiological doses) for 7 days. (c) Soleus muscle protein expression levels of MDM2 in animals treated with different doses of T3 (5, 20 and

50 physiological doses) for 7 days. (d) Photomicrographs showing general morphological features of myotube cultures originated either from primary myoblasts or from C2C12 cells. Those cultures were treated with T3(10-8M) for 3 and 2 days respectively and mRNA level of MDM2 determined. Values were expressed as means \pm SD. * p <0.05 vs control group; # p <0.05 vs T3 50X group.

3.1.2.4. MDM2 gene expression in different atrophy models

Since up to date no study has addressed MDM2 expression in different atrophy models, we decided to evaluate mRNA levels of MDM2 in animals submitted to immobilization, dexamethasone and starvation (Figure 3). Immobilization induced a modest, nonetheless significant, increase in MDM2 mRNA levels 3 days after immobilization (Figure 3a, 1.5 fold, p <0.05). Starvation, however, induced a robust increase in MDM2 mRNA levels (Figure 3b, 3.1 fold, p <0.05). Interestingly, we did not observe alterations in MDM2 mRNA levels in the animals treated by dexamethasone when compared to control group (Figure 3c).

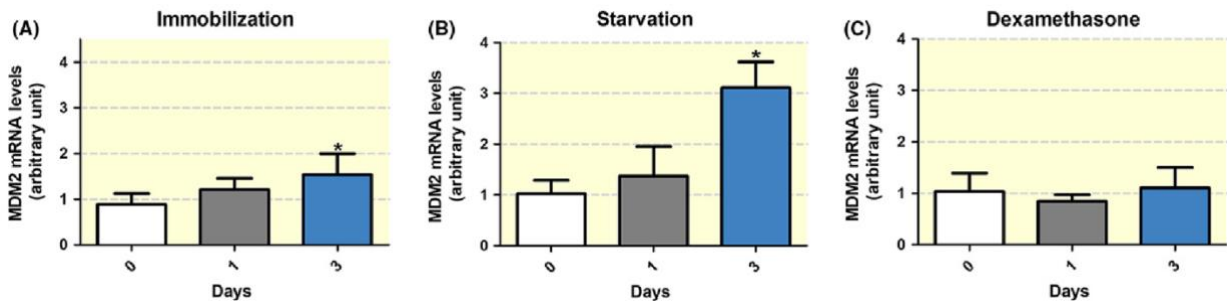


Figure 3: mRNA expression levels of MDM2 in soleus muscle in different models of atrophy. (a) Immobilization; (b) Starvation and (c) Dexamethasone (1200mg/Kg). Values were expressed as mean \pm SD. * p <0.05 vs control group.

3.1.2.5. MDM2 is up regulated by T3 in type I fibers

Next, we decided to address the tissue location of MDM2 in skeletal muscle of animals treated with T3. Under control conditions the MDM2 immunolabeling inside the

fiber was barely detectable and no distinction in the expression pattern was observed between the two main fiber types (Figure 4a-c). T3 stimulation for 1 and 7 days caused increased MDM2 immunolabeling preferentially inside the type I muscle fiber, displaying a punctuated labeling pattern evenly distributed along the fiber cross sectional area (Figure 4d-i). These results were confirmed throughout quantification of pixels absolute frequency distribution on intensity, as shown in figure 4j-l. Then to address the possible relation between calcineurin activity and MDM2 expression myotubes were treated with cyclosporine A and T3 (Figure 4m). Cyclosporine treatment caused a severe drop in MDM2 gene expression and T3 was unable to increase expression of this gene (Figure 4m).

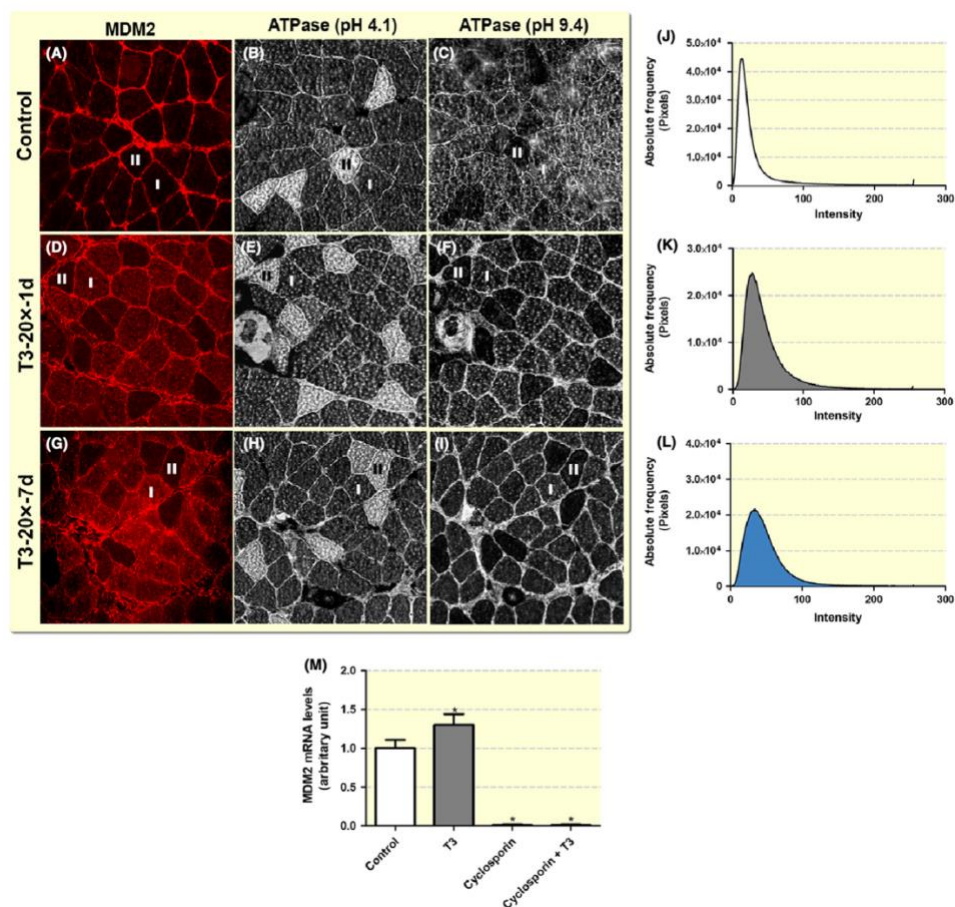


Figure 4: Tissue localization of MDM2 by immunofluorescence and skeletal muscle fiber identity by ATPase assay. a, d and g: Confocal immunofluorescence for MDM2 (red) in the soleus muscle of animals treated with T3 for 1 and 7 days (20 physiological doses). In addition, ATPase assays at acid and alkaline incubation buffers were performed to detect type I and type II fibers (b, c, e, f, h and i). Pixels absolute frequency distribution on intensity of MDM2 of the images a, d and g (j, k and l respectively). m: Expression of MDM2 in differentiated myotubes treated with T3 (10⁻⁸M), cyclosporin A (1 μ M) or both for 30 hours.

3.1.2.6. Cellular localization of MDM2 in skeletal muscle

Detailed evaluation of MDM2 immunolabeling revealed that in addition to increased expression inside the skeletal muscle fiber induced by T3, hot spots of immunopositivity were detected inside the nucleus (Figure 5a). Quantification analyses showed that ~34% of the nuclei were positive to MDM2 in T3 treated group vs ~12% in control group (Figure 5c, p<0.05). Furthermore, we have observed co-localization of DAPI, PAX7 and MDM2, demonstrating that satellite cells express MDM2, about 10% of nuclei were positive for

PAX7 and MDM2 in the control group (Figure 5b, $p < 0.05$). On the other hand, in T3 treated animals, extremely low levels of Pax7 positive nuclei were found (Figure 5b).

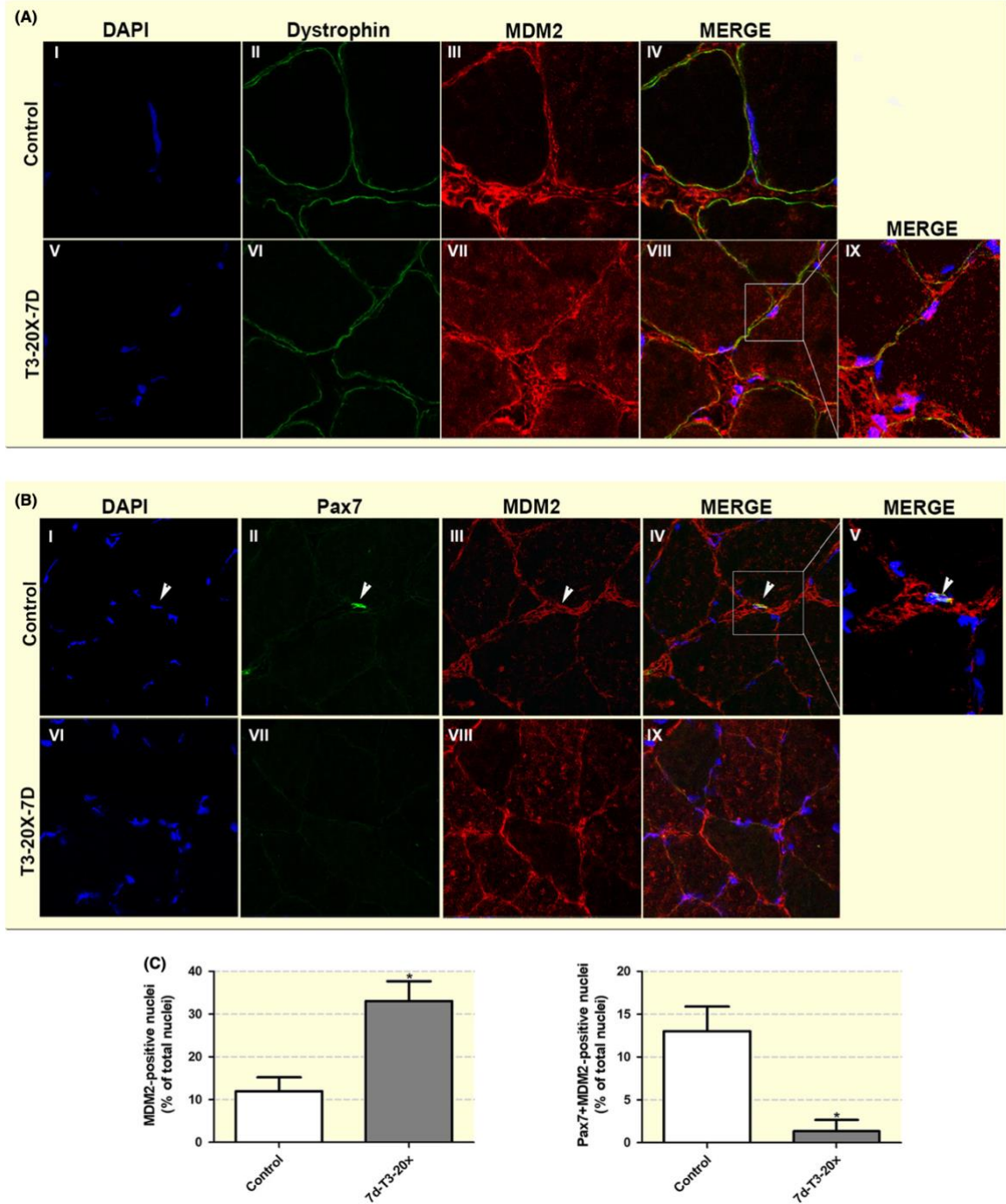


Figure 5: MDM2 is expressed in satellite cells. (a) Dystrophin/DMD (green) and MDM2 (red) were identified by confocal Immunofluorescence in soleus muscle of animals treated with T3 (20 physiological doses for 7 days). (b) PAX7 (green) and MDM2 (red) were identified by immunofluorescence under the same experimental conditions as A. DAPI staining was used (blue) for nuclei identification. (c) Quantification of

MDM2 or PAX7 plus MDM2 positive nuclei were expressed as percentage of total nuclei in soleus muscle of animals treated with T3 for 7 days.

3.1.2.7. MDM2 is a player in controlling myotube trophicity

In an attempt to understand the role of MDM2 in skeletal muscle trophicity we used cultured myoblasts that were differentiated into myotubes, which were treated with T3 and also had the interaction of MDM2 and P53 pharmacologically inhibited by Nutlin-3a. Then myotube area was determined. While vehicle did not cause any effect upon myotube area (Figure 6a-b), T3, as expected, reduced myotube area (~12%, $p < 0.05$, Figures 6a-b). When myotubes were concomitantly submitted to T3 and Nutlin-3a, the negative effect upon myotube area was enhanced (35%, $p < 0.05$ vs T3 treated group, Figure 6a-b). Nutlin-3a alone was also able to decrease myotube area at the same level as compared to the group concomitantly treated with T3 and Nutlin (Figures 6a-b, $p < 0.05$). We have also evaluated the impact of T3 and Nutlin-3a upon gene expression of Mafbx/Atrogin-1 and MuRF1. Interestingly, Nutlin-3a treatment was able to enhance the expression of both genes (1.8 and 2 fold, respectively, $p < 0.05$,) in cultured myotubes treated with T3 (Figure 6c). Notably Nutlin-3a alone was also able to increase expression of both genes (1.9 and 2.3 fold, respectively, $p < 0.05$, Figure 6c). In this cell culture system, 3 days after T3 stimulation alone did not increase levels of MAFbx/Atrogin-1 and MuRF1, although a clear drop in myotube size was observed (Figure 6b). This apparent uncoupling occurs due to the time point evaluated, for example, we have observed (data not shown) that MAFbx/Atrogin-1 was elevated 24h after stimulation.

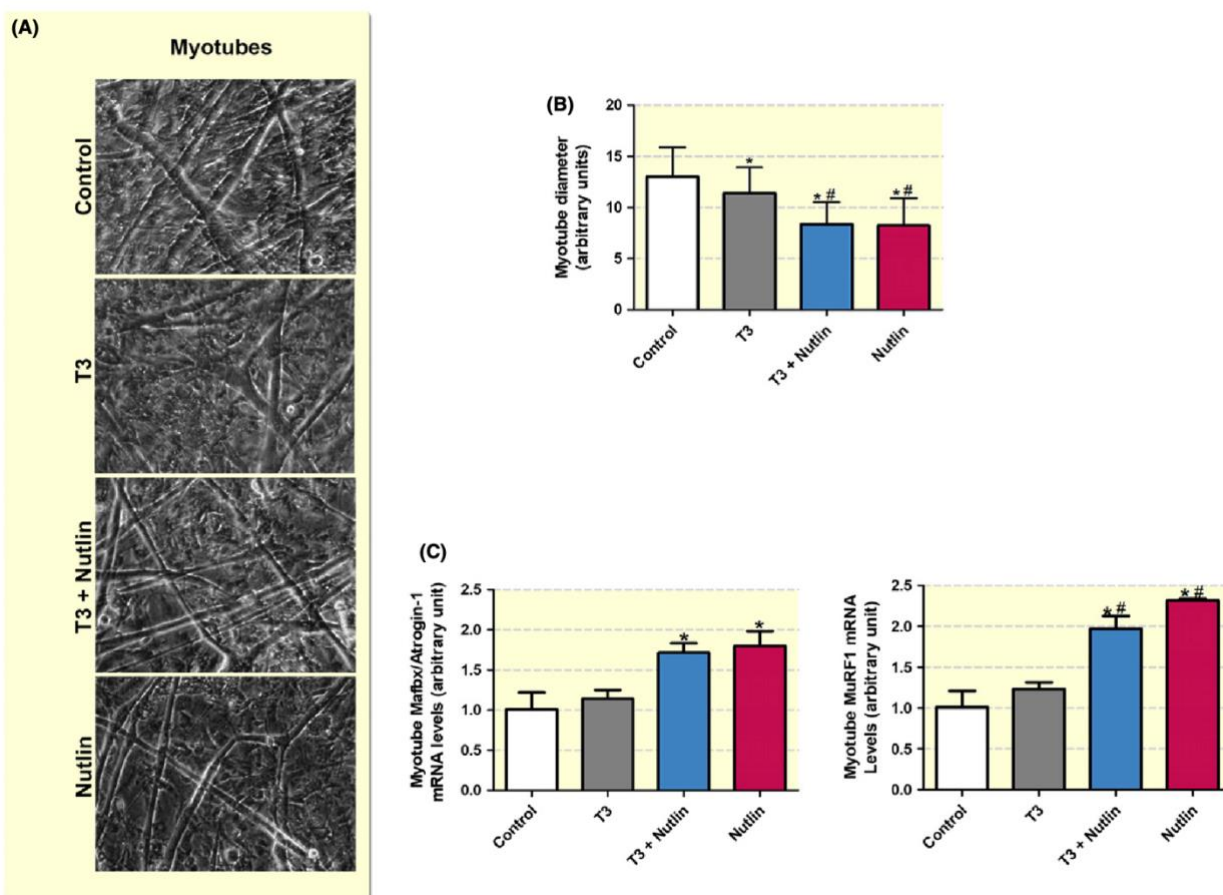


Figure 6: Influence T3 and Nutlin3 (MDM2 inhibitor) on diameter of myotubes. (a) Phase contrast microscopy of myotubes submitted to T3, Nutlin and both combined. Quantification of diameter (b) and mRNA levels of Mafbx/atrogen-1 and MuRF1 (c) in myotubes treated with T3 and Nutlin under the same experimental conditions as A. Control (untreated cells); Control+Veicle (cells treated only with the vehicle). Bars represent the mean \pm SD; * $p < 0.05$ vs control, # $p < 0.05$ vs T3.

Since gene expression of both Mafbx/Atrgin1 and MuRF1 were altered by MDM2 inhibition, we decided to address FOXO3, which is a central protein in skeletal muscle mass regulation and it has been recognized as a key player in transcriptional activation of those atrogenes. As expected we have detected nuclear localization of FOXO3 and low levels of expression in the myofibrillar area (Figure 7aI-III). Quantification analyses showed that 25% of the nuclei were positive for FOXO3 under control conditions and T3 treatment caused a strong decrease in the number of FOXO3 positive nuclei as compared to control

group (10%, $p < 0.05$, Figure 7aIV-VI,XIII). Accordingly, we also observed that T3 treatment increased immunoexpression of FOXO3 in the myofibrillar area (Figure 7aIV-VI). In a similar way myotubes treated with T3 show increased cytoplasmatic labeling and diminished nuclear immunoexpression of FOXO3 (~8%, $p < 0.05$,Figure 7aX-XII,XIV) when compared with control groups (~24%, $p < 0.05$,Figure 7aVII-IX). Western blot analysis showed that T3 promotes a strong increase in the levels of Ser253 phosphorylated FOXO3/total FOXO3 ratio (~1.8 fold, $p < 0.05$, Figure 7b).

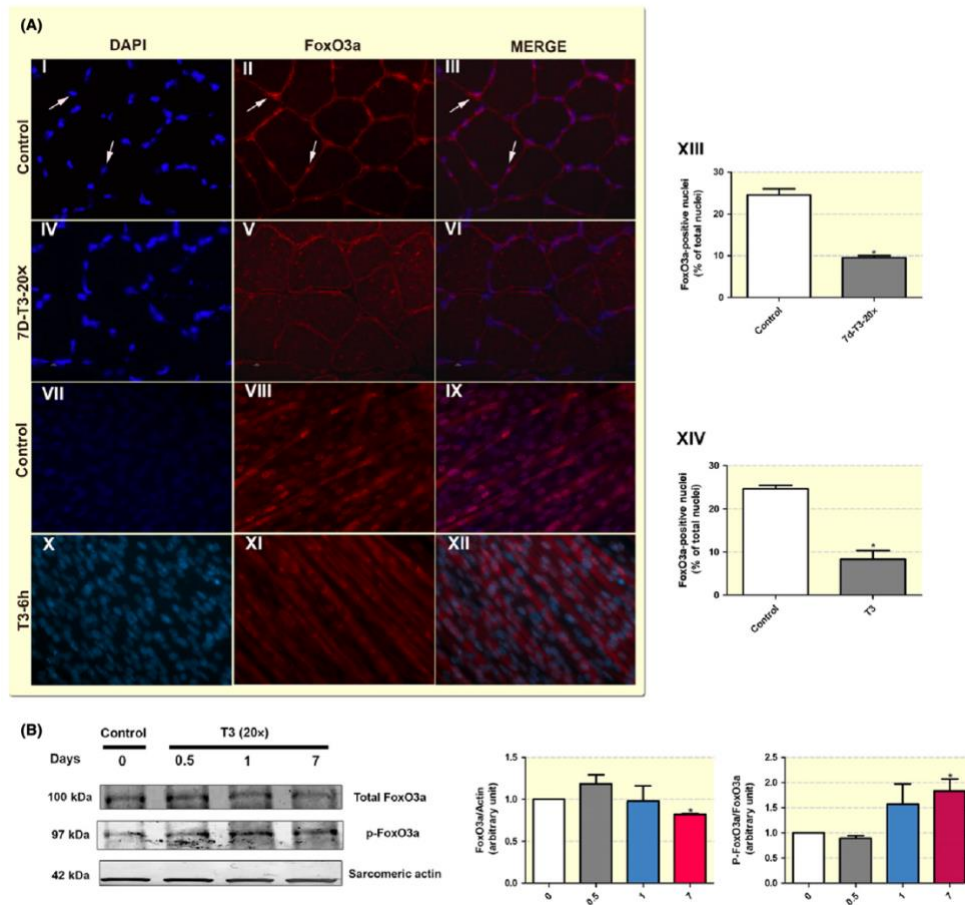
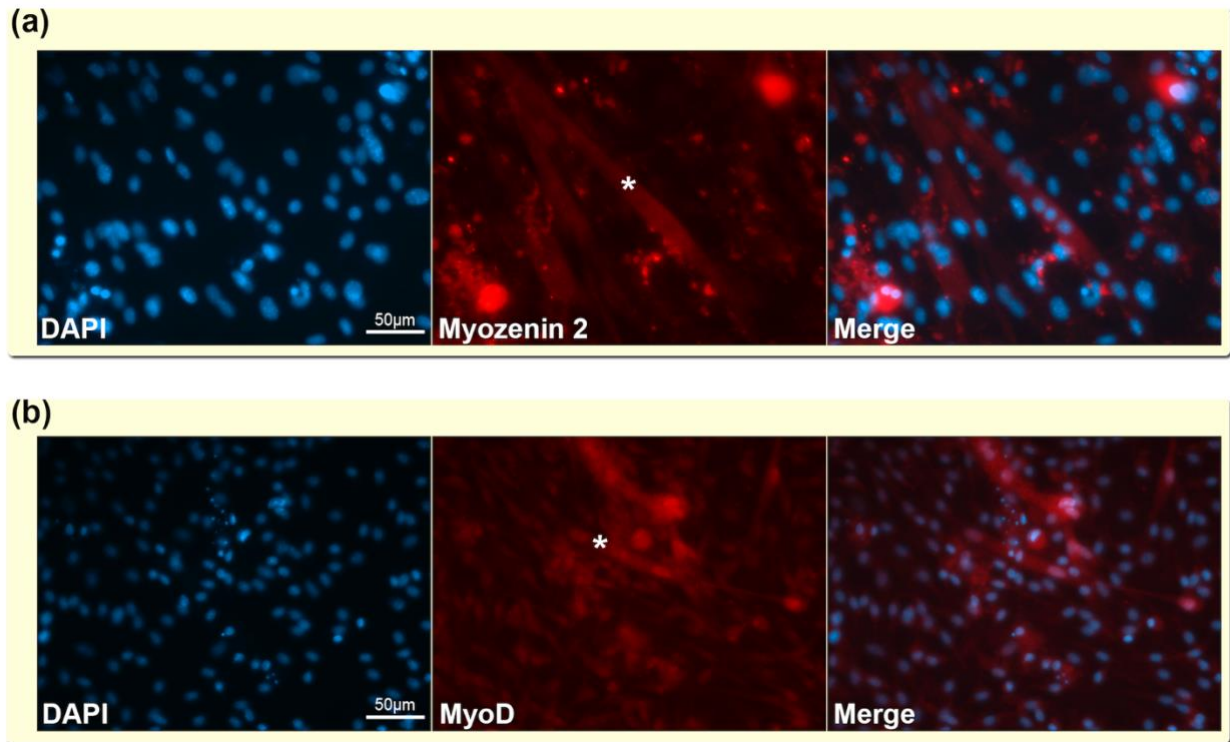


Figure 7: FOXO3 is deactivated by T3 in skeletal muscle. (a) Immunofluorescence for FOXO3 (red) and incidence of FOXO3 positive nuclei (% of total nuclei) in vivo (I-VI) and in vitro (VII-XII). (b) FOXO3 protein expression levels in soleus muscle of animals treated with T3 (20 physiological doses for 7 days). Dapi staining was used (blue) for nuclei identification. Bars represent the mean \pm SD; * $p < 0.05$ vs control.



Supplemental Figure 1: Detection of myogenic factors in primary myoblast culture. Immunofluorescence for Myozenin 2 (a) and MyoD (b) in a typical primary myoblast culture. Cells were fixed 2 days after the onset of differentiation. Asterisks indicate myotubes and Dapi staining (blue) was used for nuclei identification.

3.1.3. Discussion

In this study, by using a microarray approach, we have identified the MDM2 gene as responsive to T3 in skeletal muscle. Under T3 stimulation, it is expressed preferentially in fiber type I and also in satellite cells. In addition, we showed that MDM2 plays an important role in the pro-trophic action of T3.

We have observed that about a half of the 425 genes corresponding to proteolytic pathways are responsive to T3 and more than 80% of those are related to the ubiquitin system as compared to calpains, cathepsins and caspases, reinforcing that the proteasome is the main pathway that mediates T3 dependent proteolysis (Figures 1a-b). Out of the

responsive genes, MDM2 caught our attention because it responded to T3 similarly as MuRF1 (a hallmark of atrophy) and also because of its relatively high basal expression levels as compared to the other top responsive E3 ligases identified. In addition, recent data has suggested that MDM2 is able to ubiquitinate FOXO3, raising the possibility that this E3 ligase might be involved in control of skeletal muscle trophicity.²⁰

We have validated, throughout RT-PCR that T3 increases MDM2 mRNA level as soon as 24h after onset of hormonal treatment in soleus muscle, which is kept elevated up to 7 days of treatment (Figure 1c). Interestingly when growing doses of T3 were used, we obtained the maximal effect at 20 physiological doses. At 50 physiological doses we noticed a tendency for reduction of MDM2 at the mRNA and protein levels suggesting that higher saturating doses of T3 can trigger additional mechanisms, which can restrain the increase in MDM2 expression. The mechanisms involving T3 action on MDM2 are not dependent on systemic factors since we showed that in differentiated myotubes, T3 is able to promote a 2-fold increase in MDM2 mRNA levels (Figure 2d).

MDM2 is an oncogene overexpressed in several types of sarcomas and soft tissue tumors such as liposarcomas, osteosarcomas, fibrous histiocytomas and rhabdomyosarcoma.^{17, 21} The molecular mechanism involved in the tumorigenesis includes interaction of MDM2 with P53. The binding of MDM2 to P53 abrogates P53-mediated transactivation as well as decrease P53 levels through enhanced degradation by proteasome.¹⁸ These actions inhibit the blockade of G1 phase progression mediated by P53. Thus, overexpression of MDM2 serves as a negative regulator of P53 function. Furthermore, MDM2 interacts with the activation domains of the S-phase-promoting transcription factors E2F1 and DP1, resulting in stimulation of E2F1/DP1 transcriptional activity.²¹ Taken together, these observations indicate that MDM2 not only relieves the

proliferative blocking mediated by P53 but also promotes the G1-to-S-phase transition by stimulating E2F1/DP1 activity. Therefore, it is classically established that MDM2 is a cell cycle regulator; nonetheless its role in non-dividing cells such as the skeletal muscle fiber is still elusive. Other cell cycle regulators have been investigated in the skeletal muscle fiber which direct pro-trophic effects such as Wnt β -catenin²², mTORC1²³ and calcineurin²⁴. The results presented herein suggest that MDM2, in line with other cell cycle regulators, is involved in maintenance of skeletal muscle mass under T3 stimulation.

Based on the results obtained in the present study, it is possible to envision that MDM2 could also be involved in other conditions involving skeletal muscle trophicity such as decreased mechanical stimuli and starvation (Figure 3). Actually, it has been shown that MDM2 can ubiquitinate FOXO3 in the skeletal muscle of mice submitted to hind limb denervation^{20,25}, suggesting that MDM2 might be able to regulate skeletal muscle mass via FOXO3 inhibition.

Noteworthy, in the present study we have found that T3 is able to increase MDM2 expression specifically in the type I skeletal muscle fiber (Figure 4). Because NFAT has been described as able to bind to the MDM2 promoter²⁶ and calcineurin-NFAT pathway is considered a key player in the maintenance of type I skeletal muscle fiber phenotype, we pharmacologically inhibited calcineurin and addressed MDM2 responsiveness to T3. Our results point that MDM2 gene expression depends upon the calcineurin-NFAT pathway and also this pathway plays a key role in MDM2 responsiveness to T3 (Figure 4m). Those results are in line with the concept that the high expression of MDM2 in the type I fiber stimulated by T3 is calcineurin-NFAT dependent.

Interestingly, two THREs have been well characterized in the first intron of the MDM2 gene, therefore it is possible to conceive that the NFAT responsive element could

be spatially close to the first intron along with the basal transcriptional complex. Under stimulation with T3 only type I fiber would then provide the proper environment for increased MDM2 transcription. Since in the present study we have not performed long term experiments, up to now it is not clear what occurs with responsiveness of MDM2 as type I fibers are converted to fast twitch variants driven by T3.

T3 increases MDM2 expression homogenously, exhibiting a punctiform pattern along the sarcoplasm along the cross-sectional area of the type I fiber. In addition, we have also detected MDM2 immunolabeling inside the nucleus (Figure 5). In T3 stimulated tissue, about 30% of total nuclei is MDM2 positive, in contrast to only 10% in control group (Figure 5). Previous studies indicate that MDM2 acts in the cytoplasm²⁵, therefore the nuclear role of MDM2 in skeletal muscle remains unclear and it would be interesting to address this issue in future studies.

We have also detected MDM2 immunopositivity in satellite cells (Figure 5), leading to the possibility that this protein could play a role in the proliferation/differentiation balance of satellite cells in vivo. In fact, indirect evidence for this is observed in the study of Fu and colleagues²⁵, where it has been shown that MDM2 can improve myogenesis. It was observed that C2C12 cells treated with nandrolone, an anabolic steroid, increased Numb protein levels as well as attenuated its degradation by MDM2.²⁷ The expression of Numb in myogenic lineage has been associated with differentiation of satellite cells.^{27,28} Therefore, is possible to consider that overexpression of MDM2 in skeletal muscle plays an important role in the activity of satellite cells. Interestingly, we have detected expression of MDM2 in satellite cells mainly in basal conditions. T3 strongly decreases the expression of satellite cell markers such as MyoD, making difficult to approach the effect of T3 on MDM2 expression in satellite cells. It has been previously reported that T3

decreases such markers in orbicular muscles.²⁹ In addition, it has been shown that MDM2 can ubiquitinate and degrade C/EBPbeta, a strong activator of PAX7. This mechanism can explain why we have observed that increased MDM2 immunoeexpression is paralleled by a dramatic decrease in immunoeexpression of PAX7 (Figure 5).

In order to better understand the modulation of MDM2 in skeletal muscle we decided to measure its mRNA levels in other models of atrophy (Figure 3). Immobilization promoted a significant but rather modest increase in MDM2 gene expression. Starvation and immobilization significantly increased MDM2 gene expression, while dexamethasone treatment did not have any effect upon MDM2 gene expression. These data rise the possibility that MDM2 gene expression could play a differential role in distinct atrophy models.

In an attempt to uncover the role of MDM2 in skeletal muscle under T3 stimulation, we have pharmacologically inhibited MDM2 levels in cultured myotubes treated with T3 (Figure 6). As expected, we observed that T3 is able to decrease myotube size, highlighting the effect of T3 upon protein loss. Remarkably, myotubes treated with MDM2 inhibitor only induced a stronger sarcopenic response as compared to T3 treatment. This suggests that MDM2, by itself, might be sufficient to act positively upon myotube size. Further studies are needed to clarify this issue and also to address the operating mechanisms. When myotubes were treated with T3 and simultaneously MDM2 inhibited, a similar decrease in size was observed as compared to MDM2 inhibition alone, reinforcing the idea that MDM2 could be an autonomous positive player in myobute trophicity. The data presented herein clearly show that T3 is able to increase expression of MDM2 in the skeletal muscle fiber, therefore activation of MDM2 could be a mechanism by which T3 exerts a pro-trophic effect upon skeletal muscle.

These results are in line with the concept of a dual role of T3 in skeletal muscle: stimulating catabolic pathways, such as the proteasome system as already well established, but also stimulating anabolic pathways such as MDM2. In fact, this concept is broadly accepted in other systems such as brown adipose tissue (T3 increases lipolysis and simultaneously lipogenesis) and liver (T3 increases activity of glycolysis and gluconeogenesis).³⁰ Accordingly, in the present study we show that T3 can increase levels of phosphorylated FOXO3, keeping this important transcriptional factor inactive and at the same time increasing levels of Mafbx/Atrogin1 and MuRF1, which contain both FOXO response elements. This data shows that T3 can modulate the expression of those atrogenes independently of FoxO3. At the moment, the mechanism by which such dual effect occurs is not clear, although one possibility might rely on THREs located at the promoter of those genes, yet to be described.¹²

Another aspect strictly linked to FOXO3 activity is its cellular location. We found herein that T3 is able to strongly decrease nuclear localization of FOXO3, therefore inhibiting its activity (Figure 7). At the moment, the exact mechanisms linking T3 action upon FOXO and MDM2 are not clear and further studies are necessary to establish such link. Interestingly, though, a previous study has uncovered that MDM2 is able to ubiquitinate FOXO3, leading to subsequent degradation.²⁵ This well described mechanism pointed by Fu et al²⁵ might also be operating when T3 increases MDM2 levels. In conclusion, this study establishes a link between MDM2 and the skeletal muscle fiber mass control and unravels a mechanism involving pro-trophicity, which is utilized by T3 in skeletal muscle.

3.1.4. *Materials and Methods*

The study was conducted conform ethical principles in animals research adopted by the Brazilian College of Animals Experimentation (COBEA) and was approved by the Institute of Biomedical Sciences/University of the Sao Paulo Ethics Committee for Animal Research (#168/05).

3.1.4.1. Experimental Procedures

Male Wistar rats approximately 2 months old weighing 200-260g were housed in standard plastic cages under controlled environmental conditions (24°C; 12 hours light/dark cycle). Rats were randomized into two groups: control and hyperthyroid (T3). The hormone injected was adjusted according to body weight (BW) in order to maintain the same dosage throughout the treatment. Control animals received injections of vehicle solution. The injections were administrated once a day and the animals were treated by 0.5, 1 and 7 days. The doses of T3 (Sigma-Aldrich, St.Louis. MO) injected each day were 1.5µg, 6µg and 15µg of T3/100g body weight per day, corresponding to 5, 20 and 50 physiological doses respectively. T3 was dissolved in saline containing 40mM NaOH. After treatment the animals were killed by decapitation and the blood was collected to analyze thyroxine (T4) plasma levels. Some animals (n=4-5) were submitted to unilateral immobilization of the left hindlimb by applying a cast with total plantar extension for 1 and 3 days. Dexamethasone-induced atrophy was performed by intraperitoneal injection (1200mg/Kg) daily for 1 and 3days. For the starvation procedure animals had access only to water for 1 or 3 days.

3.1.4.2. Tissue Samples

The soleus muscle was removed, weighted, frozen in liquid nitrogen and stored at -80°C for later analysis of the mRNA and protein expression levels. The soleus muscle was transversely cut in half and one segment immersed in cold isopentane for 30 seconds. After that, the segment was cooled in liquid nitrogen, and stored at -80°C for histochemistry and immunofluorescence. To confirm effectiveness of treatment by T3, the heart weight was used as positive control.

3.1.4.3. Serum parameters

Total thyroxin (T4) serum levels were measured by commercial radioimmunoassay (RIA) kits (Schering Cis Bio International - France). The serum was separated by centrifugation (5.000 rpm; 30 minutes), immediately frozen and stored at -80°C .

3.1.4.4. Microarray analysis

Total RNA from adult rat soleus muscle was isolated using Trizol LS reagent (Life Technologies, Carlsbad, CA) in accordance with the manufacturer's instructions. Total RNA was further purified with *Rneasy Fibrous Tissue Mini Kit* (Qiagen, Austin, TX) to reach microarray RNA quality standards. The resulting phenol-free RNA was submitted to spectrophotometric analysis in a Nanodrop 1000 spectrophotometer (Thermo Scientific, Wilmington, DE) and RNA quantity determined by the A260 wavelength method. One microgram of total RNA was used in the cDNA first strand synthesis with *One-Cycle Target Labeling and Control Reagents* kit (Affymetrix, Santa Clara, CA). At the end of the cycle, samples were re-purified using the *Cleanup of Double-Strand cDNA* kit (Affymetrix, Santa

Clara, CA) and re-quantified in Nanodrop. The biotinylated-cRNA synthesis was carried out with the *in vitro* transcription (IVT) *Gene Chip Expression 3' – Amplification Reagents for IVT labeling kit* (Affymetrix, Santa Clara, CA) followed by the cRNA fragmentation at high temperature and high Mg⁺² concentration buffer. For hybridization, we used the *Gene Chip Hybridization, Wash and Stain* (Affymetrix, Santa Clara, CA). Chips were filled in with hybridization buffer, incubated at 45°C for 16 hours and then processed in the washing station (Affymetrix, Santa Clara, CA). Subsequently, chips were analyzed in a scanner and raw data files were processed using the MAS 5.0 algorithm. The fold change values for control and T3 treated groups were calculated and filtered for variations greater than 15%. Gene ontology analysis using AmiGO2³³ (<http://amigo.geneontology.org/amigo>) were applied in order to classify differential expressed genes. To address the proteolytic pathway, we filtered out genes related to “Proteolysis” (GO biological processes 0030163-protein catabolism, 0016567-ubiquitination and 0006508-proteolysis). All scripts were written in python 3.4.

3.1.4.5. Gene expression by RT- PCR

For determination of mRNA levels by RT-PCR, total RNA was isolated from soleus muscle by using the Trizol reagent (Life Technologies, Carlsbad, CA) following the manufacturer's recommendations. Total RNA (1µg) was reverse transcribed (RT) to generate cDNA. This reaction contained oligo-dT (500µg/ml), 10mM of each deoxyribonucleoside phosphate (dNTP), 5X first-strand buffer, 0.1M dithiothreitol (DTT), and 200U reverse transcriptase (SuperScri pt II; In vitrogen, San Diego, California). The RT reaction was performed at 70°C for 10 minutes, followed by 42°C for 60 minutes and

10 minutes at 95°C. The primer set for rat, Mafbx/Atrogin1, MDM2 and MuRF1 was designed by using Primer-Blast³⁴ (<http://www.ncbi.nlm.nih.gov/tools/primer-blast/>) and synthesized by IDT (Integrated DNA Technologies) according to Table 2. One microliter of cDNA was used in Real-Time PCR, containing, Syber Green Universal Master Mix II (Life Technologies, Carlsbad, CA) and the cycle parameters were: 50°C for 2 minutes, 95°C for 10 minutes, followed by 40 cycles of 95°C for 15 seconds, and 60°C for 1 minute. The fluorescence intensity was quantified and amplification plots were analyzed by a Corbett RotorGene 6000 (Qiagen, Hilden, Germany). Results were expressed using the comparative cycle threshold (CT) method as described and expression levels were represented by fold change over values derived from control animals. Amplification of cyclophilin A gene was used as an internal standard. All primer pairs were designed so at least either forward or reverse spans an exon-exon junction (Table 2).

TABLE 2 Primer sets used in real-time PCR (RT-PCR)

Primers	NCBI Accession number	Forward	Reverse
Mafbx/Atrogin-1	NM_133521.1	TACTAAGGAGCGCCATGGATACT	GTTGAATCTTCTGGAATCCAGGAT
Cyclophilin A	NM_017101.1	GCCGATGACGAGCCCTTG	TGCCGCCAGTGCCATTAT
MDM2	NM_001108099.1	GAGGATGATGAGGTCTATCG	GGAGGATTCATTTTCATTGCAC
MuRF1	NM_080903.1	TGACCAAGGAAAACAGCCACCAG	TCACTCCTTCTTCTCGTCCAGGATGG

3.1.4.6. *Western blot (WB)*

Primary antibodies used for Western blotting were: MDM2 (1:1000; Novus Biologicals, Cambridge, MA), sarcomeric Actin (1:1000; Dako, USA, used as a housekeeping protein), total FOXO3 (1:1000, Abcam, USA) and phosphorylated FOXO3 (1:1000; Cell Signaling, USA). The secondary antibodies used were: polyclonal rabbit anti-mouse immunoglobulins/AP (1:1000; Dako, USA) and polyclonal rabbit anti-rabbit immunoglobulins/AP (1:1000; Dako, USA). Soleus muscles were homogenized in an

extraction buffer termed modified RIPA buffer (0,625% Nonidet P-40; 0,625% deoxycholic acid; 0,00625M sodium phosphate pH 7,2; 1mM EDTA pH 8,0) containing 10µg/ml of protease inhibitor cocktail (SigmaAldrich). Homogenates were centrifuged at 10,000G for 10 minutes at 4 °C, and the supernatant was used. Protein concentration was determined by Bradford assay (Bio-Rad, Hercules, California), with bovine serum albumin as standard. Protein extract were run on 12% or 10% sodium dodecylsulfate–polyacrylamide gels electrophoresis (SDS-PAGE) and transferred to a nitrocellulose membrane (Bio-Rad, USA). The membranes were stained with Ponceau S to confirm the protein amount and then rinsed with Tween Tris buffered saline solution 0.5M NaCl, 50mM TrisHCl pH 7.4, and 0.1% Tween-20 (TBS-T). All membranes were incubated for 40 minutes at room temperature by blocking solution (TBS-T; 5% no-fat milk). Next the membranes were incubated overnight with primary antibodies at 4°C. After a 15 minutes wash in TBS-T solution, membranes were incubated with secondary antibodies for 1 hour at room temperature and washed again for 10 minutes in TBS-T solution. After that, membranes were incubated for 5 minutes with detection buffer (100mM Tris-HCL; 100mM sodium chloride pH9.5). Labeled proteins were detected by the alkaline phosphatase system (NBT/BCIP Stock Solution; Roche, USA).

3.1.4.7. Immunofluorescence (IF)

The primary antibodies used for immunostaining were: monoclonal-mouse MDM2 (1:1000; Novus Biologicals, Cambridge, MA), polyclonal rabbit PAX7 (1:200; Aviva Systems Biology); polyclonal rabbit dystrophin (1:250; Santa Cruz Biotechnology); polyclonal rabbit total FOXO3 (1:300; Abcam); mouse monoclonal myozenin 2 (1:250;

Santa Cruz Biotechnology). The secondary antibodies were (Table 2): goat anti-mouse IgG-Cyanine Cy2 (1:50; Jackson Lab), donkey anti-mouse Cyanine Cy3 (1:300; Jackson Lab), goat anti-rabbit IgG-Cyanine Cy2 (1:50; Jackson Lab), (4) donkey anti-rabbit IgG-Cyanine Cy3 (1:300; Jackson Lab). Cross-sections of soleus muscle for immunostaining were fixed with acetone for 10 minutes at -20°C , washed with PBS-N (PBS+ 0.1% Nonidet-40), 3 times for 5 minutes each. After that, slides were incubated with a blocking solution (PBS + 0.1% Nonidet-40 + 1% BSA) for 30 minutes at 37°C . Next, the slides were incubated with a solution containing the primary antibody overnight in a dark chamber (4°C). After washing with PBS-N, 3 times for 5 minutes each, a blocking solution containing the secondary antibody was added for 1 hour and 30 minutes in a dark chamber. The slides were then washed with PBS-N, 3 times for 5 minutes and mounted with Vectashield with 4', 6-diamidino-2-phenylindole (DAPI) (cat# H-1200, Vector Labs) and coverslipped. Images were captured on a Zeiss LSM-780 NLO microscope using Carl Zeiss Zen lite, also, the same software was used to measurement of pixels absolute frequency distribution. Images were acquired at Center of Facility of Research (CEFAP), a core facility at Institute of Biomedical Sciences, University of Sao Paulo.

3.1.4.8. Enzyme histochemical staining

Serial cross sections ($10\mu\text{m}$) obtained of the middle region soleus muscle were stained for myofibrillar ATPase activity (mATPase) after alkaline (ATPase, pH 9.4) or acid (ATPase, pH 4.1)³⁵ preincubation. Fiber type staining pattern in the alkaline pH 9.4 (dark type IIa fibers, pale type I fiber) was compared with the reverse staining pattern (pale type IIa, dark type I) in a section stained in the acid pH (pH 4.1). Acquisition of the images was

performed in the Nikon Eclipse TS 100 microscope equipped with a digital video camera and NIS-Elements BR imaging software.

3.1.4.9. Cell Culture of myoblasts

For primary culture of myoblasts, muscle samples from hind limb muscles of male FVB mice were removed and trimmed of connective tissue. Subsequently the samples were incubated with sterile phosphate buffered saline (PBS) solution and cut in short fragments to help the digestion. The minced muscles were digested in type IA collagenase 0.20% (Sigma #C9891-1G) and trypsin 0.25% (Gibco #27250-018) in 15ml of Dulbecco Modified Eagle Medium High Glucose (DMEM - Sigma #D5648). Cells were then centrifuged and cultured in growth medium (DMEM 20% FBS, 1% penicillin-streptomycin) on a bed of Matrigel (BD Bioscience, #3356234) into 24 wells culture dishes at 37°C, 5% CO₂. Cells were maintained in growth medium up to 3 days reaching 70% of confluence. After that, the medium was changed to the differentiation medium (DMEM 2% horse serum, 1% penicillin-streptomycin) to stimulate the myotube formation. After 3 days of differentiation certain wells were treated by 72 hours with T3 (3×10^{-8} M; cat #T2877, Sigma Aldrich, St. Louis. MO), the inhibitor of MDM2 named Nutlin (8 μ M; cat #18585, Cayman Chemical) or both. These treatments were used to compare the influence of T3 and MDM2 in the modulation of myotube size. As controls some wells were treated with vehicle (NaOH 40nM), and others were differentiated by 6 days without any treatment. Cell identity of this myogenic culture was confirmed by detection of myozenin 2 and MyoD (Supplemental Figure 1). Three independent experiments using cultured myotubes were performed.

Myoblasts from the muscle-derived mouse C2C12 were maintained as proliferating myoblasts in DMEM-high-glucose medium supplemented with 10% FBS, 1% penicillin-streptomycin. After reaching 90-100% confluence cells were switched to DMEM supplemented with 2% adult horse serum 1% penicillin-streptomycin, to induce fusion of myoblasts. After 2 days of differentiation certain wells were treated by 30 hours with T3 (3×10^{-8} ; cat #T2877, Sigma Aldrich, St. Louis. MO), the inhibitor of calcineurin activity named Cyclosporin A ($1 \mu\text{M}$) in DMSO or both.

3.1.4.10. Myotube Measurements

Acquisition of the images to measure the diameter of myotubes was performed in the Nikon Eclipse TS 100 microscope equipped with a digital video camera and NIS-Elements BR imaging software. Subsequently, the myotubes were measured by Image Pro-Plus Demo software. The myotubes were visualized at 100X magnification and the fields were randomly selected from four different wells for each group. At least three measurements were performed per myotube. Approximately 165 myotubes were measured per group.

3.1.4.11. Statistical Analysis

Results are reported as means \pm SD. Statistical analysis was performed using ANOVA followed by Tukey post-test analysis as appropriate. $p < 0.05$ was considered statistically significant.

3.1.5. *The completion of the Copyright Transfer and Affirmation of Originality*

The article is original, does not infringe upon any copyright or other proprietary right, is currently not under submission in another journal, and has not been previously published. There are no financial or other relationships that might lead to a conflict of interest among authors.

3.1.6. *Author contributions*

Gracielle V. Ramos, André Cruz, William J. Silva, Igor L. Baptista and João G.O. Silvestre performed experiments and wrote the paper. André Cruz and Andrei Rozanski were in charge with the *in-silico* analysis and Anselmo S. Moriscot designed the study, supervised the experiments, and wrote the paper.

3.1.7. *Acknowledgements*

We thank FAPESP and CNPq for the financial support.

3.1.8. *References*

1. Sinha, R, Yen, PM: Cellular Action of Thyroid Hormone. In: *Endotext*. edited by DE GROOT, L. J., BECK-PECCOZ, P., CHROUSOS, G., DUNGAN, K., GROSSMAN, A., HERSHMAN, J. M., KOCH, C., MCLACHLAN, R., NEW, M., REBAR, R., SINGER, F., VINIK, A., WEICKERT, M. O., South Dartmouth (MA), 2000.
2. Paris, M, Hillenweck, A, Bertrand, S, Delous, G, Escriva, H, Zalko, D, Cravedi, JP, Laudet, V: Active metabolism of thyroid hormone during metamorphosis of amphioxus. *Integrative and comparative biology*, 50: 63-74, 2010.
3. Davis, PJ, Goglia, F, Leonard, JL: Nongenomic actions of thyroid hormone. *Nature reviews Endocrinology*, 2015.
4. Mullur, R, Liu, YY, Brent, GA: Thyroid hormone regulation of metabolism. *Physiological reviews*, 94: 355-382, 2014.

5. Williams, CM, Ellis, R: Thermogenic and metabolic consequences of thyroid hormone treatment in brown and white adipose tissue. *Bioscience reports*, 5: 175-184, 1985.
6. Allain, TJ, Chambers, TJ, Flanagan, AM, McGregor, AM: Tri-iodothyronine stimulates rat osteoclastic bone resorption by an indirect effect. *The Journal of endocrinology*, 133: 327-331, 1992.
7. Bahi, L, Garnier, A, Fortin, D, Serrurier, B, Veksler, V, Bigard, AX, Ventura-Clapier, R: Differential effects of thyroid hormones on energy metabolism of rat slow- and fast-twitch muscles. *Journal of cellular physiology*, 203: 589-598, 2005.
8. Capo, LA, Sillau, AH: The effect of hyperthyroidism on capillarity and oxidative capacity in rat soleus and gastrocnemius muscles. *The Journal of physiology*, 342: 1-14, 1983.
9. Carter, WJ, van der Weijden Benjamin, WS, Faas, FH: Effect of experimental hyperthyroidism on skeletal-muscle proteolysis. *The Biochemical journal*, 194: 685-690, 1981.
10. Clément, K, Viguerie, N, Diehn, M, Alizadeh, A, Barbe, P, Thalamas, C, Storey, JD, Brown, PO, Barsh, GS, Langin, D: In Vivo Regulation of Human Skeletal Muscle Gene Expression by Thyroid Hormone. *Genome Research*, 12: 281-291, 2002.
11. Tawa, NE, Jr., Odessey, R, Goldberg, AL: Inhibitors of the proteasome reduce the accelerated proteolysis in atrophying rat skeletal muscles. *J Clin Invest*, 100: 197-203, 1997.
12. O'Neal, P, Alamdari, N, Smith, I, Poylin, V, Menconi, M, Hasselgren, PO: Experimental hyperthyroidism in rats increases the expression of the ubiquitin ligases atrogin-1 and MuRF1 and stimulates multiple proteolytic pathways in skeletal muscle. *J Cell Biochem*, 108: 963-973, 2009.
13. Chrysis, D, Chagin, A, Savendahl, L: Insulin-like growth factor-1 restores dexamethasone-induced heart growth arrest in rats: the role of the ubiquitin pathway. *Hormones*, 10: 46-56, 2011.
14. Bodine, SC, Latres, E, Baumhueter, S, Lai, VK, Nunez, L, Clarke, BA, Poueymirou, WT, Panaro, FJ, Na, E, Dharmarajan, K, Pan, ZQ, Valenzuela, DM, DeChiara, TM, Stitt, TN, Yancopoulos, GD, Glass, DJ: Identification of ubiquitin ligases required for skeletal muscle atrophy. *Science*, 294: 1704-1708, 2001.
15. Satchek, JM, Hyatt, JP, Raffaello, A, Jagoe, RT, Roy, RR, Edgerton, VR, Lecker, SH, Goldberg, AL: Rapid disuse and denervation atrophy involve transcriptional changes similar to those of muscle wasting during systemic diseases. *FASEB journal : official publication of the Federation of American Societies for Experimental Biology*, 21: 140-155, 2007.

16. Lokireddy, S, Wijesoma, IW, Sze, SK, McFarlane, C, Kambadur, R, Sharma, M: Identification of atrogin-1-targeted proteins during the myostatin-induced skeletal muscle wasting. *American journal of physiology Cell physiology*, 303: C512-529, 2012.
17. Oliner, JD, Kinzler, KW, Meltzer, PS, George, DL, Vogelstein, B: Amplification of a gene encoding a p53-associated protein in human sarcomas. *Nature*, 358: 80-83, 1992.
18. Momand, J, Wu, HH, Dasgupta, G: MDM2--master regulator of the p53 tumor suppressor protein. *Gene*, 242: 15-29, 2000.
19. Vassilev, LT, Vu, BT, Graves, B, Carvajal, D, Podlaski, F, Filipovic, Z, Kong, N, Kammlott, U, Lukacs, C, Klein, C, Fotouhi, N, Liu, EA: In vivo activation of the p53 pathway by small-molecule antagonists of MDM2. *Science*, 303: 844-848, 2004.
20. Bertaglia, E, Coletto, L, Sandri, M: Posttranslational modifications control FoxO3 activity during denervation. *American journal of physiology Cell physiology*, 302: C587-596, 2012.
21. Guo, CS, Degnin, C, Fiddler, TA, Stauffer, D, Thayer, MJ: Regulation of MyoD activity and muscle cell differentiation by MDM2, pRb, and Sp1. *J Biol Chem*, 278: 22615-22622, 2003.
22. Leal, ML, Lamas, L, Aoki, MS, Ugrinowitsch, C, Ramos, MS, Tricoli, V, Moriscot, AS: Effect of different resistance-training regimens on the WNT-signaling pathway. *European journal of applied physiology*, 111: 2535-2545, 2011.
23. Walker, DK, Dickinson, JM, Timmerman, KL, Drummond, MJ, Reidy, PT, Fry, CS, Gundermann, DM, Rasmussen, BB: Exercise, amino acids, and aging in the control of human muscle protein synthesis. *Medicine and science in sports and exercise*, 43: 2249-2258, 2011.
24. Hudson, MB, Price, SR: Calcineurin: a poorly understood regulator of muscle mass. *The international journal of biochemistry & cell biology*, 45: 2173-2178, 2013.
25. Fu, W, Ma, Q, Chen, L, Li, P, Zhang, M, Ramamoorthy, S, Nawaz, Z, Shimojima, T, Wang, H, Yang, Y, Shen, Z, Zhang, Y, Zhang, X, Nicosia, SV, Pledger, JW, Chen, J, Bai, W: MDM2 acts downstream of p53 as an E3 ligase to promote FOXO ubiquitination and degradation. *J Biol Chem*, 284: 13987-14000, 2009.
26. Zhang, X, Zhang, Z, Cheng, J, Li, M, Wang, W, Xu, W, Wang, H, Zhang, R: Transcription factor NFAT1 activates the mdm2 oncogene independent of p53. *J Biol Chem*, 287: 30468-30476, 2012.
27. Liu, XH, Yao, S, Levine, AC, Kirschenbaum, A, Pan, J, Wu, Y, Qin, W, Collier, L, Bauman, WA, Cardozo, CP: Nandrolone, an anabolic steroid, stabilizes Numb protein through inhibition of mdm2 in C2C12 myoblasts. *Journal of andrology*, 33: 1216-1223, 2012.

28. Jory, A, Le Roux, I, Gayraud-Morel, B, Rocheteau, P, Cohen-Tannoudji, M, Cumano, A, Tajbakhsh, S: Numb promotes an increase in skeletal muscle progenitor cells in the embryonic somite. *Stem cells*, 27: 2769-2780, 2009.
29. Harrison, AR, Lee, MS, McLoon, LK: Effects of elevated thyroid hormone on adult rabbit extraocular muscles. *Invest Ophthalmol Vis Sci*, 51: 183-191, 2010.
30. Feng, X, Jiang, Y, Meltzer, P, Yen, PM: Thyroid hormone regulation of hepatic genes in vivo detected by complementary DNA microarray. *Molecular endocrinology*, 14: 947-955, 2000.
31. Sandri, M, Sandri, C, Gilbert, A, Skurk, C, Calabria, E, Picard, A, Walsh, K, Schiaffino, S, Lecker, SH, Goldberg, AL: Foxo Transcription Factors Induce the Atrophy-Related Ubiquitin Ligase Atrogin-1 and Cause Skeletal Muscle Atrophy. *Cell*, 117: 399-412, 2004.
32. Waddell, DS, Baehr, LM, van den Brandt, J, Johnsen, SA, Reichardt, HM, Furlow, JD, Bodine, SC: The glucocorticoid receptor and FOXO1 synergistically activate the skeletal muscle atrophy-associated MuRF1 gene. *American Journal of Physiology - Endocrinology and Metabolism*, 295: E785-E797, 2008.
33. Carbon, S, Ireland, A, Mungall, CJ, Shu, S, Marshall, B, Lewis, S, the Ami, GOH, the Web Presence Working, G: AmiGO: online access to ontology and annotation data. *Bioinformatics*, 25: 288-289, 2009.
34. Ye, J, Coulouris, G, Zaretskaya, I, Cutcutache, I, Rozen, S, Madden, TL: Primer-BLAST: A tool to design target-specific primers for polymerase chain reaction. *BMC Bioinformatics*, 13: 134, 2012.
35. Brooke, MH, Kaiser, KK: Muscle fiber types: how many and what kind? *Archives of neurology*, 23: 369-379, 1970.

3.2. Artigo submetido: “RPTOR Inhibition is Essential for T3-induced Skeletal Muscle Atrophy Independently of mTORC-1”

Page 1 of 35

ESub : 279159 21-09-2021

Submitted to International Journal of Molecular Medicine

Rptor inhibition is essential for T3-induced skeletal muscle atrophy independently of mTORC-1

Running Title: Rptor inhibition is essential to T3-induced atrophy

Key Words: Hyperthyroidism, Myostatin, Rptor, Atrophy, T3

Submitted by: André Cruz, created on 21-09-2021

Type of Article: Article

Abstract

The thyroid hormone T3 is a key player in many signal transduction pathways, mainly by regulating nuclear transcription. In the skeletal muscle, pathologically augmented T3 signalling promotes atrophy. However, the underlying upstream mechanisms are not well understood. Thus, identifying specific transcriptome targets is crucial to developing therapeutical strategies to mitigate T3-induced atrophy. The present study addresses the effects of high levels of T3 upon the protein synthesis pathway mTOR in the rat soleus muscle. Experimental hyperthyroidism was induced in male Wistar rats (~260g) by daily doses of T3 (0.6µg Kg⁻¹) for 0.5, 1, 7, and 14 days. For in vitro experiments, myotubes were treated with T3 for 3 days. As expected, T3 induced soleus muscle atrophy (7 days: ~18%; 14 days: ~27%). By analysing global gene expression, we identified progressive downregulation of Rptor. Regarding protein content, myostatin was up-regulated on the 7th and 14th days (~1.6 and ~1.5 fold), while Rptor was down-regulated on the 7th and 14th days of treatment (~0.6 and ~0.6 fold). In addition, T3 repressed mTOR and P70S6K phosphorylation at the 7th and 14th days (~0.6 and ~0.7 fold). Notably, both myostatin knockdown and Rptor overexpression were sufficient to attenuate T3-induced skeletal muscle atrophy development significantly. Myostatin and Rptor are essential for T3-induced skeletal muscle atrophy and thus are potential therapeutic targets to prevent skeletal muscle wasting in hyperthyroidism.

Authors

Name	Institute	Email Address
Mr André Cruz	Institute of Biomedical Sciences	andreacruz@usp.br
Ms Paula K. Nascimento Alves	Institute of Biomedical Sciences	paulaketilly@usp.br
Dr William Jose Silva	Institute of Biomedical Sciences	williamsilvaj@gmail.com
Dr Andrei Rozanski	Institute of Biomedical Sciences	rozanski.andrei@gmail.com
Dr Siegfried Labeit	Institute for Integrative Pathophysiology	labeit@medma.de
Dr Anselmo Sigari Moriscot	Institute of Biomedical Sciences	moriscot@usp.br

Files

File Name	Type	Uploaded
Artigo t3 23sep2021 IJMM.docx	Manuscript	24-09-2021
IJMM fig1.tif	Figures and Images	24-09-2021
IJMM fig8.tif	Figures and Images	24-09-2021
IJMM fig4.tif	Figures and Images	24-09-2021
IJMM fig3.tif	Figures and Images	24-09-2021
IJMM fig6.tif	Figures and Images	24-09-2021

3.2.1. Introduction

Iodine-based biochemical structures are ancient in Earth's history since the spontaneous iodine binding to tyrosine generated a reactive molecule crucial for catalysing reactions in primitive unicellular organisms. Eventually, iodotyrosines signalling was integrated into the development, maturation, and maintenance of pluricellular organisms (1).

In mammals, these molecules are produced by the thyroid gland as thyroid hormones (THs), namely thyroxine (T4), and 3, 3',5-Triiodo-L-thyronine (T3), comprising major and minor portions of circulating THs, respectively (1,2). From circulation, THs are actively transported to target tissues where enzymes called deiodinases modulate THs signalling by increasing or decreasing intracellular T3 levels through iodine removal or position change in the tyrosine scaffold. Deiodinase type II increases hormonal signalling by converting T4 into T3. On the other hand, deiodinase type III reduces signalling by deactivating T3 into T2 or reverse T3 (3–5). T3 binds to specific receptors (alpha and beta isoforms), which subsequently triggers gene transcription modulation throughout the receptor's binding as dimers to specific DNA sequences called THREs (thyroid hormone responsive element). Alternatively, T3 can also exert immediate biological effects upon binding to the mentioned receptors throughout kinase activity (non-genomic effects) (6–8). The T3 mechanisms of action provide a broad range of biological effects that can be verified early on the embryonic stage controlling differentiation, maturation, growth, and postnatal maintenance of homeostasis and metabolism of several organs/tissues, such as brain, white and brown adipose tissues, bone and skeletal muscle (5,9).

Like THs, a rudimentary muscular system can be found early in animals' evolutionary history (10,11). Initially, the skeletal muscle allowed complex environmental exploration then, further specialisations linked muscle to the organism's nutritional, thermal, and immunological aspects (12,13). Thus, more recently in evolutionary history, enhanced adaptability to the surroundings is ensured since skeletal muscle can change its morphological and biochemical features following external cues, such as load status, nutritional needs, and hormonal signalling (12,14,15).

Protein turnover is the primary mechanism of adjusting both muscle mass/fibre size and function. In response to increased mechanical load, abundant nutrient availability, and anabolic hormonal signalling, a *de novo* synthesis branch led by the mechanistic target of rapamycin kinase (mTOR) pathway increases the bulk of proteins resulting in hypertrophy and consequently gain of function. In opposition, an atrophic program marked by the loss of organelles and increased protein degradation mainly by the ubiquitin-proteasome system (UPS) starts when load stimuli are absent or significantly decreased, nutrients are limited, and catabolic hormonal signalling is present (16-18). However, additional layers were added over this simplified characterisation. For instance, the mTOR pathway can be related to sarcopenic conditions in ageing, in which UPS generates free amino acids triggering mTOR, and the known negative regulator of muscle mass, myostatin, has a role in both atrophy and hypertrophy conditionally to its downstream pathways (16–18).

Not surprisingly, pathological alterations in TH levels can severely change skeletal muscle phenotype. Increased THs signalling involves skeletal muscle fibre atrophy accompanied by force weakening, increased fatigability and even sarcomere disarray at more prolonged periods. Although downstream activation of the UPS system has been

recognised as a central mechanism involved in T3 atrophy, the underlying upstream mechanisms of this hormone, including protein synthesis, have remained elusive (5,19–23).

Thus, we hypothesised that mTOR signalling inhibition along experimental hyperthyroidism would negatively impact protein turnover leading to skeletal muscle atrophy. Herein, we investigated the effects of elevated levels of T3 upon the protein synthesis pathway in the rat soleus muscle. First, investigating global expression data, we identified rapid and progressive downregulation in the regulatory associated protein of mTOR (*Rptor*), a gene encoding a complex 1 (mTORC1) subunit linked to the maintenance of the protein synthesis bulk (17,18,24).

After validation, we verified no THR_s in the *Rptor* promoter region, indicating indirect T3 action by correlated responsive components. In this sense, the myostatin pathway caught our attention due to its responsiveness to T3 and inhibitory effect upon mTOR (24–27). Thus, we further hypothesised that increased T3 levels impair mTOR function through *Rptor* downregulation throughout a mechanism comprising the myostatin pathway. In this sense, we showed that myostatin is essential to T3-induced downregulation of *Rptor* and myotube size *in vitro*. Furthermore, we demonstrated that the inhibitory effect of T3 upon *Rptor* led to weak changes in the activity of mTOR *in vivo*. Surprisingly, we verified that T3 stimulates overall protein synthesis regardless of mTOR activation. Finally, we showed that myostatin knockdown or RTPR overexpression can block T3-induced atrophy *in vivo*.

3.2.2. *Materials and Methods*

The study followed the ethical principles in animal research adopted by the Brazilian College of Animals Experimentation (COBEA) under #04/2016 approval from the Institute of Biomedical Sciences/University of São Paulo Ethics Committee on Animal Research.

3.2.2.1. Experimental hyperthyroidism in a rat model

Male Wistar rats (~ 8 weeks old) were obtained from Central Bioterium at the University of São Paulo and housed at the Department of Anatomy Bioterium. The animals were kept in controlled rooms (24°C; 12 hours light/dark cycle), in standard plastic cages lined with sawdust, and free access to chow (Nuvilab CR-1, Nuvital-Quimitia, Brazil) and water. Experimental hyperthyroidism was induced by daily intraperitoneal injections of 3, 3',5-Triiodo-L-thyronine (Sigma-Aldrich, #T2877, Germany, 0.6 µg Kg⁻¹) in-vehicle solution (0.9%NaCl, 40 mM NaOH), following the randomised groups: (1) control (CTR; vehicle injection for 7 or 14 days), T3 treated for (2) 12 hours (T3 0.5), (3) 24 hours (T3 1d), (4) seven days (T3 7d) and (5) fourteen days (T3 14d). At the end of treatment, animals were anaesthetised by isoflurane 5% and euthanised by decapitation.

3.2.2.2. Biological samples

From the animals, the collected blood (~10 ml) was placed on ice for 60 minutes, and then serum was dissociated from the clot by centrifugation (5.000 rpm; 30 minutes). Then, the heart was removed and weighed. Moreover, the soleus muscle was dissected, weighed, and transversely sectioned. The proximal section was snap-frozen in liquid

nitrogen, the distal section was immersed in liquid nitrogen-cooled isopentane for 1 minute before being frozen in liquid nitrogen. Lastly, the samples were stored at a -80 °C freezer until further analysis.

3.2.2.3. Thyroxin (T4) serum levels

According to the manufacturer's standard protocol, total thyroxin (T4) levels were quantified from serum by an immunoassay (Arbor Assays, #K050, USA).

3.2.2.4. Skeletal muscle transfection in vivo

For the procedure of plasmid delivery into the muscle via electroporation, the animals were anaesthetised intraperitoneally with a mixture of ketamine hydrochloride and xylazine (30mg kg⁻¹ and 100mg/kg, respectively). A small incision was made in the lateral region of the paw, sufficient to expose the soleus muscle, then applying five injections (5µl each, 0.4U µl⁻¹) of hyaluronidase (Sigma-Aldrich, #H3506, Germany) directly into the muscle. After 30 minutes, the muscles received five injections (5µl each) of each plasmid vector (50µg total). Subsequently, platinum-made electrodes (3x7mm) were placed parallel on opposite sides of the muscle along its long axis. A burst of pulses was delivered (6 pulses of 20 ms with 980 ms pause, 25 V, 5 mm distance between electrodes) by an electric pulse generator (built and calibrated by the Institute of Nuclear Research, Brazil).

3.2.2.5. Plasmid Constructions

The shMSTN plasmid vector was constructed according to the BLOCK-iT™ Pol II miR RNAi Expression Vector Kits manual (Invitrogen, #K4936-00, USA). The following oligonucleotide sequences were hybridised and cloned into the vector pcDNA 6.2-GW/EmGFP-miR: Top strand 5'TGCTGTTCCGTGGTAGCGTGATAATCGTTTTGGCCA CTGACTGACGATTATCACTACCACGGAA3` and Bottom strand 5`CCTGTTCCGTGGT AGTGATAATCGTCAGTCAGTGGCCAAAACGATTATCACGCTACCACGGAAC3`, containing the MSTN mRNA (NM_019151.1) RNAi (underlined). The myc-Raptor was a gift from David Sabatini (Addgene plasmid # 1859 ; <http://n2t.net/addgene:1859> ; RRID:Addgene_1859) (28).

3.2.2.6. Global gene expression

Data from a microarray from soleus muscle tissue from rats treated with T3 (Sigma-Aldrich, #T2877, Germany, 0.6 µg Kg⁻¹) for 0.5, 1, and 7 days performed previously by Ramos and collaborators (29) were filtered for mTOR pathway components and summarised on a heatmap.

3.2.2.7. Gene expression by Real-Time PCR

Fragments of the soleus muscle (~20 mg) were solubilised in TRIzol reagent (Life Technologies, #15596026, USA) by a polytron homogeniser, further total RNA isolation, and precipitation according to the manufacturer's recommendations. Subsequently, total RNA pellets were solubilised in ultrapure water, nucleic acid concentration and purity were measured on NanoDrop 1000 (Thermo-Fisher, #ND-1000, USA). Complementary DNA

was synthesised from total RNA (2 µg) using M-MLV enzyme (Promega, #M170, USA) into a reverse transcriptase reaction (50 mM Tris-HCl – pH 8.3, 7 mM MgCl₂, 40 mM KCl, 10mM DTT, 0.1 mg ml⁻¹ BSA, 0.5 mM [3H]dTTP, 0.025 mM oligo(dT), 0.25 mM poly(A), 0.01% NP-40) performed in a temperature cycle (5 minutes at 75°C then, 60 minutes at 37 °C). Finally, gene expression was accessed using equal amounts of complementary DNA in a real-time PCR reaction, comprising EvaGreen qPCR mix (Solis BioDyne, #08-36-0020, Estonia) and a specific set of primers (200nM). The reaction was set up following forty temperature cycles (15 seconds at 95°C, 30 seconds at 60°C and, 30 seconds at 72°C) in a Corbett RotorGene 6000 (Qiagen, #9001861, Germany). Fluorescence cycle threshold (Ct) was used to calculate genes relative expression abiding $\Delta\Delta\text{CT}$ method (30). All Ct values were normalised to peptidylprolyl isomerase A (*Ppia*). The primer set was both designed on Primer-Blast or previously described in the literature. Either forward or reverse sequences spans exon-exon junctions (Table I).

Table I - Primer sets used in real-time PCR (RT-PCR)

Primers	NCBI Gene ID	Forward	Reverse
Myostatin	29152	ACCCATGAAAGACGGTACAAG	TCATCACAGTCAAGCCCAAAG
Rptor	287871	CCTGATGGAGTCGGAGATGC	TCATCCGATCCTTCATTCTC
Ppia	25518	TATCTGCACTGCCAAGACTGAGTG	CTTCTTGCTGGTCTTGCCATTCC

3.2.2.8. Protein level by Western Blotting

Fragments of the soleus muscle (~20mg) were powdered in nitrogen-cold steel mortar then solubilised in radioimmunoprecipitation assay buffer (RIPA) (1 mM EDTA, pH 7.4, 0.0625% sodium deoxycholate, 0.0625% nonidet P-40, 6.2 mM sodium phosphate), including phosphatase inhibitor cocktail (1:100; Thermo-Scientific, #78447, USA), homogenates were centrifuged (10 minutes at 1000 x g at 4°C), and insoluble material was discarded. The homogenate concentrations were measured by Bradford assay (Bio-Rad, #5000006, USA) to ensure protein loading equally. Initially, an equal mass of total homogenate was loaded into SDS-PAGE gels following electrophoreses and transferred to a PVDF membrane (Thermo-Scientific, #88518, USA) to verify the specific proteins' relative levels. Then, membranes were incubated in blocking solution (tris-buffered saline with 5% BSA, 0.5 M NaCl, 50 mM tris-HCl pH 7.4 with 0.1% Tween-20 – TBST) for 1 hour at room temperature proceeding to overnight incubation in primary antibody solution at 4 °C. After 15-minutes of washing in TBST, the secondary antibody solution was incubated for 1 hour at room temperature. Finally, the NBT/BCIP (Sigma Aldrich, #B1911, USA) method detected blotted proteins and then quantified by Vision-Capt software (Vilber Lourmart, France). Primary antibodies were myostatin (MSTN, #19142-1-AP, 1µg/mL; Proteintech), glyceraldehyde-3-phosphate dehydrogenase (GAPDH, #PA1-987, 1µg/mL; Thermo Fisher), phosphatidylinositol-4,5-bisphosphate 3-kinase, catalytic subunit alpha (PI3Kca, 1µg/mL; #4255; Cell Signaling), mechanistic target of rapamycin kinase (mTOR, 1µg/mL; #2972; Cell Signaling), phosphorylated mTOR (p-mTOR, 2µg/mL; #2971; Cell Signaling), ribosomal protein S6 kinase (RPS6KB1/P70S6K, 1µg/mL; #9202; Cell Signaling), phosphorylated P70S6K (p-P70S6K, 2µg/mL; cat#9205; Cell Signaling) and alpha-tubulin (TUBA1B, #2125S, 1µg/mL; Cell Signaling). Secondary antibodies were

rabbit anti-mouse immunoglobulin/AP (polyclonal, 1 µg/mL; #D0314, Dako) and goat anti-rabbit immunoglobulin/AP (polyclonal, 1 µg/mL; #D0487, Dako).

3.2.2.9. Histological analysis and immunofluorescence

Cryopreserved samples were sectioned in a cryostat (Leica, #CM3050, Germany), then the 10 µm cross-sections were stained by Hematoxylin (Amresco, #0701, USA) and Eosin (Amresco, #0109, USA). For fibre typing and cross-section area measurements, immunofluorescence was used to detect myosin heavy chain (MHC) type I (1:250, Sigma-Aldrich, #M8421, Germany), type II (1:250, Sigma-Aldrich, #M4276, Germany), and laminin (1:1000, Sigma-Aldrich, #L9393, Germany). First, soleus muscle sections were fixed in acetone (10 minutes at -20°C), washed in TBS with 0.3% Triton x-100 (three 5-minutes rounds), and incubated in blocking solution (1% BSA in TBS+0.3% Triton x-100) for 1 hour at room temperature. After overnight incubation in primary antibody, slides were washed (three 5-minutes rounds), incubated in secondary antibody solution for 1 hour at room temperature, washed again (three 5-minutes rounds), and mounted in mounting media with 4',6-diamidino-2-phenylindole (Vector Laboratories, #H-1200, USA) under coverslips. Finally, pictures were acquired under a light microscope for H/E staining (Carl Zeiss Microscopy, Axio Scope.A1, Germany) and fluorescence microscope for MHC localisation (Carl Zeiss Microscopy, Axio Scope.A1, Germany). SMAD3 nuclear colocalisation imaging throughout the Z-axis was performed at a confocal microscope (Carl Zeiss Microscopy, LSM 780-NLO, Germany). Fibre cross-sectional area and MHC type proportions were measured on ImageJ software (version 2.0; NIH).

3.2.2.10. Cell Culture of Myoblasts and RNAi transfection

Muscle-derived C2C12 (ATCC, CRL-1772, USA) myoblasts were differentiated and maintained as described in Ramos and collaborators (29). Then, two days after the onset of differentiation, cells were transfected with 30nM of scrambled (Ambion, #AM4511, USA) and Myostatin (Ambion, S70075, USA) siRNAs for 12 hours using lipofectamine 2000 (Invitrogen, #LF2000, USA) following the manufacturer instructions.

3.2.2.11. Statistical analysis

Results are reported as means \pm SD. Statistical analysis was performed using t-test or Mann Whitney, and Kruskal-Wallis or ANOVA followed by Tukey post-test analysis as appropriate. $p < 0.05$ was considered statistically significant.

3.2.3. Results

3.2.3.1. Effects of supraphysiological T3 dose upon biometric features

Consistent with previous studies, thyroid hormone treatment produced changes in whole-body attributes (Table II). Overall, T3 treatment for seven and fourteen days led to reduced body weight (7 days: ~10%; 14 days: ~13%), soleus muscle atrophy (7 days: ~18%; 14 days: ~23%), and cardiac hypertrophy (7 days: ~22%; 14 days: ~23%). Accordingly, muscle and heart mass normalised by nose-to-anus length showed significant low (7 days: ~18%; 14 days: ~27%) and high (7 days: ~22%; 14 days: ~21%) ratios, respectively. Furthermore, plasma levels of T4 declined progressively after one day of T3 stimulation, reaching the lowest levels after seven and fourteen days (1 day: ~38%;

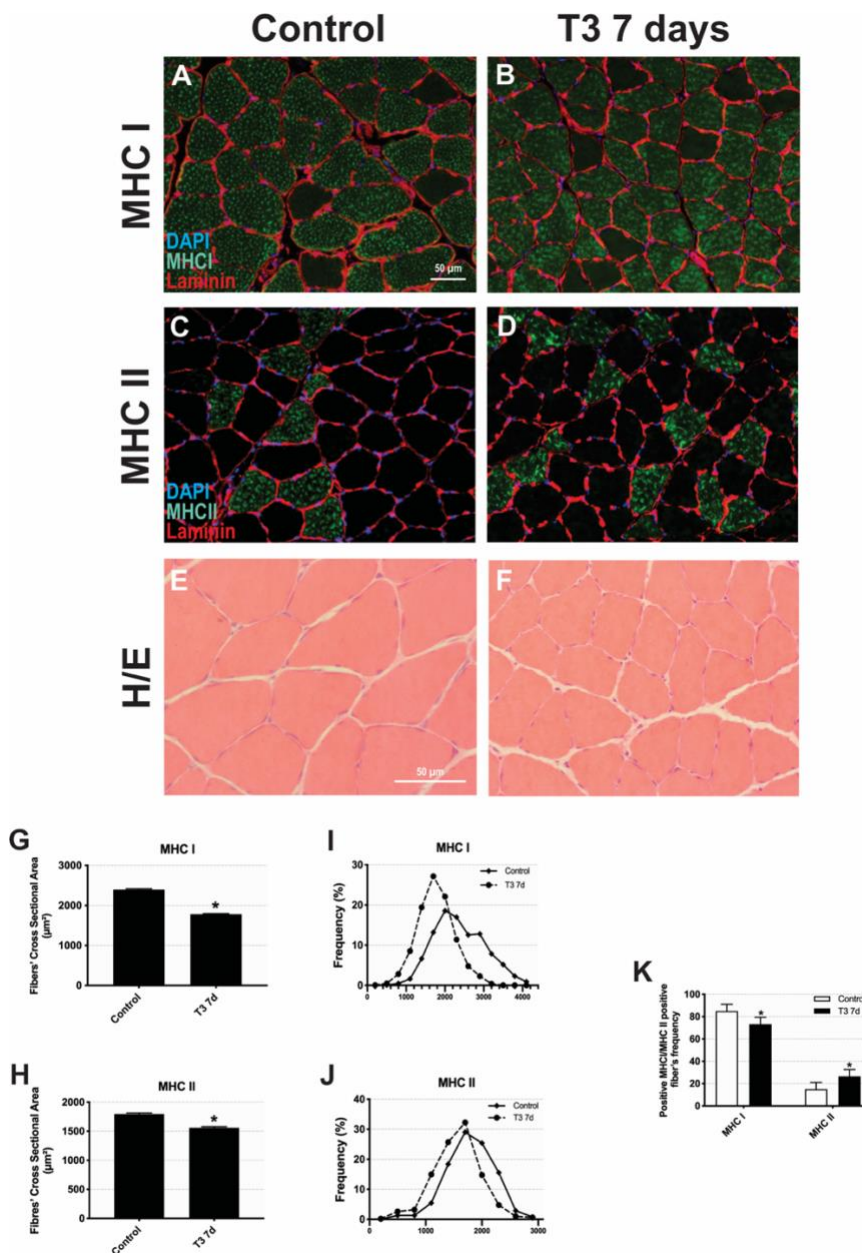
7 days: ~87%; 14 days: ~84%). We conclude that typical hallmarks of T3-induced atrophy were established on the 7th and 14th days of experimental hyperthyroidism.

Table II: Biometric measurements of nose-to-anus length (NAL), bodyweight (BW), heart weight (HW), soleus muscle weight (MW), HW/NAL ratio, MW/NAL ratio, and free T4 from T3 treated rats for 12 hours (T3 0.5d), 24 hours (T3 1d), 7 days (T3 7d), 14 days (T3 14d), and their respective controls.

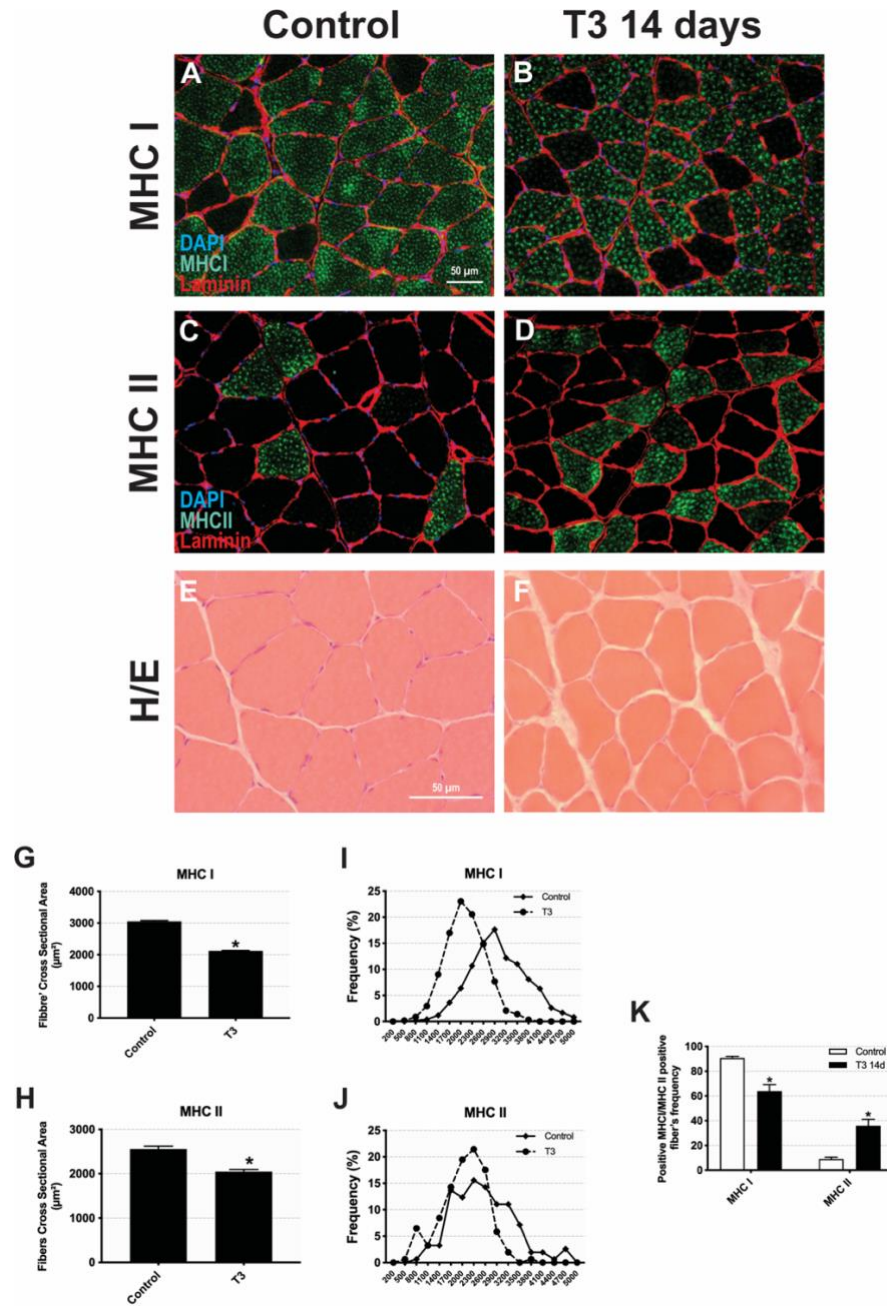
Groups	NAL (cm)	BW (g)	HW (mg)	MW (mg)	HW/NAL (mg/cm)	MW/NAL (mg/cm)	T4 (nmol/L)
Control (n=5)	21.62 ± 0.41	254.8 ± 22.70	790.62 ± 64.35	108.07 ± 9.72	36.56 ± 2.72	5.00 ± 0.39	51.81 ± 10.25
T3 0.5d (n=5)	21.7 ± 0.76	248.56 ± 20.36	843.47 ± 54.58	98.99 ± 10.67	38.85 ± 1.64	4.57 ± 0.54	39.98 ± 5.32
T3 1d (n=5)	21.30 ± 0.67	260.72 ± 21.91	845.79 ± 77.14	112.27 ± 10.92	39.71 ± 3.35	5.27 ± 0.41	32.07 ± 7.30*
Control (n=10)	23.56 ± 0.68	352.18 ± 37.78	1108.63 ± 140.78	142.22 ± 19.23	47.14 ± 6.59	6.03 ± 0.75	57.43 ± 2.61
T3 7d (n=10)	23.45 ± 1.48	314.84 ± 27.62*	1350.30 ± 204.10*	117.07 ± 24.05*	57.68 ± 7.30*	4.97 ± 0.82*	7.40 ± 1.09*
Control (n=10)	23.01 ± 1.25	369.73 ± 58.96	966.88 ± 179.69	153.03 ± 32.49	40.93 ± 8.54	6.71 ± 1.72	57.95 ± 3.28
T3 14d (n=9)	24.11 ± 1.38	320.90 ± 28.65*	1192.79 ± 193.60*	118.40 ± 23.59*	49.48 ± 7.74*	4.91 ± 0.91*	9.38 ± 2.40*

Centimeter (cm); gram (g); milligram (mg); nanomolar per liter (nmol L⁻¹)
Data are show as means ± standart deviation. * p< 0.05 v. Control

Considering that atrophy was obtained after seven and fourteen days of T3 treatment, we investigated soleus muscle myofiber's area and metabolic properties at these time points (Figures 1 and 2). As expected, we verified an overall decrease in muscle fibres' cross-sectional area (CSA) after T3 treatment. Interestingly, the CSA reduction was accentuated in the slow-twitch fibres at the seven-day (MHC I: ~26%; MHC II: ~13%) and fourteen-day time-points (MHC I: ~ 31%; MHC II: ~20%; Figures 1G-J and 2G-J). Additionally, experimental hyperthyroidism induced a slow-to-fast twitch conversion phenotype (Figures 1A-F,K and 2A-F,K), with a significant reduction in MCH I positive fibres (7 days: ~12%; 14 days: ~ 27%) and augmented MHC II labelling (7 days: ~12%; 14 days: ~27%).



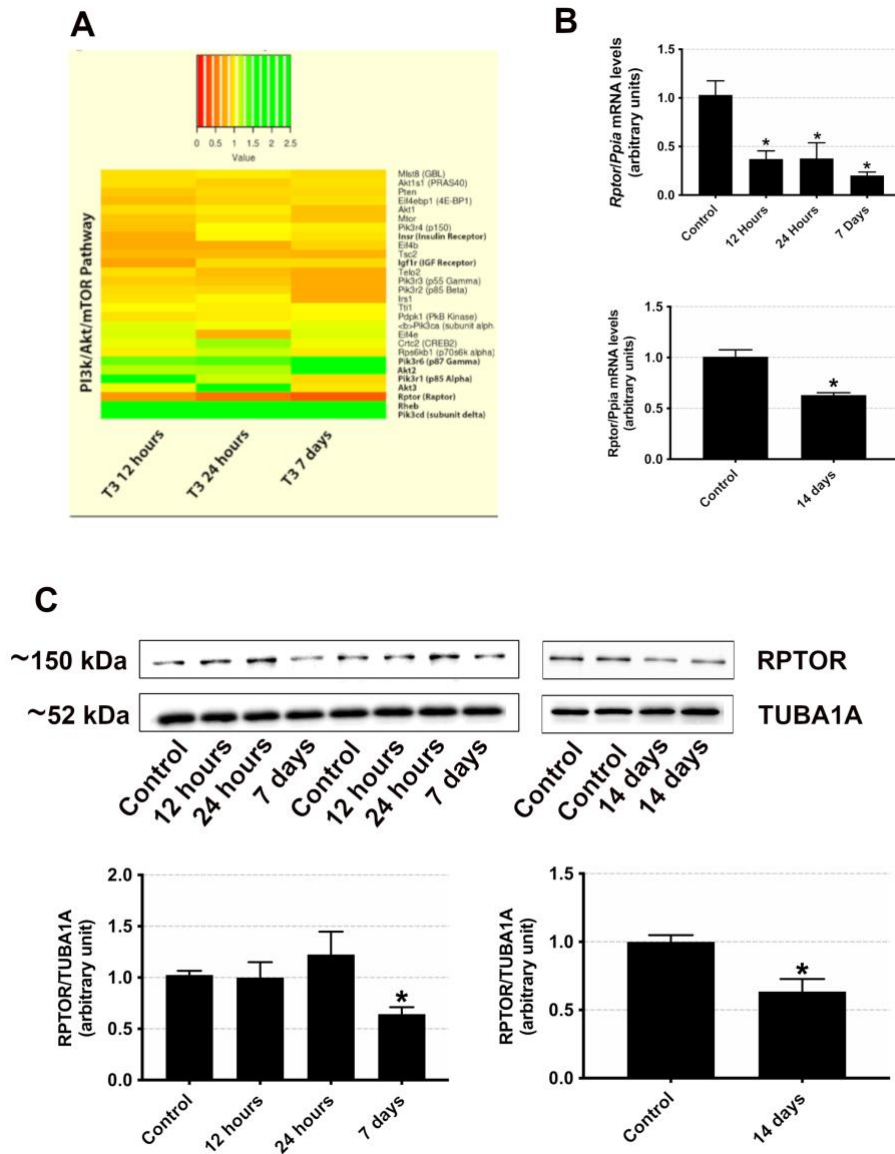
Artigo 2 Figure 1: T3 supraphysiological injections for seven days resulted in decreased fibre's cross-sectional area and slow-to-fast type switch in the soleus muscle of rats. (A-B) Soleus muscle cross-section photomicrographs (n=5 per group, 200x magnification) depicting myosin heavy chain type I labelled fibres (MHC I, green) outlined by laminin labelling (red). (C-D) Soleus muscle cross-section photomicrographs (n=5 per group, 200x magnification) depicting myosin heavy chain type II labelled fibres (MHC II, green) outlined by laminin labelling (red). (E-F) Soleus muscle cross-section photomicrographs stained by haematoxylin and eosin (n=5, 400x magnification). (G) MHC I positive fibres' cross-section area (µm²; n= ~1500 fibres per group). (H) MHC II positive fibres' cross-section area (µm²; n= ~500 fibres per group). (I) MHC I positive fibres' cross-section area frequency distribution. (J) MHC II positive fibres' cross-section area frequency distribution. (K) Frequency of MHC I and MHC II positive fibres. All results are shown as means ± SD. Mann Whitney test was applied to verify differences among the groups. * p<0.05 versus the control group.



Artigo 2 Figure 2: T3 supraphysiological injections for fourteen days resulted in decreased fibre's cross-sectional area and slow-to-fast type switch in the soleus muscle of rats. (A-B) Soleus muscle cross-section photomicrographs (n=5 per group, 200x magnification) depicting myosin heavy chain type I labelled fibres (MHC I, green) outlined by laminin labelling (red). (C-D) Soleus muscle cross-section photomicrographs (n=5 per group, 200x magnification) depicting myosin heavy chain type II labelled fibres (MHCII, green) outlined by laminin labelling (red). Soleus muscle cross-section photomicrographs stained by haematoxylin and eosin (n=5, 400x magnification). (G) MHC I positive fibres' cross-section area (μm^2 ; n= ~1500 fibres per group). (H) MHC II positive fibres' cross-section area (μm^2 ; n= ~500 fibres per group). (I) MHC I positive fibres' cross-section area frequency distribution. (J) MHC II positive fibres' cross-section area frequency distribution. (K) Frequency of MHC I and MHC II positive fibres. All results are shown as means \pm SD. Mann Whitney test was applied to verify differences among the groups. * $p < 0.05$ versus the control group.

3.2.3.2. Global gene expression analysis of mTOR components

Analysing a microarray, we previously showed that T3 injections up-regulate several E3 ubiquitin-ligases, possibly increasing the protein breakdown ratio. However, investigating the underlying mechanisms on MDM2 E3 ubiquitin-ligase unveiled an active T3-induced pro-trophic mechanism (29). Therefore, in the present study, we explored a previously published microarray focusing on mTOR-related genes' regulation throughout the onset of the experimental hyperthyroidism (12 hours, 24 hours, and 7 days). *Rptor*'s fast and robust down-regulation (12 hours: ~37%; 24 hours: ~52%; 7 days: ~61%) stood out in the compared transcriptomes, consistent with its prominent role in mTORC1 complex functionality (Figure 3A).

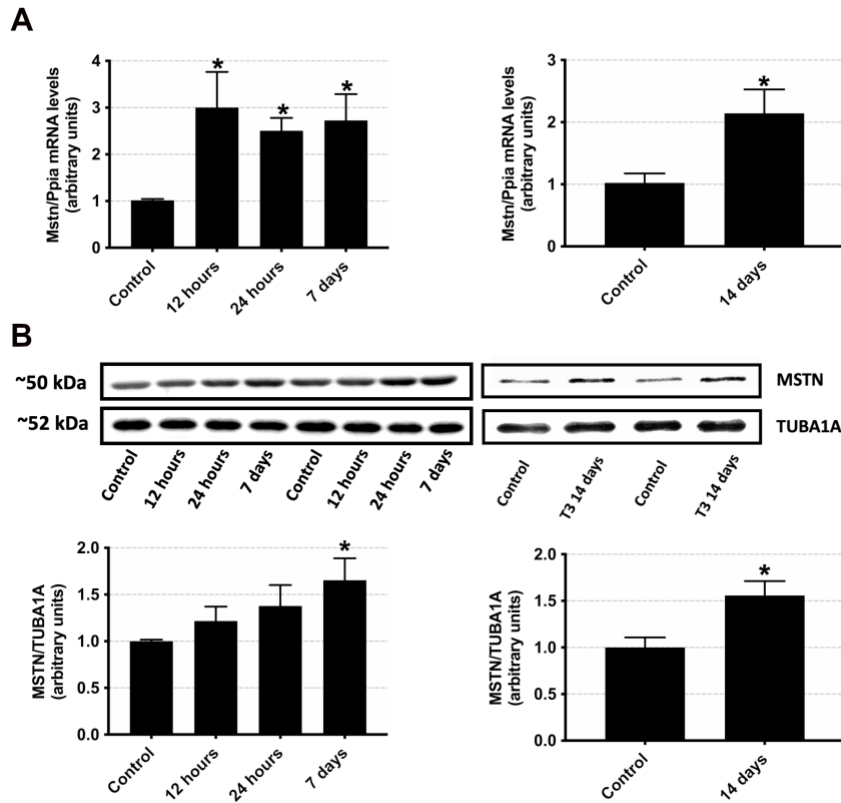


Artigo 2 Figure 3: Rptor gene expression and protein levels were downregulated during experimental hyperthyroidism on the soleus muscle of rats. (A) Global gene expression of mTOR components up-regulated (green) or down-regulated (red) are represented in a heat map. Gene names in bold highlight significant changes from the control group (fold change ~40%). (B) Rptor expression was analysed by real-time PCR in the groups treated for twelve hours, twenty-four hours, and seven days (top; n=5) or fourteen days (bottom; n=4). Rptor values were normalised by Ppia expression (C) Western blot analysis of RPTOR protein levels in the groups treated for twelve hours, twenty-four hours, and seven days (top left; n=5) or fourteen days (top right; n=8). Densitometric analysis of RPTOR fold change from the groups treated for twelve hours, twenty-four hours, and seven days (bottom left) or fourteen days (bottom right) were normalised by TUBA1A levels. Values are expressed as means \pm SD. T-test was applied to verify differences among two groups. On the other hand, two-way ANOVA followed by Tukey's post hoc test was used to evaluate more than two groups. * $p < 0.05$ versus control group.

3.2.3.3. T3 inhibits Raptor and promotes Myostatin expression

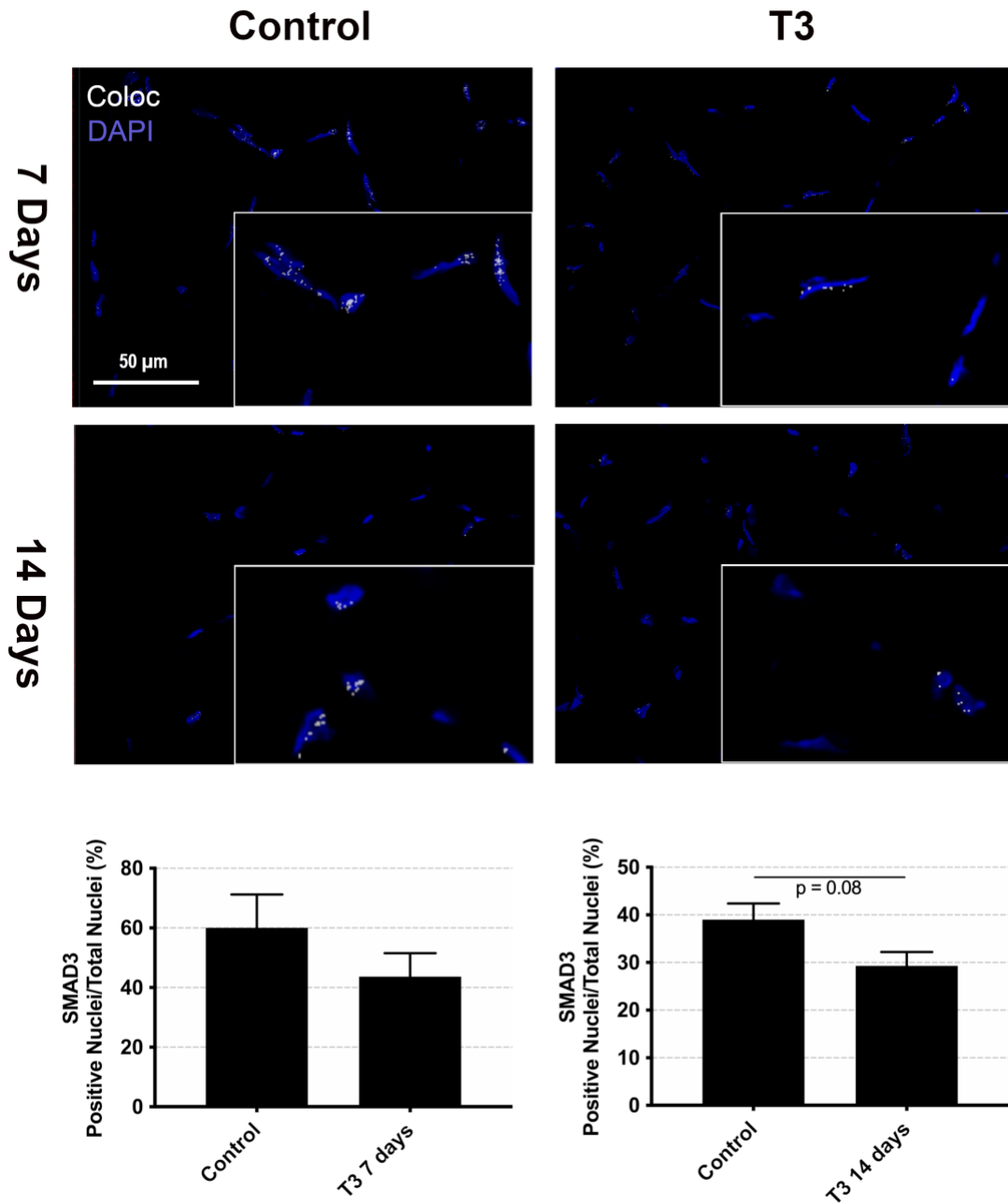
By real-time reverse transcription-polymerase chain reaction (RT-qPCR), we confirmed *Raptor* reduced gene expression (Figure 3B) after T3 treatment for twelve hours, twenty-four hours, seven days, and fourteen days (~0.4 fold, ~0.4 fold, ~0.2 fold, and ~0.6 fold, respectively). The impact upon protein levels was significant after seven days (~0.6 fold) and fourteen days (~0.6 fold) of T3 treatment (Figure 3C).

Since we could not find T3 responsive elements on the *Raptor* promoter region by *in silico* evaluation (data not shown), and previous work has not found such elements in *Raptor* promoter (31), we hypothesised that T3 might induce *Raptor* downregulation indirectly. Therefore, we explored myostatin (*Mstn*) because the *Mstn* promoter is responsive to T3 and can lead to *Raptor* regulation (27). Indeed, *Mstn* expression (Figure 4A) was swiftly and strongly up-regulated by T3 in all-time points analysed (12 hours: ~3 fold, 24 hours: ~2.5 fold, 7 days: ~2.7 fold, 14 days: ~2 fold). Also, MSTN protein levels (Figure 4B) were expressively elevated at 7 (~1.6 fold) and 14-days (~1.5 fold) of T3 treatment.



Artigo 2 Figure 4: Myostatin gene expression and protein levels were upregulated during experimental hyperthyroidism. (A) Myostatin expression was analysed by real-time PCR in groups treated for twelve hours, twenty-four hours, and seven days (left; n=5) or fourteen days (right; n=4). Myostatin values were normalised by Ppia expression. (B) Western blot analysis of myostatin protein levels in the groups treated for twelve hours, twenty-four hours, and seven days (top left; n=5) or fourteen days (top right; n=4). Densitometric analysis of myostatin fold change from the groups treated for twelve hours, twenty-four hours, and seven days (bottom left) or fourteen days (bottom right) were normalised by TUBA1A levels. Values are expressed as means \pm SD. T-test was applied to verify differences among two groups. On the other hand, two-way ANOVA followed by Tukey's post hoc test was used to evaluate more than two groups. * $p < 0.05$ versus control group.

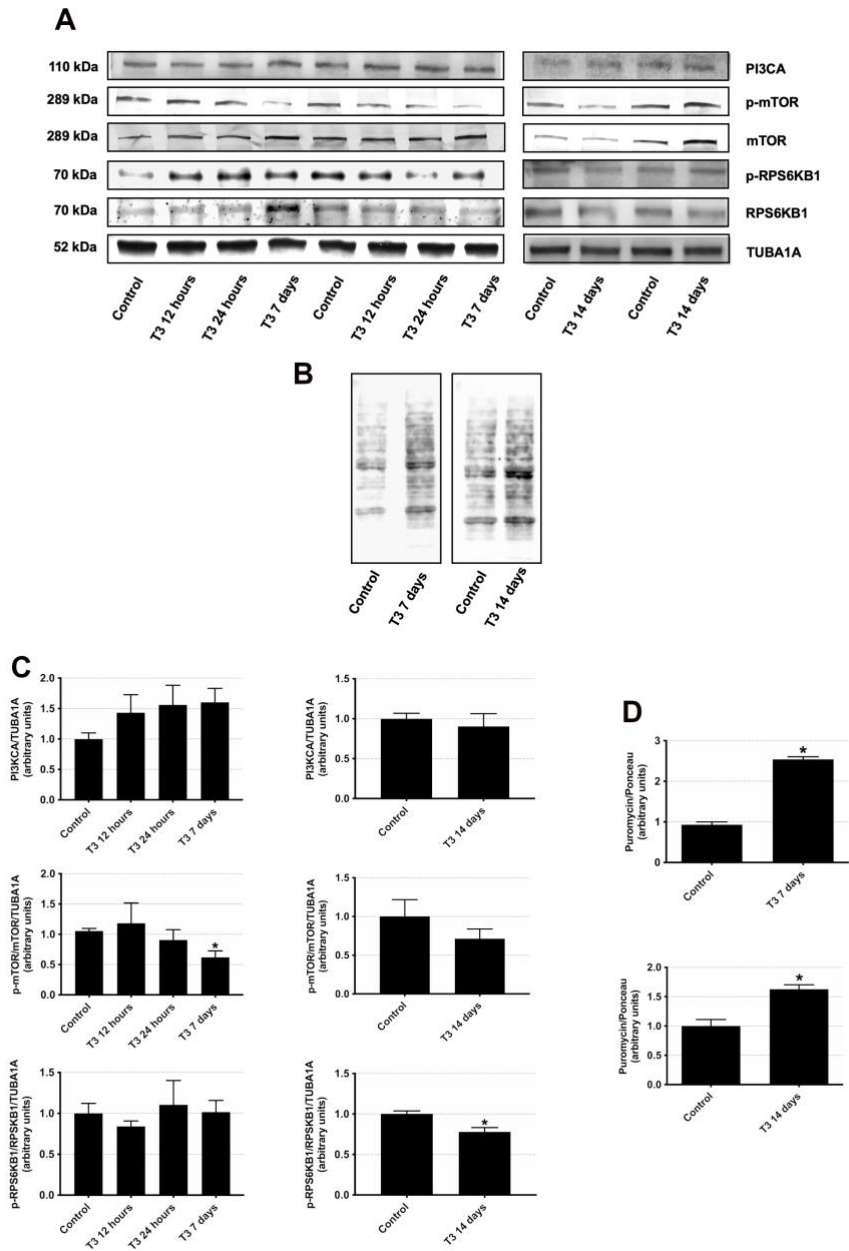
Surprisingly, the elevated MSTN levels we found in skeletal muscle were not accompanied by the SMAD canonical pathway induction. Indeed, we observed that T3 treatment for seven and fourteen days tended to reduce the number of SMAD family member 3 (SMAD3) positive nuclei (7 days: 17%, $p=0.3$; 14 days: 10%, $p=0.08$) when compared to controls (Figure 5).



Artigo 2 Figure 5: SMAD3 nuclei colocalisation inquiry by confocal immunofluorescence analysis. (Top) Representative photomicrographs displaying SMAD3/nuclei colocalisation in soleus muscle from rats seven and fourteen days after T3 injections (400x amplification). DAPI (blue) and SMAD3 colocalisation (white). (Bottom) SMAD3 positive nuclei in soleus muscle of rats treated with T3 for seven days (n=3) or fourteen days (n=4). Values are expressed as means ± SD. Mann Whitney test was applied to verify differences between groups.

3.2.3.4. T3 supraphysiological injections increase de novo protein synthesis despite reduced mTOR phosphorylation

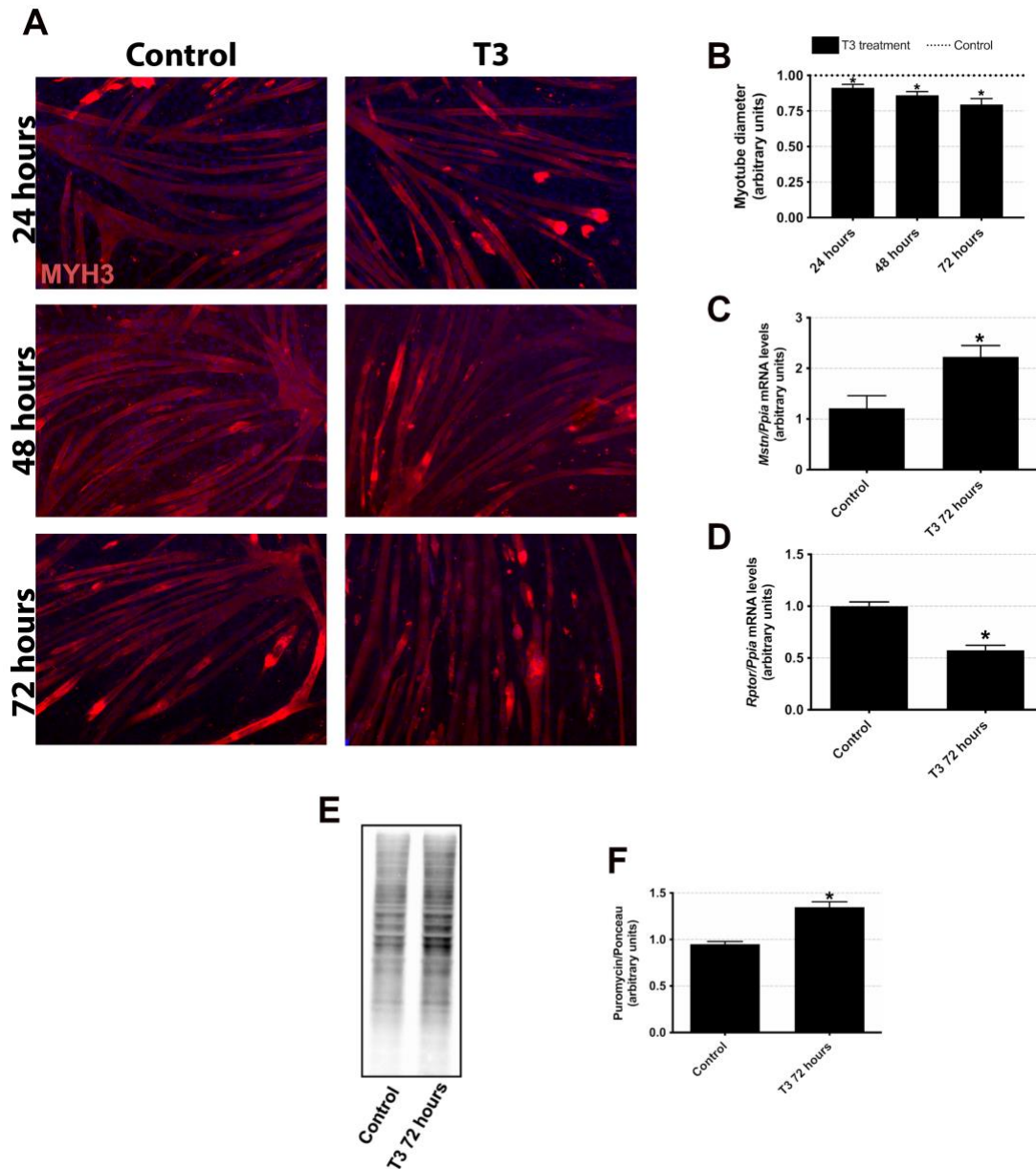
Both RPTOR inhibition and MSTN increase could negatively impact mTORC1 normal function impairing protein synthesis. Thus, we verified the protein levels of PI3KCA, mTOR, phosphorylated-mTOR, RPS6KB1/P70S6K and, phosphorylated-RPS6KB1/P70S6K (Figure 6A,C) along with total *de novo* protein synthesis (Figure 6B,D). In this sense, T3 injections for seven days inhibited mTOR phosphorylation (7 days: ~0.6 fold). A similar result was observed in RPS6KB1 phosphorylation only at the fourteen-day group (14 days: ~0.7 fold). No significant alterations were observed in PI3KCA protein levels. Unexpectedly, experimental hyperthyroidism enhanced *de novo* protein synthesis at seven days and fourteen days treated groups (~ 2.5 fold and ~ 1.6 fold, respectively).



Artigo 2 Figure 6: Protein levels of mTORC1 components during experimental hyperthyroidism. (A) Western blot analysis of PI3KCA, mTOR, phosphorylated-mTOR, RPS6KB1/P70S6K, and phosphorylated-RPS6KB1/P70S6K during experimental hyperthyroidism for twelve hours, twenty-four hours, and seven days (n=5) (right) or 14 days (n=6) (left). (B) Western blot analysis of puromycin incorporation in soleus muscle of rats treated with T3 for seven days (left) or fourteen days (right) (n=3). (C) Densitometric analysis of fold change in PI3KCA, phosphorylated-mTOR and phosphorylated-RPS6KB1/P70S6K at twelve hours, twenty-four hours, seven days (left) and fourteen days (right). (D) Densitometric analysis of fold change in puromycin incorporation in soleus muscle of rats treated with T3 for seven days (top) or fourteen days (bottom). Values were normalised by TUBA1A expression and expressed as mean fold change \pm SD. T-test was applied to verify differences among two groups. On the other hand, two-way ANOVA followed by Tukey's post hoc test was applied to evaluate more than two groups. * $p < 0.05$ versus control.

3.2.3.5. T3 triggers in vivo similar alterations in myotubes from C2C12 lineage

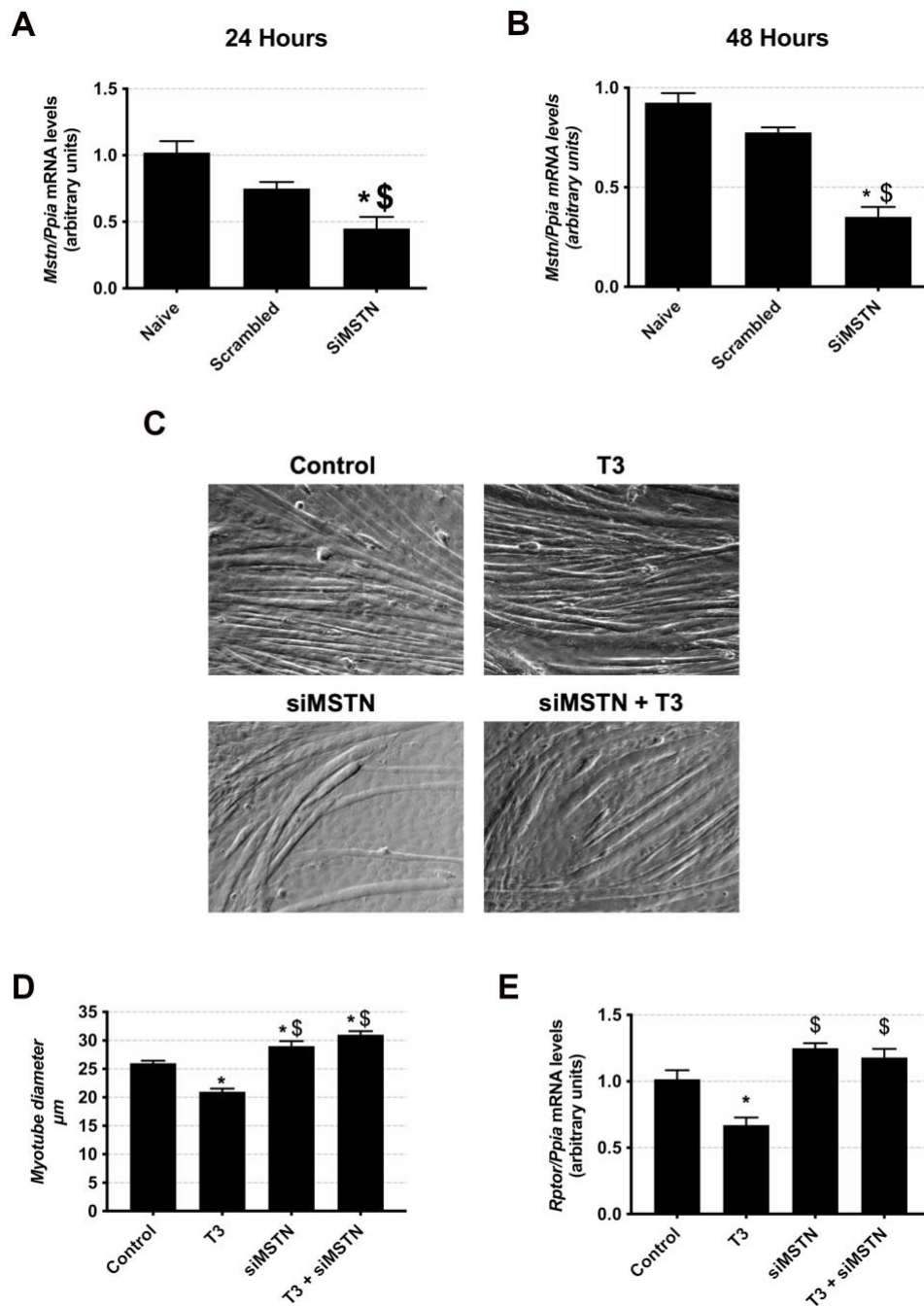
Since experimental hyperthyroidism phenotype leads to multi-organ morphological and functional alterations, the molecular effects in *Rptor*, *Mstn*, and *de novo* protein synthesis could be a counteraction to full body events rather than a direct T3 mechanism within the muscle cell. Hence, we established a supraphysiological T3-level environment in mature myotubes differentiated from C2C12 lineage cells. We found that myotubes diameter promptly decreases upon T3 exposition (Figure 7A, B) with accentuated effects seen after seventy-two hours (24 hours: ~10%, 48 hours: ~15%, 72 hours: ~20%). Therefore, we utilised the seventy-two hours' time-point for downstream analysis. In agreement with the in vivo data, we found that T3 induces *Mstn* (Figure 7C; ~2 fold) and inhibits *Rptor* (Figure 7D, ~0.6 fold) gene expression while stimulates *de novo* protein synthesis (Figure 7E-F; ~1.3 fold).



Artigo 2 Figure 7: Thyroid hormone treatment induces morphological and molecular alterations in mature myotubes. (A) Representative photomicrographs from mature myotubes (embMCH positive) treated with T3 for twenty-four hours (top; n=5), forty-eight hours (middle; n=5) and seventy-two hours (bottom; n=5). (B) Myotubes diameter measurements in arbitrary units (n=90 per group). (C) Myostatin mRNA levels from myotubes treated with T3 for seventy-two hours were analysed by RT-PCR and normalised by Ppia expression. (D) Rptor mRNA levels from myotubes treated with T3 for seventy-two hours were analysed by RT-PCR and normalised by Ppia expression. (E) Western blot analysis of puromycin incorporation in myotubes treated with T3 for seventy-two hours (n=3). (F) Densitometric analysis of fold change in puromycin incorporation levels from the seventy-two hours' time-point. Values are expressed as mean fold change \pm SD. T-test was applied to verify differences among two groups. On the other hand, one-way ANOVA followed by Tukey's post hoc test was applied to evaluate more than two groups. * $p < 0.05$ versus control.

3.2.3.6. Myostatin knockdown protects myotubes from T3 effects in vitro

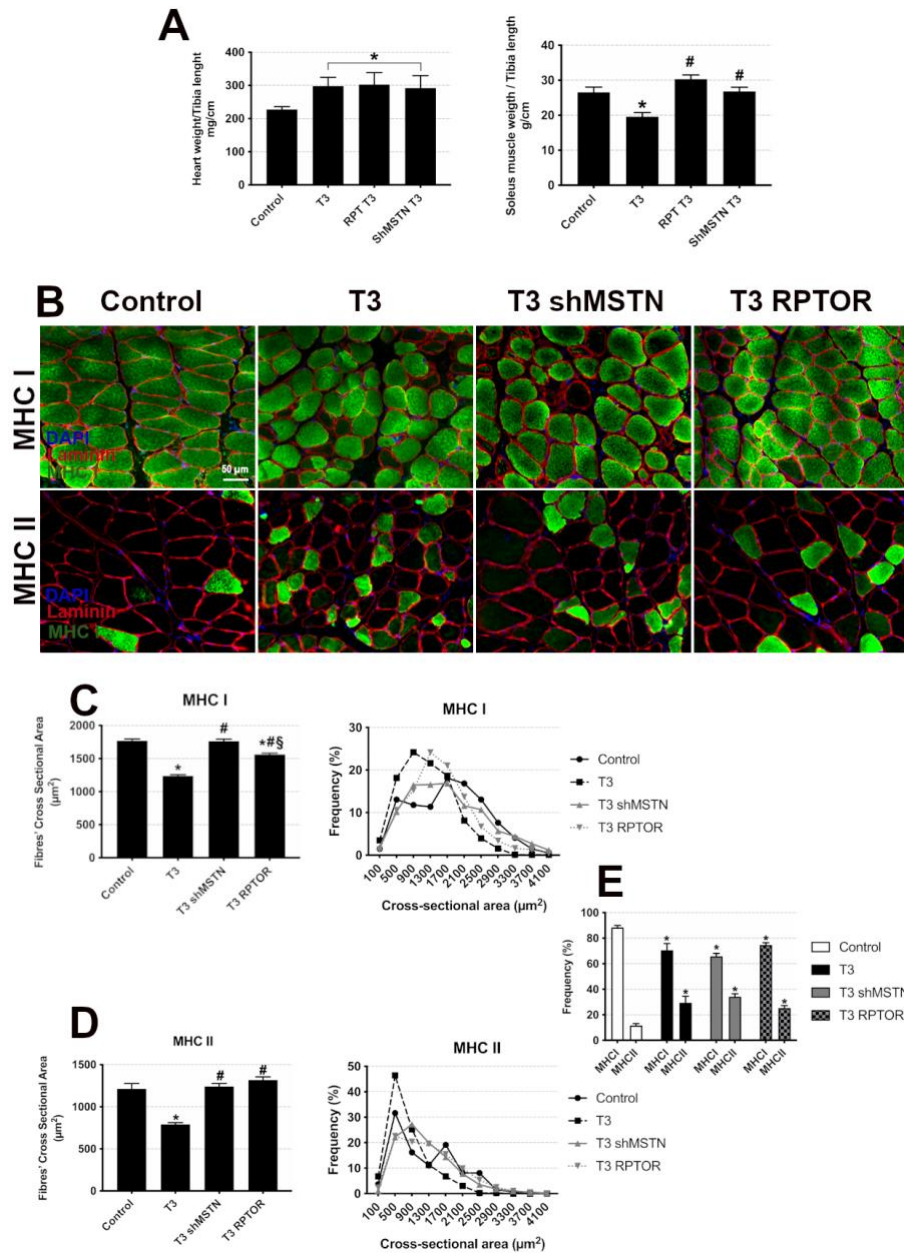
Next, we considered *Mstn*'s role in T3-induced *Rptor* inhibition and myotube size reduction. Accordingly, we knocked down *Mstn* in C2C12 differentiated myotubes (24 hours: ~0.45-fold, 48 hours: ~0.35-fold, Figure 8A,B). Interestingly, *Mstn* knockdown blocked T3 declining effects on myotube size (Control: 26 μ m, T3: 21 μ m, siMSTN: 29 μ m, T3 + siMSTN: 31 μ m, Figure 8C,D) and *Rptor* expression (T3: ~0.7-fold, siMSTN: ~1.2-fold, T3 + siMSTN: ~1.2-fold, Figure 8E).



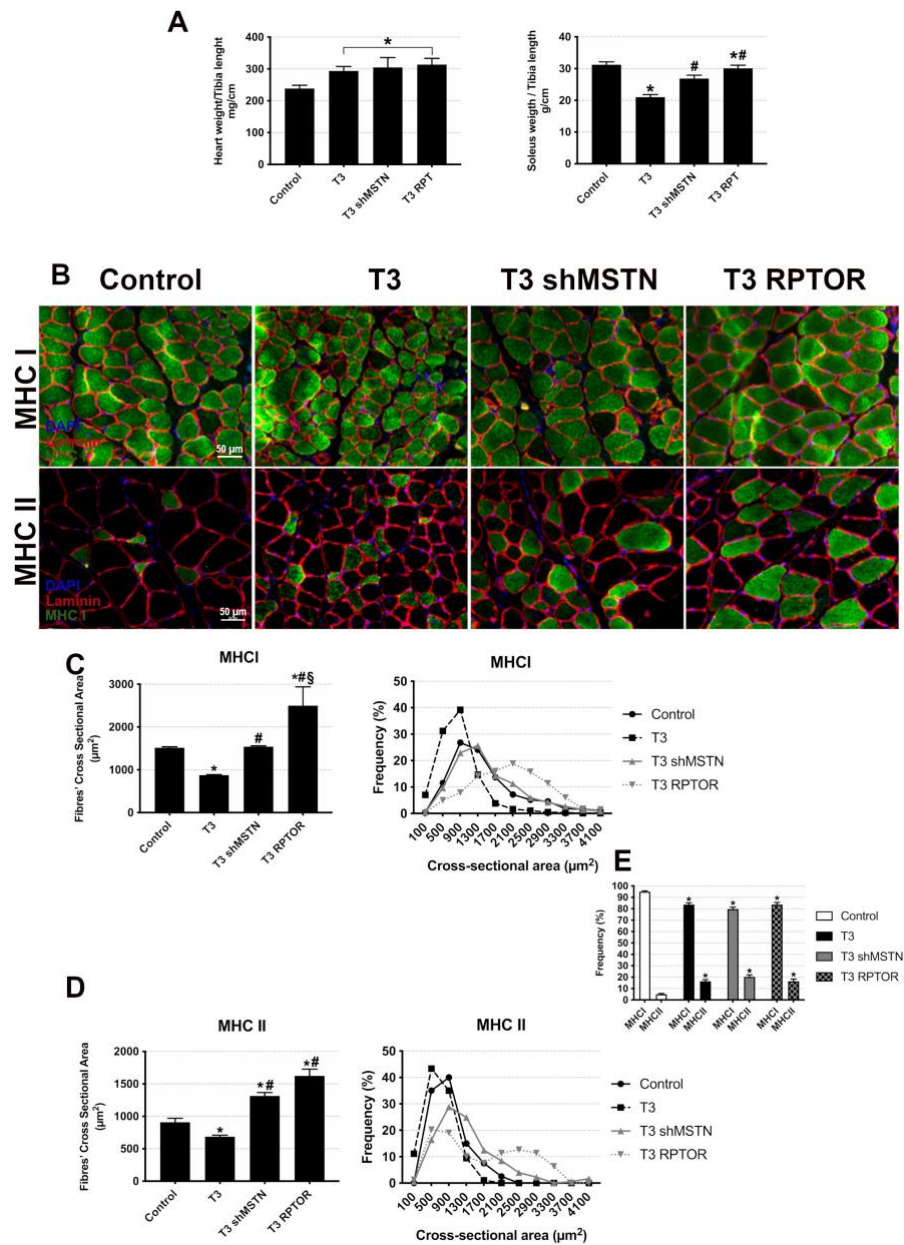
Artigo 2 Figure 8: Myostatin knockdown blocked T3 effects upon myotube size and Rptor gene expression. Myostatin mRNA levels from myotubes treated with scrambled RNA or Myostatin siRNA for twenty-four hours (A; n=5) or forty-eight hours (B; n=5) were evaluated by RT-PCR. (C) Representative photomicrographs from mature myotubes treated with T3 for seventy-two hours with scrambled RNA or myostatin siRNA. (D) Myotubes size measurements in micrometres (n= 60 per group). (E) Rptor mRNA levels from myotubes treated with T3 for seventy-two hours with scrambled RNA or myostatin siRNA were analysed by RT-PCR (n=4). Values are expressed as mean fold change ± SD. One-way ANOVA followed by Tukey's post hoc test was applied to evaluate differences between groups. * p<0.05 versus control or naive groups; § p<0.05 versus T3 or scrambled groups.

3.2.3.7. Myostatin knockdown and Rptor overexpression protects skeletal muscle from T3-induced atrophy

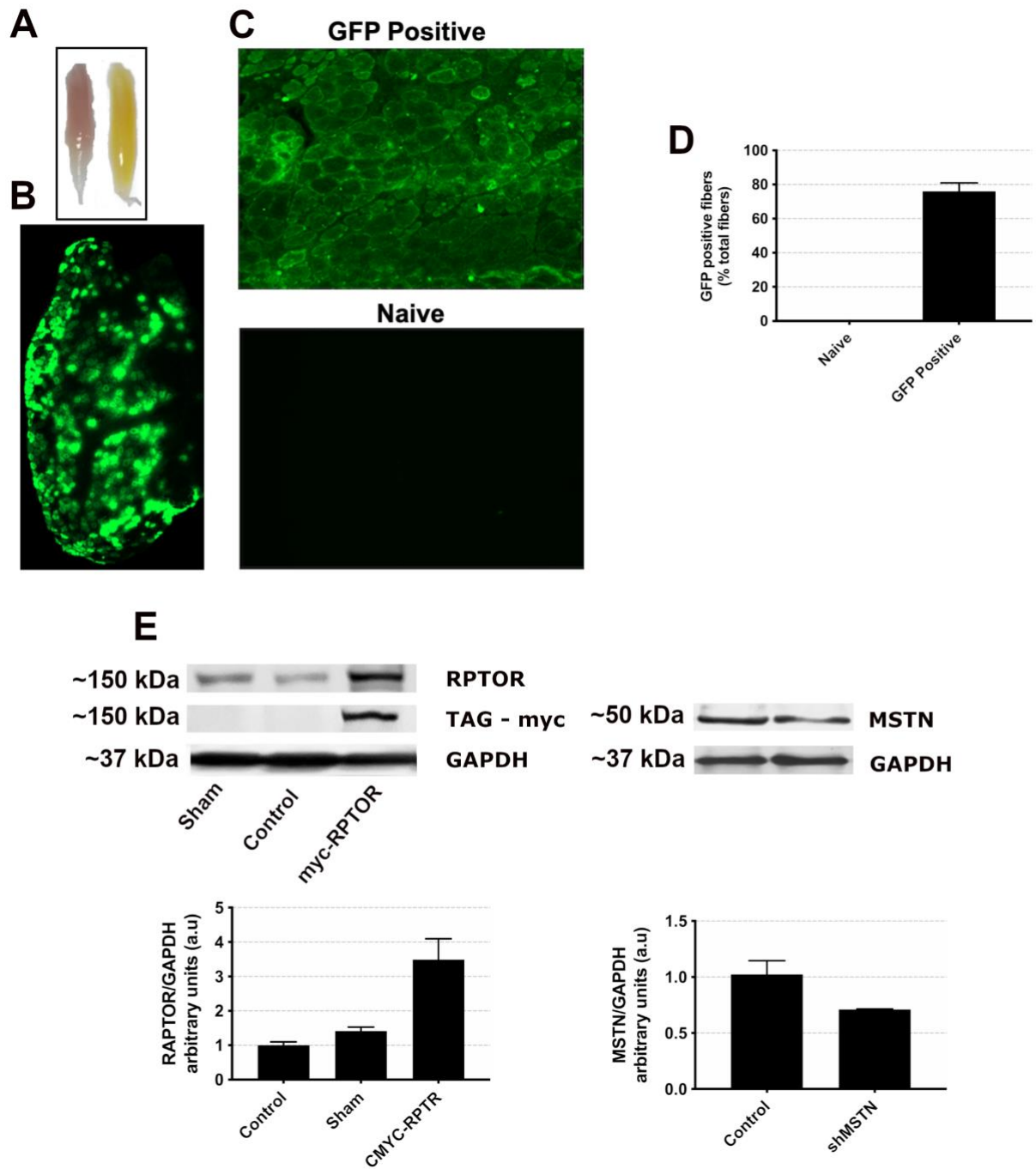
Finally, we tested whether MSTN knockdown or RPTOR overexpression protects skeletal muscle mass from T3-induced atrophy (Figures 9 and 10). We notice that both MSTN knockdown and RPTOR overexpression led to the protection of skeletal muscle mass from T3-induced atrophy for seven (Figure 9A; CTR: 27.16 ± 3.94 g; T3: 19.7 ± 2.78 g; T3 shMSTN: 27.53 ± 2.48 g; T3 RPTOR 27.79 ± 2.24 g) and fourteen days (Figure 10A; CTR: 31.21 ± 2.04 g; T3: 21.03 ± 1.90 g; T3 shMSTN: 26.89 ± 2.58 g; T3 RPTOR 30.11 ± 2.58 g). Similarly, the T3-induced CSA reduction was protected at the seven-day (Figure 9B-D; MHC I - CTR: $1768 \pm 893.8 \mu\text{m}^2$; T3: $1238 \pm 622.4 \mu\text{m}^2$; T3 shMSTN: $1764 \pm 992.1 \mu\text{m}^2$; T3 RPTOR $1562 \pm 761 \mu\text{m}^2$; MHC II CTR: $1213 \pm 730.4 \mu\text{m}^2$; T3: $790.3 \pm 472 \mu\text{m}^2$; T3 shMSTN: $1242 \pm 731.5 \mu\text{m}^2$; T3 RPTOR $1316 \pm 783.2 \mu\text{m}^2$) and fourteen-day (Figure 10B-D; MHC I - CTR: $1515 \pm 915.3 \mu\text{m}^2$; T3: $877.2 \pm 516.1 \mu\text{m}^2$; T3 shMSTN: $1542 \pm 795.1 \mu\text{m}^2$; T3 RPTOR $2498 \pm 15189 \mu\text{m}^2$; MHC II CTR: $725.8 \pm 405.5 \mu\text{m}^2$; T3: $621.6 \pm 348.1 \mu\text{m}^2$; T3 shMSTN: $1207 \pm 659.3 \mu\text{m}^2$; T3 RPTOR $1720 \pm 884.2 \mu\text{m}^2$) groups. Interestingly, the slow-to-fast phenotype induced by T3 was maintained in all groups (Figures 9E and 10E).



Artigo 2 Figure 9: Myostatin knockdown and RPTOR overexpression protect skeletal muscle from seven-day T3-induced atrophy. (A) Heart mass normalised by tibia length (left, n=5) and soleus muscle mass normalised by tibia length (right, n=5). (B) Soleus muscle cross-section photomicrographs (n=5 per group, 200x magnification) depicting myosin heavy chain type I (top; MHC I; green) or myosin heavy chain type II (bottom; MHC II; green) labelled fibres outlined by laminin labelling (red) in the groups: control (empty vector), T3 (empty vector + T3 injections), T3 + shMSTN (myostatin knockdown + T3 injections) and Rptor+T3 (Rptor overexpression + T3 injections) groups. (C) MHC I positive fibres' cross-section area mean (left) (μm²; n= ~1200 fibres per group) and frequency distribution (right). (D) MHC II positive fibres' cross-section area mean (left) (μm²; n= ~1200 fibres per group) and frequency distribution (right). (E) MCH I and MHC II positive fibres frequency among groups. Values are expressed as mean fold change ± SD. Kruskal Wallis test was applied to verify differences among the groups. * p<0.05 versus control group. # p<0.05 versus T3 group. § p<0.05 versus T3 shMSTN group.



Artigo 2 Figure 10: Myostatin knockdown and RPTOR overexpression protect skeletal muscle from fourteen-day T3-induced atrophy. (A) Heart mass normalised by tibia length (left, n=5) and soleus muscle mass normalised by tibia length (right, n=5). (B) Soleus muscle cross-section photomicrographs (n=5 per group, 200x magnification) depicting myosin heavy chain type I (top; MHC I; green) or myosin heavy chain type II (bottom; MHC II; green) labelled fibres outlined by laminin labelling (red) in the groups: control (empty vector), T3 (empty vector + T3 injections), T3 + shMSTN (myostatin knockdown + T3 injections) and Rptor+T3 (Rptor overexpression + T3 injections) groups. (C) MHC I positive fibres' cross-section area mean (left) (µm²; n= ~1200 fibres per group) and frequency distribution (right). (D) MHC II positive fibres' cross-section area mean (left) (µm²; n= ~1200 fibres per group) and frequency distribution (right). (E) MCH I and MHC II positive fibres frequency among groups. Values are expressed as mean fold change ± SD. Kruskal Wallis test was applied to verify differences among the groups. * p<0.05 versus control group. # p<0.05 versus T3 group. § p<0.05 versus T3 shMSTN group.



Artigo 2 Supplemental Figure 1: Soleus muscle electroporation efficiency. (A) Macrophotograph from naive (left) and electroporated (right) soleus muscle. (B) Panoramic photomicrograph of electroporated muscle. (C) Photomicrograph of electroporated (top) and electroporated (bottom) soleus muscle. (D) Electroporation efficiency in the percentage of transfected cells. (E) Western blot analysis of electroporated soleus muscles with Rptor expression plasmid (left; n=2) or MSTN shRNA (right; n=2).

3.2.4. Discussion

Thyroid hormone-related disorders are currently positioned as the second most prevalent endocrine disorder being hyperthyroidism the most common (32). This situation persists despite the current diagnosis and treatment capabilities. It is estimated that approximately one billion people are still vulnerable to TH-related illness (33), and skeletal muscle is susceptible to thyroid hormone fluctuations (34), leading mainly to hyperthyroidism related to myopathies and atrophy (35).

In this study, we induced experimental hyperthyroidism to explore THs underlying mechanisms on skeletal muscle mass regulation (29,36–38). The success of the model employed herein was attested by reduced body weight, skeletal muscle atrophy (declined mass and CSA), heart hypertrophy and low levels of T4 (Table II) (38–41). Furthermore, we verified typical T3-induced slow-to-fast fibre type shift (Figures 1 and 2), characterised by a decrease in MHCI positive fibres (42–45).

The unbalanced protein turnover is at the core of experimental hyperthyroidism-related atrophy, and it is well established that increased proteolysis is a major player (38,46–48). In a previous study, we have identified the proteasome related E3 ligase named MDM2 as responsive to T3, although, surprisingly, MDM2 is required to muscle mass maintenance, highlighting concomitant anabolic effects in T3-induced atrophy (29). Actually, the impact of T3 upon protein synthesis, a much less explored field, is still elusive (48–50). Certain studies have found that T3 does not change protein synthesis (51) and others that protein synthesis is increased (41); therefore, further investigation is required to fully understand T3 actions in skeletal muscle.

Stimulated by the above-mentioned previous results, we explored the same microarray database and identified decreased *Rptor* gene expression, validated at mRNA and protein levels (Figure 3), suggesting compromised anabolic signalling since *Rptor* ablation is related to mTORC1 dysfunction, myopathies and skeletal muscle loss (24,52,53). Because we have not found thyroid hormone-responsive elements (THRE) on the *Rptor* regulatory region, as corroborated by Finotti and collaborators (31), we reasoned that *Rptor* could be indirectly inhibited by a T3-responsive gene. In this sense, *Mstn* caught our attention due to the presence of a described positive THRE (25,26). Furthermore, previous work has suggested feedback regulation between myostatin and mTORC1-*Rptor* (27,54).

Herein, we confirmed that myostatin gene expression and protein levels were elevated by T3 (Figure 4), surprisingly with no evidence of SMAD3 activation (Figure 5). In fact, T3 has been shown to inhibit SMAD3 phosphorylation, nuclear translocation and DNA binding in the liver (55). Further, transforming growth factor-beta (TGFBI)-induced SMAD3 activation was described to be blocked by T3(55), which is associated with fibrosis in the human liver (56). Since TGFBI and MSTN share a common receptor, we foresee that T3 could exert a dual effect on skeletal muscle by increasing myostatin levels while impairing SMAD3 activation. In this sense, *Rptor* could be inhibited by a SMAD3-independent mechanism (57). Another non-exclusive possibility contemplates that the T3 could increase SMAD3/SP1 affinity inside the nucleus, inhibiting transcription. It has been shown that SP1 can bind to SMAD3 and increase the transactivation of SP1 responsive genes (58,59). Noteworthy, the *Rptor* regulatory region is particularly rich in SP1 sites (31).

Since *Rptor* ablation is related to mTORC1 dysfunction, we also verified the impact of experimental hyperthyroidism upon mTORC1 components and overall protein synthesis. We noticed elevated protein synthesis after T3 treatment for seven and fourteen days despite inhibited mTOR and P70S6K phosphorylation, respectively (Figure 6). These results evince the remarkable complexity of mTORC1 activity on regulating protein synthesis and skeletal muscle mass under different conditions. For instance, initial work suggested *Rptor* crucial role in maintaining mTORC1 activity and skeletal muscle mass (24). However, it has been shown that *Rptor* knockout followed by decreased basal levels of protein synthesis did not affect the skeletal muscle mass maintenance (60). Surprisingly, hypertrophic stimuli can activate mTORC1 downstream components and induce de novo protein synthesis independently of mTOR/RPTOR activity (52). In this sense, Short and collaborators found that T3 can elevate protein synthesis without activating mTORC1 components (41), evoking mTORC1-independent T3 prototropic mechanisms.

The atrophic effect of T3 in parallel to elevated protein synthesis is still an intriguing issue. A plain possibility contemplates that experimental hyperthyroidism induction of proteolysis overlays the anabolic signaling, leading to reduced fibre size (46). On the other hand, the protein synthesis could be triggered by the high levels of free amino acids released by the intense proteolysis (61), which would be insufficient to maintain balanced protein turnover. Another non-exclusive possibility includes that T3 could drive mistranslated misfolded proteins, not representing an actual increase in quality-controlled proteins. In fact, it has been shown, in other experimental conditions, involving mTORC1 target disruption, that induced protein synthesis can induce misfolded proteins (62).

Finally, we manipulated the levels of Rptor and myostatin in the experimental hyperthyroidism model to explore further the role of those proteins in the onset of T3 dependent skeletal muscle atrophy. Myostatin knockdown was able to block T3-induced skeletal muscle atrophy in vitro (Figure 8) and in vivo (Figures 9 and 10). This effect could be associated with a boost in the mTORC1-independent mechanism of protein synthesis induced by myostatin inhibition (63) or a negative impact upon proteolytic pathway since myostatin knockdown could inhibit nuclear factor kappa B (NFkB)-dependent tripartite motif-containing 63 (TRIM63/MuRF1) upregulation, lessening the protein degradation (57). Likewise, our results show that RPTOR overexpression could block T3-induced atrophy in vivo, probably by equilibrating mTORC1 normal function restabilising the translation of properly folded proteins that can compose the bulk of myofibrillar components. Interestingly, our results indicate that T3 induces slow-to-fast fibre shift and skeletal muscle atrophy by distinct mechanisms. For instance, T3 was shown to induce the fibre type changing through the regulation of the mir133a (64), corroborating a new layer to T3-induced changes. In conclusion, this study established that Rptor/myostatin are essential in T3-induced atrophy program by a mechanism independent of mTORC1 inhibition.

3.2.5. *Acknowledgements*

We thank FAPESP and CNPq for their financial support.

3.2.6. *Funding*

The São Paulo Research Foundation supported this work (FAPESP) fellowships #2017/09398-8, #2018/24419-4, #2019/08996-4, and by the Research Grant

2015/04090-0. This work was also supported by the Brazilian National Research Foundation (CNPq), Leducq Foundation, Award #FLQ13CVD04, and the European Union (GA#645648, "Muscle Stress Relief").

3.2.7. Availability of data and materials

The datasets used and/or analysed during the current study are available from the corresponding author on reasonable request.

3.2.8. Author's contributions

AC and AM designed the study. AC, PA, WS and AR carried out experiments and analysed the data. AC wrote the manuscript. AM and SL contributed to data interpretation, supervision, and manuscript revision and funding. AC and PA confirm the authenticity of the raw data. All the authors have read and approved the final manuscript.

3.2.9. Ethics approval and consent to participate

The study followed the ethical principles in animal research adopted by the Brazilian College of Animals Experimentation (COBEA) under #04/2016 approval from the Institute of Biomedical Sciences/University of São Paulo Ethics Committee on Animal Research.

3.2.10. Patient consent for publication

Not applicable

3.2.11. Competing interests

The authors declare that they have no competing interests

3.2.12. References

1. Crockford SJ: Evolutionary roots of iodine and thyroid hormones in cell-cell signaling. *Integr Comp Biol* 49: 155–166, 2009.
2. Laurberg P: Mechanisms governing the relative proportions of thyroxine and 3,5,3'-triiodothyronine in thyroid secretion. *Metabolism* 33: 379–392, 1984.
3. Salvatore D, Simonides WS, Dentice M, Zavacki AM and Larsen PR: Thyroid hormones and skeletal muscle - New insights and potential implications. *Nat Rev Endocrinol* 10: 206–214, 2014.
4. Bianco AC: Minireview: Cracking the metabolic code for thyroid hormone signaling. *Endocrinology* 152: 3306–3311, 2011.
5. Lee J, Kim N and Milanesi A: Thyroid hormone signaling in muscle development, repair and metabolism. *J Endocrinol Diabetes Obes* 2: 1046–1055, 2014.
6. Salvatore D, Pansini V, Simonides WS, Dentice M, Zavacki AM, Ma B and Larsen PR: Thyroid hormones and skeletal muscle — new insights and potential implications. *10*: 206–214, 2014.
7. Cao X, Kambe F, Moeller LC, Refetoff S and Seo H: Thyroid hormone induces rapid activation of Akt/protein kinase B-mammalian target of rapamycin-p70S6K cascade through phosphatidylinositol 3-kinase in human fibroblasts. *Mol Endocrinol* 19: 102–112, 2005.
8. Hammes SR and Davis PJ: Overlapping nongenomic and genomic actions of thyroid hormone and steroids. *Best Pract Res Clin Endocrinol Metab* 29: 581–593, 2015.
9. Forhead AJ and Fowden AL: Thyroid hormones in fetal growth and parturition maturation. *J Endocrinol* 221, 2014.
10. Steinmetz PRH, Kraus JEM, Larroux C, *et al.*: Independent evolution of striated muscles in cnidarians and bilaterians. *Nature* 487: 231–234, 2012.
11. Lee LA, Karabina A, Broadwell LJ and Leinwand LA: The ancient sarcomeric myosins found in specialised muscles. *Skelet Muscle* 9: 7, 2019.
12. Hill J and Olson EN: *Muscle: Fundamental Biology and Mechanisms of Disease*. Academic Press, 2012.
13. Béchet D, Tassa A, Combaret L, Taillandier D and Attaix D: Regulation of skeletal muscle proteolysis by amino acids. *J Ren Nutr* 15: 18–22, 2005.
14. Goldberg AL: Protein turnover in skeletal muscle. II. Effects of denervation and cortisone on protein catabolism in skeletal muscle. *J Biol Chem* 244: 3223–9, 1969.

15. Goldberg AL: Protein turnover in skeletal muscle. I. Protein Catabolism During Work-Induced Hypertrophy and Growth induced with Growth Hormone. *J Biol Chem* 244: 3217–3222, 1969.
16. Peris-Moreno D, Taillandier D and Polge C: MuRF1/TRIM63, master regulator of muscle mass. *Int J Mol Sci* 21: 1–39, 2020.
17. Schiaffino S, Dyar KA, Ciciliot S, Blaauw B and Sandri M: Mechanisms regulating skeletal muscle growth and atrophy. *FEBS J* 280: 4294–4314, 2013.
18. Vainshtein A and Sandri M: Signaling pathways that control muscle mass. *Int J Mol Sci* 21: 1–32, 2020.
19. Olson BR, Klein I, Benner R, Burdett R, Trzepacz P and Levey GS: Hyperthyroid myopathy and the response to treatment. *Thyroid* 1: 137–141, 1991.
20. Clément K, Viguerie N, Diehn M, *et al.*: In vivo regulation of human skeletal muscle gene expression by thyroid hormone. *Genome Res* 12: 281–291, 2002.
21. Al-Zubeidi H, Demeterco C and Jones KL: Thyrotoxic, hypokalemic periodic paralysis (THPP) in adolescents. *J Pediatr Endocrinol Metab* 28: 157–161, 2015.
22. Biondi B: Graves' Disease. Springer New York, New York, NY, 2015.
23. Carter WJ, Benjamin WSV and Faas FH: Effect of experimental hyperthyroidism on skeletal-muscle proteolysis. *Biochem J* 194: 685–690, 1981.
24. Bentzinger CF, Romanino K, Cloëtta D, *et al.*: Skeletal Muscle-Specific Ablation of raptor, but Not of rictor, Causes Metabolic Changes and Results in Muscle Dystrophy. *Cell Metab* 8: 411–424, 2008.
25. Kun M, Mallidis C, Artaza J, Taylor W, Gonzalez-Cadavid N and Bhasin S: Characterisation of 5'-regulatory region of human myostatin gene: Regulation by dexamethasone in vitro. *Am J Physiol - Endocrinol Metab* 281: 1128–1136, 2001.
26. Ma Y, Chen X, Li Q, An X and Chen Y: Effect of thyroid hormone on the gene expression of myostatin in rat skeletal muscle. *Asian-Australas J Anim Sci* 22: 275–281, 2009.
27. Trendelenburg AU, Meyer A, Rohner D, Boyle J, Hatakeyama S and Glass DJ: Myostatin reduces Akt/TORC1/p70S6K signaling, inhibiting myoblast differentiation and myotube size. *AJP Cell Physiol* 296: C1258–C1270, 2009.
28. Sarbassov DD, Ali SM, Kim D-H, *et al.*: Rictor, a Novel Binding Partner of mTOR, Defines a Rapamycin-Insensitive and Raptor-Independent Pathway that Regulates the Cytoskeleton. *Curr Biol* 14: 1296–1302, 2004.
29. Ramos G V, Cruz A, Silva WJ, Rozanski A, Baptista IL, Silvestre JG and Moriscot AS: Thyroid hormone upregulates MDM2 in rat type I fibre: Implications for skeletal muscle mass regulation. *Acta Physiol* 222: e13003, 2018.
30. Livak KJ and Schmittgen TD: Analysis of relative gene expression data using real-time quantitative PCR and the 2(-Delta Delta C(T)) Method. *Methods San Diego Calif* 25: 402–408, 2001.
31. Finotti A, Bianchi N, Fabbri E, Borgatti M, Breveglieri G, Gasparello J and Gambari R: Erythroid induction of K562 cells treated with mithramycin is associated with

- inhibition of raptor gene transcription and mammalian target of rapamycin complex 1 (mTORC1) functions. *Pharmacol Res* 91: 57–68, 2015.
32. Heuck C, Kallner A, Kanagasabapathy A and Riesen W: *Diagnosis and Monitoring of Diseases of The Thyroid.*, 2000.
 33. Taylor PN, Albrecht D, Scholz A, Gutierrez-buey G, Lazarus JH, Dayan CM and Okosieme OE: *Global epidemiology of hyperthyroidism and hypothyroidism.*, 2018.
 34. Park YS, Chang Y, Lee Y-T, Shin H, Ryu S and Yoon KJ: The prospective relationship between low muscle mass and thyroid hormones among 198 069 euthyroid men and women ; comparing different definitions of low muscle mass. *Int J Clin Pract* 75: 1–9, 2021.
 35. Ramsay IAN: *THYROID DISEASE AND MUSCLE DYSFUNCTION.* William Heinemann Medical Books, London, 1974.
 36. Souza KDP, Goulart F and Nunes MT: *Effect of neonatal hyperthyroidism on GH gene expression reprogramming and physiological repercussions in rat adulthood.*, 2004.
 37. Bianco AC, Anderson G, Forrest D, *et al.*: *American Thyroid Association Guide to Investigating Thyroid Hormone Economy and Action in Rodent and Cell Models.* *Thyroid* 24: 88–168, 2014.
 38. O'Neal P, Alamdari N, Smith I, Poylin V, Menconi M and Hasselgren P-O: *Experimental hyperthyroidism in rats increases the expression of the ubiquitin ligases atrogin-1 and MuRF1 and stimulates multiple proteolytic pathways in skeletal muscle.* *J Cell Biochem* 108: 963–973, 2009.
 39. Bahi L, Garnier A, Fortin D, Serrurier B, Veksler V and Bigard AX: *Differential Effects of Thyroid Hormones on Energy Metabolism of Rat Slow- and Fast-Twitch Muscles.* *598: 589–598*, 2005.
 40. Postler TS, Budak MT, Khurana TS and Rubinstein NA: *Influence of hyperthyroid conditions on gene expression in extraocular muscles of rats.* *Physiol Genomics* 37: 231–238, 2009.
 41. Short KR, Nygren J and Nair KS: *Effect of T3-induced hyperthyroidism on mitochondrial and cytoplasmic protein synthesis rates in oxidative and glycolytic tissues in rats.* *Am J Physiol - Endocrinol Metab* 292: 642–647, 2007.
 42. Larsson L, R UMULLE, Li X and Schiaffino S: *Thyroid hormone regulation of myosin heavy chain isoform composition in young and old rats , w i t h special reference t o IIX myosin.* 109–116, 1995.
 43. Li X, Hughes SM, Salviati G, Teresi A and Larsson L: *Thyroid hormone effects on contractility and myosin composition of soleus muscle and single fibres from young and old rats.* 555–567, 1996.
 44. Miyabara EH, Aoki MS, Soares AG, *et al.*: *Thyroid hormone receptor- β -selective agonist GC-24 spares skeletal muscle type I to II fiber shift.* 233–241, 2005.

45. VAN ER LINDER C, Simonides WS, Muller A, *et al.*: Fiber-specific regulation of Ca²⁺ + -ATPase isoform expression by thyroid hormone in rat skeletal muscle. *Am Physiol Soc*, 1996.
46. Angeras U and Hasselgren PO.: Protein turnover in different types of skeletal muscle during experimental hyperthyroidism in rats. *Acta Endocrinol (Copenh)* 109: 90–95, 1985.
47. Tawa NE, Odessey R and Goldberg AL: Inhibitors of the proteasome reduce the accelerated proteolysis in atrophying rat skeletal muscles. *J Clin Invest* 100: 197–203, 1997.
48. Clément K, Viguerie N, Diehn M, *et al.*: In vivo regulation of human skeletal muscle gene expression by thyroid hormone. *Genome Res* 12: 281–291, 2002.
49. Flaim KE, Li JB and Jefferson LS: Effects of thyroxine on protein turnover in rat skeletal muscle. *Am J Physiol Endocrinol Metab Gastrointest Physiol* 4, 1978.
50. MORRISON WL, GIBSON JNA, JUNG RT and RENNIE MJ: Skeletal muscle and whole body protein turnover in thyroid disease. *Eur J Clin Invest* 18: 62–68, 1988.
51. Kazakov VM and Kovalenko TM: Experimental Thyrotoxic myopathy: Radioautography of protein synthesis in skeletal muscle and motor neurons of spinal cord. *Neuromuscul Disord* 5: 47–52, 1995.
52. You JS, McNally RM, Jacobs BL, *et al.*: The role of raptor in the mechanical load-induced regulation of mTOR signaling, protein synthesis, and skeletal muscle hypertrophy. *FASEB J* 33: 4021–4034, 2019.
53. Guertin DA, Stevens DM, Thoreen CC, *et al.*: Ablation in Mice of the mTORC Components raptor, rictor, or mLST8 Reveals that mTORC2 Is Required for Signaling to Akt-FOXO and PKC α , but Not S6K1. *Dev Cell* 11: 859–871, 2006.
54. Sartori R, Milan G, Patron M, Mammucari C, Blaauw B, Abraham R and Sandri M: Smad2 and 3 transcription factors control muscle mass in adulthood. *Am J Physiol - Cell Physiol* 296: 1248–1257, 2009.
55. Alonso-Merino E, Orozco RM, Ruíz-Llorente L, *et al.*: Thyroid hormones inhibit TGF- β signaling and attenuate fibrotic responses. *Proc Natl Acad Sci U S A* 113: E3451–E3460, 2016.
56. Du J, Chai S, Zhao X, Sun J, Zhang X and Huo L: Association between thyroid hormone levels and advanced liver fibrosis in patients with type 2 diabetes mellitus and non-alcoholic fatty liver disease. *Diabetes Metab Syndr Obes Targets Ther* 14: 2399–2406, 2021.
57. Sriram S, Subramanian S, Juvvuna PK, *et al.*: Myostatin augments muscle-specific ring finger protein-1 expression through an NF- κ B independent mechanism in SMAD3 null muscle. *Mol Endocrinol* 28: 317–330, 2014.
58. Botella LM, Sánchez-Elsner T, Rius C, Corbí A and Bernabéu C: Identification of a Critical Sp1 Site within the Endoglin Promoter and Its Involvement in the Transforming Growth Factor- β Stimulation. *J Biol Chem* 276: 34486–34494, 2001.

59. Poncelet AC and Schnaper HW: Sp1 and Smad Proteins Cooperate to Mediate Transforming Growth Factor- β 1-induced α 2(I) Collagen Expression in Human Glomerular Mesangial Cells. *J Biol Chem* 276: 6983–6992, 2001.
60. Ham AS, Chojnowska K, Tintignac LA, *et al.*: mTORC1 signalling is not essential for the maintenance of muscle mass and function in adult sedentary mice. *J Cachexia Sarcopenia Muscle* 11: 259–273, 2020.
61. Zhang Y, Nicholatos J, Dreier JR, *et al.*: Coordinated regulation of protein synthesis and degradation by mTORC1. *Nature* 513: 440–443, 2014.
62. Marabita M, Baraldo M, Solagna F, *et al.*: S6K1 Is Required for Increasing Skeletal Muscle Force during Hypertrophy. *Cell Rep* 17: 501–513, 2016.
63. Welle S, Burgess K and Mehta S: Stimulation of skeletal muscle myofibrillar protein synthesis, p70 S6 kinase phosphorylation, and ribosomal protein S6 phosphorylation by inhibition of myostatin in mature mice. *Am J Physiol - Endocrinol Metab* 296: 567–572, 2009.
64. Zhang D, Wang X, Li Y, *et al.*: Thyroid hormone regulates muscle fiber type conversion via miR-133a1. *J Cell Biol* 207: 753–766, 2014.

4 Apresentação dos Artigos (Discussão)

As doenças relacionadas ao desequilíbrio nos níveis de hormônios tireoidianos, hipertireoidismo e hipotireoidismo, apresentam prevalência mundial de aproximadamente 2% da população, sendo predominante em regiões com suficiência em iodo nutricional, como o Brasil [90] (Taylor, 2018). Os músculos cardíaco e esquelético possuem alta sensibilidade às flutuações nos hormônios tireoidianos, apresentando patologias significativas a essas alterações. Em particular, o hipertireoidismo induz atrofia muscular esquelética, diminuição na força e alta fatigabilidade, de modo que, além da importância clínica, a resposta do tecido muscular ao T3 é conveniente ao estudo dos mecanismos de controle de massa.

Dessa forma, os artigos apresentados no corpo desta tese compartilham o objetivo de explorar o padrão da expressão global de genes durante o hipertireoidismo experimental. No artigo “THYROID HORMONE UPREGULATES MDM2 IN RAT TYPE I FIBER: IMPLICATIONS FOR SKELETAL MUSCLE MASS REGULATION” (Artigo 1), explorou-se a regulação de genes do sistema ubiquitina proteassoma. Já no artigo “RPTOR IS ESSENTIAL FOR T3-INDUCED SKELETAL MUSCLE ATROPHY INDEPENDENTLY OF MTORC-1” (Artigo 2), investigou-se a regulação de genes da via de síntese mTOR.

Em ambos, o modelo animal utilizado para a indução do hipertireoidismo resultou em aumento da massa cardíaca, redução dos níveis de T4, atrofia do músculo soleus (Tabela 1 – Artigo 1; Tabela 1 e Figuras 1 e 2 – Artigo 2) e indução de mudança do tipo de fibras musculares com diminuição da prevalência de fibras do tipo I e preponderância

de fibras do tipo II (Figuras 1 e 2 – Artigo 2). Esses resultados corroboram a indução do hipertireoidismo e estão de acordo com dados encontrados na literatura. 37-40 (artigo 2)

Isto posto, realizou-se a análise do padrão global da expressão gênica no músculo soleus de animais com indução de hipertireoidismo por 12 horas, 24 horas e 7 dias, focando-se nos componentes da via ubiquitina proteasoma e mTOR, que identificaram a indução da E3 ligase MDM2 (Figura 1 – Artigo 1) e a inibição de RPTOR (Figura 3 – Artigo 2), respectivamente.

Essas respostas foram validadas *in vivo* e *in vitro*. No primeiro caso, identificou-se que a resposta de MDM2 ocorria especificamente 20x os níveis fisiológicos, com aumento da expressão gênica e proteica no sétimo dia (Figura 2 – Artigo 1). Com base nesses resultados a regulação de RPTOR foi avaliada apenas no hipertireoidismo experimental com 20x os níveis fisiológicos, entretanto, adicionou-se um grupo tratado por quatorze dias, visando identificar a estabilidade da regulação durante a manutenção da atrofia. Assim, foi verificada a diminuição da expressão gênica e proteica de RPTOR também no sétimo e décimo quarto dia (Figura 3 – Artigo 2). Já no processo de validação em cultura celular, verificou-se que a utilização de T3 por três dias resulta em diminuição do diâmetro dos miotubos provenientes de cultura primária (Figura 6 – Artigo 1) e C2C12 (Figura 7 – Artigo 2), com aumento na expressão de MDM2 (Figura 2 – Artigo 1) e redução na expressão de RPTOR (Figura 7 – Artigo 2), respectivamente.

A respeito dos mecanismos envolvidos na regulação da massa e esses genes de interesse, os artigos exploram vias intracelulares distintas. O Artigo 1 demonstra que a indução na expressão de MDM2 é dependente de NFAT e é essencial para um mecanismo de proteção de massa induzido por T3 (Figura 6 – Artigo 1), possivelmente, ao fosforilar e inativar FoxO (Figuras 6 e 7 – Artigo 1). Já o Artigo 2 demonstrou que a

inibição de RPTOR por T3 ocorre de maneira indireta, provavelmente por um mecanismo dependente de miostatina (Figuras 4 e 5 – Artigo 2). Além disso, revelou que T3 induz a síntese de proteínas mesmo reduzindo a fosforilação de mTOR e P70S6k de maneira assíncrona (Figuras 6 e 7 – Artigo 2). Por fim, verificou-se que a inibição da miostatina e a hiperexpressão de RPTOR bloqueiam o efeito da atrofia induzida pelo hormônio tireoidiano (Figuras 9 e 10 – Artigo 2).

Em suma os resultados de ambos os artigos demonstram que estímulos antagônicos se encontram em atividade durante o hipertireoidismo, por exemplo, a reduzida translocação de SMAD3 (Figura 5 – Artigo 2) e FoxO (Figura 6 – Artigo 1) para o núcleo e o aumento na expressão dos atrogenes (Figura 1 – Artigo 1), além da inibição de RPTOR e componentes de mTORC1 com elevada síntese proteica. Esses resultados ilustram a necessidade de estudos que verifiquem a relação entre as vias de síntese e degradação e sua regulação mútua durante o hipertireoidismo experimental, para que, mecanismos mais completos de controle de massa possam ser identificados.

5 REFERÊNCIAS

- [1] Schrodinger E. O que é vida?: o aspecto físico da célula viva: Seguido de “Mente e matéria” e “Fragmentos autobiográficos.” 1ª edição. São Paulo: Editora Unesp; 2007.
- [2] Crockford SJ. Evolutionary roots of iodine and thyroid hormones in cell-cell signaling. *Integr Comp Biol* 2009;49:155–66. <https://doi.org/10.1093/icb/icp053>.
- [3] Weiss MC, Preiner M, Xavier JC, Zimorski V, Martin WF. The last universal common ancestor between ancient Earth chemistry and the onset of genetics. *PLoS Genet* 2018;14:e1007518. <https://doi.org/10.1371/journal.pgen.1007518>.
- [4] Barry BA, Babcock GT. Tyrosine radicals are involved in the photosynthetic oxygen-evolving system. *Proc Natl Acad Sci U S A* 1987;84:7099–103. <https://doi.org/10.1073/pnas.84.20.7099>.
- [5] Guo Z, He J, Barry BA. Calcium, conformational selection, and redox-active tyrosine YZ in the photosynthetic oxygen-evolving cluster. *Proc Natl Acad Sci U S A* 2018;115:5658–63. <https://doi.org/10.1073/pnas.1800758115>.
- [6] Björn LO, Govindjee U. The evolution of photosynthesis and its environmental impact. *Photobiol — Sci Life Light 2nd Ed* 2008:255–87. https://doi.org/10.1007/978-0-387-72655-7_12.
- [7] Fenical W. Halogenation in the Rhodophyta a Review. *J Phycol* 1975;11:245–59. <https://doi.org/10.1111/j.1529-8817.1975.tb02775.x>.
- [8] Fowden L. Radioactive Iodine Incorporation into Organic Compounds of Various Angiosperms. *Physiol Plant* 1959;12:657–64. <https://doi.org/10.1111/j.1399-3054.1959.tb08900.x>.
- [9] La Barre S, Potin P, Leblanc C, Delage L. The halogenated metabolism of brown algae (Phaeophyta), its biological importance and its environmental significance. *Mar Drugs* 2010;8:988–1010. <https://doi.org/10.3390/md8040988>.
- [10] Smoleń S, Kowalska I, Halka M, Ledwożyw-Smoleń I, Grzanka M, Skoczylas Ł, et al. Selected Aspects of Iodate and Iodosalicylate Metabolism in Lettuce Including the Activity of Vanadium Dependent Haloperoxidases as Affected by Exogenous Vanadium. *Agronomy* 2020;10:1. <https://doi.org/10.3390/agronomy10010001>.
- [11] Reis LTC, Da Silva MRD, Costa SL, Velozo EDS, Batista R, Da Cunha Lima ST. Estrogen and Thyroid Hormone Receptor Activation by Medicinal Plants from Bahia, Brazil. *Medicines* 2018;5:8. <https://doi.org/10.3390/medicines5010008>.
- [12] Heyland A, Moroz LL. Cross-kingdom hormonal signaling: an insight from thyroid hormone functions in marine larvae. *J Exp Biol* 2005;208:4355–61. <https://doi.org/10.1242/jeb.01877>.
- [13] Sebastiano V. Evolutionary Significance of Iodine. *Curr Chem Biol* 2011;5:155–62.
- [14] Eales JG. Iodine Metabolism and Thyroid-Related Functions in Organisms Lacking Thyroid Follicles: Are Thyroid Hormones also Vitamins? 1997. <https://journals.sagepub.com/doi/abs/10.3181/00379727-214-44098> (accessed September 8, 2021).
- [15] Taylor E, Heyland A. Evolution of thyroid hormone signaling in animals: Non-genomic and genomic modes of action. *Mol Cell Endocrinol* 2017;459:14–20. <https://doi.org/10.1016/j.mce.2017.05.019>.

- [16] Heyland A, Hodin J, Reitzel AM. Hormone signaling in evolution and development: a non-model system approaches. *BioEssays* 2005;27:64–75. <https://doi.org/10.1002/bies.20136>.
- [17] Nyström E, E.B. Berg G, K.G. Jansson S, Tarring O, V. Valdemarsson S. *Thyroid Disease in Adults*. 2011 edition. Heidelberg: Springer; 2011.
- [18] Moore K, Dalley AF, Agur AMR. *Anatomia Orientada Para A Clínica*. 7° edição. Rio de Janeiro, Brasil: Guanabara Koogan; 2014.
- [19] Drake RL, Vogl W, Mitchell AWM. *Gray's Anatomy For Student*. 1st Edition. Oxford, Reino Unido: Churchill Livingstone; 2004.
- [20] Ross MH, Pawlina W. *Histology: A Text and Atlas With Correlated Cell and Molecular Biology*. 7th Edition. Filadélfia, Estados Unidos Da América: Wolters Kluwer Health; 2015.
- [21] La Perle KMD, Dintzis SM. *Endocrine Sysem. Comp. Anat. Histol. Mouse Rat Hum. Atlas*. 2nd ed., Oxford, Reino Unido: Academic Press; 2017.
- [22] Lowrie DJ. *Histology: An Essential Textbook*. Nova Iorque, Estados Unidos Da América: Thieme; 2020.
- [23] Ilie IR. *Introduction to Endocrinology*. Cham, Suíça: Springer Nature; 2020.
- [24] Kronenberg HM, Melmed S, Polonsky KS, Larsen PR. *Williams Textbook of Endocrinology*. 11th Edition. Filadélfia, Estados Unidos Da América: Elsevier; 2007.
- [25] Carvalho DP, Dupuy C. Thyroid hormone biosynthesis and release. *Mol Cell Endocrinol* 2017;458:6–15. <https://doi.org/10.1016/j.mce.2017.01.038>.
- [26] Tortora GJ, Derrickson B. *Principles of Anatomy & Physiology*. 14th Edition. Massachussets, Estados Unidos Da América: Wiley; 2014.
- [27] Mendoza A, Hollenberg AN. New insights into thyroid hormone action. *Pharmacol Ther* 2017;173:135–45. <https://doi.org/10.1016/j.pharmthera.2017.02.012>.
- [28] Cicatiello AG, Di Girolamo D, Dentice M. Metabolic Effects of the Intracellular Regulation of Thyroid Hormone: Old Players, New Concepts. *Front Endocrinol* 2018;9:474. <https://doi.org/10.3389/fendo.2018.00474>.
- [29] Gereben B, Zavacki AM, Ribich S, Kim BW, Huang SA, Simonides WS, et al. Cellular and molecular basis of deiodinase-regulated thyroid hormone signaling. *Endocr Rev* 2008;29:898–938. <https://doi.org/10.1210/er.2008-0019>.
- [30] Astapova I, Hollenberg AN. The in vivo role of nuclear receptor corepressors in thyroid hormone action. *Biochim Biophys Acta* 2013;1830:3876–81. <https://doi.org/10.1016/j.bbagen.2012.07.001>.
- [31] Cheng S-Y, Leonard JL, Davis PJ. Molecular aspects of thyroid hormone actions. *Endocr Rev* 2010;31:139–70. <https://doi.org/10.1210/er.2009-0007>.
- [32] Zhang J, Lazar MA. The Mechanism of Action of Thyroid Hormones. *Annu Rev Physiol* 2000;62:439–66. <https://doi.org/10.1146/annurev.physiol.62.1.439>.
- [33] Yen PM. Physiological and molecular basis of thyroid hormone action. *Physiol Rev* 2001;81:1097–142. <https://doi.org/10.1152/physrev.2001.81.3.1097>.
- [34] Salvatore D, Simonides WS, Dentice M, Zavacki AM, Larsen PR. Thyroid hormones and skeletal muscle--new insights and potential implications. *Nat Rev Endocrinol* 2014;10:206–14. <https://doi.org/10.1038/nrendo.2013.238>.
- [35] Cao X, Kambe F, Moeller LC, Refetoff S, Seo H. Thyroid hormone induces rapid activation of Akt/protein kinase B-mammalian target of rapamycin-p70S6K cascade through phosphatidylinositol 3-kinase in human fibroblasts. *Mol Endocrinol Baltim Md* 2005;19:102–12. <https://doi.org/10.1210/me.2004-0093>.

- [36] Irrcher I, Walkinshaw DR, Sheehan TE, Hood DA. Thyroid hormone (T3) rapidly activates p38 and AMPK in skeletal muscle in vivo. *J Appl Physiol Bethesda Md* 1985 2008;104:178–85. <https://doi.org/10.1152/japplphysiol.00643.2007>.
- [37] Davis PJ, Leonard JL, Davis FB. Mechanisms of nongenomic actions of thyroid hormone. *Front Neuroendocrinol* 2008;29:211–8. <https://doi.org/10.1016/j.yfrne.2007.09.003>.
- [38] Hammes SR, Davis PJ. Overlapping nongenomic and genomic actions of thyroid hormone and steroids. *Best Pract Res Clin Endocrinol Metab* 2015;29:581–93. <https://doi.org/10.1016/j.beem.2015.04.001>.
- [39] Grüters A, Biebermann H, Krude H. Neonatal thyroid disorders. *Horm Res* 2003;59 Suppl 1:24–9. <https://doi.org/10.1159/000067841>.
- [40] Buchholz DR. More similar than you think: Frog metamorphosis as a model of human perinatal endocrinology. *Dev Biol* 2015;408:188–95. <https://doi.org/10.1016/j.ydbio.2015.02.018>.
- [41] Moog NK, Entringer S, Heim C, Wadhwa PD, Kathmann N, Buss C. Influence of maternal thyroid hormones during gestation on fetal brain development. *Neuroscience* 2017;342:68–100. <https://doi.org/10.1016/j.neuroscience.2015.09.070>.
- [42] Forhead AJ, Fowden AL. Thyroid hormones in fetal growth and parturition maturation. *J Endocrinol* 2014;221:R87–103. <https://doi.org/10.1530/JOE-14-0025>.
- [43] Lee J-W, Kim N-H, Milanesi A. Thyroid Hormone Signaling in Muscle Development, Repair and Metabolism. *J Endocrinol Diabetes Obes* 2014;2:1046.
- [44] Klein RZ, Mitchell ML. Maternal hypothyroidism and child development. A review. *Horm Res* 1999;52:55–9. <https://doi.org/10.1159/000023435>.
- [45] Préau L, Fini JB, Morvan-Dubois G, Demeneix B. Thyroid hormone signaling during early neurogenesis and its significance as a vulnerable window for endocrine disruption. *Biochim Biophys Acta* 2015;1849:112–21. <https://doi.org/10.1016/j.bbagr.2014.06.015>.
- [46] Kahaly GJ, Dillmann WH. Thyroid hormone action in the heart. *Endocr Rev* 2005;26:704–28. <https://doi.org/10.1210/er.2003-0033>.
- [47] Williams JE. Patients' early. *Med J Aust* 1969;2:54–5.
- [48] Al-Zubeidi H, Demeterco C, Jones KL. Thyrotoxic, hypokalemic periodic paralysis (THPP) in adolescents. *J Pediatr Endocrinol Metab JPEM* 2015;28:157–61. <https://doi.org/10.1515/jpem-2014-0016>.
- [49] Bahn RS. *Graves' Disease: A Comprehensive Guide for Clinicians*. 1st ed. Nova Iorque, Estados Unidos Da América: Springer; 2015.
- [50] Lee LA, Karabina A, Broadwell LJ, Leinwand LA. The ancient sarcomeric myosins found in specialized muscles. *Skelet Muscle* 2019;9:7. <https://doi.org/10.1186/s13395-019-0192-3>.
- [51] Lindstedt S, Nishikawa K. Huxleys' Missing Filament: Form and Function of Titin in Vertebrate Striated Muscle. *Annu Rev Physiol* 2017;79:145–66. <https://doi.org/10.1146/annurev-physiol-022516-034152>.
- [52] Steinmetz PRH, Kraus JEM, Larroux C, Hammel JU, Amon-Hassenzahl A, Houliston E, et al. Independent evolution of striated muscles in cnidarians and bilaterians. *Nature* 2012;487:231–4. <https://doi.org/10.1038/nature11180>.

- [53] Lee LA, Karabina A, Broadwell LJ, Leinwand LA. The ancient sarcomeric myosins found in specialized muscles. *Skelet Muscle* 2019;9:7. <https://doi.org/10.1186/s13395-019-0192-3>.
- [54] Janssen I, Heymsfield SB, Wang ZM, Ross R. Skeletal muscle mass and distribution in 468 men and women aged 18-88 yr. *J Appl Physiol Bethesda Md* 1985 2000;89:81–8. <https://doi.org/10.1152/jappl.2000.89.1.81>.
- [55] Gibala MJ. Using exercise training to understand control of skeletal muscle metabolism. *Appl Physiol Nutr Metab Physiol Appl Nutr Metab* 2017;42:108–10. <https://doi.org/10.1139/apnm-2016-0356>.
- [56] Béchet D, Tassa A, Combaret L, Taillandier D, Attaix D. Regulation of skeletal muscle proteolysis by amino acids. *J Ren Nutr* 2005;15:18–22. <https://doi.org/10.1053/j.jrn.2004.09.005>.
- [57] Hill JA, Olson EN. *Muscle: Fundamental Biology and Mechanisms of Disease*. vol. 1. 1st ed. Boston, Estados Unidos Da América: Academic Press; 2012.
- [58] Goodin AD-, Yelizarov D. Evolution of movement process as a key for human cognition. *Cuad Neuropsicol Panam J Neuropsychol* 2018;12.
- [59] Schoenfeld BJ. The mechanisms of muscle hypertrophy and their application to resistance training. *J Strength Cond Res* 2010;24:2857–72. <https://doi.org/10.1519/JSC.0b013e3181e840f3>.
- [60] Herbst KL, Bhasin S. Testosterone action on skeletal muscle. *Curr Opin Clin Nutr Metab Care* 2004;7:271–7. <https://doi.org/10.1097/00075197-200405000-00006>.
- [61] Goldspink G, Howells KF. Work-induced hypertrophy in exercised normal muscles of different ages and the reversibility of hypertrophy after cessation of exercise. *J Physiol* 1974;239:179–93. <https://doi.org/10.1113/jphysiol.1974.sp010562>.
- [62] Sandri M. Signaling in muscle atrophy and hypertrophy. *Physiol Bethesda Md* 2008;23:160–70. <https://doi.org/10.1152/physiol.00041.2007>.
- [63] Zhang P, Chen X, Fan M. Signaling mechanisms involved in disuse muscle atrophy. *Med Hypotheses* 2007;69:310–21. <https://doi.org/10.1016/j.mehy.2006.11.043>.
- [64] Goldberg AL. Protein turnover in skeletal muscle. I. Protein catabolism during work-induced hypertrophy and growth induced with growth hormone. *J Biol Chem* 1969;244:3217–22.
- [65] Goldberg AL. Protein turnover in skeletal muscle. II. Effects of denervation and cortisone on protein catabolism in skeletal muscle. *J Biol Chem* 1969;244:3223–9.
- [66] Peris-Moreno D, Taillandier D, Polge C. MuRF1/TRIM63, Master Regulator of Muscle Mass. *Int J Mol Sci* 2020;21:E6663. <https://doi.org/10.3390/ijms21186663>.
- [67] Schiaffino S, Dyar KA, Ciciliot S, Blaauw B, Sandri M. Mechanisms regulating skeletal muscle growth and atrophy. *FEBS J* 2013;280:4294–314. <https://doi.org/10.1111/febs.12253>.
- [68] Vainshtein A, Sandri M. Signaling Pathways That Control Muscle Mass. *Int J Mol Sci* 2020;21:E4759. <https://doi.org/10.3390/ijms21134759>.
- [69] Egerman MA, Glass DJ. Signaling pathways controlling skeletal muscle mass. *Crit Rev Biochem Mol Biol* 2014;49:59–68. <https://doi.org/10.3109/10409238.2013.857291>.
- [70] Smith LW, Smith JD, Criswell DS. Involvement of nitric oxide synthase in skeletal muscle adaptation to chronic overload. *J Appl Physiol Bethesda Md* 1985 2002;92:2005–11. <https://doi.org/10.1152/japplphysiol.00950.2001>.

- [71] Aline G, Sotiropoulos A. Srf: A key factor controlling skeletal muscle hypertrophy by enhancing the recruitment of muscle stem cells. *Bioarchitecture* 2012;2:88–90. <https://doi.org/10.4161/bioa.20699>.
- [72] Gonçalves DA, Silveira WA, Manfredi LH, Graça FA, Armani A, Bertaglia E, et al. Insulin/IGF1 signalling mediates the effects of β_2 -adrenergic agonist on muscle proteostasis and growth. *J Cachexia Sarcopenia Muscle* 2019;10:455–75. <https://doi.org/10.1002/jcsm.12395>.
- [73] Lee SJ, McPherron AC. Regulation of myostatin activity and muscle growth. *Proc Natl Acad Sci U S A* 2001;98:9306–11. <https://doi.org/10.1073/pnas.151270098>.
- [74] Bonaldo P, Sandri M. Cellular and molecular mechanisms of muscle atrophy. *Dis Model Mech* 2013;6:25–39. <https://doi.org/10.1242/dmm.010389>.
- [75] Sabatini DM. Twenty-five years of mTOR: Uncovering the link from nutrients to growth. *Proc Natl Acad Sci* 2017;114:11818–25. <https://doi.org/10.1073/pnas.1716173114>.
- [76] Weichhart T. mTOR. Nova Iorque, Estados Unidos Da América: Springer; 2012. <https://doi.org/10.1007/978-1-61779-430-8>.
- [77] Yoon M-S. mTOR as a Key Regulator in Maintaining Skeletal Muscle Mass. *Front Physiol* 2017;8:788. <https://doi.org/10.3389/fphys.2017.00788>.
- [78] Ben-Sahra I, Manning BD. mTORC1 signaling and the metabolic control of cell growth. *Curr Opin Cell Biol* 2017;45:72–82. <https://doi.org/10.1016/j.ccb.2017.02.012>.
- [79] Liu J, Pan M, Huang D, Guo Y, Yang M, Zhang W, et al. Myostatin-1 Inhibits Cell Proliferation by Inhibiting the mTOR Signal Pathway and MRFs, and Activating the Ubiquitin-Proteasomal System in Skeletal Muscle Cells of Japanese Flounder *Paralichthys olivaceus*. *Cells* 2020;9:E2376. <https://doi.org/10.3390/cells9112376>.
- [80] Trendelenburg AU, Meyer A, Rohner D, Boyle J, Hatakeyama S, Glass DJ. Myostatin reduces Akt/TORC1/p70S6K signaling, inhibiting myoblast differentiation and myotube size. *Am J Physiol Cell Physiol* 2009;296:C1258-1270. <https://doi.org/10.1152/ajpcell.00105.2009>.
- [81] Hitachi K, Nakatani M, Tsuchida K. Myostatin signaling regulates Akt activity via the regulation of miR-486 expression. *Int J Biochem Cell Biol* 2014;47:93–103. <https://doi.org/10.1016/j.biocel.2013.12.003>.
- [82] Wang D-T, Yang Y-J, Huang R-H, Zhang Z-H, Lin X. Myostatin Activates the Ubiquitin-Proteasome and Autophagy-Lysosome Systems Contributing to Muscle Wasting in Chronic Kidney Disease. *Oxid Med Cell Longev* 2015;2015:684965. <https://doi.org/10.1155/2015/684965>.
- [83] Sriram S, Subramanian S, Juvvuna PK, Ge X, Lokireddy S, McFarlane CD, et al. Myostatin augments muscle-specific ring finger protein-1 expression through an NF- κ B independent mechanism in SMAD3 null muscle. *Mol Endocrinol Baltim Md* 2014;28:317–30. <https://doi.org/10.1210/me.2013-1179>.
- [84] Bodine SC, Latres E, Baumhueter S, Lai VK, Nunez L, Clarke BA, et al. Identification of ubiquitin ligases required for skeletal muscle atrophy. *Science* 2001;294:1704–8. <https://doi.org/10.1126/science.1065874>.
- [85] Lokireddy S, Wijesoma IW, Sze SK, McFarlane C, Kambadur R, Sharma M. Identification of atrogen-1-targeted proteins during the myostatin-induced skeletal muscle wasting. *Am J Physiol Cell Physiol* 2012;303:C512-529. <https://doi.org/10.1152/ajpcell.00402.2011>.

- [86] Baehr LM, Furlow JD, Bodine SC. Muscle sparing in muscle RING finger 1 null mice: response to synthetic glucocorticoids. *J Physiol* 2011;589:4759–76. <https://doi.org/10.1113/jphysiol.2011.212845>.
- [87] Bowen TS, Adams V, Werner S, Fischer T, Vinke P, Brogger MN, et al. Small-molecule inhibition of MuRF1 attenuates skeletal muscle atrophy and dysfunction in cardiac cachexia. *J Cachexia Sarcopenia Muscle* 2017;8:939–53. <https://doi.org/10.1002/jcsm.12233>.
- [88] Labeit S, Kohl CH, Witt CC, Labeit D, Jung J, Granzier H. Modulation of Muscle Atrophy, Fatigue and MLC Phosphorylation by MuRF1 as Indicated by Hindlimb Suspension Studies on MuRF1-KO Mice. *J Biomed Biotechnol* 2010;2010. <https://doi.org/10.1155/2010/693741>.
- [89] Hershko A, Ciechanover A. The ubiquitin system. *Annu Rev Biochem* 1998;67:425–79. <https://doi.org/10.1146/annurev.biochem.67.1.425>.
- [90] Taylor PN, Albrecht D, Scholz A, Gutierrez-Buey G, Lazarus JH, Dayan CM, et al. Global epidemiology of hyperthyroidism and hypothyroidism. *Nat Rev Endocrinol* 2018;14:301–16. <https://doi.org/10.1038/nrendo.2018.18>.

6 ANEXOS

6.1. Autorização uso artigo “Thyroid hormone upregulates MDM2 in rat type I fibre: Implications for skeletal muscle mass regulation”

JOHN WILEY AND SONS LICENSE
TERMS AND CONDITIONS

Jul 22, 2021

This Agreement between Mr. André Cruz ("You") and John Wiley and Sons ("John Wiley and Sons") consists of your license details and the terms and conditions provided by John Wiley and Sons and Copyright Clearance Center.

License Number 5114401071735

License date Jul 22, 2021

Licensed Content Publisher John Wiley and Sons

Licensed Content Publication Acta Physiologica

Licensed Content Title Thyroid hormone upregulates MDM2 in rat type I fibre: Implications for skeletal muscle mass regulation

Licensed Content Author A. S. Moriscot, J. G. Silvestre, I. L. Baptista, et al

Licensed Content Date Dec 18, 2017

Licensed Content Volume 222

Licensed Content Issue 4

Licensed
Content Pages 15

Type of use Dissertation/Thesis

Requestor type Author of this Wiley article

Format Print and electronic

Portion Full article

Will you be translating? No

Title Identification and characterization of cellular/molecular mechanisms involved in skeletal muscle mass regulation by experimental hyperthyroidism

Institution name University of São Paulo

Expected presentation date Oct 2021

Order reference number 30

Requestor Location
Mr. André Cruz
Av. Professor Lineu Prestes, 2415
Lab 02, subsolo02, ICB3
São Paulo, São Paulo 05508-000
Brazil
Attn: Mr. André Cruz

Publisher Tax ID EU826007151

Total 0.00 USD

Terms and Conditions

TERMS AND CONDITIONS

This copyrighted material is owned by or exclusively licensed to John Wiley & Sons, Inc. or one of its group companies (each a "Wiley Company") or handled on behalf of a society with which a Wiley Company has exclusive publishing rights in relation to a particular work (collectively "WILEY"). By clicking "accept" in connection with completing this licensing transaction, you agree that the following terms and conditions apply to this transaction (along with the billing and payment terms and conditions established by the Copyright Clearance Center Inc., ("CCC's Billing and Payment terms and conditions"), at the time that you opened your RightsLink account (these are available at any time at <http://myaccount.copyright.com>).

Terms and Conditions

- The materials you have requested permission to reproduce or reuse (the "Wiley Materials") are protected by copyright.
- You are hereby granted a personal, non-exclusive, non-sub licensable (on a stand-alone basis), non-transferable, worldwide, limited license to reproduce the Wiley Materials for the purpose specified in the licensing process. This license, **and any CONTENT (PDF or image file) purchased as part of your order**, is for a one-time use only and limited to any maximum distribution number specified in the license. The first instance of republication or reuse granted by this license must be completed within two years of the date of the grant of this license (although copies prepared before the end date may be distributed thereafter). The Wiley Materials shall not be used in any other manner or for any other purpose, beyond what is granted in the license. Permission is granted subject to an appropriate acknowledgement given to the author, title of the material/book/journal and the publisher. You shall also duplicate the copyright notice that appears in the Wiley publication in your use of the Wiley Material. Permission is also granted on the understanding that nowhere in the text is a previously published source acknowledged for all or part of this Wiley Material. Any third party content is expressly excluded from this permission.
- With respect to the Wiley Materials, all rights are reserved. Except as expressly granted by the terms of the license, no part of the Wiley Materials may be copied, modified, adapted (except for minor reformatting required by the new Publication), translated, reproduced, transferred or distributed, in any form or by any means, and no derivative works may be made based on the Wiley Materials without the prior permission of the respective copyright owner. **For STM Signatory Publishers clearing permission under the terms of the [STM Permissions Guidelines](#) only, the terms of the license are extended to include subsequent editions and for editions in other languages, provided such editions are for the work as a whole in situ and does not involve the separate exploitation of the permitted figures or extracts**, You may not alter, remove or suppress in any manner any copyright, trademark or other notices displayed by the Wiley Materials. You may not license, rent, sell, loan, lease, pledge, offer as security, transfer or assign the Wiley Materials on a stand-alone basis, or any of the rights granted to you hereunder to any other person.
- The Wiley Materials and all of the intellectual property rights therein shall at all times

remain the exclusive property of John Wiley & Sons Inc, the Wiley Companies, or their respective licensors, and your interest therein is only that of having possession of and the right to reproduce the Wiley Materials pursuant to Section 2 herein during the continuance of this Agreement. You agree that you own no right, title or interest in or to the Wiley Materials or any of the intellectual property rights therein. You shall have no rights hereunder other than the license as provided for above in Section 2. No right, license or interest to any trademark, trade name, service mark or other branding ("Marks") of WILEY or its licensors is granted hereunder, and you agree that you shall not assert any such right, license or interest with respect thereto

- NEITHER WILEY NOR ITS LICENSORS MAKES ANY WARRANTY OR REPRESENTATION OF ANY KIND TO YOU OR ANY THIRD PARTY, EXPRESS, IMPLIED OR STATUTORY, WITH RESPECT TO THE MATERIALS OR THE ACCURACY OF ANY INFORMATION CONTAINED IN THE MATERIALS, INCLUDING, WITHOUT LIMITATION, ANY IMPLIED WARRANTY OF MERCHANTABILITY, ACCURACY, SATISFACTORY QUALITY, FITNESS FOR A PARTICULAR PURPOSE, USABILITY, INTEGRATION OR NON-INFRINGEMENT AND ALL SUCH WARRANTIES ARE HEREBY EXCLUDED BY WILEY AND ITS LICENSORS AND WAIVED BY YOU.
- WILEY shall have the right to terminate this Agreement immediately upon breach of this Agreement by you.
- You shall indemnify, defend and hold harmless WILEY, its Licensors and their respective directors, officers, agents and employees, from and against any actual or threatened claims, demands, causes of action or proceedings arising from any breach of this Agreement by you.
- IN NO EVENT SHALL WILEY OR ITS LICENSORS BE LIABLE TO YOU OR ANY OTHER PARTY OR ANY OTHER PERSON OR ENTITY FOR ANY SPECIAL, CONSEQUENTIAL, INCIDENTAL, INDIRECT, EXEMPLARY OR PUNITIVE DAMAGES, HOWEVER CAUSED, ARISING OUT OF OR IN CONNECTION WITH THE DOWNLOADING, PROVISIONING, VIEWING OR USE OF THE MATERIALS REGARDLESS OF THE FORM OF ACTION, WHETHER FOR BREACH OF CONTRACT, BREACH OF WARRANTY, TORT, NEGLIGENCE, INFRINGEMENT OR OTHERWISE (INCLUDING, WITHOUT LIMITATION, DAMAGES BASED ON LOSS OF PROFITS, DATA, FILES, USE, BUSINESS OPPORTUNITY OR CLAIMS OF THIRD PARTIES), AND WHETHER OR NOT THE PARTY HAS BEEN ADVISED OF THE POSSIBILITY OF SUCH DAMAGES. THIS LIMITATION SHALL APPLY NOTWITHSTANDING ANY FAILURE OF ESSENTIAL PURPOSE OF ANY LIMITED REMEDY PROVIDED HEREIN.
- Should any provision of this Agreement be held by a court of competent jurisdiction to be illegal, invalid, or unenforceable, that provision shall be deemed amended to achieve as nearly as possible the same economic effect as the original provision, and the legality, validity and enforceability of the remaining provisions of this Agreement shall not be affected or impaired thereby.
- The failure of either party to enforce any term or condition of this Agreement shall not constitute a waiver of either party's right to enforce each and every term and condition of this Agreement. No breach under this agreement shall be deemed waived or excused by either party unless such waiver or consent is in writing signed by the party

granting such waiver or consent. The waiver by or consent of a party to a breach of any provision of this Agreement shall not operate or be construed as a waiver of or consent to any other or subsequent breach by such other party.

- This Agreement may not be assigned (including by operation of law or otherwise) by you without WILEY's prior written consent.
- Any fee required for this permission shall be non-refundable after thirty (30) days from receipt by the CCC.
- These terms and conditions together with CCC's Billing and Payment terms and conditions (which are incorporated herein) form the entire agreement between you and WILEY concerning this licensing transaction and (in the absence of fraud) supersedes all prior agreements and representations of the parties, oral or written. This Agreement may not be amended except in writing signed by both parties. This Agreement shall be binding upon and inure to the benefit of the parties' successors, legal representatives, and authorized assigns.
- In the event of any conflict between your obligations established by these terms and conditions and those established by CCC's Billing and Payment terms and conditions, these terms and conditions shall prevail.
- WILEY expressly reserves all rights not specifically granted in the combination of (i) the license details provided by you and accepted in the course of this licensing transaction, (ii) these terms and conditions and (iii) CCC's Billing and Payment terms and conditions.
- This Agreement will be void if the Type of Use, Format, Circulation, or Requestor Type was misrepresented during the licensing process.
- This Agreement shall be governed by and construed in accordance with the laws of the State of New York, USA, without regards to such state's conflict of law rules. Any legal action, suit or proceeding arising out of or relating to these Terms and Conditions or the breach thereof shall be instituted in a court of competent jurisdiction in New York County in the State of New York in the United States of America and each party hereby consents and submits to the personal jurisdiction of such court, waives any objection to venue in such court and consents to service of process by registered or certified mail, return receipt requested, at the last known address of such party.

WILEY OPEN ACCESS TERMS AND CONDITIONS

Wiley Publishes Open Access Articles in fully Open Access Journals and in Subscription journals offering Online Open. Although most of the fully Open Access journals publish open access articles under the terms of the Creative Commons Attribution (CC BY) License only, the subscription journals and a few of the Open Access Journals offer a choice of Creative Commons Licenses. The license type is clearly identified on the article.

The Creative Commons Attribution License

The [Creative Commons Attribution License \(CC-BY\)](#) allows users to copy, distribute and transmit an article, adapt the article and make commercial use of the article. The CC-BY license permits commercial and non-

Creative Commons Attribution Non-Commercial License

The [Creative Commons Attribution Non-Commercial \(CC-BY-NC\) License](#) permits use, distribution and reproduction in any medium, provided the original work is properly cited and is not used for commercial purposes.(see below)

Creative Commons Attribution-Non-Commercial-NoDerivs License

The [Creative Commons Attribution Non-Commercial-NoDerivs License](#) (CC-BY-NC-ND) permits use, distribution and reproduction in any medium, provided the original work is properly cited, is not used for commercial purposes and no modifications or adaptations are made. (see below)

Use by commercial "for-profit" organizations

Use of Wiley Open Access articles for commercial, promotional, or marketing purposes requires further explicit permission from Wiley and will be subject to a fee.

Further details can be found on Wiley Online Library
<http://olabout.wiley.com/WileyCDA/Section/id-410895.html>

Other Terms and Conditions:

v1.10 Last updated September 2015

Questions? customercare@copyright.com or +1-855-239-3415 (toll free in the US) or +1-978-646-2777.

6.2. Autorização para uso do artigo “Skeletal Muscle Anti-Atrophic Effects of Leucine Involve Myostatin Inhibition”

Mary Ann Liebert, Inc. Copyright Transfer Agreement

Article Title: SKELETAL MUSCLE ANTI-ATROPHIC EFFECTS OF LEUCINE INVOLVE MYOSTATIN INHIBITION

Name of Author: Mr. André Cruz

Journal Name: DNA and Cell Biology

1. The Contribution

The Author(s) hereby affirm(s):

- A. The Contribution entitled "SKELETAL MUSCLE ANTI-ATROPHIC EFFECTS OF LEUCINE INVOLVE MYOSTATIN INHIBITION" is to be published in DNA and Cell Biology.
- B. Applicable Supplementary Material shall be published with Contribution in DNA and Cell Biology.

2. Obligations of the Authors(s)

The Author(s) warrant(s):

- A. Contribution and Supplementary Material is original and no part has been plagiarized, fabricated, or manipulated.
- B. All individuals identified as Authors* contributed to the Contribution, and all individuals who contributed are listed as Authors on the Contribution. [*See below for definition of "Author."]
- C. Contribution is not under consideration in another publication and has not been published elsewhere, or in any other language.
- D. Contribution and Supplementary Material contains no libelous or unlawful statements; does not infringe upon the rights (including without limitation the copyright, patent, or trademark rights) or the privacy of others; does not contain material or instructions that might cause harm or injury.
- E. If applicable, Contribution meets all ethical guidelines and/or Internal Review Board approval in the treatment of human and animal studies (see Instructions for Authors), or meets the requirements set forth by the Declaration of Helsinki.
- F. Names and all identifying features or information have been removed from the Contribution's figures, tables, text, and Supplemental Material.
- G. Obtained re-use permission for excerpts from copyrighted works owned by third parties and attribution to the sources have been included in the Contribution.
- H. Author(s) have disclosed any conflicts of interest within the Contribution as a paragraph before the reference section.
- I. All contributing Authors are aware of the rights and conditions set forth in this agreement.
- J. The Authors(s) will indemnify Mary Ann Liebert, Inc., against any costs, expenses, or damages, which may incur, or of which Mary Ann Liebert, Inc., may become liable as a result from any breach of these warranties contained herein. These representations and warranties may be extended to third parties by Mary Ann Liebert, Inc.

***Authorship is defined as:**

- *Substantial contributions to the conception or design of the work; or the acquisition, analysis, or interpretation of data for the work; AND*
- *Drafting the work or revising it critically for important intellectual content; AND*
- *Final approval of the version to be published; AND*
- *Agreement to be accountable for all aspects of the work in ensuring that questions related to the accuracy or integrity of any part of the work are appropriately investigated and resolved.*

3. Grant of Right

3.1. The Author(s) grant the copyright of this Contribution, including any graphic and/or video elements therein (e.g. illustrations, charts, moving images), is hereby assigned for good and valuable consideration to Mary Ann Liebert, Inc., effective if and when the Contribution is accepted for publication and to the extent assignable if assignability is restricted by applicable law or regulations. If copyright cannot be assigned to Mary Ann Liebert, Inc., because the Author(s) are government employees then the Author(s) agree to inform Mary Ann Liebert, Inc.

CCC RightsLink®

Home Help Live Chat André Cruz ▾

 **Skeletal Muscle Anti-Atrophic Effects of Leucine Involve Myostatin Inhibition**
Author: André Cruz, Andrea Ferian, Paula K.N. Alves, et al
Publication: DNA and Cell Biology
Publisher: Mary Ann Liebert, Inc.
Date: Dec 1, 2020
Copyright © 2020, Mary Ann Liebert, Inc.

Permissions Request

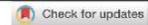
Mary Ann Liebert, Inc. publishers does not require authors of the content being used to obtain a license for their personal reuse of full article, charts/graphs/tables or text excerpt.

[BACK](#) [CLOSE WINDOW](#)

© 2021 Copyright - All Rights Reserved | Copyright Clearance Center, Inc. | Privacy statement | Terms and Conditions
Comments? We would like to hear from you. E-mail us at customer-care@copyright.com

6.3. Artigos Publicados em Colaboração

6.3.1. “miR-29c improves skeletal muscle mass and function throughout myocyte proliferation and differentiation and by repressing atrophy-related genes”



Received: 24 July 2018 | Revised: 2 March 2019 | Accepted: 31 March 2019
DOI: 10.1111/apha.13278

REGULAR PAPER

ACTA PHYSIOLOGICA

miR-29c improves skeletal muscle mass and function throughout myocyte proliferation and differentiation and by repressing atrophy-related genes

William José Silva¹ | Flavia Aparecida Graça¹ | André Cruz¹ |
João Guilherme Silvestre¹ | Siegfried Labeit² | Elen Haruka Miyabara¹ |
Chao Yun Irene Yan³ | Da Zhi Wang⁴ | Anselmo Sigari Moriscot¹

¹Department of Anatomy, Institute of Biomedical Sciences, University of Sao Paulo, Sao Paulo, Brazil

²Faculty for Clinical Medicine Mannheim of the University of Heidelberg, Institute for Integrative Pathophysiology, Universitätsmedizin Mannheim, Mannheim, Germany

³Department of Cell Biology, Institute of Biomedical Sciences, University of Sao Paulo, Sao Paulo, Brazil

⁴Department of Cardiology, Boston Children's Hospital, Harvard Medical School, Boston, Massachusetts

Correspondence

Anselmo Sigari Moriscot, Department of Anatomy, Institute of Biomedical Sciences, University of Sao Paulo, 2415, Av. Professor Lineu Prestes, Sao Paulo 05508-000, Brazil. Email: moriscot@usp.br

Funding information

Leducq Foundation, Grant/Award Number: FLQ13CVD04; Sao Paulo Research Foundation (FAPESP), Grant/Award Number: 645648; National Institutes of Health, Grant/Award Number: HL085635 and HL116919; European Union for financial support (Horizon 2020 project Muscle Stress Relief network), Grant/Award Number: 645648; Conselho Nacional de Desenvolvimento Científico e Tecnológico

See Editorial Commentary: Falcone, G. 2019. A new role of miR-29c as a potent inducer of skeletal muscle hypertrophy. *Acta Physiol.* 226, e13320.

William José Silva and Flavia Aparecida Graça contributed equally to the work.

This is an open access article under the terms of the Creative Commons Attribution-NonCommercial License, which permits use, distribution and reproduction in any medium, provided the original work is properly cited and is not used for commercial purposes.

© 2019 The Authors. *Acta Physiologica* published by John Wiley & Sons Ltd on behalf of Scandinavian Physiological Society

Acta Physiologica. 2019;226:e13278.
<https://doi.org/10.1111/apha.13278>

wileyonlinelibrary.com/journal/apha | 1 of 19

Abstract

Aim: To identify microRNAs (miRs) involved in the regulation of skeletal muscle mass. For that purpose, we have initially utilized an in silico analysis, resulting in the identification of miR-29c as a positive regulator of muscle mass.

Methods: miR-29c was electrotransferred to the tibialis anterior to address its morphometric and functional properties and to determine the level of satellite cell proliferation and differentiation. qPCR was used to investigate the effect of miR-29c overexpression on trophicity-related genes. C2C12 cells were used to determine the impact of miR-29c on myogenesis and a luciferase reporter assay was used to evaluate the ability of miR-29c to bind to the MuRF1 3'UTR.

Results: The overexpression of miR-29c in the tibialis anterior increased muscle mass by 40%, with a corresponding increase in fibre cross-sectional area and force and a 30% increase in length. In addition, satellite cell proliferation and differentiation were increased. In C2C12 cells, miR-29c oligonucleotides caused increased levels of differentiation, as evidenced by an increase in eMHC immunostaining and the myotube fusion index. Accordingly, the mRNA levels of myogenic markers were also increased. Mechanistically, the overexpression of miR-29c inhibited the expression of the muscle atrophic factors MuRF1, Atrogin-1 and HDAC4. For the key atrogene MuRF1, we found that miR-29c can bind to its 3'UTR to mediate repression.

Conclusions: The results herein suggest that miR-29c can improve skeletal muscle size and function by stimulating satellite cell proliferation and repressing atrophy-related genes. Taken together, our results indicate that miR-29c might be useful as a future therapeutic device in diseases involving decreased skeletal muscle mass.

KEYWORDS

atrophy, hypertrophy, miR-29c, myogenesis, skeletal muscle, trophicity

6.3.2. "The E3 ligase MuRF2 plays a key role in the functional capacity of skeletal muscle fibroblasts"

Brazilian Journal of Medical and Biological Research (2019) 52(9): e8551, <http://dx.doi.org/10.1590/1414-431X20198551>
ISSN 1414-431X Research Article



1/10

The E3 ligase MuRF2 plays a key role in the functional capacity of skeletal muscle fibroblasts

J.G. Silvestre¹, I.L. Baptista², W.J. Silva¹, A. Cruz¹, M.T. Silva¹, E.H. Miyabara¹,
S. Labeit³, and A.S. Moriscot¹

¹Departamento de Anatomia, Instituto de Ciências Biomédicas, Universidade de São Paulo, São Paulo, SP, Brasil

²Faculdade de Ciências Aplicadas, UNICAMP, Limeira, SP, Brasil

³Institute for Integrative Pathophysiology, Mannheim Medical University, Faculty for Clinical Medicine Mannheim, University of Heidelberg, Mannheim, Germany

Abstract

Fibroblasts are a highly heterogeneous population of cells, being found in a large number of different tissues. These cells produce the extracellular matrix, which is essential to preserve structural integrity of connective tissues. Fibroblasts are frequently engaged in migration and remodeling, exerting traction forces in the extracellular matrix, which is crucial for matrix deposition and wound healing. In addition, previous studies performed on primary myoblasts suggest that the E3 ligase MuRF2 might function as a cytoskeleton adaptor. Here, we hypothesized that MuRF2 also plays a functional role in skeletal muscle fibroblasts. We found that skeletal muscle fibroblasts express MuRF2 and its siRNA knock-down promoted decreased fibroblast migration, cell border accumulation of polymerized actin, and down-regulation of the phospho-Akt expression. Our results indicated that MuRF2 was necessary to maintain the actin cytoskeleton functionality in skeletal muscle fibroblasts via Akt activity and exerted an important role in extracellular matrix remodeling in the skeletal muscle tissue.

Key words: Fibroblast; Skeletal muscle; Migration; MuRF2; E3 ligase; Wound healing

Introduction

Mesenchymal cells are known for giving rise to a large number of connective tissue cells such as myoblasts, chondroblasts, adipocytes, osteoblasts, and fibroblasts. Fibroblasts, in turn, are a highly heterogeneous population of cells, and can be found in different tissues (1), being the most abundant stromal cell type (2). The extracellular matrix (ECM), produced by fibroblasts, plays essential roles in preserving the structural integrity of connective tissues and during healing progression (1). In skeletal muscle tissue, fibroblasts are one of the most abundant cell population (3). The ECM is an important scaffold for skeletal muscle fibers and is involved in force transmission and protection against mechanical trauma (4).

Regeneration of skeletal muscle is a highly complex process that involves the activation of a large number of intracellular and cell-to-cell responses (5,6). Although it is widely known that the regeneration process relies upon satellite cells in order to repair the skeletal muscle fiber and recover function, the much less understood fibroblasts also play an important role. Recently, there has been increasing evidence of a role for the ECM in signaling through regulatory molecules (7). Interestingly,

however, it is known that excessive ECM can impair muscle function and hinder muscle regeneration (8,9). In wound repair, fibroblasts proliferate and differentiate into active states, secreting important components of the ECM. These cells also intensely engage in migration and remodeling and exert traction forces in the ECM (10).

The migratory capacity of fibroblasts is crucial for matrix deposition and wound healing (11), and recent studies highlight the importance of correct cytoskeleton arrangement for fibroblast migration. Noteworthy, it has been shown that Akt activity is crucial for the establishment of actin filaments at the edge of fibroblasts during the migration process (12). Recently, it has been shown that E3 ubiquitin ligases play important roles in cytoskeleton dynamics towards proper migration (13).

The E3 ubiquitin ligases are proteins that play essential roles in cellular homeostasis and in the degradation of mutated misfolded or damaged proteins (14,15). In skeletal muscle tissue, an important family of E3 ubiquitin ligases initially named muscle-specific RING finger (MuRFs) has been described (16). Subsequently, MuRFs were categorized as MuRF1 (17) and MuRF2 (18). MuRF2 can establish

Correspondence: A.S. Moriscot: <moriscot@usp.br>

Received February 21, 2019 | Accepted July 11, 2019

Braz J Med Biol Res | doi: 10.1590/1414-431X20198551

6.3.3. “Small-Molecule Chemical Knockdown of MuRF1 in Melanoma Bearing Mice Attenuates Tumor Cachexia Associated Myopathy”



Article

Small-Molecule Chemical Knockdown of MuRF1 in Melanoma Bearing Mice Attenuates Tumor Cachexia Associated Myopathy

Volker Adams ^{1,2,*}, Victoria Gußen ^{1,†}, Sergey Zozulya ³, André Cruz ⁴, Anselmo Moriscot ⁴, Axel Linke ^{1,2} and Siegfried Labeit ⁵

¹ Laboratory of Molecular and Experimental Cardiology, TU Dresden, Heart Center Dresden, 1307 Dresden, Germany; victoria.gussen@gmx.de (V.G.); Axel.linke@tu-dresden.de (A.L.)

² Dresden Cardiovascular Research Institute and Core Laboratories GmbH, 01067 Dresden, Germany

³ Department of Drug Research, Enamine-Bienta Ltd., 02000 Kiev, Ukraine; s.zozulya@enamine.net

⁴ Department of Anatomy, Institute of Biomedical Sciences, University of Sao Paulo, Sao Paulo 05508-000, Brazil; andrecruz@usp.br (A.C.); moriscot@usp.br (A.M.)

⁵ Medical Faculty Mannheim, University of Heidelberg, 68167 Mannheim, Germany; labeit@medma.de

* Correspondence: volker.adams@mailbox.tu-dresden.de; Tel.: +49-(0)3514586627

† These authors contributed equally to this work.

Received: 4 September 2020; Accepted: 21 September 2020; Published: 11 October 2020



Abstract: Patients with malignant tumors frequently suffer during disease progression from a syndrome referred to as cancer cachexia (CaCax): CaCax includes skeletal muscle atrophy and weakness, loss of bodyweight, and fat tissues. Currently, there are no FDA (Food and Drug Administration) approved treatments available for CaCax. Here, we studied skeletal muscle atrophy and dysfunction in a murine CaCax model by injecting B16F10 melanoma cells into mouse thighs and followed mice during melanoma outgrowth. Skeletal muscles developed progressive weakness as detected by wire hang tests (WHTs) during days 13–23. Individual muscles analyzed at day 24 had atrophy, mitochondrial dysfunction, augmented metabolic reactive oxygen species (ROS) stress, and a catabolically activated ubiquitin proteasome system (UPS), including upregulated MuRF1. Accordingly, we tested as an experimental intervention of recently identified small molecules, Myomed-205 and -946, that inhibit MuRF1 activity and MuRF1/MuRF2 expression. Results indicate that MuRF1 inhibitor fed attenuated induction of MuRF1 in tumor stressed muscles. In addition, the compounds augmented muscle performance in WHTs and attenuated muscle weight loss. Myomed-205 and -946 also rescued citrate synthase and complex-1 activities in tumor-stressed muscles, possibly suggesting that mitochondrial-metabolic and muscle wasting effects in this CaCax model are mechanistically connected. Inhibition of MuRF1 during tumor cachexia may represent a suitable strategy to attenuate skeletal muscle atrophy and dysfunction.

Keywords: cancer cachexia; melanoma tumors; muscle wasting; mitochondrial metabolism; MuRF1; chemical biology

1. Introduction

The term cancer cachexia (CaCax) was introduced to describe a heterogeneous group of syndromes where malignancy is the underlying cause of a general cachexia. CaCax in patients is highly variable and depends on the underlying tumor as well as its treatment [1–4]. Solid tumors of the pancreas, lung, liver, and gastrointestinal tract are typically associated with cancer cachexia [3]. Overall, it has been estimated that about 50–80% of all malignancies include cancer cachexia, and cancer cachexia may account for as much as 20% of all cancer deaths [2]. Cachexia progression has also been correlated

6.3.4. “Leucine Supplementation Decreases HDAC4 Expression and Nuclear Localization in Skeletal Muscle Fiber of Rats Submitted to Hindlimb Immobilization”



Article

Leucine Supplementation Decreases HDAC4 Expression and Nuclear Localization in Skeletal Muscle Fiber of Rats Submitted to Hindlimb Immobilization

Paula K. N. Alves ¹, André Cruz ¹, William J. Silva ¹, Siegfried Labeit ^{2,3} and Anselmo S. Moriscot ^{1,*}

¹ Department of Anatomy, Institute of Biomedical Sciences, University of Sao Paulo, Sao Paulo 05508000, Brazil; paulaketilly@usp.br (P.K.N.A.); andrecruz@usp.br (A.C.); williamsilvaj@gmail.com (W.J.S.)

² Faculty for Clinical Medicine Mannheim of the University of Heidelberg, Institute for Integrative Pathophysiology, Universitätsmedizin Mannheim, 68169 Mannheim, Germany; labeit@medma.de

³ Myomedix GmbH, 69151 Neckargemund, Germany

* Correspondence: moriscot@usp.br

Received: 22 September 2020; Accepted: 26 November 2020; Published: 2 December 2020



Abstract: In this study we surveyed a rat skeletal muscle RNA-Seq for genes that are induced by hindlimb immobilization and, in turn, become attenuated by leucine supplementation. This approach, in search of leucine-atrophy protection mediating genes, identified histone deacetylase 4 (*HDAC4*) as highly responsive to both hindlimb immobilization and leucine supplementation. We then examined the impact of leucine on *HDAC4* expression, tissue localization, and target genes. A total of 76 male Wistar rats (~280 g) were submitted to hindlimb immobilization and/or leucine supplementation for 3, 7 and 12 days. These animals were euthanized, and soleus muscle was removed for further analysis. RNA-Seq analysis of hindlimb immobilized rats indicated a sharp induction ($\log_2 = 3.4$) of *HDAC4* expression which was attenuated by leucine supplementation (~50%). Real-time PCR and protein expression analysis by Western blot confirmed increased *HDAC4* mRNA after 7 days of hindlimb immobilization and mitigation of induction by leucine supplementation. Regarding the *HDAC4* localization, the proportion of positive nuclei was higher in the immobilized group and decreased after leucine supplementation. Also, we found a marked decrease of myogenin and *MAFbx-atrogin-1* mRNA levels upon leucine supplementation, while *CAMKII* and *DACH2* mRNA levels were increased by leucine supplementation. Our data suggest that *HDAC4* inhibition might be involved in the anti-atrophic effects of leucine.

Keywords: atrophy; skeletal muscle; *HDAC4*; *MAFbx*; *MYOG*; leucine supplementation

1. Introduction

Skeletal muscle shows a high degree of adaptability to external pressure, such as injury and mechanical load. When the mechanical load decreases, reducing skeletal muscle burden, molecular mechanisms are triggered promoting muscle atrophy. Most of this signaling acts on protein turnover, modifying the protein synthesis and degradation balance, favoring a scenario where protein breakdown exceeds the synthesis of new proteins [1,2].

Many conditions can induce skeletal muscle atrophy, such as extended periods of limb disuse/immobilization [3–5], long-lasting bed rest [6], microgravity [5], physical inactivity [7], denervation [8], malignant cachexia [9], long-term corticoid treatment [10], and inflammation [11]. Generally, the atrophic process is highly integrated, embracing gene transcription and enzyme activity

6.3.5. “Regulation of Glucose Metabolism by MuRF1 and Treatment of Myopathy in Diabetic Mice with Small Molecules Targeting MuRF1”



International Journal of
Molecular Sciences



Article

Regulation of Glucose Metabolism by MuRF1 and Treatment of Myopathy in Diabetic Mice with Small Molecules Targeting MuRF1

Siegfried Labeit ^{1,2,*}, Stephanie Hirner ¹, Julijus Bogomolovas ³, André Cruz ⁴, Moldir Myrzabekova ⁵, Anselmo Moriscot ⁴, Thomas Scott Bowen ⁶ and Volker Adams ^{7,8}

¹ Department of Anesthesiology, Medical Faculty Mannheim, University of Heidelberg, 68169 Mannheim, Germany; stephanie.hirner@gmx.de

² Myomedix GmbH, 69151 Neckargemünd, Germany

³ Zentralinstitut für Seelische Gesundheit, 68159 Mannheim, Germany; jbogomolovas@ucsd.edu

⁴ Department of Anatomy, Institute of Biomedical Sciences, University of Sao Paulo, 05508-000 Sao Paulo, Brazil; andreacruz@usp.br (A.C.); moriscot@usp.br (A.M.)

⁵ Scientific Research Institute of Biology and Biotechnology Problems, al-Farabi Kasakh National University, Almaty 050040, Kazakhstan; moldir.myrzabek@gmail.com

⁶ School of Biomedical Sciences, University of Leeds, Leeds LS2 9JT, UK; T.S.Bowen@leeds.ac.uk

⁷ Laboratory of Molecular and Experimental Cardiology, TU Dresden, Heart Center Dresden, 01307 Dresden, Germany; volker.adams@mailbox.tu-dresden.de

⁸ Dresden Cardiovascular Research Institute and Core Laboratories GmbH, 01307 Dresden, Germany

* Correspondence: labeit@medma.de; Tel.: +0049-(0)6223-71738



Citation: Labeit, S.; Hirner, S.; Bogomolovas, J.; Cruz, A.; Myrzabekova, M.; Moriscot, A.; Bowen, T.S.; Adams, V. Regulation of Glucose Metabolism by MuRF1 and Treatment of Myopathy in Diabetic Mice with Small Molecules Targeting MuRF1. *Int. J. Mol. Sci.* **2021**, *22*, 2225. <https://doi.org/10.3390/ijms22042225>

Academic Editor: Henri Bernardi

Received: 15 October 2020

Accepted: 15 February 2021

Published: 23 February 2021

Publisher's Note: MDPI stays neutral with regard to jurisdictional claims in published maps and institutional affiliations.



Copyright: © 2021 by the authors. Licensee MDPI, Basel, Switzerland. This article is an open access article distributed under the terms and conditions of the Creative Commons Attribution (CC BY) license (<https://creativecommons.org/licenses/by/4.0/>).

Abstract: The muscle-specific ubiquitin ligase MuRF1 regulates muscle catabolism during chronic wasting states, although its roles in general metabolism are less-studied. Here, we metabolically profiled MuRF1-deficient knockout mice. We also included knockout mice for MuRF2 as its closely related gene homolog. MuRF1 and MuRF2-KO (knockout) mice have elevated serum glucose, elevated triglycerides, and reduced glucose tolerance. In addition, MuRF2-KO mice have a reduced tolerance to a fat-rich diet. Western blot and enzymatic studies on MuRF1-KO skeletal muscle showed perturbed FoxO-Akt signaling, elevated Akt-Ser-473 activation, and downregulated oxidative mitochondrial metabolism, indicating potential mechanisms for MuRF1,2-dependent glucose and fat metabolism regulation. Consistent with this, the adenoviral re-expression of MuRF1 in KO mice normalized Akt-Ser-473, serum glucose, and triglycerides. Finally, we tested the MuRF1/2 inhibitors MyoMed-205 and MyoMed-946 in a mouse model for type 2 diabetes mellitus (T2DM). After 28 days of treatment, T2DM mice developed progressive muscle weakness detected by wire hang tests, but this was attenuated by the MyoMed-205 treatment. While MyoMed-205 and MyoMed-946 had no significant effects on serum glucose, they did normalize the lymphocyte-granulocyte counts in diabetic sera as indicators of the immune response. Thus, small molecules directed to MuRF1 may be useful in attenuating skeletal muscle strength loss in T2DM conditions.

Keywords: diabetes mellitus; glucose and muscle metabolism; MuRF1; MuRF2; chemical biology

1. Introduction

A secondary progressive loss of muscle mass or sarcopenia in chronic diseases is an increasing medical issue, particularly in the ageing population of developed countries [1,2]. The underlying causes are frequently multifactorial, such as aging-dependent inactivity and malnutrition. Myofibril loss, also referred to as sarcopenia, becomes further exacerbated when patients suffer from additional cachexia-promoting states, such as diabetes, sepsis, or inflammation, that further promote general muscle catabolism [3,4]. The molecular mechanisms that underlie the development of muscle wasting include downregulation of the translation of muscle proteins, activation of their degradation by site-specific proteases

6.4. Artigos Completos Publicados – Primeira autoria

ORIGINAL ARTICLE

Thyroid hormone upregulates MDM2 in rat type I fibre: Implications for skeletal muscle mass regulation

G. V. Ramos | A. Cruz  | W. J. Silva | A. Rozanski | I. L. Baptista | J. G. Silvestre | A. S. Moriscot

Department of Anatomy, Institute of Biomedical Sciences, University of Sao Paulo, Sao Paulo, Brazil

Correspondence

A. S. Moriscot, Department of Anatomy, Institute of Biomedical Sciences, University of São Paulo, São Paulo, Brazil.
Email: moriscot@usp.br

Funding information

This work was supported by the Sao Paulo Research Foundation (FAPESP) fellowships #2010/50321-0, #2012/22488-2, #2012/13315-7, #2012/13071-0, #2012/22488-4, #2017/09398-8, and by the Research Grant 2015/04090-0. This work was also supported by the Brazilian National Research Foundation CNPq grant #201123/2010-1.

Abstract

Aim: Based upon a microarray assay, we have identified that triiodothyronine (T3) upregulates MDM2 gene expression in the rat skeletal muscle. As MDM2 protein is an E3 ligase, we hypothesized that this enzyme could play a role in T3 effects on skeletal muscle mass control.

Methods: To test our hypothesis, male rats (2 months old) were randomly assigned into the following groups: intact controls, treated with 20 physiological doses of T3 for 0.5, 1 and 7 days, or with 5, 20 and 50 physiological doses of T3 for 7 days. For in vitro experiments, myotubes and C2C12 cells were treated with T3 for 3 days.

Results: After validation of the microarray finding throughout RT-PCR and confirmation that T3 induces increases in MDM2 protein expression in a dose-dependent manner, we observed that MDM2 was upregulated by T3 exclusively in fibre type I. Moreover, detailed histological evaluation showed that MDM2 overexpression distributes punctiformly along the cross section of the fibre and also inside nuclei. MDM2 colocalizes with PAX7 in control muscle and T3 downregulates this myogenic factor. Pharmacological inhibition of MDM2 in cultured myotubes caused a severe decrease in their diameter (~35%, $P < .001$ vs Control), enhancing the effect of T3 (from ~12% to ~35%, $P < .001$) alone upon myotube diameter and mRNA levels of atrogenes. Finally, we observed that FOXO3 (MDM2 target) is kept outside the nucleus under T3 stimulation.

Conclusion: Our results indicate that MDM2 might be involved in the pro-trophic effects of T3 in skeletal muscle.

KEYWORDS

atrophy, E3 Ligase, MDM2, skeletal muscle, T3

1 | INTRODUCTION

T3 is a key hormone broadly involved in many biological processes, including development, differentiation and metabolism. It is well known that hypothyroidism can lead to

developmental malformations including delayed growth, abnormal neurogenesis, deafness and cardiac defects.¹ The importance of T3 is also well recognized by its conserved expression from amphioxus to humans.²

At the molecular level, T3 is well known to act as an activator of the receptors TR α and TR β . These receptors are expressed in different tissues in the postnatal phase and

Ramos and Cruz equally contributed to this study.

are associated with specific DNA sequences denominated THREs (thyroid hormone-responsive element), located in target genes. These receptors can form homodimers or heterodimers with partners such as RAR, RXR and VDR. When the complex T3-TR is formed, transcriptional modulation of the target gene occurs, a mechanism that mediates most of the biological effects of the hormone and is known as genomic action. More recently, non-genomic effects mediated by T3 in the plasma membrane, cytoplasm and mitochondria have been well described.³ Furthermore, T3 signalling is modulated by plasma membrane selective transport, interactions of TR with co-repressors and co-activators, crosstalk with other intracellular pathways and by the configuration of the THREs. Finally, levels of T3 also can be regulated by deiodinases.^{1,4}

An interesting aspect of T3 action is its dual effect in many systems: for example, elevated levels of this hormone can increase lipogenesis and lipolysis in both white and brown fat tissue.⁵ In bone tissue, T3 can simultaneously increase osteoblastic and osteoclastic activity.⁶ In skeletal muscle, supra-physiological levels of T3 can increase expression of fast twitch myosin heavy chain proteins and simultaneously increase mitochondrial content and myoglobin expression, leading to skeletal muscle fibres that have increased fast twitch power and also increased aerobic capacity.⁷ Regarding skeletal muscle mass control, T3 is well described to increase protein breakdown.^{8,9} On the other hand, it has been suggested that T3 can also activate protein synthesis pathways.¹⁰ The net output of these two opposing forces results in a sarcopenic status. The precise molecular players in these two effects (catabolic vs anabolic) of T3 are not well understood, and their identification and characterization can unravel new targets for therapeutic strategies emphasizing spared mass.

Previous observations have shown that high levels of T3 stimulate the ubiquitin-proteasome-dependent protein breakdown in skeletal muscle,^{11,12} which is considered to be the main pathway of proteolysis of myofibrillar proteins in skeletal muscle.¹³ In this system, E3 ligases ubiquitinate target proteins that will be directed and degraded at the 26S proteasome. F-box protein 32 (MAFbx/Atrogin-1) and tripartite motif containing 63 (muscle RING Finger 1/MuRF1) are two E3 ligases abundantly expressed in skeletal muscles and have been directly implicated in muscle wasting in several catabolic conditions; therefore, they were named as atrogenes.^{14–16} On the other hand, it is unlikely that these two E3 ligases can account for all the massive ubiquitination that occurs under atrophic conditions; therefore, it is possible that additional E3 ligases play a role in skeletal muscle mass control. Accordingly, new E3 ligases need to be identified and explored to deepen the understanding on the effects of T3 upon skeletal muscle.

In this study, we have used a microarray approach aiming to identify additional E3 ligases responsive to thyroid

hormone. Out of the E3 ligases identified, MDM2 caught our attention because of reproducibility and levels of responsiveness to T3. MDM2 is an oncogene overexpressed in several types of human sarcomas. Oliner and colleagues¹⁷ have shown amplification of MDM2 in approximately 30% of osteosarcomas and soft tissue tumours. Previous observations have evidenced that MDM2 speeds the tumour cells growth throughout interactions with several cell cycle regulatory proteins, including P53 a key cell cycle restrainer. Under physiological conditions, MDM2 plays a crucial role for cell survival by keeping P53 appropriated repressed into the cell. This regulatory mechanism is important because increased P53 levels can cause cell cycle arrest and apoptosis.^{18,19}

In this study, we have identified and characterized MDM2 gene responsiveness to T3 in skeletal muscle, determining expression levels and tissue/cellular localization. Furthermore, we have shown in vitro that MDM2 is essential for myotube diameter maintenance. These data emphasize that in addition to activating proteolytic pathways, T3 might also be involved in contention of proteolysis by increasing MDM2 expression.

2 | RESULTS

2.1 | Effect of T3 on body, heart and skeletal muscle weights and on serum T4 levels

Our first step was to confirm the recognized effects of supra-physiological doses of T3 upon body, heart and skeletal muscle weight and serum T4 levels. We observed no significant differences in body weight among all groups. On the other hand, heart weight and heart weight/naso-tail length ratio were significantly increased after 7 days of treatment with T3 (~11.5% and ~11.8% higher than control, respectively, $P < .05$, Table 1). Accordingly, soleus muscle weight and weight/naso-tail length ratio significantly decreased (~11.4% and ~13.5% lower than control, respectively, $P < .05$, Table 1) at 7 days of treatment with T3. As expected, treatment with T3 decreased T4 plasma levels (~90.8% lower than Control, $P < .05$, Table 1).

2.2 | Gene expression level of E3 ligases by microarray and RT-PCR

Using the microarray approach, it was possible to simultaneously analyse 425 genes corresponding to proteolytic pathways (GO: protein catabolism process, ubiquitination and proteolysis). Out of those genes, 55% (233 genes) were regulated by T3 (Figure 1A) and interestingly, out of those, 185 genes belonged to the ubiquitin-proteasome pathway category (Figure 1A). The majority of the T3-responsive genes in the ubiquitin-proteasome category corresponded to E3 ligases (166 genes) (Figure 1A). The responsiveness of E3 ligases

TABLE 1 General data of T4 serum levels, body weight (BW), naso-tail (NT), heart weight (HW), muscle weight (MW) and HW/NT, MW/NT ratios of animals treated with 20 physiological doses of T3. n = 8

Groups	T4 (nmol/L)	BW (g)	NT (cm)	HW (mg)	Soleus MW (mg)	HW/NT (mg/cm)	MW/NT (mg/cm)
Control	44.23 ± 13.59	246.33 ± 24.11	21.09 ± 0.46	851.00 ± 48.18	89.00 ± 8.12	40.34 ± 1.68	4.22 ± 0.33
T3-0.5 day	33.24 ± 10.25	218.35 ± 7.79	20.68 ± 0.79	803.13 ± 39.72	80.31 ± 6.31	38.89 ± 2.24	3.88 ± 0.22
T3-1 day	27.89 ± 9.34*	217.89 ± 19.08	20.21 ± 0.57*	775.50 ± 35.58	81.69 ± 6.98	38.40 ± 2.11	4.01 ± 0.32
T3-7 days	4.05 ± 0.54*	228.08 ± 14.25	21.06 ± 0.50	949.38 ± 84.42*	78.81 ± 6.15*	45.12 ± 4.49*	3.65 ± 0.45*

Values expressed as mean ± SD.

* $P < .05$ vs Control

that presented elevated expression at all experimental time points is shown in Figure 1B. Among T3-responsive E3 ligases, MDM2 caught our attention because of the similarity of response comparing to MuRF1 and also because of high gross basal expression (~1500, data not shown), in contrast to the other top responsive genes (FBXO45:~7, ASB3:~130, BIRC3:~180, KLHL2:~140, data not shown). Therefore, we decided to focus the investigation on MDM2. The upregulation of MDM2 to T3 was validated by RT-PCR (Figure 1C). Similarly to the microarray assay, MDM2 showed upregulation 12 hours after the onset of T3 treatment and lasted up to 7 days. For comparison purposes, the responsiveness of two classical E3 ligases was measured: MAFbx/Atrogin-1 and MuRF1 in skeletal muscle. As expected, those E3 ligases were upregulated by T3 (Figure 1C).

2.3 | MDM2 expression levels in vivo and in vitro

In agreement with mRNA levels, we found that T3 increased MDM2 protein levels at 7 days of treatment (Figure 2A, $P < .05$). Next, we evaluated the effect of increasing doses of T3 upon MDM2 gene and protein expression. MDM2 mRNA expression was increased by 20 physiological doses of T3 (2.4-fold, $P < .05$) and non-responsive at 5 and 50 physiological doses of T3 (Figure 2B). These results were also noticed at the protein level, except at 50 physiological doses where we observed lower levels of MDM2 protein when compared to control (Figure 2C; $P < .05$). In a primary myoblast culture differentiated to myotubes, we observed that MDM2 is also upregulated by T3 (~1.8-fold, Figure 2D, $P < .05$). Similar response can be observed at a C2C12 culture differentiated to myotubes treated with T3 for 48 hours (~1.4-fold, Figure 2D, $P < .05$).

2.4 | MDM2 gene expression in different atrophy models

Since up to date no study has addressed MDM2 expression in different atrophy models, we decided to evaluate mRNA

levels of MDM2 in animals submitted to immobilization, dexamethasone and starvation (Figure 3). Immobilization induced a modest, nonetheless significant, increase in MDM2 mRNA levels 3 days after immobilization (Figure 3A, 1.5-fold, $P < .05$). Starvation, however, induced a robust increase in MDM2 mRNA levels (Figure 3B, 3.1-fold, $P < .05$). Interestingly, we did not observe alterations in MDM2 mRNA levels in the animals treated with dexamethasone when compared to control group (Figure 3C).

2.5 | MDM2 is upregulated by T3 in type I fibres

Next, we decided to address the tissue location of MDM2 in skeletal muscle of animals treated with T3. Under control conditions, the MDM2 immunolabelling inside the fibre was barely detectable and no distinction in the expression pattern was observed between the two main fibre types (Figure 4A–C). T3 stimulation for 1 and 7 days caused increased MDM2 immunolabelling preferentially inside the type I muscle fibre, displaying a punctuated labelling pattern evenly distributed along the fibre cross-sectional area (Figure 4D–I). These results were confirmed throughout quantification of pixels absolute frequency distribution on intensity, as shown in Figure 4J–L. Then, to address the possible relation between calcineurin activity and MDM2 expression, myotubes were treated with cyclosporine A and T3 (Figure 4M). Cyclosporine treatment caused a severe drop in MDM2 gene expression and T3 was unable to increase expression of this gene (Figure 4M).

2.6 | Cellular localization of MDM2 in skeletal muscle

Detailed evaluation of MDM2 immunolabelling revealed that in addition to increased expression inside the skeletal muscle fibre induced by T3, hot spots of immunopositivity were detected inside the nucleus (Figure 5A). Quantification analyses showed that ~34% of the nuclei were positive to MDM2

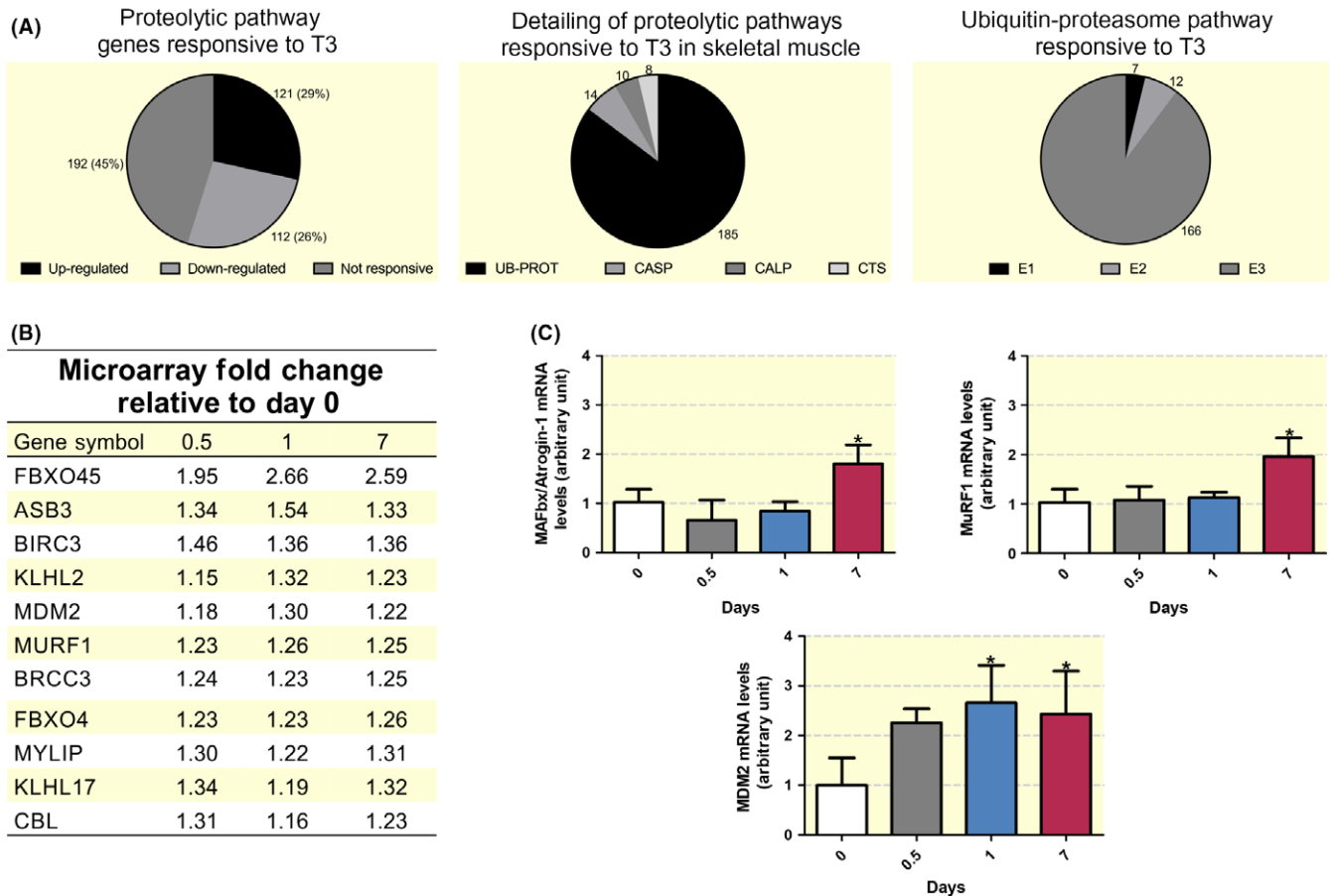


FIGURE 1 Microarray-based global gene expression analysis of proteolytic pathways responsive to T3 in the soleus muscle. A, Proteolysis overall gene expression responsiveness to T3; categories considered were ubiquitin-proteasome (UB-PROT), caspases (CASP), calpains (CALP) and cathepsins (CTS) B, Fold change in mRNA levels of responsive E3 ligases after 0.5, 1 and 7 days of treatment with T3 (fold change of ≥ 1.15 relative to the control group was considered responsive). C, mRNA levels of Mafbx/Atrogin-1, MuRF1 and MDM2 after treatment with T3 for 0.5, 1 and 7 days determined by RT-PCR. Values were expressed as means \pm SD. * $P < .05$ vs control group

in T3-treated group vs $\sim 12\%$ in control group (Figure 5C, $P < .05$). Furthermore, we have observed colocalization of DAPI, PAX7 and MDM2, demonstrating that satellite cells express MDM2, about 10% of nuclei were positive for PAX7 and MDM2 in the control group (Figure 5B-C, $P < .05$). On the other hand, in T3-treated animals, extremely low levels of Pax7-positive nuclei were found (Figure 5B-C).

2.7 | MDM2 is a player in controlling myotube trophicity

In an attempt to understand the role of MDM2 in skeletal muscle trophicity, we used cultured myoblasts that were differentiated into myotubes, which were treated with T3 and also had the interaction of MDM2 and P53 pharmacologically inhibited by Nutlin-3a. Then, myotube area was determined. T3, as expected, reduced myotube area ($\sim 12\%$, $P < .05$, Figures 6A,B). When myotubes were concomitantly submitted to T3 and Nutlin-3a, the negative effect upon myotube area was enhanced (35%, $P < .05$ vs

T3-treated group, Figure 6A,B). Nutlin-3a alone was also able to decrease myotube area at the same level as compared to the group concomitantly treated with T3 and Nutlin (Figure 6A,B, $P < .05$). We have also evaluated the impact of T3 and Nutlin-3a upon gene expression of Mafbx/Atrogin-1 and MuRF1. Interestingly, Nutlin-3a treatment was able to enhance the expression of both genes (1.8-fold and twofold, respectively, $P < .05$) in cultured myotubes treated with T3 (Figure 6C). Notably, Nutlin-3a alone was also able to increase expression of both genes (1.9-fold and 2.3-fold, respectively, $P < .05$, Figure 6C). In this cell culture system, 3 days after T3 stimulation alone did not increase levels of MAFbx/Atrogin-1 and MuRF1, although a clear drop in myotube size was observed (Figure 6B). This apparent uncoupling occurs due to the time point evaluated; for example, we have observed (data not shown) that MAFbx/Atrogin-1 was elevated 24 hours after stimulation.

As gene expression of both Mafbx/Atrogin-1 and MuRF1 was altered by MDM2 inhibition, we decided to address FOXO3, which is a central protein in skeletal muscle mass

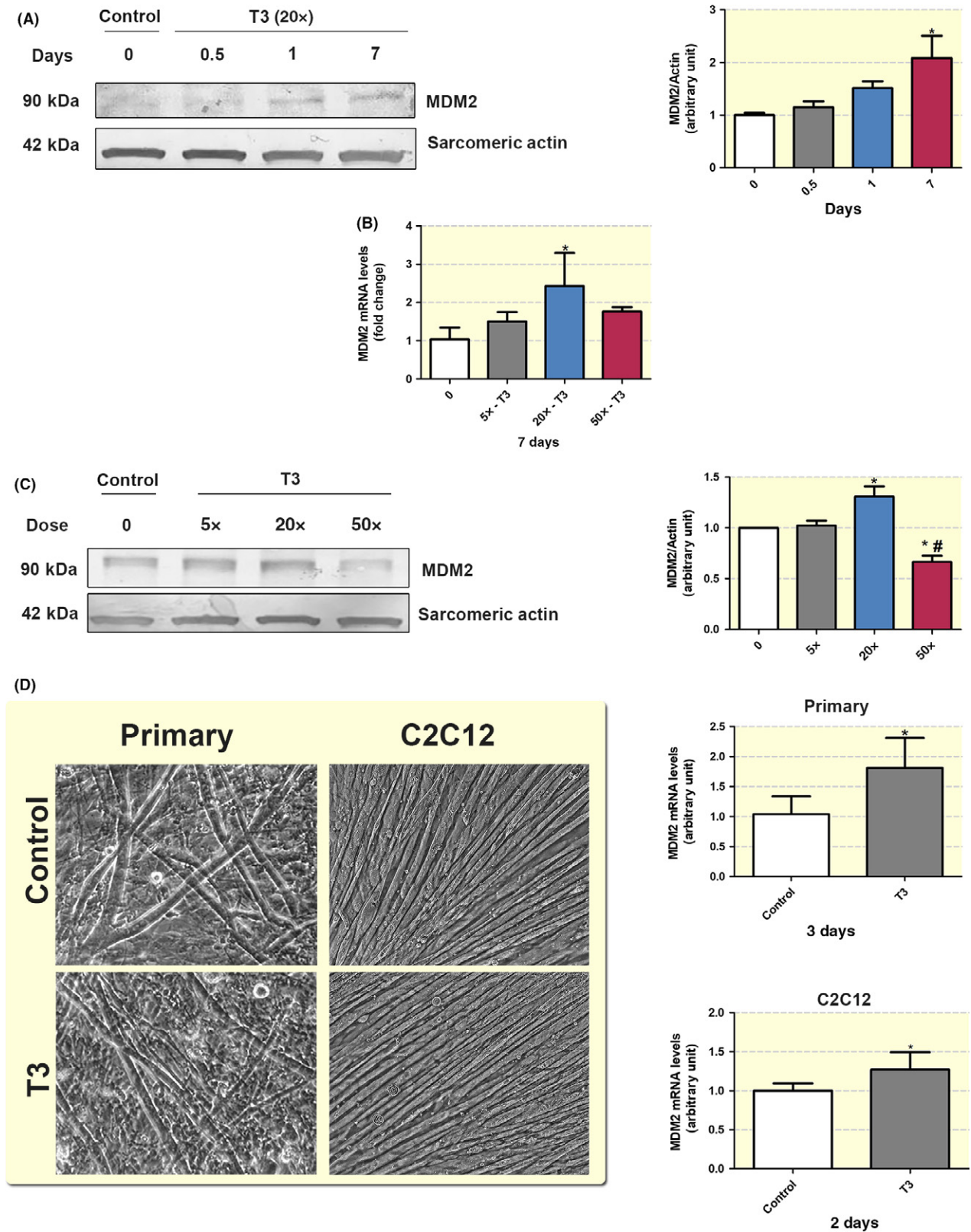


FIGURE 2 T3 increases MDM2 expression in vivo and in vitro. A, MDM2 protein expression in soleus muscle of T3 (20 physiological doses)-treated animals for 0.5, 1 and 7 days. B, MDM2 mRNA expression level in soleus muscle after treatment with different doses of T3 (5, 20 and 50 physiological doses) for 7 days. C, Soleus muscle protein expression levels of MDM2 in animals treated with different doses of T3 (5, 20 and 50 physiological doses) for 7 days. D, Photomicrographs showing general morphological features of myotube cultures originated either from primary myoblasts or from C2C12 cells. Those cultures were treated with T3 (10^{-8} M) for 3 and 2 days, respectively, and mRNA level of MDM2 determined. Values were expressed as means \pm SD. * $P < .05$ vs control group; # $P < .05$ vs T3 20x group

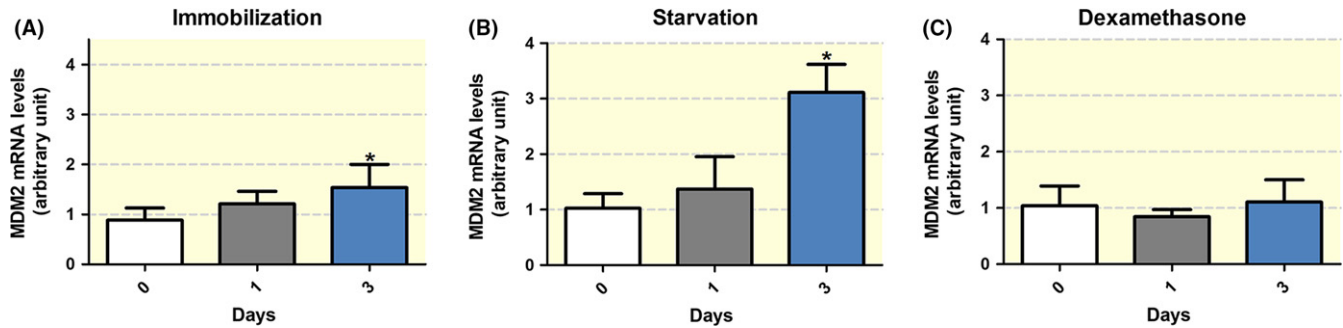


FIGURE 3 mRNA expression levels of MDM2 in soleus muscle in different models of atrophy. A, Immobilization; B, starvation and C, dexamethasone (1200 mg/Kg). Values were expressed as mean \pm SD. * $P < .05$ vs control group

regulation and it has been recognized as a key player in transcriptional activation of those atrogens. As expected, we have detected nuclear localization of FOXO3 and low levels of expression in the myofibrillar area (Figure 7A[I–III]) in vivo. Quantification analyses showed that 25% of the nuclei were positive for FOXO3 under control conditions and T3 treatment caused a strong decrease in the number of FOXO3-positive nuclei as compared to control group (10%, $P < .05$, Figure 7A: IV–VI, XIII). Accordingly, we also observed that T3 treatment increased immunexpression of FOXO3 in the myofibrillar area (Figure 7A: IV–VI). In a similar way, C2C12 derived cultured myotubes treated with T3 show increased cytoplasmic labelling and diminished nuclear immunexpression of FOXO3 (~8%, $P < .05$, Figure 7A: X–XII, XIV) when compared with control groups (~24%, $P < .05$, Figure 7A: VII–IX). Western blot analysis showed that T3 promotes a strong increase in the levels of Ser253 phosphorylated FOXO3/total FOXO3 ratio in skeletal muscle (~1.8-fold, $P < .05$, Figure 7B).

3 | DISCUSSION

In this study, using a microarray approach, we have identified the MDM2 gene as responsive to T3 in skeletal muscle. Under T3 stimulation, it is expressed preferentially in fibre type I and also in satellite cells. In addition, we showed that MDM2 plays an important role in the trophic action of T3.

We have observed that about a half of the 425 genes corresponding to proteolytic pathways are responsive to T3 and more than 80% of those are related to the ubiquitin system as compared to calpains, cathepsins and caspases, reinforcing that the proteasome is the main pathway that mediates T3-dependent proteolysis (Figure 1A,B). Out of the responsive genes, MDM2 caught our attention because it responded to T3 similarly as MuRF1 (a hallmark of atrophy) and also because of its relatively high basal expression levels as compared to the other top responsive E3

ligases identified. In addition, recent data have suggested that MDM2 is able to ubiquitinate FOXO3, raising the possibility that this E3 ligase might be involved in control of skeletal muscle trophicity.²⁰

We have validated, throughout RT-PCR that T3 increases MDM2 mRNA level as soon as 24 hours after onset of hormonal treatment in soleus muscle, which is kept elevated up to 7 days of treatment (Figure 1C). Interestingly, when growing doses of T3 were used, we obtained the maximal effect at 20 physiological doses. At 50 physiological doses, we noticed a tendency for reduction in MDM2 at the mRNA and protein levels suggesting that higher saturating doses of T3 can trigger additional mechanisms, which can restrain the increase in MDM2 expression. The mechanisms involving T3 action on MDM2 are not dependent on systemic factors as we showed that in differentiated myotubes, T3 is able to promote a twofold increase in MDM2 mRNA levels (Figure 2D).

MDM2 is an oncogene overexpressed in several types of sarcomas and soft tissue tumours such as liposarcomas, osteosarcomas, fibrous histiocytomas and rhabdomyosarcoma.^{17,21} The molecular mechanism involved in the tumorigenesis includes interaction of MDM2 with P53. The binding of MDM2 to P53 abrogates P53-mediated transactivation and decreases P53 levels through enhanced degradation by proteasome.¹⁸ These actions inhibit the blockade of G1 phase progression mediated by P53. Thus, overexpression of MDM2 serves as a negative regulator of P53 function. Furthermore, MDM2 interacts with the activation domains of the S-phase-promoting transcription factors E2F1 and DP1, resulting in stimulation of E2F1/DP1 transcriptional activity.²¹ Taken together, these observations indicate that MDM2 not only relieves the proliferative blocking mediated by P53 but also promotes the G1-to-S-phase transition by stimulating E2F1/DP1 activity. Therefore, it is classically established that MDM2 is a cell cycle regulator; nonetheless, its role in non-dividing cells such as the skeletal muscle fibre is still elusive. Other cell cycle

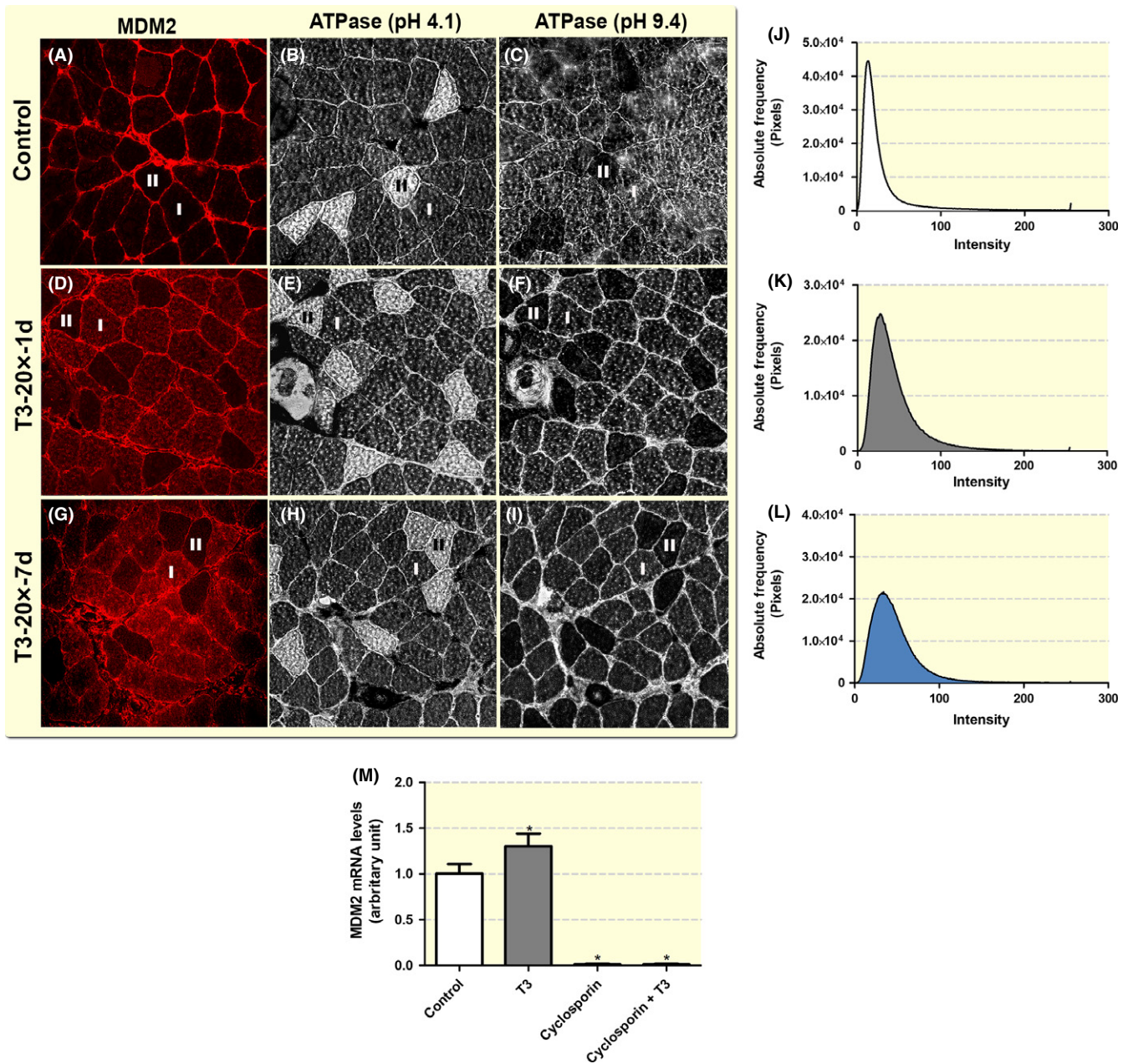


FIGURE 4 Tissue localization of MDM2 by immunofluorescence and skeletal muscle fibre identity by ATPase assay. (A, D, G) Confocal immunofluorescence for MDM2 (red) in the soleus muscle of animals treated with T3 for 1 and 7 days (20 physiological doses). In addition, ATPase assays at acid and alkaline incubation buffers were performed to detect type I and type II fibres (B, C, E, F, H, I). Pixels absolute frequency distribution on intensity of MDM2 of the images A, D and G (J, K and L, respectively). M: Expression of MDM2 in differentiated myotubes treated with T3 (10^{-8} M), cyclosporin A (1 μ M) or both for 30 hours. Values were expressed as mean \pm SD. * $P < .05$ vs control group

regulators have been investigated in the skeletal muscle fibre which direct pro-trophic effects such as Wnt β -catenin,²² mTORC1²³ and calcineurin.²⁴ The results presented herein suggest that MDM2, in line with other cell cycle regulators, is involved in maintenance of skeletal muscle mass under T3 stimulation.

Based on the results obtained in the present study, it is possible to envision that MDM2 could also be involved in other conditions involving skeletal muscle trophicity such

as decreased mechanical stimuli and starvation (Figure 3). Actually, it has been shown that MDM2 can ubiquitinate FOXO3 in the skeletal muscle of mice submitted to hindlimb denervation,^{20,25} suggesting that MDM2 might be able to regulate skeletal muscle mass via FOXO3 inhibition.

Noteworthy, in the present study we have found that T3 is able to increase MDM2 expression specifically in the type I skeletal muscle fibre (Figure 4). Because NFAT has

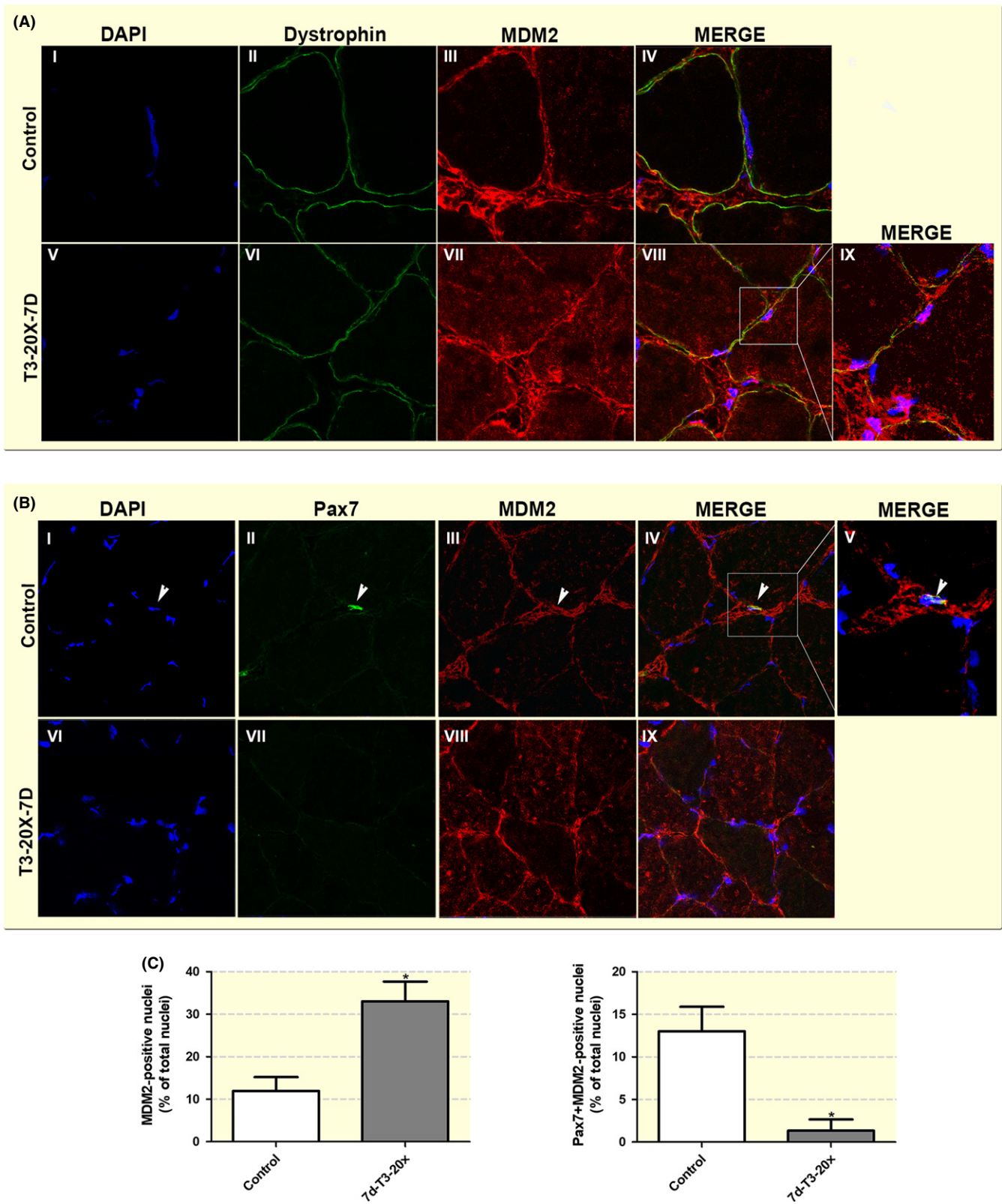


FIGURE 5 MDM2 is expressed in satellite cells. A, Dystrophin/DMD (green) and MDM2 (red) were identified by confocal immunofluorescence in soleus muscle of animals treated with T3 (20 physiological doses for 7 days). B, PAX7 (green) and MDM2 (red) were identified by immunofluorescence under the same experimental conditions as A. DAPI staining was used (blue) for nuclei identification. C, Quantification of MDM2 or PAX7 plus MDM2-positive nuclei was expressed as percentage of total nuclei in soleus muscle of animals treated with T3 for 7 days. Values were expressed as mean \pm SD. * $P < .05$ vs control group

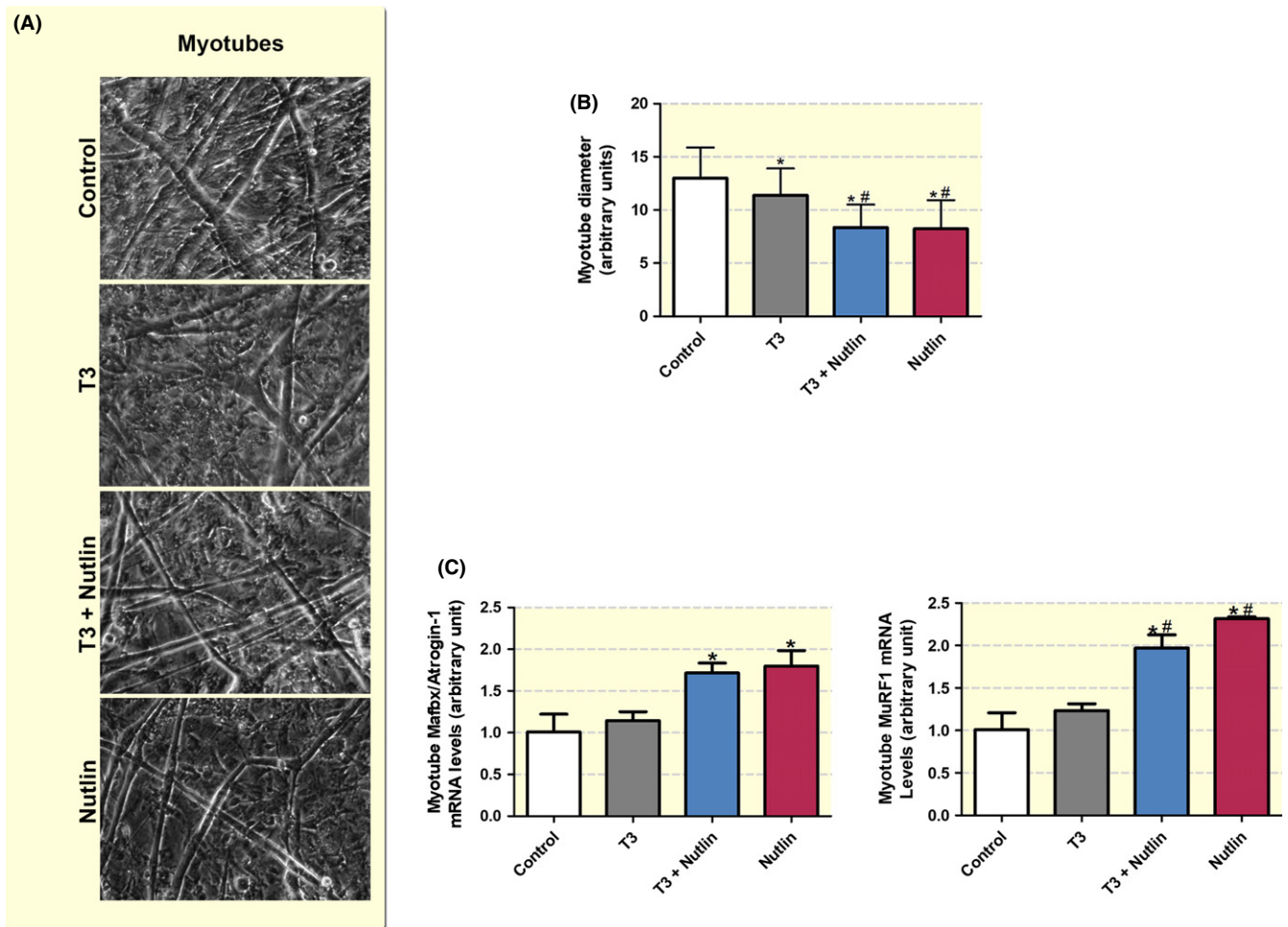


FIGURE 6 Influence T3 and Nutlin-3 (MDM2 inhibitor) on diameter of myotubes. (A) Phase-contrast microscopy of myotubes submitted to T3, Nutlin and both combined. Quantification of diameter (B) and mRNA levels of Mafbx/Atrogin-1 and MuRF1 (C) in myotubes treated with T3 and Nutlin under the same experimental conditions as A. Bars represent the mean \pm SD; * $P < .05$ vs control, # $P < .05$ vs T3

been described as able to bind to the MDM2 promoter²⁶ and calcineurin-NFAT pathway is considered a key player in the maintenance of type I skeletal muscle fibre phenotype, we pharmacologically inhibited calcineurin and addressed MDM2 responsiveness to T3. Our results point that MDM2 gene expression depends upon the calcineurin-NFAT pathway and also this pathway plays a key role in MDM2 responsiveness to T3 (Figure 4M). Those results are in line with the concept that the high expression of MDM2 in the type I fibre stimulated by T3 is calcineurin-NFAT dependent.

Interestingly, two THREs have been well characterized in the first intron of the MDM2 gene; therefore, it is possible to conceive that the NFAT responsive element could be spatially close to the first intron along with the basal transcriptional complex. Under stimulation with T3, only type I fibre would then provide the proper environment for increased MDM2 transcription. Since in the present study we have not performed long-term experiments, up to now it is not clear

what occurs with responsiveness of MDM2 as type I fibres are converted to fast twitch variants driven by T3.

T3 increases MDM2 expression homogeneously, exhibiting a punctiform pattern along the sarcoplasm along the cross-sectional area of the type I fibre. In addition, we have also detected MDM2 immunolabelling inside the nucleus (Figure 5). In T3 stimulated tissue, about 30% of total nuclei is MDM2 positive, in contrast to only 10% in control group (Figure 5). Previous studies indicate that MDM2 acts in the cytoplasm;²⁵ therefore, the nuclear role of MDM2 in skeletal muscle remains unclear and it would be interesting to address this issue in future studies.

We have also detected MDM2 immunopositivity in satellite cells (Figure 5), leading to the possibility that this protein could play a role in the proliferation/differentiation balance of satellite cells in vivo. In fact, indirect evidence for this is observed in the study of Fu and colleagues,²⁵ where it has been shown that MDM2 can improve myogenesis. It was observed that C2C12 cells treated with

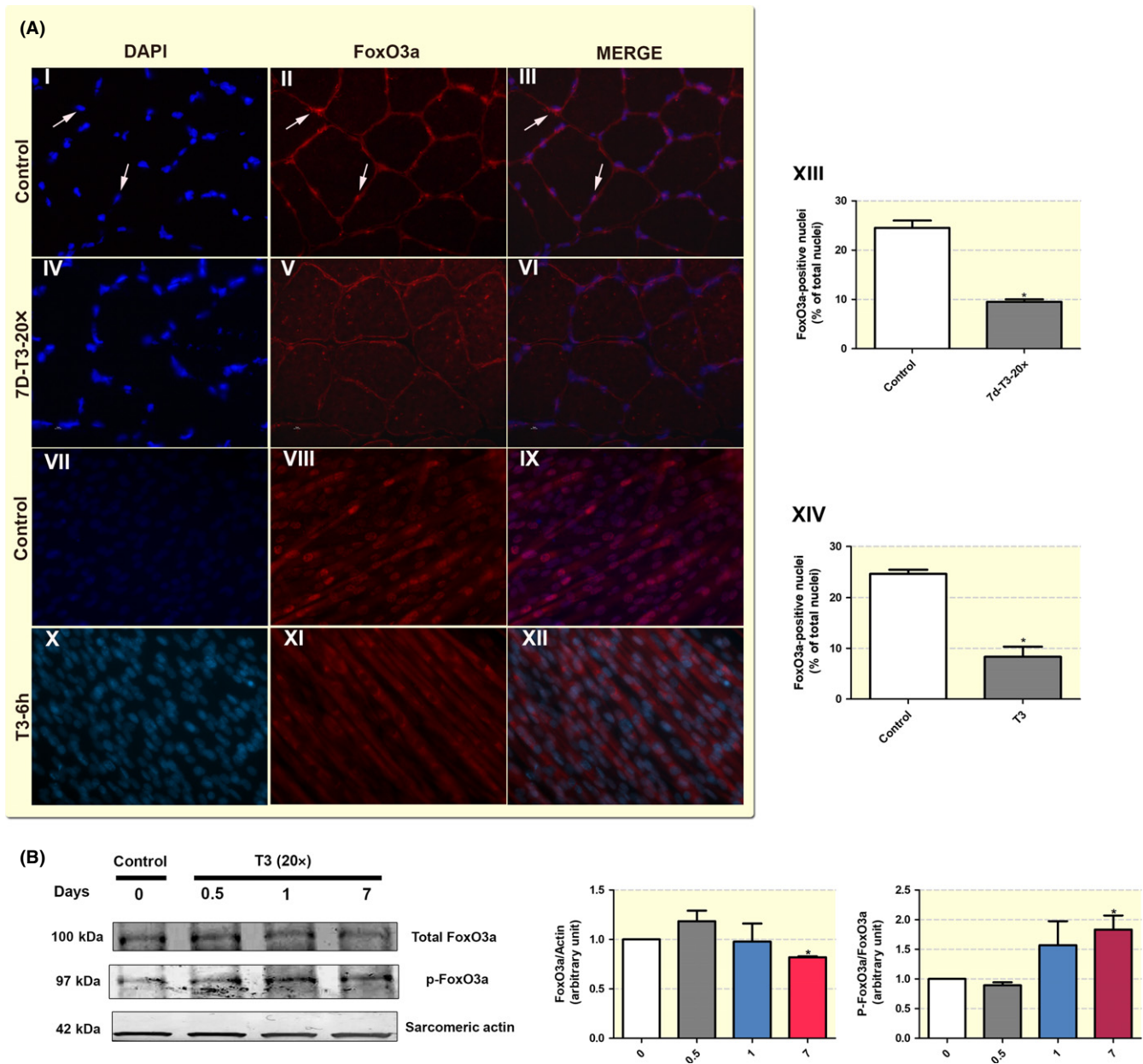


FIGURE 7 FOXO3 is deactivated by T3 in skeletal muscle. A, Immunofluorescence for FOXO3 (red) and incidence of FOXO3-positive nuclei (% of total nuclei) in vivo (I-VI) and in vitro (VII-XII). B, FOXO3 protein expression levels in soleus muscle of animals treated with T3 (20 physiological doses for 7 days). Dapi staining was used (blue) for nuclei identification. Bars represent the mean \pm SD; * $P < .05$ vs control

nandrolone, an anabolic steroid, increased Numb protein levels as well as attenuated its degradation by MDM2.²⁷ The expression of Numb in myogenic lineage has been associated with differentiation of satellite cells.^{27,28} Therefore, it is possible to consider that overexpression of MDM2 in skeletal muscle plays an important role in the activity of satellite cells. Interestingly, we have detected expression of MDM2 in satellite cells mainly in basal conditions. T3 strongly decreases the expression of satellite cell markers such as MyoD, making difficult to approach the effect of T3 on MDM2 expression in satellite cells. It has been previously reported that T3 decreases such

markers in orbicular muscles.²⁹ In addition, it has been shown that MDM2 can ubiquitinate and degrade C/EBP-beta, a strong activator of PAX7. This mechanism can explain why we have observed that increased MDM2 immunoeexpression is paralleled by a dramatic decrease in immunoeexpression of PAX7 (Figure 5).

In order to better understand the modulation of MDM2 in skeletal muscle, we decided to measure its mRNA levels in other models of atrophy (Figure 3). Immobilization promoted a significant but rather modest increase in MDM2 gene expression. Starvation and immobilization significantly increased MDM2 gene expression, while dexamethasone

treatment did not have any effect upon MDM2 gene expression. These data rise the possibility that MDM2 gene expression could play a differential role in distinct atrophy models.

In an attempt to uncover the role of MDM2 in skeletal muscle under T3 stimulation, we have pharmacologically inhibited MDM2 levels in cultured myotubes treated with T3 (Figure 6). As expected, we observed that T3 is able to decrease myotube size, highlighting the effect of T3 upon protein loss. Remarkably, myotubes treated with MDM2 inhibitor only induced a stronger sarcopenic response as compared to T3 treatment. This suggests that MDM2, by itself, might be sufficient to act positively upon myotube size. Further studies are needed to clarify this issue and also to address the operating mechanisms. When myotubes were treated with T3 and simultaneously MDM2 inhibited, a similar decrease in size was observed as compared to MDM2 inhibition alone, reinforcing the idea that MDM2 could be an autonomous positive player in myotube trophicity. The data presented herein clearly show that T3 is able to increase expression of MDM2 in the skeletal muscle fibre; therefore, activation of MDM2 could be a mechanism by which T3 exerts a pro-trophic effect upon skeletal muscle.

These results are in line with the concept of a dual role of T3 in skeletal muscle: stimulating catabolic pathways, such as the proteasome system as already well established, but also stimulating anabolic pathways such as MDM2. In fact, this concept is broadly accepted in other systems such as brown adipose tissue (T3 increases lipolysis and simultaneously lipogenesis) and liver (T3 increases activity of glycolysis and gluconeogenesis).³⁰ Accordingly, in the present study we show that T3 can increase levels of phosphorylated FOXO3, keeping this important transcriptional factor inactive and at the same time increasing levels of Mafbx/Atrogin-1 and MuRF1, which contain both FOXO response elements.^{31,32} These data show that T3 can modulate the expression of those atrogenes independently of FoxO3. At the moment, the mechanism by which such dual effect occurs is not clear, although one possibility might rely on THREs located at the promoter of those genes, yet to be described.¹²

Another aspect strictly linked to FOXO3 activity is its cellular location. We found herein that T3 is able to strongly decrease nuclear localization of FOXO3, therefore inhibiting its activity (Figure 7). At the moment, the exact mechanisms linking T3 action upon FOXO and MDM2 are not clear and further studies are necessary to establish such link. Interestingly, though, a previous study has uncovered that MDM2 is able to ubiquitinate FOXO3, leading to subsequent degradation.²⁵ This well-described mechanism pointed by Fu et al²⁵ might also be operating when T3 increases MDM2 levels. In conclusion, this study establishes a link between MDM2 and the skeletal muscle fibre

mass control and unravels a mechanism involving pro-trophicity, which is utilized by T3 in skeletal muscle.

4 | MATERIALS AND METHODS

The study was conducted conform ethical principles in animals research adopted by the Brazilian College of Animals Experimentation (COBEA) and was approved by the Institute of Biomedical Sciences/University of the Sao Paulo Ethics Committee for Animal Research (#168/05).

4.1 | Experimental procedures

Male Wistar rats of approximately 2 months old weighing 200–260 g were housed in standard plastic cages under controlled environmental conditions (24°C; 12-hour light/dark cycle). Animals were randomized into two groups: control and hyperthyroid (T3). The hormone injected was adjusted according to body weight (BW) to maintain the same dosage throughout the treatment. Control animals received injections of vehicle solution. The injections were administrated once a day, and the animals were treated by 0.5, 1 and 7 days. The doses of T3 (Sigma-Aldrich, St.Louis, MO, USA) injected each day were 1.5, 6 and 15 µg of T3/100 g body weight per day, corresponding to 5, 20 and 50 physiological doses, respectively. T3 was dissolved in saline containing 40 mM NaOH. After treatment, the animals were killed by decapitation and the blood was collected to analyse thyroxine (T4) plasma levels. Some animals (n = 4-5) were submitted to unilateral immobilization of the left hindlimb by applying a cast with total plantar extension for 1 and 3 days. Dexamethasone-induced atrophy was performed by intraperitoneal injection (1200 mg/kg) daily for 1 and 3 days. For the starvation procedure, animals had access only to water for 1 or 3 days.

4.2 | Tissue samples

The soleus muscle was removed, weighed, frozen in liquid nitrogen and stored at –80°C for later analysis of the mRNA and protein expression levels. The soleus muscle was transversely cut in half, and one segment immersed in cold isopentane for 30 seconds. After that, the segment was cooled in liquid nitrogen and stored at –80°C for histochemistry and immunofluorescence. To confirm effectiveness of treatment by T3, the heart weight was used as positive control.

4.3 | Serum parameters

Total thyroxine (T4) serum levels were measured by commercial radioimmunoassay (RIA) kits (Schering Cis Bio

International—France). The serum was separated by centrifugation (4500 g; 30 minutes), immediately frozen and stored at -80°C .

4.4 | Microarray analysis

Total RNA from adult rat soleus muscle was isolated using Trizol LS reagent (Life Technologies, Carlsbad, CA, USA) in accordance with the manufacturer's instructions. Total RNA was further purified with *Rneasy Fibrous Tissue Mini Kit* (Qiagen, Austin, TX, USA) to reach microarray RNA quality standards. The resulting phenol-free RNA was submitted to spectrophotometric analysis in a Nanodrop 1000 spectrophotometer (Thermo Scientific, Wilmington, DE, USA) and RNA quantity determined by the A260 wavelength method. One microgram of total RNA was used in the cDNA first-strand synthesis with *One-Cycle Target Labelling and Control Reagents* kit (Affymetrix, Santa Clara, CA, USA). At the end of the cycle, samples were repurified using the *Cleanup of Double-Strand cDNA* kit (Affymetrix) and requantified in Nanodrop. The biotinylated-cRNA synthesis was carried out with the in vitro transcription (IVT) *Gene Chip Expression 3'-Amplification Reagents for IVT labelling kit* (Affymetrix) followed by the cRNA fragmentation at high temperature and high Mg^{2+} concentration buffer. For hybridization, we used the *Gene Chip Hybridization, Wash and Stain* (Affymetrix). Chips were filled in with hybridization buffer, incubated at 45°C for 16 hours and then processed in the washing station (Affymetrix). Subsequently, chips were analysed in a scanner and raw data files were processed using the MAS 5.0 algorithm. The fold change values for control and T3-treated groups were calculated and filtered for variations greater than 15%. Gene ontology analysis using AmiGO2³³ (<http://amigo.geneontology.org/amigo>) was applied to classify differential expressed genes. To address the proteolytic pathway, we filtered out genes related to "proteolysis" (GO biological processes 0030163-protein catabolism, 0016567-ubiquitination and 0006508-proteolysis). All scripts were written in python 3.4.

4.5 | Gene expression by RT-PCR

For determination of mRNA levels by RT-PCR, total RNA was isolated from soleus muscle using the Trizol reagent

(Life Technologies) following the manufacturer's recommendations. Total RNA (1 μg) was reverse transcribed (RT) to generate cDNA. This reaction contained oligo-dT (500 $\mu\text{g}/\text{ml}$), 10 mM of each deoxyribonucleoside phosphate (dNTP), $5\times$ first-strand buffer, 0.1 M dithiothreitol (DTT) and 200U reverse transcriptase (SuperScript II; Invitrogen, San Diego, CA, USA). The RT reaction was performed at 70°C for 10 minutes, followed by 42°C for 60 minutes and 10 minutes at 95°C . The primer set for rat, Mafbx/Atrogin-1, MDM2 and MuRF1 was designed using Primer-BLAST³⁴ (http://www.ncbi.nlm.nih.gov/tools/prime_r-blast/) and synthesized by IDT (Integrated DNA Technologies, Coralville, IA, USA) according to Table 2. One microlitre of cDNA was used in real-time PCR, containing Syber Green Universal Master Mix II (Life Technologies), and the cycle parameters were as follows: 50°C for 2 minutes, 95°C for 10 minutes, followed by 40 cycles of 95°C for 15 seconds, and 60°C for 1 minute. The fluorescence intensity was quantified, and amplification plots were analysed by a Corbett RotorGene 6000 (Qiagen, Hilden, Germany). Results were expressed using the comparative cycle threshold (CT) method as described, and expression levels were represented by fold change over values derived from control animals. Amplification of cyclophilin A gene was used as an internal standard. All primer pairs were designed so at least either forward or reverse spans an exon-exon junction (Table 2).

4.6 | Western blot

Primary antibodies used for Western blotting were as follows: MDM2 (1:1000; Novus Biologicals, Cambridge, MA, USA), sarcomeric Actin (1:1000; Dako, Santa Clara, CA, USA, used as a housekeeping protein), total FOXO3 (1:1000; Abcam, San Francisco, CA, USA) and phosphorylated FOXO3 (1:1000; Cell Signaling, Danvers, MA, USA). The secondary antibodies used were as follows: polyclonal rabbit anti-mouse immunoglobulins/AP (1:1000; Dako) and polyclonal rabbit anti-rabbit immunoglobulins/AP (1:1000; Dako). Soleus muscles were homogenized in an extraction buffer termed modified RIPA buffer (0.625% Nonidet P-40; 0.625% deoxycholic acid; 0.00625 M sodium phosphate pH 7.2; 1 mM EDTA pH 8.0) containing 10 $\mu\text{g}/\text{ml}$ of protease inhibitor cocktail (Sigma-Aldrich). Homogenates were centrifuged at

TABLE 2 Primer sets used in real-time PCR (RT-PCR)

Primers	NCBI Accession number	Forward	Reverse
Mafbx/Atrogin-1	NM_133521.1	TACTAAGGAGCGCCATGGATACT	GTTGAATCTTCTGGAATCCAGGAT
Cyclophilin A	NM_017101.1	GCCGATGACGAGCCCTTG	TGCCGCCAGTGCCATTAT
MDM2	NM_001108099.1	GAGGATGATGAGGTCTATCG	GGAGGATTCATTTTCATTGCAC
MuRF1	NM_080903.1	TGACCAAGGAAAACAGCCACCAG	TCACTCCTTCTCTCGTCCAGGATGG

10 000 G for 10 minutes at 4°C, and the supernatant was used. Protein concentration was determined by Bradford assay (Bio-Rad, Hercules, CA, USA), with bovine serum albumin as standard. Protein extract was run on 12% or 10% sodium dodecyl sulphate-polyacrylamide gels electrophoresis (SDS-PAGE) and transferred to a nitrocellulose membrane (Bio-Rad). The membranes were stained with Ponceau S to confirm the protein amount and then rinsed with Tween Tris-buffered saline solution 0.5 M NaCl, 50 mM Tris-HCl pH 7.4 and 0.1% Tween-20 (TBS-T). All membranes were incubated for 40 minutes at room temperature by blocking solution (TBS-T; 5% no-fat milk). Next, the membranes were incubated overnight with primary antibodies at 4°C. After a 15-minutes wash in TBS-T solution, membranes were incubated with secondary antibodies for 1 hour at room temperature and washed again for 10 minutes in TBS-T solution. After that, membranes were incubated for 5 minutes with detection buffer (100 mM Tris-HCL; 100 mM sodium chloride pH9.5). Labelled proteins were detected by the alkaline phosphatase system (NBT/BCIP Stock Solution; Roche, USA).

4.7 | Immunofluorescence

The primary antibodies used for immunostaining were as follows: monoclonal mouse MDM2 (1:1000; Novus Biologicals); polyclonal rabbit PAX7 (1:200; Aviva Systems Biology, San Diego, CA, USA); polyclonal rabbit dystrophin (1:250; Santa Cruz Biotechnology, Dallas, TX, USA); polyclonal rabbit total FOXO3 (1:300; Abcam); mouse monoclonal myozenin 2 (1:250; Santa Cruz Biotechnology). The secondary antibodies were (Table 2) as follows: goat anti-mouse IgG-Cyanine Cy2 (1:50; Jackson Lab Bar Harbor, ME, USA), donkey anti-mouse Cyanine Cy3 (1:300; Jackson Lab), goat anti-rabbit IgG-Cyanine Cy2 (1:50; Jackson Lab), (4) donkey anti-rabbit IgG-Cyanine Cy3 (1:300; Jackson Lab). Cross sections of soleus muscle for immunostaining were fixed with acetone for 10 minutes at -20°C and washed with PBS-N (PBS⁺ 0.1% Nonidet-40), 3 times for 5 minutes each. After that, slides were incubated with a blocking solution (PBS⁺ 0.1% Nonidet-40 + 1% BSA) for 30 minutes at 37°C. Next, the slides were incubated with a solution containing the primary antibody overnight in a dark chamber (4°C). After washing with PBS-N, 3 times for 5 minutes each, a blocking solution containing the secondary antibody was added for 1 hour and 30 minutes in a dark chamber. The slides were then washed with PBS-N, 3 times for 5 minutes and mounted with Vectashield with 4', 6-diamidino-2-phenylindole (DAPI) (cat# H-1200, Vector Labs) and coverslipped. Images were captured on a Zeiss LSM-780 NLO microscope using Carl Zeiss Zen lite and also the same software was used to measurement of pixels absolute frequency

distribution. Images were acquired at Center of Facility of Research (CEFAP), a core facility at Institute of Biomedical Sciences, University of Sao Paulo.

4.8 | Enzyme histochemical staining

Serial cross sections (10 µm) obtained of the middle region soleus muscle were stained for myofibrillar ATPase activity (mATPase) after alkaline (ATPase, pH 9.4) or acid (ATPase, pH 4.1)³⁵ preincubation. Fibre type staining pattern in the alkaline pH 9.4 (dark type IIa fibres, pale type I fibre) was compared with the reverse staining pattern (pale type IIa, dark type I) in a section stained in the acid pH (pH 4.1). Acquisition of the images was performed in the Nikon Eclipse TS 100 microscope equipped with a digital video camera and NIS-Elements BR imaging software.

4.9 | Cell Culture of myoblasts

For primary culture of myoblasts, muscle samples from hindlimb muscles of male FVB mice were removed and trimmed of connective tissue. Subsequently, the samples were incubated with sterile phosphate-buffered saline (PBS) solution and cut in short fragments to help the digestion. The minced muscles were digested in type IA collagenase 0.20% (Sigma #C9891-1G) and trypsin 0.25% (Gibco #27250-018) in 15 ml of Dulbecco's modified Eagle's medium high glucose (DMEM—Sigma #D5648). Cells were then centrifuged and cultured in growth medium (DMEM 20% FBS, 1% penicillin-streptomycin) on a bed of Matrigel (BD Bioscience, #3356234) into 24-well culture dishes at 37°C, 5% CO₂. Cells were maintained in growth medium up to 3 days reaching 70% of confluence. After that, the medium was changed to the differentiation medium (DMEM 2% horse serum, 1% penicillin-streptomycin) to stimulate the myotube formation. After 3 days of differentiation, certain wells were treated by 72 hours with T3 (3×10^{-8} M; cat #T2877, Sigma-Aldrich), the inhibitor of MDM2 named Nutlin (8 µM; cat #18585, Cayman Chemical) or both. These treatments were used to compare the influence of T3 and MDM2 in the modulation of myotube size. As controls some wells were treated with vehicle (NaOH 40 nM), and others were differentiated by 6 days without any treatment. Cell identity of this myogenic culture was confirmed by detection of myozenin 2 and MyoD (Figure S1). Three independent experiments using cultured myotubes were performed.

Myoblasts from the muscle-derived mouse C2C12 were maintained as proliferating myoblasts in DMEM-high-glucose medium supplemented with 10% FBS, 1% penicillin-streptomycin. After reaching 90%-100% confluence, cells were switched to DMEM supplemented with 2% adult horse serum 1% penicillin-streptomycin, to induce fusion of myoblasts. After 2 days of differentiation, certain wells were

treated by 30 hours with T3 (3×10^{-8} ; cat #T2877, Sigma-Aldrich), the inhibitor of calcineurin activity named cyclosporin A (1 μ M) in DMSO or both.

4.10 | Myotube measurements

Acquisition of the images to measure the diameter of myotubes was performed in the Nikon Eclipse TS 100 microscope equipped with a digital video camera and NIS-Elements BR imaging software. Subsequently, the myotubes were measured by Image-Pro-Plus Demo software. The myotubes were visualized at 100 \times magnification, and the fields were randomly selected from four different wells for each group. At least three measurements were performed per myotube. Approximately 165 myotubes were measured per group.

4.11 | Statistical analysis

Results are reported as means \pm SD. Statistical analysis was performed using ANOVA followed by Tukey post-test analysis as appropriate. $P < .05$ was considered statistically significant.

4.12 | The completion of the copyright transfer and affirmation of originality

The article is original, does not infringe upon any copyright or other proprietary right, is currently not under submission in another journal and has not been previously published. There are no financial or other relationships that might lead to a conflict of interest among authors.

ACKNOWLEDGEMENTS

We thank FAPESP and CNPq for the financial support.

AUTHOR CONTRIBUTIONS

Gracielle V. Ramos, André Cruz, William J. Silva, Igor L. Baptista and João G.O. Silvestre performed experiments and wrote the manuscript. André Cruz and Andrei Rozanski were in charge with the *in silico* analysis, and Anselmo S. Moriscot designed the study, supervised the experiments and wrote the manuscript.

CONFLICT OF INTEREST

The authors have nothing to disclose.

ORCID

A. Cruz  <http://orcid.org/0000-0001-7977-8752>

REFERENCES

1. Sinha R, Yen PM. Cellular action of thyroid hormone. In: de Groot LJ, Beck-Peccoz P, Chrousos G, Dungan K, Grossman A, Hershman JM, Koch C, Mclachlan R, New M, Rebar R, Singer F, Vinik A, Weickert MO, eds. *Endotext*. South Dartmouth, MA: MDText.com, Inc.; 2000 [internet] Available from: <https://www.ncbi.nlm.nih.gov/books/NBK285568/>.
2. Paris M, Hillenweck A, Bertrand S, et al. Active metabolism of thyroid hormone during metamorphosis of amphioxus. *Integr Comp Biol*. 2010;50:63-74.
3. Davis PJ, Goglia F, Leonard JL. Nongenomic actions of thyroid hormone. *Nat Rev Endocrinol*. 2015;12:111-121.
4. Mullur R, Liu YY, Brent GA. Thyroid hormone regulation of metabolism. *Physiol Rev*. 2014;94:355-382.
5. Williams CM, Ellis R. Thermogenic and metabolic consequences of thyroid hormone treatment in brown and white adipose tissue. *Biosci Rep*. 1985;5:175-184.
6. Allain TJ, Chambers TJ, Flanagan AM, McGregor AM. Triiodothyronine stimulates rat osteoclastic bone resorption by an indirect effect. *J Endocrinol*. 1992;133:327-331.
7. Bahi L, Garnier A, Fortin D, et al. Differential effects of thyroid hormones on energy metabolism of rat slow- and fast-twitch muscles. *J Cell Physiol*. 2005;203:589-598.
8. Capo LA, Sillau AH. The effect of hyperthyroidism on capillarity and oxidative capacity in rat soleus and gastrocnemius muscles. *J Physiol*. 1983;342:1-14.
9. Carter WJ, van der Weijden Benjamin WS, Faas FH. Effect of experimental hyperthyroidism on skeletal-muscle proteolysis. *Biochem J*. 1981;194:685-690.
10. Clément K, Viguier N, Diehn M, et al. In vivo regulation of human skeletal muscle gene expression by thyroid hormone. *Genome Res*. 2002;12:281-291.
11. Tawa NE Jr, Odessey R, Goldberg AL. Inhibitors of the proteasome reduce the accelerated proteolysis in atrophying rat skeletal muscles. *J Clin Invest*. 1997;100:197-203.
12. O'Neal P, Alamdari N, Smith I, Poylin V, Menconi M, Hasselgren PO. Experimental hyperthyroidism in rats increases the expression of the ubiquitin ligases atrogin-1 and MuRF1 and stimulates multiple proteolytic pathways in skeletal muscle. *J Cell Biochem*. 2009;108:963-973.
13. Chrysis D, Chagin A, Savendahl L. Insulin-like growth factor-1 restores dexamethasone-induced heart growth arrest in rats: the role of the ubiquitin pathway. *Hormones (Athens)*. 2011;10:46-56.
14. Bodine SC, Latres E, Baumhueter S, et al. Identification of ubiquitin ligases required for skeletal muscle atrophy. *Science*. 2001;294:1704-1708.
15. Satchek JM, Hyatt JP, Raffaello A, et al. Rapid disuse and denervation atrophy involve transcriptional changes similar to those of muscle wasting during systemic diseases. *FASEB J*. 2007;21:140-155.
16. Lokireddy S, Wijesoma IW, Sze SK, McFarlane C, Kambadur R, Sharma M. Identification of atrogin-1-targeted proteins during the myostatin-induced skeletal muscle wasting. *Am J Physiol Cell Physiol*. 2012;303:C512-C529.
17. Oliner JD, Kinzler KW, Meltzer PS, George DL, Vogelstein B. Amplification of a gene encoding a p53-associated protein in human sarcomas. *Nature*. 1992;358:80-83.

18. Momand J, Wu HH, Dasgupta G. MDM2—master regulator of the p53 tumor suppressor protein. *Gene*. 2000;242:15-29.
19. Vassilev LT, Vu BT, Graves B, et al. In vivo activation of the p53 pathway by small-molecule antagonists of MDM2. *Science*. 2004;303:844-848.
20. Bertaggia E, Coletto L, Sandri M. Posttranslational modifications control FoxO3 activity during denervation. *Am J Physiol Cell Physiol*. 2012;302:C587-C596.
21. Guo CS, Degnin C, Fiddler TA, Stauffer D, Thayer MJ. Regulation of MyoD activity and muscle cell differentiation by MDM2, pRb, and Sp1. *J Biol Chem*. 2003;278:22615-22622.
22. Leal ML, Lamas L, Aoki MS, et al. Effect of different resistance-training regimens on the WNT-signaling pathway. *Eur J Appl Physiol*. 2011;111:2535-2545.
23. Walker DK, Dickinson JM, Timmerman KL, et al. Exercise, amino acids, and aging in the control of human muscle protein synthesis. *Med Sci Sports Exerc*. 2011;43:2249-2258.
24. Hudson MB, Price SR. Calcineurin: a poorly understood regulator of muscle mass. *Int J Biochem Cell Biol*. 2013;45:2173-2178.
25. Fu W, Ma Q, Chen L, et al. MDM2 acts downstream of p53 as an E3 ligase to promote FOXO ubiquitination and degradation. *J Biol Chem*. 2009;284:13987-14000.
26. Zhang X, Zhang Z, Cheng J, et al. Transcription factor NFAT1 activates the mdm2 oncogene independent of p53. *J Biol Chem*. 2012;287:30468-30476.
27. Liu XH, Yao S, Levine AC, et al. Nandrolone, an anabolic steroid, stabilizes Numb protein through inhibition of mdm2 in C2C12 myoblasts. *J Androl*. 2012;33:1216-1223.
28. Jory A, Le Roux I, Gayraud-Morel B, et al. Numb promotes an increase in skeletal muscle progenitor cells in the embryonic somite. *Stem Cells*. 2009;27:2769-2780.
29. Harrison AR, Lee MS, McLoon LK. Effects of elevated thyroid hormone on adult rabbit extraocular muscles. *Invest Ophthalmol Vis Sci*. 2010;51:183-191.
30. Feng X, Jiang Y, Meltzer P, Yen PM. Thyroid hormone regulation of hepatic genes in vivo detected by complementary DNA microarray. *Mol Endocrinol*. 2000;14:947-955.
31. Sandri M, Sandri C, Gilbert A, et al. Foxo transcription factors induce the atrophy-related ubiquitin ligase atrogin-1 and cause skeletal muscle atrophy. *Cell*. 2004;117:399-412.
32. Waddell DS, Baehr LM, van den Brandt J, et al. The glucocorticoid receptor and FOXO1 synergistically activate the skeletal muscle atrophy-associated MuRF1 gene. *Am J Physiol Endocrinol Metab*. 2008;295:E785-E797.
33. Carbon S, Ireland A, Mungall CJ, et al. AmiGO: online access to ontology and annotation data. *Bioinformatics*. 2009;25:288-289.
34. Ye J, Coulouris G, Zaretskaya I, Cutcutache I, Rozen S, Madden TL. Primer-BLAST: a tool to design target-specific primers for polymerase chain reaction. *BMC Bioinformatics*. 2012;13:134.
35. Brooke MH, Kaiser KK. Muscle fiber types: how many and what kind? *Arch Neurol*. 1970;23:369-379.

SUPPORTING INFORMATION

Additional Supporting Information may be found online in the supporting information tab for this article.

How to cite this article: Ramos GV, Cruz A, Silva WJ, et al. Thyroid hormone upregulates MDM2 in rat type I fibre: Implications for skeletal muscle mass regulation. *Acta Physiol*. 2018;222:e13003. <https://doi.org/10.1111/apha.13003>

Skeletal Muscle Anti-Atrophic Effects of Leucine Involve Myostatin Inhibition

André Cruz,^{1,*} Andrea Ferian,^{1,*} Paula K.N. Alves,¹ William Jose Silva,¹ Mirella Ribeiro Bento,¹ Alexander Gasch,² Siegfried Labeit,² and Anselmo Sigari Moriscot¹

Lack of mechanical load leads to skeletal muscle atrophy, and one major underlying mechanism involves the myostatin pathway that negatively regulates protein synthesis and also activates Atrogin-1/MAFbx and MuRF1 genes. In hindlimb immobilization, leucine was observed to attenuate the upregulation of the referred atrogenes, thereby shortening the impact on fiber cross-sectional area, nonetheless, the possible connection with myostatin is still elusive. This study sought to verify the impact of leucine supplementation on myostatin expression. Male Wistar rats were supplemented with leucine and hindlimb immobilized for 3 and 7 days, after which soleus muscles were removed for morphometric measurements and analyzed for gene and protein expression by real-time PCR and Western blotting, respectively. Muscle wasting was prominent 7 days after immobilization, as expected, leucine feeding mitigated this effect. Atrogin-1/MAFbx gene expression was upregulated only after 3 days of immobilization, and this effect was attenuated by leucine supplementation. Atrogin-1/MAFbx protein levels were elevated after 7 days of immobilization, which leucine supplementation was not able to lessen. On the other hand, myostatin gene expression was upregulated in immobilization for 3 and 7 days, which returned to normal levels after leucine supplementation. Myostatin protein levels followed gene expression at a 3-day time point only. Follistatin gene expression was upregulated during immobilization and accentuated by leucine after 3 days of supplementation. Concerning protein expression, follistatin was not altered neither by immobilization nor in immobilized animals treated with leucine. In conclusion, leucine protects against skeletal muscle mass loss during disuse, and the underlying molecular mechanisms appear to involve myostatin inhibition and Atrogin-1 normalization independently of follistatin signaling.

Keywords: leucine, cast immobilization, mass loss, myostatin

Introduction

IN HUMANS, ~40% OF the body mass corresponds to skeletal muscle, and primary factors, such as movement, nutritional reserve, immunological equilibrium, and energetic metabolism, depend on this tissue for maintenance and health (Janssen *et al.*, 2000). This wide range of contexts is fulfilled by the remarkable capacity of muscle to adapt, and load status, nutritional needs, and even hormones affect the skeletal muscle mass and function (Hill and Olson, 2012).

Regarding load status, increased stimulation will often induce muscle hypertrophy. In contrast, the lack of mechanical load often induces skeletal muscle atrophy. This phenomenon, known as disuse, is evident in cases in which healthy humans undergo a period of inactivity by limb im-

mobilization or bed rest (Brooks and Myburgh, 2014; Wall *et al.*, 2014).

The absence of weight and tension stimuli on skeletal muscle leads to significant physiological and molecular changes, affecting almost every aspect of muscle function. For example, after 2 to 5 weeks of inactivity, metabolic rate and insulin sensitivity adapt to lower loads (Brooks and Myburgh, 2014; Wall *et al.*, 2014). At the single myocyte level, complex and not fully understood mechanisms trigger enhanced proteolysis on top of reduced *de novo* protein synthesis, leading to an overall loss of sarcomeres. Although the specific gene networks that drive anabolic and catabolic signaling in each type of muscle wasting requires further understanding, the outcome of this altered protein turnover is atrophy (Jackman and Kandarian, 2004). Atrophy, also known as muscle wasting, is characterized by depletion of organelles and proteins with major impact

¹Department of Anatomy, Institute of Biomedical Sciences, University of São Paulo, São Paulo, Brazil.

²Institute for Integrative Pathophysiology, Faculty for Clinical Medicine Mannheim of the University of Heidelberg, Mannheim, Germany.

*These authors contributed equally to the study.

upon myofibrillar content through the ubiquitin/proteasome system (UPS) degradation (Sandri, 2008).

In this regard, myostatin is an interesting signaling factor, since it negatively regulates protein synthesis and myogenesis, while also inducing protein breakdown (Trendelenburg *et al.*, 2009; Elkina *et al.*, 2011; Lokireddy *et al.*, 2011; Lokireddy *et al.*, 2012; Wang *et al.*, 2015). With regard to muscle protein breakdown, the UPS, and particularly the so-called E3 ligases are essential to target proteins, which are then directed and degraded at the 26S proteasome. Among these enzymes, both Atrogin-1/MAFbx and MuRF1 are induced by several atrophic models and are thus designated atrogenes. In disuse, these atrogenes are especially upregulated and are considered a requirement for muscle atrophy and substrate specificity (Bodine *et al.*, 2001; Bodine and Baehr, 2014).

Several studies aimed to downregulate atrogenes and/or to decrease protein breakdown by using amino acid supplementation, including leucine. This amino acid has been shown to attenuate mass loss driven by immobilization in rat soleus muscle (Anthony *et al.*, 2000; Ventrucci *et al.*, 2001; van Norren *et al.*, 2009; Peters *et al.*, 2011; Baptista *et al.*, 2013; Pereira *et al.*, 2014).

Baptista *et al.* (2010) noted that leucine supplementation severely minimizes the Atrogin-1/MAFbx and MuRF-1 upregulation peak induced by cast immobilization for 3 days, shortening the effects of disuse on the cross-sectional area (CSA) of type I fibers. The capacity of leucine to induce protein synthesis while attenuating atrogene expression raises the possibility of its interaction with the myostatin pathway. Therefore, we investigated, in this study, in a rat skeletal muscle atrophy model, whether leucine effects are correlated to myostatin expression.

Materials and Methods

Experimental groups and animals

Experimental procedures were allowed by COBEA (Colégio Brasileiro de Experimentação Animal) under #88 approval from the Ethics Committee CEUA (Comissão de Ética no Uso de Animais). The animals, 2-month-old Wistar rats, were supplied by Central Bioterium at University of São Paulo.

Animals accessed food and water *ad libitum*, and the circadian cycle was maintained by a 12-h light/12-h dark protocol. Then, animals were arbitrarily sorted into groups as follows: (1) control group (CON; nonchallenged rats that received saline solution through gavage); (2) leucine group (LEU; nonchallenged rats that received leucine solution through gavage); (3) immobilized group (IMOB; hindlimb immobilized rats that received saline solution through gavage); and (4) immobilized and supplemented with leucine (IMOB+LEU; hindlimb immobilized rats that received leu-

cine solution through gavage). The immobilization and supplementation procedures were conducted for 3 and 7 days.

Hindlimb Immobilization and supplementation process

For hindlimb immobilization, animals were anesthetized by a ketamine and xylazine mixture (30 mg/kg rat of ketamine and 10 mg/kg rat of xylazine). Then, micropore tape was attached at the left rat hindlimb such that the whole limb was maintained in the extended position, and the soleus muscle fixed in a shortened position. After drying, the cast was involved in a galvanized steel wire mesh (2 mm opening), which was subsequently fixed by a 0.5 mm diameter steel galvanized wire. The purpose of involving the cast with a mesh was to prevent it to be chewed by the animal.

A standard rat chow was provided for all groups (Nuvilab CR-1, Nuvital-Quimtia, Brazil) and a high dose of leucine was applied through gavage. The animals received two rounds of leucine supplementation (L-Leucine, Ajinomoto) consisting of a 2.7 g/kg/day body mass, prepared in 0.9% saline. All the treatments began 3 days before immobilization, and the control group received 0.9% saline on the same gavage volumes. After each set period, the animals were euthanized by cervical dislocation. The soleus muscle was then isolated, measured, and dry weighed. To obtain dry weight, muscles were kept at 60°C until stable mass was reached (Gissel, 2010). Finally, the muscle samples were frozen in liquid nitrogen and kept at -80°C until they were analyzed.

Gene expression analysis by real-time PCR

Real-time polymerase chain reaction (PCR) was utilized to measure mRNA levels. First, from soleus muscle, total RNA was isolated by TRIzol reagent (Life Technologies, Carlsbad, CA). Then, cDNA was synthesized by reverse transcriptase reaction.

This reaction involved 1 µg of total RNA, 500 µg/mL of oligo-dT, 0.1 M dithiothreitol (DTT), 200 U reverse transcriptase (SuperScript II; Invitrogen, San Diego, California), 10 mM of deoxyribonucleoside phosphate (dNTP), and 5 × first-strand buffer. The reaction was carried on a thermal cycler at 70°C for 10 min, 42°C for 60 min, and 95°C for 10 min.

Primer sets for rats mice were designed on the Primer Blast platform targeting the following genes: Myostatin, Follistatin, MAFbx/Atrogin-1, MuRF-1, and Cyclophilin A. Either 5' or 3' primer spanned exon-exon junctions (Table 1).

Real-time PCR templates were mixed at SYBR Green Universal Master Mix II (Life Technologies, Carlsbad, CA), 5' primer, and 3' primer. Then, the samples were incubated at 50°C for 2 min and 95°C for 10 min, followed by 40 cycles of 95°C for 15 s and 60°C for 1 min. The fluorescence intensity was quantified by a RotorGene 6000 (Qiagen, Germany).

TABLE 1. PRIMER SETS USED IN REAL-TIME PCR

Primers	NCBI Accession Number	Forward	Reverse
Myostatin	NM-019151.1	CTACCACGGAAACAATCATTACCA	AGCAACATTTGGGCTTTCCAT
Follistatin	NM-012561.2	AGGGAAAGTGTATCAAAGCAAAGTC	AACCTTGAAATCCCATAGGCATT
MAFbx/Atrogin-1	NM-133521.1	TACTAAGGAGCGCCATGGATACT	GTTGAATCTTCTGGAATCCAGGAT
Cyclophilin A	NM-017101.1	GGATTCATGTGCCAGGGTGG	CACATGCTTGCCATCCAGCC

A comparative threshold method in which gene expression was defined as the fold change over control values was utilized to obtain the results. Cyclophilin A was standardized as a housekeeping gene.

Western blotting

Soleus muscle was homogenized in modified RIPA buffer (1 mM EDTA pH 8.0, 0.00625 M sodium phosphate pH 7.2, 0.625% deoxycholic acid, 0.625% Nonidet P-40), including 10 µg/mL of protease inhibitor cocktail (Sigma-Aldrich). Then, the samples were centrifuged at 10,000 g for 10 min at 4°C. The total amount of protein was quantified by Bradford Assay (Bio-Rad, Hercules, CA) using bovine serum albumin (BSA) as a standard.

Samples of those homogenates were passed through SDS-PAGE gel (sodium dodecyl sulfate/polyacrylamide) by electrophoresis and then transferred to a nitrocellulose membrane (Bio-Rad). To confirm the transfer and the equal protein load, Ponceau S staining was applied. After that step, the membranes were blocked for 1 h (5% BSA in tris-buffered saline +0.1% Tween-20 at room temperature) followed by primary antibody overnight incubation at 4°C. Next, the membranes were washed for 15 min and maintained for 1 h in secondary antibody solution at room temperature. After a 15-min wash, the alkaline phosphatase system detected label proteins. Primary antibodies were Atrogin-1/MAFbx (#AP2041, 1:1000; ECM Biosciences), Myostatin (#19142-1-AP, 1:1000; Proteintech), Follistatin (#PA5-19787, 1:500; Thermo Fisher), *GAPDH* (#PA1-987, 1:3000; Thermo Fisher) and alpha-tubulin (#2125S, 1:1000; Cell Signaling). Secondary antibodies were rabbit anti-mouse immunoglobulin/AP (polyclonal, 1:10,000; Dako) and goat anti-rabbit immunoglobulin/AP (polyclonal, 1:10,000; Dako). Images were obtained and quantified by Vision-Capt software (Wilber Lourmart, France).

Histological analysis

Cross-sections measuring 10 µm were made in a cryostat (Leica CM3050, Nussloch, Germany). These transverse sections were stained with Hematoxylin and Eosin, and pictures were subsequently acquired under a light microscope. CSA of the fibers were measured by the freehand tool on ImageJ software (version 2.0; NIH), ~500 fibers per group were measured and procedures were conducted blinded. The total number of fibers was estimated as shown in Ceglia *et al.* (2013).

Statistical analysis

The results were reported as the mean ± standard deviation (SD). As recommended, two-way analysis of variance followed by Tukey's posttest was applied. $p < 0.05$ was considered to be statistically significant.

Results

Leucine mitigates disuse-induced muscle wasting on the soleus muscle of rats

First, we confirmed the recognized effect of leucine in the protection of muscle mass in a disuse atrophy model (Figs. 1

and 2). After 3 days of cast immobilization, rat soleus muscle from nonsupplemented animals showed reduced mass (~20%; Fig. 1B), although no changes were detected in fiber number and CSA (Fig. 1C, D, respectively).

One week of hindlimb immobilization induced a 40% mass loss, whereas immobilized and leucine-supplemented animals exhibited a 30% decrease (Fig. 2B). Interestingly, leucine supplementation alone induced a 15% increase in mass (Fig. 2B). Regarding CSA of fibers, immobilized animals exhibited a 50% decrease in area, in contrast, immobilized animals that received daily doses of leucine for 7 days showed only about 17% reduction when compared with the control group (Fig. 2A, D). No changes were observed in total fiber counts. The effect of leucine on CSAs was restricted to the atrophy stress state. In summary, these results certify that the model utilized herein to induce atrophy and supplementation with leucine was accomplished efficiently.

Atrogin-1/MAFbx gene expression was upregulated upon immobilization and attenuated by leucine supplementation

To further certify the immobilization model and leucine treatment efficiency, we evaluate Atrogin-1/MAFbx gene expression and protein content over 3 and 7 days of immobilization and/or leucine supplementation (Fig. 3).

By the third day (Fig. 3A) of immobilization, Atrogin-1/MAFbx gene expression was upregulated (~4-fold) and mitigated by leucine supplementation (~1.5-fold). On the seventh day (Fig. 3C), however, Atrogin-1/MAFbx gene expression was similar to control values in immobilization, as well as leucine-treated groups. Leucine supplementation alone did not affect the expression of this gene at any time. Concerning protein expression, no changes among groups were observed at the 3-day time point (Fig. 3B). On the other hand, at 7-day time point Atrogin-1/MAFbx protein levels increased by immobilization, although leucine was not able to impair this rise (Fig. 3D; imob: ~3-fold; imob leu: ~3-fold).

Myostatin was upregulated on immobilization and attenuated by leucine supplementation

As expected, immobilization was able to induce myostatin gene expression by 3 and 7 days (~3 and 1.7-fold, respectively). This elevation was reduced by leucine supplementation to the level of the control group at all time points (Fig. 4A, C).

Protein expression was in line with mRNA data on the third day, being elevated by immobilization (~1.6-fold). At this time point, leucine supplementation in immobilized animals was able to block the rise in myostatin protein expression, setting it to the level of the control group (Fig. 4B). At 7 days, myostatin protein expression remains unchanged in all groups analyzed (Fig. 4D).

Follistatin gene expression was upregulated on immobilization and accentuated by leucine at third-day

Considering that myostatin expression was modulated by leucine, we decided to verify the expression of the inhibitor of myostatin, follistatin. We observed that immobilization induced increased follistatin expression on the third and on the seventh day (Fig. 5A, C). On the third day of immobilization, leucine supplementation induces upregulation of

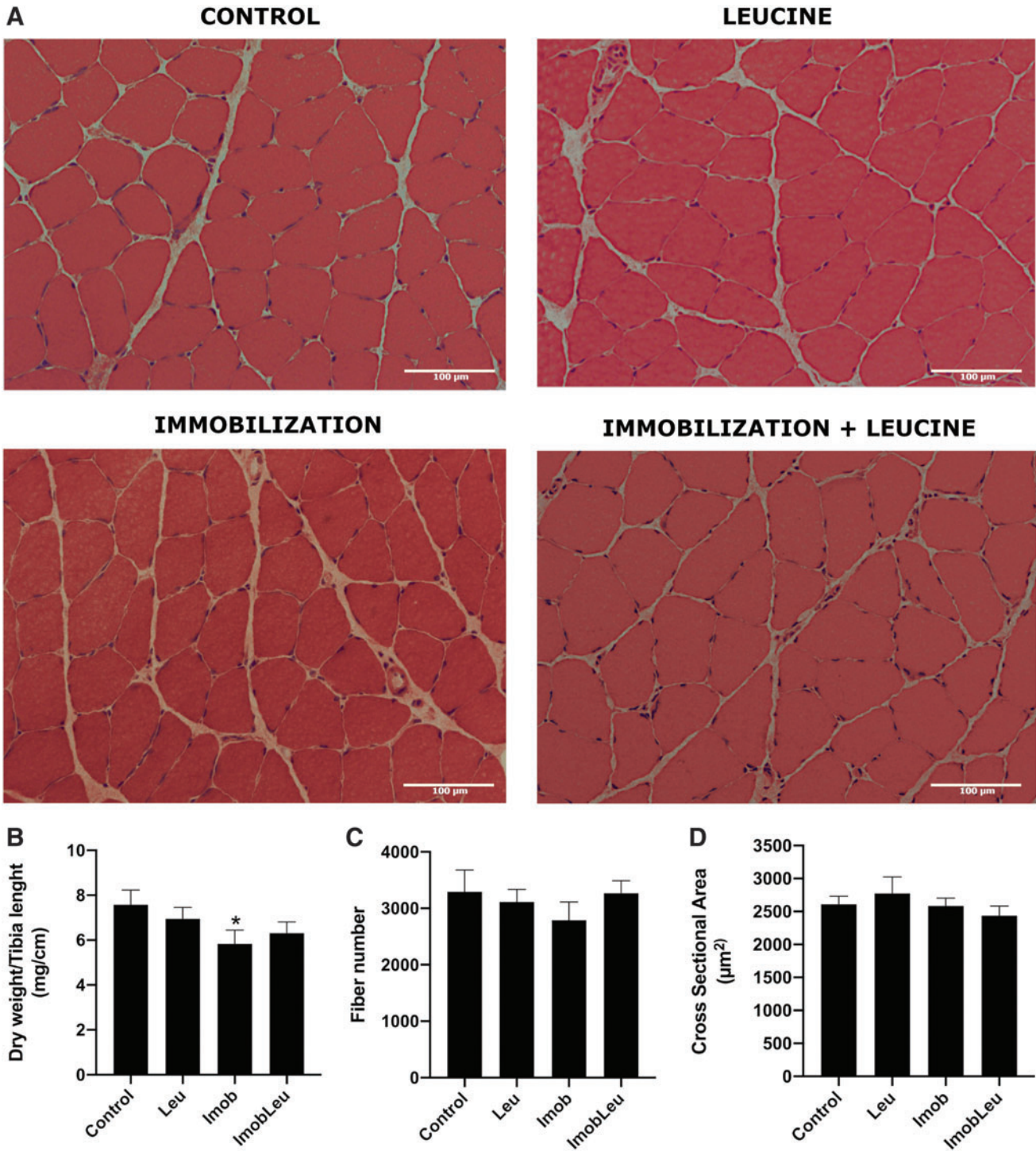


FIG. 1. (A) H&E staining of soleus cross-sections from groups: control, leucine (leu), immobilization (imob), and immobilization plus leucine (imob leu) for 3 days. (B) The dry weight of soleus muscle at 3-day time point in the groups: control, leu, imob, and imob leu. The muscle weight was normalized by tibia length. (C) Number of soleus muscle fibers of rats after 3-day time point in the groups: control, leu, imob, and imob leu. (D) Cross-sectional area of fibers in the soleus muscle of rats after 3 days of immobilization (imob), leucine supplementation (leu), or immobilization plus leucine supplementation (imob leu). Values are mean + SD. * $p < 0.05$ versus control. H&E, Hematoxylin and Eosin; SD, standard deviation. Color images are available online.

follistatin gene expression on a significant scale (~ 3.7 -fold) as compared with control. Remarkably, leucine supplementation in immobilized animals for 3 days further elevated follistatin gene expression very strongly (~ 14 -fold). On the seventh day, follistatin gene expression persisted elevated in

immobilized animals (~ 6 -fold) and leucine supplementation in immobilized animals did not produce enhanced follistatin mRNA levels as in the 3-day group (Fig. 5C). In contrast to gene expression, follistatin protein content was unchanged at 3 and 7 days (Fig. 5B, D).

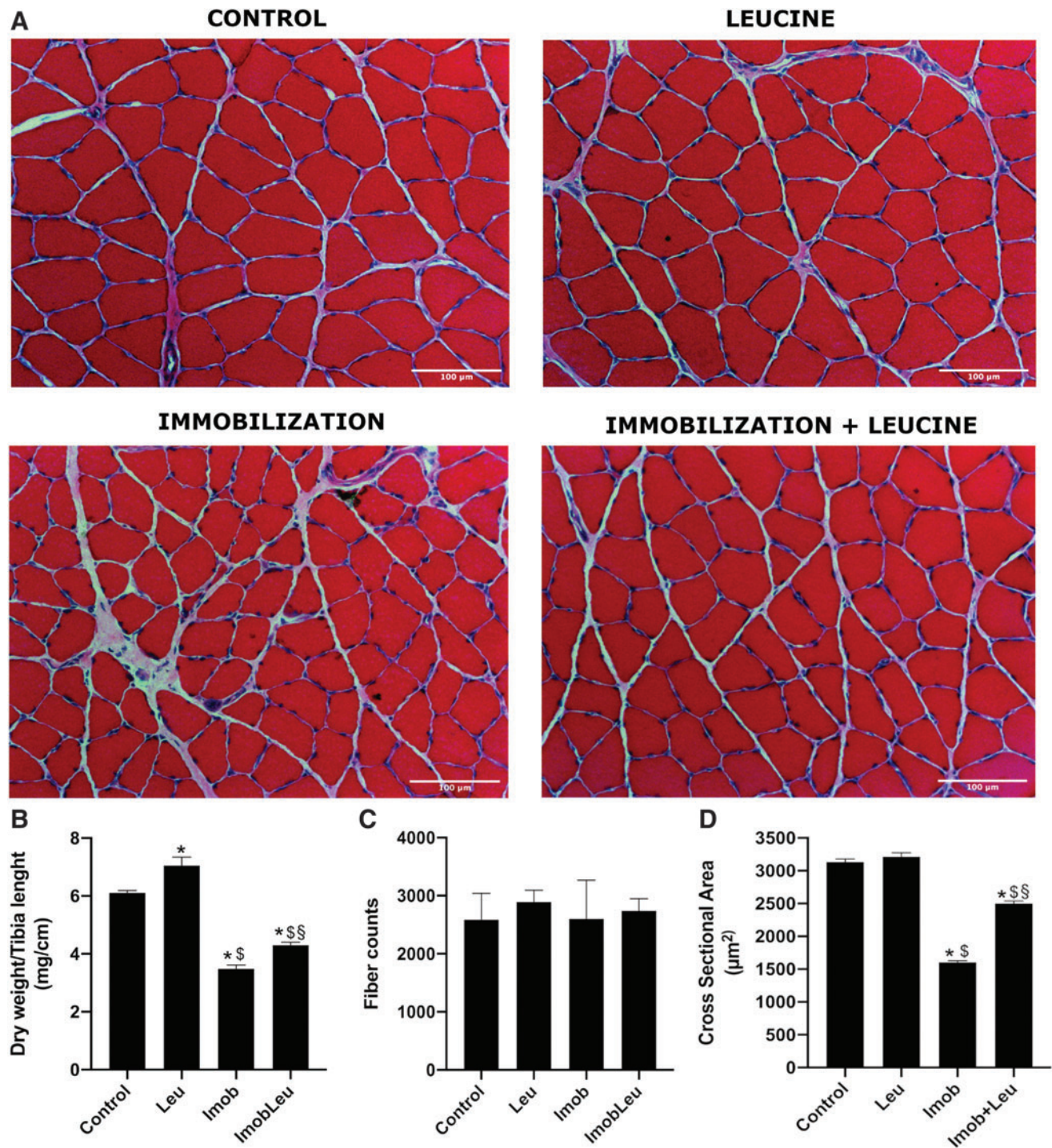


FIG. 2. (A) H&E staining of soleus cross-sections at 7-day time point from groups: control, leucine (leu), immobilization (imob), and immobilization plus leucine (imob leu). (B) Dry weight of soleus muscle at 7-day time point in the groups: control, leu, imob, and imob leu. The muscle weight was normalized by tibia length. (C) Number of soleus muscle fibers of rats after 7-day time point in the groups: control, leu, imob, and imob leu. (D) Cross-sectional area of fibers in the soleus muscle of rats after 7 days of immobilization (imob), leucine supplementation (leu), or immobilization plus leucine supplementation (imobleu). Values are mean + SD. * $p < 0.05$ versus control, § $p < 0.05$ versus leu, §§ $p < 0.05$ versus imob leu. Color images are available online.

Discussion

Although starvation, glucocorticoid treatment, cachexia, kidney failure, aging, and mechanical unload are widespread examples of skeletal muscle mass loss, such models can

modulate specific genes and even specific pathways (Sachek *et al.*, 2007). Among those models, mechanical unloading (i.e., cast immobilization) allows significant clinical insights to be reached regarding conditions where patients were submitted to bone fracture, peripheral nerve injury, or

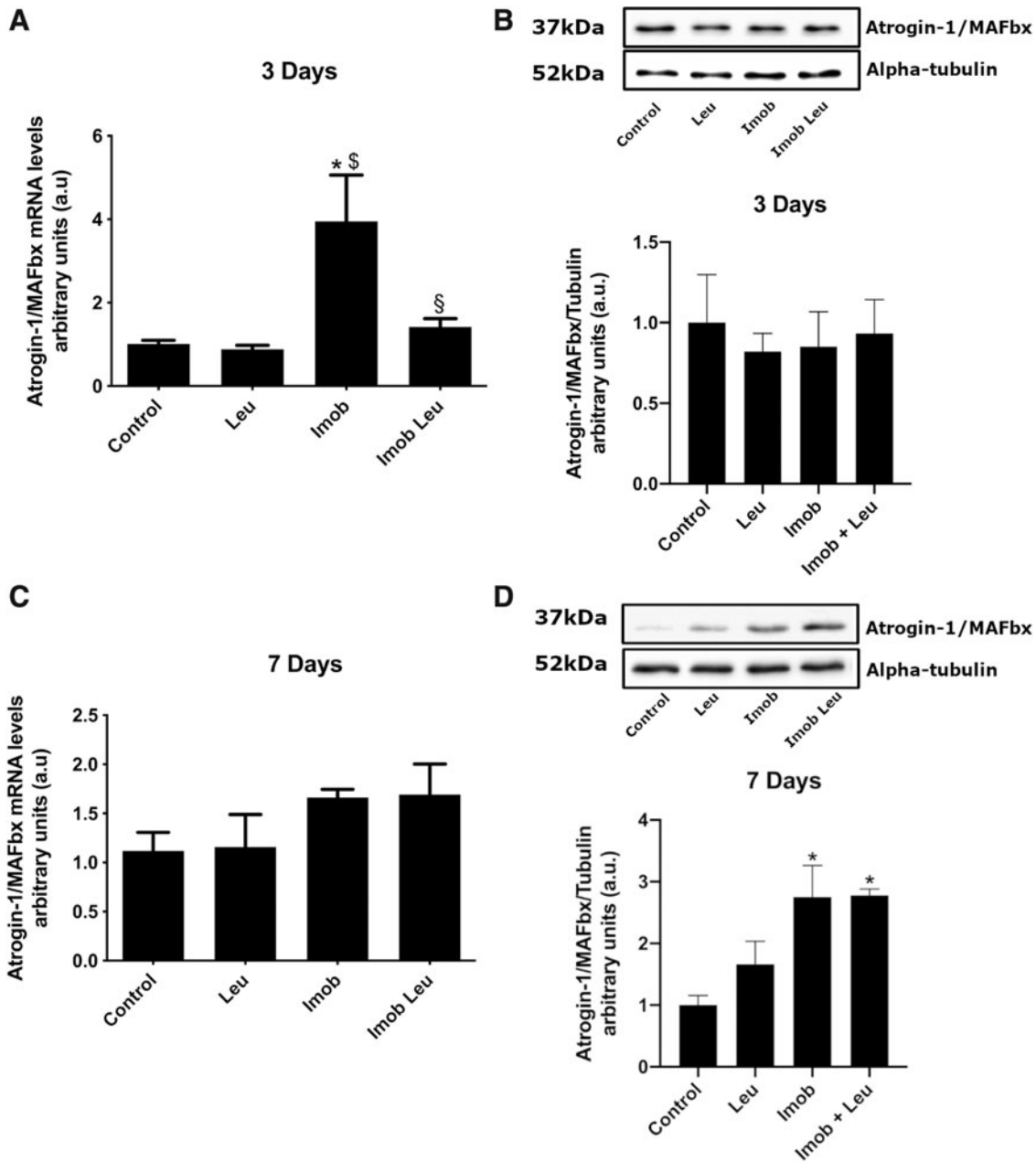


FIG. 3. (A and C) Atrogin-1/MAFbx gene expression in the soleus muscle of rats from groups: control, leucine (leu), immobilization (imob), and immobilization plus leucine (imob leu) for 3 and 7 days. Arbitrary units express the results, which were normalized by the cyclophilin A expression. (B and D) Atrogin-1/MAFbx protein levels in soleus muscle of rats from groups: control, leu, imob, and imob leu for 3 and 7 days. Alpha-tubulin protein content was used as a loading control. ^{*} $p < 0.05$ versus control, ^{\$} $p < 0.05$ versus leu, [§] $p < 0.05$ versus imob.

joint surgery. In humans, skeletal muscle wasting after mechanical unloading is detectable as early as 5 days following a decrease in strength and local metabolic changes, such as increased insulin resistance (Appell, 1990; Wall *et al.*, 2014).

In rodents, cast immobilization as a model of mechanical unloading results in a rapid and consistent mass loss, also resulting in decreased force. Moreover, in this model, slow-twitch fibers are the most affected, which is in line with clinical conditions involving cast immobilization in humans (Booth and Kelso, 1973; Brooks and Myburgh, 2014). Indeed, in the present study, when we cast-hindlimb-immobilized rats for 3 and 7 days, the soleus muscle

(~90% slow-twitch fibers) showed a consistent loss of mass (~23% and ~40% decrease, respectively). After 1 week of cast immobilization, the CSA of the fibers was also reduced ~48% when compared with control, indicating that the atrophy model used in this study was successfully employed (Figs. 1 and 2). Accordingly, the atrophy obtained in this study using the hindlimb immobilization model agrees with previous studies; for example, Baptista *et al.* (2013) observed ~40% decrease in soleus mass and CSA in rat soleus muscle 1 week after immobilization. No changes were found regarding total number of fibers, which is in line with the study of Cardenas *et al.* (1977) and Nicks *et al.* (1989),

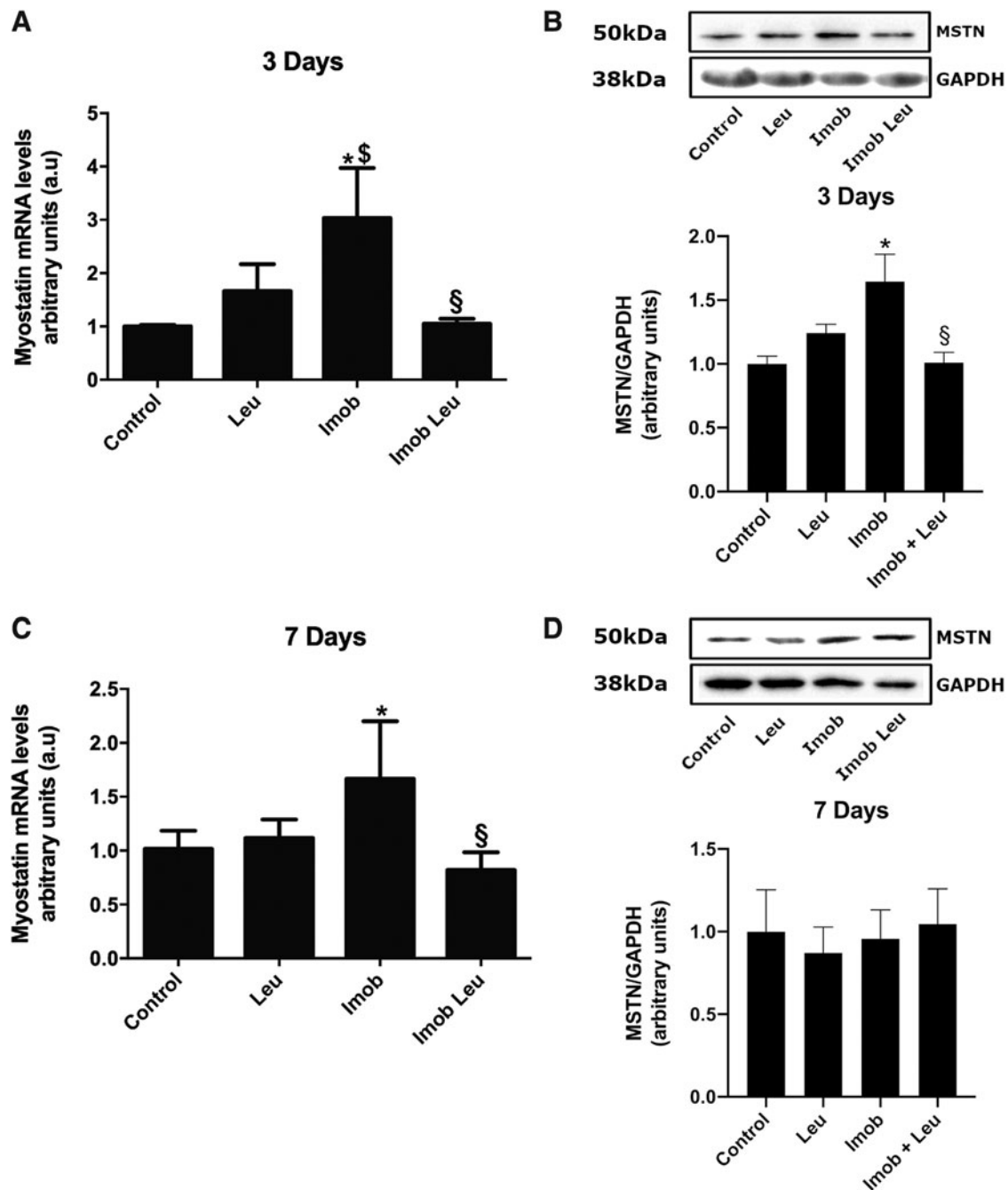


FIG. 4. (A and C) Myostatin gene expression in the soleus muscle of rats from groups: control, leucine (leu), immobilization (imob), and immobilization plus leucine (imob leu) for 3 and 7 days. Arbitrary units express the results that were normalized by the cyclophilin A expression. (B and D) Myostatin protein levels in the soleus muscle of rats from groups: control, leu, imob, and imob leu for 3 and 7 days. The *GAPDH* protein content was used as a loading control. * $p < 0.05$ versus control, $^{\$}p < 0.05$ versus leu, $^{\$}p < 0.05$ versus imob.

which showed that skeletal muscle atrophy induced by immobilization do not occur through fiber number loss.

Several approaches have been employed aiming to mitigate skeletal muscle wasting, such as resistive physical exercise (Shen *et al.*, 2018), blockage, or stimulation of certain intracellular pathways with antibodies or recombinant proteins, i.e., myostatin antibodies or follistatin overexpression (Sepulveda *et al.*, 2015; Camporez *et al.*, 2016; Desgeorges

et al., 2017). Other noninvasive methods have been used, and supplementation with L-leucine appears to be an attractive strategy. It has been shown that leucine is capable of minimizing mass loss in cachexia, cancer, injury, and immobilization in rodents (Anthony *et al.*, 2000; Ventrucchi *et al.*, 2001; van Norren *et al.*, 2009; Peters *et al.*, 2011; Baptista *et al.*, 2013; Pereira *et al.*, 2014). However, in humans, the anti-atrophic effects of leucine supplementation are still

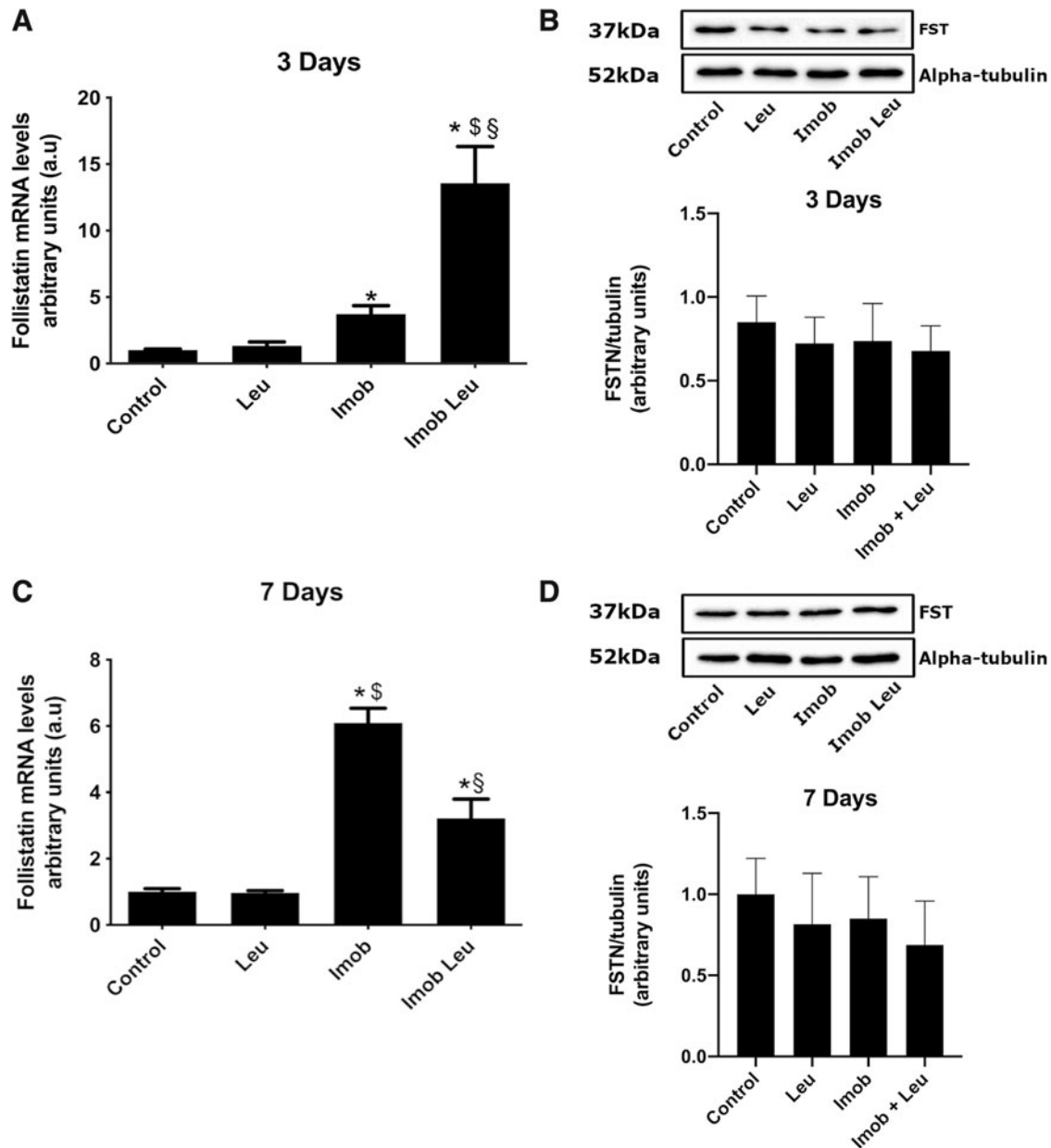


FIG. 5. (A and C) Follistatin gene expression in soleus muscle of rats from groups: control, leucine (leu), immobilization (imob), and immobilization plus leucine (imob leu) for 3 and 7 days. Arbitrary units express the results that were normalized by the cyclophilin A expression. (B and D) Follistatin protein levels in the soleus muscle of rats from groups: control, leu, imob, and imob leu for 3 and 7 days. Alpha-tubulin protein content was used as a loading control. * $p < 0.05$ versus control, [§] $p < 0.05$ versus leu, ^{§§} $p < 0.05$ versus imob.

under debate. In certain studies, the protective effect of leucine is reported, while other authors found no protective effect. The differences in age of subjects, time of leucine supplementation (i.e., pre- vs. postprandial), and differences in dosage might explain those somewhat conflicting results (Ham *et al.*, 2014; English *et al.*, 2016; Ispoglou *et al.*, 2016, 2017; Mitchell *et al.*, 2017; Wolfe, 2017; Backx *et al.*, 2018).

To track the atrophic process at the molecular level, we monitored Atrogin-1/MAFbx gene and protein expression 3 and 7 days after hindlimb immobilization (Fig. 3). It has been previously shown that this atrogin gene expression peaks at a 3-day time point (Bodine *et al.*, 2001; Baptista

et al., 2010; Okamoto *et al.*, 2011), and as expected, we observed an increased Atrogin-1/MAFbx expression 3 days after immobilization. Leucine supplementation mitigated this increase, again demonstrating that the atrophy and leucine supplementation model employed in this study was efficient.

Nonetheless, atrogenes may not be the only components in muscle mass control. Indeed, other interrelated pathways, such as myostatin, do play a role, and in this study, we decided to evaluate whether leucine supplementation can modulate myostatin expression in skeletal muscle under disuse.

As expected, we found elevated levels of myostatin gene expression after 3 and 7 days of immobilization, and

interestingly, leucine supplementation completely blocked this effect (Fig. 4A, C). Additionally, at the protein level, leucine blocked the rise in myostatin driven by 3 days of immobilization (Fig. 4B). On the other hand, no differences were found in myostatin protein levels among the groups after 7 days of immobilization (Fig. 4D). These data helped to elucidate the anti-atrophic effects of leucine, suggesting that myostatin mRNA regulation plays a role in the skeletal muscle atrophy and is sensitive to leucine.

The leucine effects on myostatin mRNA during immobilization could be related to transcription and posttranscriptional modulation. At transcriptional level, myostatin expression can be induced by the transcription factor FoxO (Allen and Unterman, 2007; Grade *et al.*, 2019). Accordingly, FoxO activity is increased in disuse atrophy (Senf *et al.*, 2010; Baptista *et al.*, 2017) and leucine supplementation is able to decrease FoxO nuclear translocation during immobilization (Baptista *et al.*, 2017). This effect could therefore be related to myostatin mRNA response both to immobilization and leucine.

Another possible mechanism includes posttranscriptional modulation by microRNAs. The miR-27 family of microRNAs has been shown to target and degrade myostatin and FoxO mRNAs, reducing their biological availability (Guttilla and White, 2009; Huang *et al.*, 2012; Miretti *et al.*, 2013). Interestingly, members of this family are upregulated by leucine supplementation (Chen *et al.*, 2013); in this sense, the myostatin downregulation induced by leucine seen in this study could be related to miR-27 action upon myostatin itself and FoxO mRNAs. The dynamics of miR-27 expression during immobilization and supplementation is an interesting topic to address in forthcoming studies.

Although it is well known that regulation of myostatin by follistatin occurs by protein/protein interactions (Amthor, 2004; Sepulveda *et al.*, 2015), we decided to verify follistatin expression because mRNA and protein levels can provide input on the possible amount of follistatin in the extracellular environment.

Follistatin overexpression promotes skeletal muscle hypertrophy and is known to ameliorate pathology in mdx, amyotrophic lateral sclerosis mice, and spinal muscular atrophy (Rose *et al.*, 2009; Sepulveda *et al.*, 2015; Iskenderian *et al.*, 2018).

Interestingly, we were not able to find studies examining the regulation of follistatin expression in cast immobilization. In this study, surprisingly, we show that immobilization alone can strongly induce follistatin gene expression at 3 and 7 days after immobilization (Fig. 5A, C). Notably, leucine supplementation can boost the increase in follistatin driven by immobilization (from ~3.7-fold to 14-fold). At 7 days of immobilization, follistatin mRNA levels were similar to those of the 3-day group, and the boost in follistatin mRNA driven by leucine was no longer observable.

In spite of changes in mRNA expression, we did not find a corresponding increase in follistatin protein levels; indeed, we found no changes in the levels of this protein in cast-immobilized animals (Fig. 5B, D). These results indicate that leucine can exert its anti-atrophic effect by decreasing myostatin protein expression independently of follistatin at the protein level. On the other hand, it is intriguing that such a strong response of follistatin occurs exclusively at the mRNA level. We envision that follistatin mRNA rise could be related to molecular mechanisms other than pro-

tein/protein interactions, such as those related to noncoding RNAs (Nie *et al.*, 2015). For example, follistatin mRNA could generate a currently uncharacterized microRNAs that would, in turn, be able to inhibit mRNAs coding for stimulators of myostatin, such as NF- κ B-p65, MYOD, MYF5, and NFAT, all of which are known to be transactivators of the myostatin promoter. Alternatively, those microRNAs could even target myostatin mRNA itself (Huang *et al.*, 2012; Qiu *et al.*, 2013; Grade *et al.*, 2019).

In fact, several studies have shown that mRNAs are able to produce functional microRNAs, and regulatory loops have been described (Ladewig *et al.*, 2012; Ha and Kim, 2014; Titov and Vorozheykin, 2018). Nonetheless, to the best of our knowledge, at present, no study has directly demonstrated microRNAs originating from follistatin mRNA, although it has been shown that in the follistatin family, follistatin-like 1 (FSLT1) can produce miR-198 on its last exon (Hinske *et al.*, 2010; Sundaram *et al.*, 2013). Finally, additional recently described noncoding RNAs, such as circRNA and lncRNAs, could also be hosted in the follistatin gene and be related to proatrophic pathways.

This type of mechanism involving noncoding RNAs has been recently linked to skeletal muscle plasticity, including myogenesis and atrophy (Weng *et al.*, 2018; Peng *et al.*, 2019).

Conclusion

We demonstrated that leucine protects skeletal muscle mass loss by disuse through myostatin inhibition independently of follistatin signaling.

Acknowledgments

The authors thank FAPESP and CNPq for financial support. They are also grateful to the Foundation Leducq (network 13CVD04), and the European Union (Horizon 2020 grant agreement no. 645648 “Muscle Stress Relief”).

Disclosure Statement

No competing financial interests exist.

Funding Information

This work was supported by the São Paulo Research Foundation (FAPESP) fellowships #2017/09398-8, #2013/15040-8, #2018/24419-4, #2012/22488-2, #2013/19387-2, Research Grant 2015/04090-0 and CNPq. This work was also supported by Leducq Foundation, Award #FLQ13CVD04, and the European Union (GA#645648, “Muscle Stress Relief”).

References

- Allen, D.L., and Unterman, T.G. (2007). Regulation of myostatin expression and myoblast differentiation by FoxO and SMAD transcription factors. *Am J Physiol Cell Physiol* **292**, C188–C199.
- Amthor, H. (2004). Follistatin complexes myostatin and antagonizes Myostatin-mediated inhibition of myogenesis. *Dev Biol* **270**, 19–30.
- Anthony, J.C., Anthony, T.G., Kimball, S.R., Vary, T.C., and Jefferson, L.S. (2000). Orally administered leucine stimulates protein synthesis in skeletal muscle of postabsorptive rats in association with increased eIF4F formation. *J Nutr* **130**, 139–145.

- Appell, H.-J. (1990). Muscular atrophy following immobilisation. *Sports Med* **10**, 42–58.
- Backx, E.M.P., Horstman, A.M.H., Marzuca-Nassr, G.N., van Kranenburg, J., Smeets, J.S., Fuchs, C.J., *et al.* (2018). Leucine supplementation does not attenuate skeletal muscle loss during leg immobilization in healthy, young men. *Nutrients* **10**, 635.
- Baptista, I.L., Leal, M.L., Artioli, G.G., Aoki, M.S., Fiamoncini, J., Turri, A.O., *et al.* (2010). Leucine attenuates skeletal muscle wasting via inhibition of ubiquitin ligases. *Muscle Nerve* **41**, 800–808.
- Baptista, I.L., Silva, W.J., Artioli, G.G., Guilherme, J.P.L.F., Leal, M.L., Aoki, M.S., *et al.* (2013). Leucine and HMB differentially modulate proteasome system in skeletal muscle under different sarcopenic conditions. *PLoS One* **8**, e76752.
- Baptista, I.L., Silvestre, J.G., Silva, W.J., Labeit, S., and Moriscot, A.S. (2017). FoxO3a suppression and VPS34 activity are essential to anti-atrophic effects of leucine in skeletal muscle. *Cell Tissue Res* **369**, 381–394.
- Bodine, S.C., and Baehr, L.M. (2014). Skeletal muscle atrophy and the E3 ubiquitin ligases MuRF1 and MAFbx/atrogin-1. *Am J Physiol Endocrinol Metab* **307**, E469–E484.
- Bodine, S.C., Latres, E., Baumhueter, S., Lai, V.K., Nunez, L., Clarke, B.A., *et al.* (2001). Identification of ubiquitin ligases required for skeletal muscle atrophy. *Science* **294**, 1704–1708.
- Booth, F.W., and Kelso, J.R. (1973). Production of rat muscle atrophy by cast fixation. *J Appl Physiol* **34**, 404–406.
- Brooks, N.E., and Myburgh, K.H. (2014). Skeletal muscle wasting with disuse atrophy is multi-dimensional: the response and interaction of myonuclei, satellite cells, and signaling pathways. *Front Physiol* **5**, 99.
- Camporez, J-P.G., Petersen, M.C., Abudukadier, A., Moreira, G.V., Jurczak, M.J., Friedman, G., *et al.* (2016). Anti-myostatin antibody increases muscle mass and strength and improves insulin sensitivity in old mice. *Proc Natl Acad Sci U S A* **113**, 2212–2217.
- Cardenas, D.D., Stolov, W.C., and Hardy, R. (1977). Muscle fiber number in immobilization atrophy. *Arch Phys Med Rehabil* **58**, 423–426.
- Ceglia, L., Niramitmahapanya, S., Price, L.L., Harris, S.S., Fielding, R.A., and Dawson-Hughes, B. (2013). An evaluation of the reliability of muscle fiber cross-sectional area and fiber number measurements in rat skeletal muscle. *Biol Proced Online* **15**, 6.
- Chen, X., Huang, Z., Chen, D., Yang, T., and Liu, G. (2013). MicroRNA-27a is induced by leucine and contributes to leucine-induced proliferation promotion in C2C12 cells. *Int J Mol Sci* **14**, 14076–14084.
- Desgeorges, M.M., Devillard, X., Toutain, J., Castells, J., Divoux, D., Arnould, D.F., *et al.* (2017). Pharmacological inhibition of myostatin improves skeletal muscle mass and function in a mouse model of stroke. *Sci Rep* **7**, 14000.
- Elkina, Y., von Haehling, S., Anker, S.D., and Springer, J. (2011). The role of myostatin in muscle wasting: an overview. *J Cachexia Sarcopenia Muscle* **2**, 143–151.
- English, K.L., Mettler, J.A., Ellison, J.B., Mamerow, M.M., Arentson-Lantz, E., Pattarini, J.M., *et al.* (2016). Leucine partially protects muscle mass and function during bed rest in middle-aged adults. *Am J Clin Nutr* **103**, 465–473.
- Grade, C.V.C., Mantovani, C.S., and Alvares, L.E. (2019). Myostatin gene promoter: structure, conservation and importance as a target for muscle modulation. *J Anim Sci Biotechnol* **10**, 32.
- Gissel, H. (2010). Effects of varying pulse parameters on ion homeostasis, cellular integrity, and force following electroporation of rat muscle in vivo. *Am J Physiol Regul Integr Comp Physiol* **298**, 918–929.
- Guttilla, I.K., and White, B.A. (2009). Coordinate regulation of FoxO1 by miR-27a, miR-96, and miR-182 in breast cancer cells. *J Biol Chem* **284**, 23204–23216.
- Ha, M., and Kim, V.N. (2014). Regulation of microRNA biogenesis. *Nat Rev Mol Cell Biol* **15**, 509–524.
- Ham, D.J., Caldow, M.K., Lynch, G.S., and Koopman, R. (2014). Leucine as a treatment for muscle wasting: a critical review. *Clin Nutr* **33**, 937–945.
- Hill, J.A., and Olson, E.N. (2012). *Muscle fundamental biology and mechanisms of disease*, first edition. Academic Press, Boston, MA.
- Hinske, L.C.G., AF Galante, P., Kuo, W.P., and Ohno-Machado, L. (2010). A potential role for intragenic miRNAs on their hosts' interactome. *BMC Genomics* **11**, 533.
- Huang, Z., Chen, X., Yu, B., He, J., and Chen, D. (2012). MicroRNA-27a promotes myoblast proliferation by targeting myostatin. *Biochem Biophys Res Commun* **423**, 265–269.
- Iskenderian, A., Liu, N., Deng, Q., Huang, Y., Shen, C., Palmieri, K., *et al.* (2018). Myostatin and activin blockade by engineered follistatin results in hypertrophy and improves dystrophic pathology in mdx mouse more than myostatin blockade alone. *Skeletal Muscle* **8**, 34.
- Ispoglou, T., Deighton, K., King, R.F., White, H., and Lees, M. (2017). Novel essential amino acid supplements enriched with L-leucine facilitate increased protein and energy intakes in older women: a randomised controlled trial. *Nutr J* **16**, 75.
- Ispoglou, T., White, H., Preston, T., McElhone, S., McKenna, J., and Hind, K. (2016). Double-blind, placebo-controlled pilot trial of L-Leucine-enriched amino-acid mixtures on body composition and physical performance in men and women aged 65–75 years. *Eur J Clin Nutr* **70**, 182–188.
- Jackman, R.W., and Kandarian, S.C. (2004). The molecular basis of skeletal muscle atrophy. *Am J Physiol Cell Physiol* **287**, C834–C843.
- Janssen, I., Heymsfield, S.B., Wang, Z., and Ross, R. (2000). Skeletal muscle mass and distribution in 468 men and women aged 18–88 yr. *J Appl Physiol* **89**, 81–88.
- Ladewig, E., Okamura, K., Flynt, A.S., Westholm, J.O., and Lai, E.C. (2012). Discovery of hundreds of mirtrons in mouse and human small RNA data. *Genome Res* **22**, 1634–1645.
- Lokireddy, S., Mouly, V., Butler-Browne, G., Gluckman, P.D., Sharma, M., Kambadur R., *et al.* (2011). Myostatin promotes the wasting of human myoblast cultures through promoting ubiquitin-proteasome pathway-mediated loss of sarcomeric proteins. *Am J Physiol Cell Physiol* **301**, C1316–C1324.
- Lokireddy, S., Wijesoma, I.W., Sze, S.K., McFarlane, C., Kambadur, R., and Sharma, M. (2012). Identification of atrogin-1-targeted proteins during the myostatin-induced skeletal muscle wasting. *Am J Physiol Cell Physiol* **303**, C512–C529.
- Miretti, S., Martignani, E., Accornero, P., and Baratta, M. (2013). Functional effect of mir-27b on myostatin expression: a relationship in piedmontese cattle with double-muscling phenotype. *BMC Genomics* **14**, 194.
- Mitchell, W.K., Phillips, B.E., Hill, I., Greenhaff, P., Lund, J.N., Williams, J.P., *et al.* (2017). Human skeletal muscle is refractory to the anabolic effects of leucine during the

- postprandial muscle-full period in older men. *Clin Sci* **131**, 2643–2653.
- Nicks, DK, Beneke, WM, Key, RM, and Timson, BF. (1989). Muscle fibre size and number following immobilisation atrophy. *J Anatomy* **163**, 1–5.
- Nie, M., Deng, Z-L., Liu, J., and Wang, D-Z. (2015). Non-coding RNAs, emerging regulators of skeletal muscle development and diseases. *Biomed Res Int* **2015**, 676575.
- Okamoto, T., Torii, S., and Machida, S. (2011). Differential gene expression of muscle-specific ubiquitin ligase MAFbx/Atrogin-1 and MuRF1 in response to immobilization-induced atrophy of slow-twitch and fast-twitch muscles. *J Physiol Sci* **61**, 537.
- Peng, S., Song, C., Li, H., Cao, X., Ma, Y., Wang, X., *et al.* (2019). Circular RNA SNX29 sponges miR-744 to regulate proliferation and differentiation of myoblasts by activating the Wnt5a/Ca2+ signaling pathway. *Mol Ther Nucleic Acids* **16**, 481–493.
- Pereira, M.G., Silva, M.T., Carlassara, E.O.C., Gonçalves, D.A., Abrahamsohn, P.A., Kettelhut, I.C., *et al.* (2014). Leucine supplementation accelerates connective tissue repair of injured tibialis anterior muscle. *Nutrients* **6**, 3981–4001.
- Peters, S.J., van Helvoort, A., Kegler, D., Argilès, J.M., Luiking, Y.C., Laviano, A., *et al.* (2011). Dose-dependent effects of leucine supplementation on preservation of muscle mass in cancer cachectic mice. *Oncol Rep* **26**, 247–254.
- Qiu, J., Thapaliya, S., Runkana, A., Yang, Y., Tsien, C., Mohan, M.L., *et al.* (2013). Hyperammonemia in cirrhosis induces transcriptional regulation of myostatin by an NF- κ B-mediated mechanism. *Proc Natl Acad Sci U S A* **110**, 18162–18167.
- Rose FF Jr, Mattis, V.B., Rindt, H., and Lorson, C.L. (2009). Delivery of recombinant follistatin lessens disease severity in a mouse model of spinal muscular atrophy. *Hum Mol Genet* **18**, 997–1005.
- Sacheck, J.M., Hyatt, J-P.K., Raffaello, A., Jagoe, R.T., Roy, R.R., Edgerton, V.R., *et al.* (2007). Rapid disuse and denervation atrophy involve transcriptional changes similar to those of muscle wasting during systemic diseases. *FASEB J* **21**, 140–155.
- Sandri, M. (2008). Signaling in muscle atrophy and hypertrophy. *Physiology* **23**, 160–170.
- Senf, S.M., Dodd, S.L., and Judge, A.R. (2010). FOXO signaling is required for disuse muscle atrophy and is directly regulated by Hsp70. *Am J Physiol Cell Physiol* **298**, 38–45.
- Sepulveda, P.V., Lamon, S., Hagg, A., Thomson, R.E., Winbanks, C.E., Qian, H., *et al.* (2015). Evaluation of follistatin as a therapeutic in models of skeletal muscle atrophy associated with denervation and tenotomy. *Sci Rep* **5**, 17535.
- Shen, L., Meng, X., Zhang, Z., and Wang, T. (2018). Physical exercise for muscle atrophy. *Adv Exp Med Biol* **1088**, 529–545.
- Sundaram, G.M., Common, J.E.A., Gopal, F.E., Srikanta, S., Lakshman, K., Lunny, D.P., *et al.* (2013). “See-saw” expression of microRNA-198 and FSTL1 from a single transcript in wound healing. *Nature* **495**, 103–106.
- Titov, I.I., and Vorozheykin, P.S. (2018). Comparing miRNA structure of mirtrons and non-mirtrons. *BMC Genomics* **19**, 114.
- Trendelenburg, A.U., Meyer, A., Rohner, D., Boyle, J., Hatakeyama, S., and Glass, D.J. (2009). Myostatin reduces Akt/TORC1/p70S6K signaling, inhibiting myoblast differentiation and myotube size. *Am J Physiol Cell Physiol* **296**, C1258–C1270.
- van Norren, K., Kegler, D., Argilès, J.M., Luiking, Y., Gorse-link, M., Laviano, A., *et al.* (2009). Dietary supplementation with a specific combination of high protein, leucine, and fish oil improves muscle function and daily activity in tumour-bearing cachectic mice. *Br J Cancer* **100**, 713–722.
- Ventrucci, G., Mello, M.A.R., and Gomes-Marcondes, M.C.C. (2001). Effect of a leucine-supplemented diet on body composition changes in pregnant rats bearing Walker 256 tumor. *Braz J Med Biol Res* **34**, 333–338.
- Wall, B.T., Dirks, M.L., Snijders, T., Senden, J.M.G., Dolmans, J., and van Loon, L.J.C. (2014). Substantial skeletal muscle loss occurs during only 5 days of disuse. *Acta Physiol* **210**, 600–611.
- Wang, D-T., Yang, Y-J., Huang, R-H., Zhang, Z-H., and Lin, X. (2015). Myostatin activates the ubiquitin-proteasome and autophagy-lysosome systems contributing to muscle wasting in chronic kidney disease. *Oxid Med Cell Longev* **2015**, 684965.
- Weng, J., Zhang, P., Yin, X., and Jiang, B. (2018). The whole transcriptome involved in denervated muscle atrophy following peripheral nerve injury. *Front Mol Neurosci* **11**, 69.
- Wolfe, R.R. (2017). Branched-chain amino acids and muscle protein synthesis in humans: myth or reality? *J Int Soc Sports Nutr* **14**, 30.

Address correspondence to:
 Anselmo Sigari Moriscot, PhD
 Department of Anatomy, (ICB-III)
 Institute of Biomedical Sciences
 University of São Paulo
 Avenida Lineu Prestes 2415
 São Paulo 05508-000
 Brazil

E-mail: moriscot@usp.br

Received for publication March 3, 2020; received in revised form August 28, 2020; accepted September 8, 2020.